LIÈGE université
GIGA institute

LIÈGE université

Rasa3 controls turnover of endothelial cell adhesion and vascular lumen integrity by a Rap1-dependent mechanism

ORBAN Tanguy

Promotor : Pr. Franck Dequiedt

Laboratory of Protein Signaling and Interactions

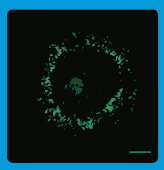

siRasa3

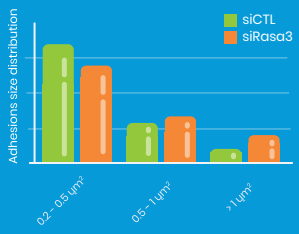

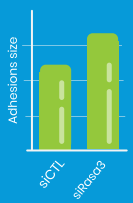

Thesis submitted to attain the degree of Doctor of Sciences

Academic Year 2018-2019

Examination committee

Prof. Dr. **Catherine Sadzot** (Committee Chair)

Laboratory of Virology and Immunology GIGA-Research, University of Liège, B-4000 Liège, Belgium.

Prof. Dr. **Franck Dequiedt** (Promoter)

Laboratory of Protein Signaling and Interactions (PSI), GIGA-Research, University of Liège, B-4000 Liège, Belgium.

Prof. Dr. **Stephane Schurmans**

Laboratory of Functional Genetics, GIGA-Research, University of Liège, B-4000 Liège, Belgium.

Dr. **Angeliki Malliri**

Cell Signalling Group, Cancer Research UK Manchester Institute, The University of Manchester, Alderley Park, SK10 4TG, UK.

Dr **Ilse Geudens**

VIB-KU Leuven Center for Cancer Biology, Campus Gasthuisberg 3000 LEUVEN

Dr. **Ingrid Struman**

Laboratory of Molecular Angiogenesis, GIGA-Research, University of Liège, B-4000 Liège, Belgium.

Dr. **Isabelle Manfroid**

Laboratory of Zebrafish Development and Disease Models, GIGA-Research, University of Liège, B-4000 Liège, Belgium.

Résumé

Rasa3 est une protéine activatrice des *small GTPases* et fait partie de la famille GAP1 qui cible Ras et Rap1. Bien que l'inactivation catalytique ou la délétion de Rasa3 en souris résulte en de nombreuses hémorragies et à la létalité embryonnaire, la fonction biologique sous-jacente à ces défauts reste inconnue. Ici, via une combinaison d'approche *in vivo* en souris et zebrafish et *in vitro* en HUVECs, nous avons identifié un rôle clé de Rasa3 dans le développement vasculaire.

L'ablation spécifique de Rasa3 dans les cellules endothéliales de la souris récapitule complétement le phénotype observé chez les souris Rasa3$^{-/-}$. Des défauts de lumenisation ont été mis en évidence chez les souris où Rasa3 est spécifiquement inactivée dans la lignée endothéliale ainsi que dans le zébrafish via l'utilisation d'un morpholino.

In vitro en HUVECs, la déplétion de Rasa3 augmente l'activation de l'intégrine β1, l'adhésion des cellules à la matrice extracellulaire entrainant une diminution de la migration cellulaire et unblocage de la tubulogenèse. Durant la migration, les cellules déplétées pour Rasa3 exhibent des adhésions plus larges et plus matures résultant d'une perturbation des processus d'assemblage et de désassemblage entrainant une augmentation de leur durée de vie. Ces défauts sont dus à une hyperactivation de Rap1 et à un blocage dans la signalisation FAK/Src. De plus, la déplétion de Rasa3 augmente la stabilité des jonctions cellule-cellule résultant en une diminution de la perméabilité. Finalement, des défauts d'adhésion et d'étalement des péricytes (cellules impliquées dans les interactions hétérotypic avec les cellules endothéliales) ont été observés *in vivo* en souris et *in vitro* en HUVECs.

L'ensemble de ces résultats indique que Rasa3 est un régulateur critique de Rap1 dans les cellules endothéliales en régulant les propriétés d'adhésion et la maintenance de l'intégrité du lumen.

Remerciements

On dit toujours que les remerciements sont la partie la plus simple de l'écriture d'une thèse… et pourtant, voilà une semaine que j'ai fini mes corrections et que je n'arrive pas à m'y mettre.

Cette thèse n'aurait pas vu le jour sans votre aide et je tiens donc à grandement vous remercier.

Tout d'abord je tiens à remercier mon promoteur Franck, de m'avoir accueilli au sein de son laboratoire et de m'avoir préparé pour affronter le jury FRIA. Je te remercie pour ton aide au cours de la thèse pour les manips ainsi que pour la bonne ambiance instaurée au labo avec les barbecues et le ski.

Cependant, mon aventure au GIGA n'a pas commencé dans le labo de Franck, mais bien dans le laboratoire de virologie où j'ai effectué mon mémoire. Je remercie le Dr. Yvette Habraken d'avoir été présente pour répondre à mes questions et surtout d'avoir su supporter mon humour particulier : « Bonjouuuuuuuuur Yvette ».

Durant ce mémoire j'ai pu rencontrer Adeline. Un GRAND merci d'avoir passé autant de temps sur la conception de ma couverture de thèse ainsi que les intercalaires. Je te remercie aussi pour m'avoir donné ma filleule Aurore (j'en profite aussi pour remercier Arnaud parce que sur ce coup la tu n'étais pas toute seule ;)). Mais avant ces histoires de bébés, couverture de thèse… il y a avait les délires entre 2 collègues qui partageaient un bureau. Merci pour tout.

Ensuite j'ai débarqué chez Franck où l'on m'a proposé de travailler sur la protéine Rasa3 en collaboration avec une équipe du +4. Je remercie le Dr. Patricia Molina Ortiz pour son aide durant les différentes étapes de ma thèse ainsi que Stéphane Schurmans sans qui cette collaboration n'aurait pu avoir lieu.

Je remercie également le Dr.Maud Martin qui avait commencé ce projet et qui a su répondre à mes nombreuses questions. Merci, de m'avoir accueilli et encadré pendant mes 2 semaines à Utrecht.

Un énorme merci à Tina d'avoir pris le temps de relire cette thèse en détail et d'être toujours disponible pour une question. Merci à toi et j'espère plein de bonnes choses pour la suite.

A la petite portugaise Alex, tout simplement merci pour TOUT. Pour les manips, les sorties, les repas,… j'espère bien vite venir te rendre visite à Boston. Tes expressions si particulières manquent au labo pour cette fin de thèse ;).

Johnny !!! Le pompier du labo, l'huile indispensable au moteur du laboratoire. C'est simple, sans toi, le labo s'écroule. Mon partenaire du « gang des bananes » devenu ami, un grand merci pour toute l'aide pendant ces 4 années et j'espère continuer à te voir après.

*Aux 3 gonzesses/meufs (Quelle vulgarité dans ces termes !!!). Je parle évidement de Charlotte, Megan et Emeline. Il y a d'abord la calme, douce et posée Charlotte. Nous qui partageons cette passion des légumes ! Merci pour la découverte du poireau, aubergines, roquette, carottes, poivrons, échalotes, brocolis … je mangerai bien un Huggy's ;) Pas toujours facile d'être ma voisine au bench et au bureau pour rester concentrée, alors Merci (tout en faisant chick chicky boom chick chicky boom). On en vient ensuite à la distinguée et raffinée Megan (La triplé n°4). Parce que oui, Megan elle peut cracher et parler avec un accent de barlos ; ça passe parce qu'elle va dans des étoilés ;) Merci de m'avoir accompagné dans mes délires de baraki (Dissssssssssssss !!!!). Pour terminer il y a la lucide et perspicace Emeline, celle qui comprend toujours tout correctement. « Bonjour Emeline, bienvenue au Labo », « Quoi qu'est-ce que tu dis avec ton sp**** ? » « Silence gênant … ». Merci pour ces moments d'incompréhension (surtout de ta part) ainsi que d'avoir été ma maman à la piscine.*

Bartémide, Bartholomé, Bartitude, Bartichaut, bon je ne sais plus ! Je vais t'appeler Léo. Merci de m'avoir bien fait rire avec cet humour unique que seul toi comprends.

A mes 2 petits esclaves Nicolas (moi au moins je ne t'oublie pas) et Audrey que j'ai encadré pendant un an. Merci d'avoir fait avancer mon projet et de bien m'avoir fait marrer.

Merci aux filles de chez Denis (Céline, Lola, Amandine et Sarah) d'avoir insufflé un air nouveau (je dirais même un vent de fraicheur) au sein du laboratoire (surtout toi Amandine). Quant à toi Lola, merci pour ces petits coups de téléphone si sympathique ;). J'en profite du coup pour remercier MON Fripon.

Merci également aux membres du labo de JC. Marco, Despoina, Pierre et Deeya. JC, merci à toi pour les encouragements et ton aide pendant ces 4 ans.

LA CLEEEEEEEEE !!!!! Même si cela te rendait folle, cela t'a fait aussi bien rire. Merci Mimi pour ta bonne humeur et courage pour la suite.

Merci à mon ami François pour cette grenadine de café pur sucre gracieusement offerte. Merci d'être devenu un si bon ami ces dernières années. J'espère que l'on va continuer ces petites séances de squash (les balles dans ma gueule en moins) ainsi que le sport et la bonne bouffe (parce que oui, la liste des restos que l'on doit gouter s'allonge de plus en plus ;)). Fatcha ti, je ne pouvais pas oublier Vinciane (sexy, même sans sourcils). Toujours agréable d'avoir une personne avec un grand sourire chaque matin, alors Merci.

Je remercie le reste de l'équipe Viral Vectors, Manu et Alex R. Manu merci de m'avoir fait découvrir l'escalade (même si j'ai un peu abandonné mais je vais m'y remettre).

Alors Julien (c'est la seule partie des remerciements qui n'aura pas été corrigée donc il y aura probablement des fautes :p), Merci pour tes nombreuses invitations à des repas « petits fours », raclette, moules à Knokke (99% sont restées des invitations ;)). Merci d'avoir été mon collègue préféré avec qui j'ai pu rigoler énormément pendant ces années.

Merci au labo Viro, les voisins d'à côté. Cédric, merci pour ces petits matchs de tennis/squash partagés durant ces 4 ans. Merci à Catherine pour sa bonne humeur durant les temps de midi ainsi que l'organisation de barbecues/tartiflette. Merci également à Sylvie, Fatima et Marco.

Sans eux je n'aurais rien appris, merci aux anciens ; Cécile, Laura, Greg, Laurent, Cha T et Marielle. Sans vous cela n'aurait pas été la même chose alors merci.

Pour les petits nouveaux, Zahrat, Margaud, Alice (en espérant que tu réussisses le FRIA). Courage à vous, ce n'est que le commencement ;). Margaud (bonsoir…), merci d'avoir pris le temps pour cette table de matière qui m'a beaucoup énervé.

Alors Judit, parce que la petite enfant gâtée a besoin d'un paragraphe à elle toute seule :p Merci pour ta joie de vivre (parfois un peu trop, même beaucoup trop). Tu me manqueras quand même un minimum.

Pas simple de dompter le petit zébrafish, Merci à la team zebra (principalement Alice, Jordane et Anne-so) pour la bonne humeur dans ce sombre couloir du -2.

Simplement parce qu'on l'oublie souvent, un énorme merci à Fabienne pour ses chiques qui me font descendre chercher les colis.

Alors ils ont tenté de rester dans le labo mais n'y sont pas arrivé (à mon grand regret), je remercie Quentin et Géraldine (microbe). Quentin merci pour les invitations régulières à bouffer du gras ;).

C'est toujours un honneur d'être choisi comme parrain. Merci Renaud et Manon de m'avoir donné mon premier filleul, Elliot, et de m'avoir encouragé tout le long de ma thèse.

Je termine en remerciant ma maman, mon papa et mes 3 sœurs (et les beaufs). Merci de m'avoir permis de faire ces études et de les avoir financées (même si parmi vous 5 je ne suis pas certain que vous sauriez me dire exactement ce que j'ai étudié).

Après 4 années, cette thèse se termine et marque le début d'une nouvelle aventure (cette phrase est d'un cliché…) Au fil de ces 4 années, j'ai rencontré de nombreux collègues qui, pour certains, sont devenus de véritables amis que je tiens à garder. J'espère vous revoir tous très vite ;).

List of abbreviations

ADF	Actin depolymerization factor
ADP	Adenosine diphosphate
AJ	Adherens junction
Arp2/3	Actin-related protein 2/3
ATP	Adenosine triphosphate
Btk	Bruton tyrosine kinase
CAM	Ca2+ activation calmodulin
cAMP	Cyclic adenosine monophosphate
cDNA	complementary DNA
Cdc42	Cell division control protein 42 homolog
CVP	Caudal vein plexus
DA	Dorsal aorta
DAG	Diacylglycerol
DH	Dbl homology
DLAV	Dorsal longitudinal anastomotic vessel
Dll4	Delta-like4
DNA	Deoxyribonucleic acid
Dpf	Days post-fertilization
EBM	Endothelial basal medium
EC	Endothelial cell
ECM	Extracellular matrix
EDG1	Endothelial differentiation gene 1
EGF	Epidermal growth factor
EGFR	Epidermal growth factor receptor
EGTA	Ethylene glycol tetraacetic acid
ERK	Extracellular signal-related kinase
ESAM	Endothelial selective adhesion molecule
FA	Focal adhesion

FAJ	Focal adherens jonction
FAK	Focal adhesion kinase
FB	Fibrillar adhesion
FBS	Fetal bovine serum
FGF	Fibroblast growth factor
FGFR	Fibroblast growth factor receptor
FH	Formin homology
FITC	Fluorescein isothiocyanate
FX	Focal complex
GAP	GTPase activating protein
GAPDH	Glyceraldehyde-3-phosphate dehydrogenase
GDP	Guanine diphosphate
GDI	Guanine nucleotide dissociation inhibitor
GEF	Guanine nucleotide exchanger factor
GFP	Green fluorescent protein
GTP	Guanine triphosphate
HB-EGF	Heparin-binding EGF like growth factor
HBVP	Human brain vascular pericyte
HDMEC	Human dermal microvascular endothelial cell
HeLa	Henrietta Lacks
HIF	Hypoxia inducible factor
HMEC	Human microvascular endothelial cell
Hpf	Hours post-fertilization
HUVEC	Human umbilical vein endothelial cell
IP3	Inositol trisphosphate
IP4	Inositol tetraphosphate
IQ	Calmodulin-binding motif
ISV	intersegmental vessel
JAM	Junctional adhesion molecule
MAPK	Mitogen-activated protein kinase

MC	Mural cell
MCL	Myosin light chain
MCLK	Myosin light chain kinase
mDia	mammalian diaphanous
MMP	Matrix metalloproteinase
mRNA	Messenger RNA
NGF	Nerve growth factor
PAI1	Plasminogen activator inhibitor 1
PAK	P21-activated kinase
PCV	Posterior cardinal vein
PDGF	Platelet-derived growth factor
PECAM	Platelet endothelial cell adhesion molecules
PH	Pleckstrin homology
PI3K	Phosphatidylinositol-3-kinase
PIP2	Phosphatidylinositol (4,5) bisphosphate
PIP3	Phosphatidylinositol (3,4,5) trisphosphate
PKC	Protein kinase C
PLC	Phospholipase C
PTU	1-phenyl-2 thiourea
qRT-PCR	Quantitative reverse transcription polymerase chain reaction
RAC1	Ras-related C3 botulinum toxin substrate 1
RAP1	Ras-related protein 1
RAS	Rat sarcoma
RASA2	Ras p21 protein activator 2
RASA3	Ras p21 protein activator 3
RASA4	Ras p21 protein activator 4
RASAL	Ras p21 protein activator like
REM	Ras exchange motif
RhoA	Ras homolog gene family member A

RNA	Ribonucleic acid
ROCK	Rho-associated protein kinase
RU	Relative Units
S1P	Sphingosine-1-phosphate
Scat	Severe combined anemia and thrombocytopenia
SCID	Severe combined immune deficient
SH2	Src homology domain 2
SH3	Scr homology domain 3
siRNA	small-interfering RNA
SIV	Sub-intestinal vessel
TGF	Transforming growth factor
TJ	Tight junction
TNFα	Tumor necrosis factor alpha
VEGF	Vascular endothelial growth factor
VEGFR	Vascular endothelial growth factor receptor
VE-PTP	Vascular endothelial protein tyrosine phosphatase
VVO	Vesiculo vacuolar organelle
WASP	Wiskott-Aldrich syndrome protein
WAVE	WASP-family verprolin-homologous protein
WH	WASP homology

Table of contents

Introduction

1. Vascular Development

The cardiovascular system is the first functional organ that is formed in the vertebrate embryo. It plays a crucial role by providing nutrients and oxygen to different organs and by evacuating metabolic wastes. The formation of this huge and complex network of blood vessels requires two distinct mechanisms, called vasculogenesis and angiogenesis. The vascular system consists of blood vessels (arteries, veins, arterioles, venules and capillaries) and lymphatic vessels. The blood vascular system transports blood (containing oxygen, metabolites and carbon dioxide) from the heart into the tissues of different organs where exchanges occur and brings it back to the heart. On the other hand, the lymphatic system plays a crucial role in immunity and drains the lymph (interstitial liquid) from tissues, allowing organs' detoxification. Small blood vessels consist of a monolayer of endothelial cells, associated sometimes with pericytes, and surrounded by a basal membrane. Larger vessels contain additional layers (muscular smooth cells) in order to resist higher pressure [1–6].

1.1. Vasculogenesis

During the first steps of embryogenesis, oxygen and nutrients required for growth diffuse passively. Rapidly however, with expansion of the embryo, passive diffusion is unable to meet the needs for correct development of embryos, leading to the formation of a primitive vascular network by vasculogenesis. This mechanism (vasculogenesis) is the process by which *de novo* vessels are formed [4,5].

Endothelial and blood cells share a common precursor: hemangioblasts derived from mesoderm. Hemangioblasts are precursors of angioblasts and hematopoietic cells, which differentiate respectively into endothelial cells and blood cells. Once hemangioblasts differentiate into angioblasts,

they migrate and coalesce, giving rise to the first blood vessels. The early vessels are formed in two distinct places: in the yolk sac (extraembryonic) and in the embryo (intraembryonic) [4,7,8].

Extraembryonic vessel formation is the first sign of vascular system formation (**Figure 1**). Cells derived from mesoderm (hemangioblastes) migrate, aggregate and form clusters called blood islands. Cells found at the cell periphery of blood islands (angioblasts) later differentiate into endothelial cells forming the endothelium while the cells found in the center later differentiate into hematopoietic cells. The aggregation of blood islands results in the formation of the primitive vascular network necessary for providing oxygen and nutrients to the embryo. Once formed, the primitive vascular network is further developed by angiogenesis [4,9–11].

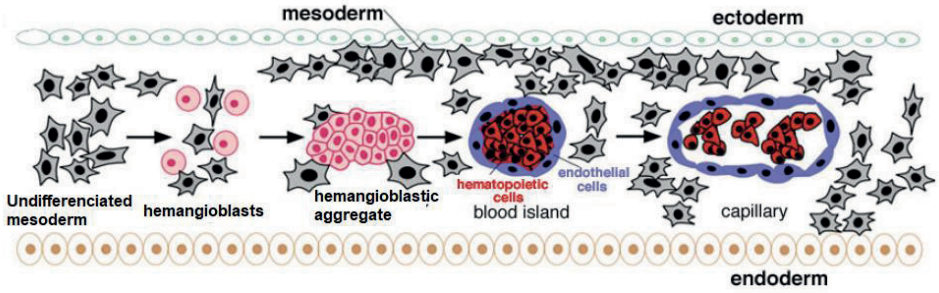

Figure 1: Illustration of vascular development by vasculogenesis. The process by which new vessels are formed *de novo* is called vasculogenesis. Undifferentiated mesoderm cells differentiate into hemangioblasts which aggregate into blood islands. The layer of cells found at the periphery of blood islands (angioblasts) give rise to endothelial cells while the core cells of blood islands differentiate into blood cells. Blood islands then aggregate and finally form the primitive vascular network (Adapted from [10]).

In intraembryonic vessel formation, in contrast to blood island development, angioblasts migrate individually then coalesce to form the pair of dorsal aortae and the cardinal vein in the absence of hematopoiesis. The extra- and intraembryonic vasculatures connect while the embryo is still able to obtain oxygen and nutrients by passive diffusion [8,9,12].

The formation of early vessels is rapidly followed by their differentiation into arteries and veins (arteriovenous differentiation) induced by blood flow. Arteriovenous differentiation is a crucial process that has long been considered to be induced by blood circulation. However, it has been shown that endothelial cells from blood islands express some arterial markers before blood flow begins [13–15].

Many regulators of developmental vasculogenesis have been identified throughout the years. Fibroblast growth factors (FGFs), in particular FGF2, are implicated in the induction of angioblasts from the mesoderm. In addition, the Indian hedgehog protein (Ihh) of the hedgehog family is required for correct blood island formation. Although its exact role is still unknown, the transforming growth factor-β (TGF-β) has also been shown to be necessary during vasculogenesis. The master regulators of vasculogenesis are the vascular endothelial growth factor (VEGF) and the angiopoietins. Indeed, VEGF-A and its receptors VEGFR-1 and VEGFR-2 are expressed very early during embryonic development. VEGF-A and VEGFR-2 are both expressed in blood islands [9,11]. In the past, the formation of new vessels in adults was principally attributed to angiogenesis. However, different studies have demonstrated that vasculogenesis also occurs in adults and requires circulating endothelial progenitor cells, though the mechanism is still unclear [8].

1.2. Angiogenesis

Angiogenesis is defined as the process by which new blood vessels are formed from pre-existing ones. The primitive plexus formed by vasculogenesis is remodeled by angiogenesis, leading to the formation of a complex and functional vascular network. Angiogenesis plays a crucial role in embryonic development but also in adults, where it can be induced during wound healing and the menstrual cycle. Finally, angiogenenic processes are also required during the development of tumors and in some pathologies such as rheumatoid polyarthritis [1,3,9,16]

Three types of angiogenesis have been observed: sprouting angiogenesis, intussusceptive angiogenesis and looping angiogenesis [17].

a. Sprouting angiogenesis

Sprouting angiogenesis is the most common angiogenesis process observed during embryonic development and tumor growth. This process can be divided into different phases (**Figure 2**). First, vessels are in a quiescent state in the absence of pro-angiogenic stimuli. Once pro-angiogenic signals increase, endothelial cells lose their cell-cell junctions and proteases degrade the surrounding extracellular matrix (ECM). Then, endothelial cells initiate the formation of the new vessels in the direction of pro-angiogenic signals. Once in contact with other vessels, the newly formed vessels fuse by anastomosis and are stabilized and matured by the deposition of a new ECM and by the recruitment of pericytes. The stabilization of the new vessels is followed by a return to the quiescent endothelial cell state. The molecular and cellular mechanisms regulating sprouting angiogenesis will be described in a following section [3,5,9,16,18–20].

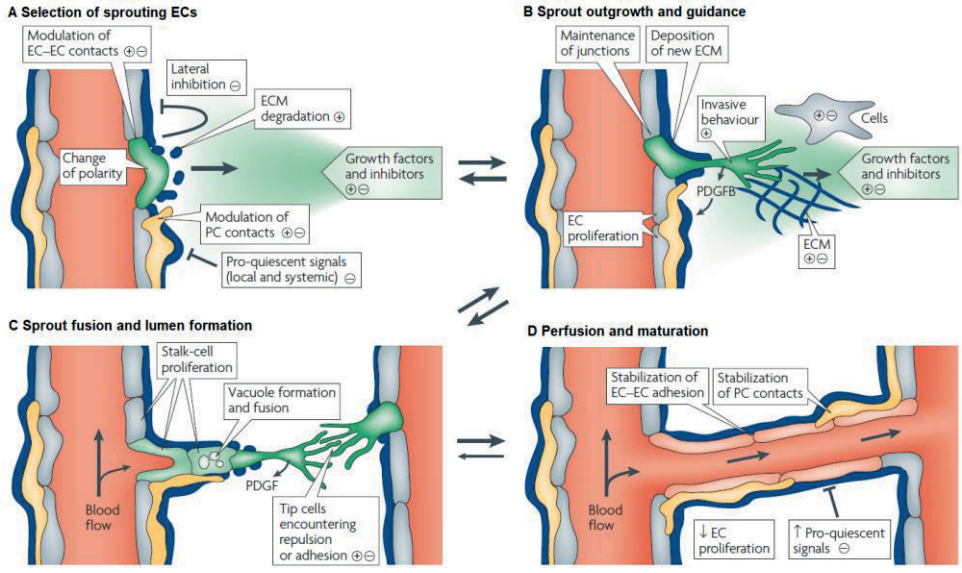

Figure 2: Illustration of sprouting angiogenesis mechanism. In the absence of stimuli, endothelial cells are maintained in a quiescent state. (**A**) Increases in pro-angiogenic factors such as VEGF-A induce angiogenesis. Some endothelial cells (in green) can sprout, becoming motile and invasive. The sprouting requires the disassembly of cell-cell junctions and the degradation of the extracellular-matrix (ECM). (**B**) The new vessel is guided by a VEGF gradient. Production of PDGFβ by the tip cells (in green) results in the recruitment of pericytes along the new vessel. (**C**) Once the tip cell of the new vessel encounters another tip cell, the vessels fuse by anastomosis while the lumen forms. (**D**) The EC-EC junctions and EC-pericyte junctions are stabilized, allowing establishment of a continuous lumen. Cells then return to a quiescent state and blood flow brings oxygen and reduces pro-angiogenic signals (Adapted from [18]).

b. Intussusceptive angiogenesis

Intussusceptive angiogenesis is the process by which new capillaries are formed by the longitudinal division of one capillary into two new functional capillaries. Compared to sprouting angiogenesis, intussusceptive

angiogenesis is a rapid process and does not require the proliferation of endothelial cells or VEGF signaling. Though little is known about its regulation, intussusceptive angiogenesis can be divided into different phases (**Figure 3**). First, endothelial cells from opposite sides of the capillary wall migrate to the center of the lumen forming the "interendothelial transluminal bridge". Then the cells rearrange themselves, inducing perfusion inside the capillary and forming structures called pillars, which are covered by pericytes and a basal membrane. Finally, once the pillar is formed and stabilized it can orient endothelial cells, allowing pillar elongation and continuing the division of the new vessel [16,21,22].

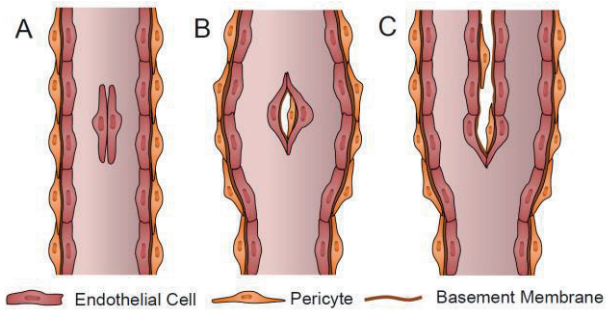

Figure 3: Illustration of intussusceptive angiogenesis. (**A**) Endothelial cells from opposite sides of the capillary migrate centripetally in the lumen. (B) These endothelial cells assemble into structures called pillars after induction of a protrusion in the capillary. (C) Stabilized pillars can orient and elongate endothelial cells leading to the division of the new vessel (Adapted from [16]).

c. Looping angiogenesis

Looping angiogenesis (**Figure 4**), which is independent of VEGF signaling, is a rapid process observed during wound healing that requires the remodeling and contraction of the extracellular matrix (ECM) by myofibroblasts. This remodeling of ECM induces tension that drags vessels

from the surrounding vascularized area into the remodeling area (or avascular region). The new vessels dragged into the avascular region can then elongate using other angiogenic processes [16,23,24].

Figure 4: Illustration of looping angiogenesis. Fibroblasts migrate and differentiate into myofibroblasts (Black) in the ECM around a vascularized region. Myofibroblast contraction induces tension inside of the remodeling area, resulting in the translocation of the surrounding vessels into the avascular region (Adapted from [17]).

1.3. Sprouting angiogenesis: molecular and cellular mechanisms

1.3.1. Induction of sprouting angiogenesis

At the beginning of embryonic development, oxygen and nutrients are assimilated by the embryo via passive diffusion. As the embryo grows, the eventual decrease in oxygen supply results in the stabilization of the transcription factor HIF-α (hypoxia inducible factor), leading to the transcription of its target genes. Among these genes is VEGF-A, the master regulator of angiogenic processes. The VEGF (vascular endothelial growth factor) family consists of 5 secreted growth factors; VEGF-A, -B, -C, -D and the placental growth factor (PGF), that bind 3 tyrosine kinase membrane receptors: VEGFR-1, -2 and -3. The following section will focus on VEGF-A and its receptors, VEGFR1 and VEGFR2 [9,11,18,19].

VEGF-A can bind both VEGFR-1 and VEGFR-2 receptors, but with higher affinity to VEGFR-1. However, sprouting angiogenesis is mediated by the kinase activity of the VEGFR-2 receptor after the binding of VEGF-A. Indeed, the VEGFR-1 receptor displays weak kinase activity that counteracts pro-angiogenic signaling. Moreover, VEGFR-1 can also be found as a soluble receptor, VEGFR1s, that sequesters VEGF-A in the extracellular medium and prevents its association with VEGFR-2, resulting in a decrease in pro-angiogenic signals [9,19,20,25].

The angiopoietins (Ang1 and Ang2) are soluble factors that bind the Tie2 receptor expressed by endothelial cells. Ang1 is produced by pericytes or vascular smooth muscle cells. The binding of Ang1 to Tie2 results in the maintenance of vascular quiescence. However, Ang2 acts as an antagonist to Ang1/Tie2 signaling. Indeed, Ang2 is produced by endothelial cells and its expression is activated by VEGF-A. Binding of Ang2 to the Tie2 receptor is implicated in removing cells from quiescence, inducing sprouting and the migration of endothelial cells [9,11,25–27]. Fibroblast growth factors (FGF1, FGF2 and FGF4) bind to FGF receptors (FGFR1 and FGFR2), lead to endothelial cell proliferation and activate matrix metalloproteinases (MMPs) that are required for extracellular matrix degradation [25].

A critical step initiating sprouting angiogenesis is the detachment of mural cells (pericytes and vascular smooth muscle cells) from endothelial cells and the degradation of the extracellular matrix by MMPs. The binding of Ang2 to its receptor Tie2 has been shown to participate in the detachment of pericytes. The detachment of mural cells allows the expression of MT-MMP1, leading to ECM degradation [25,28,29].

1.3.2. Mechanism of tip cell and stalk cell selection

Once pro-angiogenic signals are detected, endothelial cells specialize into tip cells, stalk cells and phalanx cells (**Figure 5**).

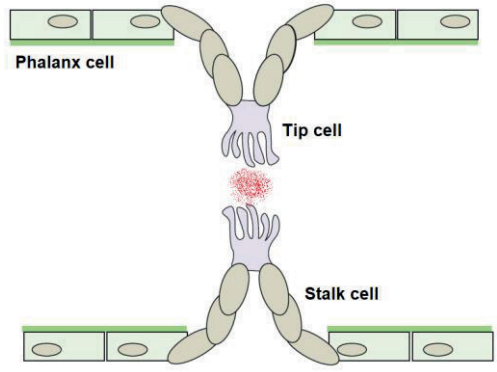

Figure 5: Specialization of endothelial cells during sprouting angiogenesis. Pro-angiogenic signals (red) induce specialization of endothelial cells. Tip cells (violet) have many filopodia and guide the new vessel towards the growth factors. Stalk cells (adjacent to tip cells) are proliferative cells that extend the new vessel. Phalanx cells stay quiescent in the origin vessel (Adpated from [20]).

The tip cells are mobile cells that lead the neovessel towards the growth factors. They are characterized by the presence of many filipodia and do not display proliferative capacities. The stalk cells, directly adjacent to the tip cells, allow the extension of the new vessel. Unlike tip cells, stalk cells have few filopodia, proliferate, maintain their EC-EC junctions and have a lumen. Finally, phalanx cells are cells that remain in a quiescent state in the origin vessel [3,5,18–20].

The main signaling pathways implicated in tip and stalk cell selection during sprouting angiogenesis are the VEGF and Notch signaling pathways (**Figure 6**).

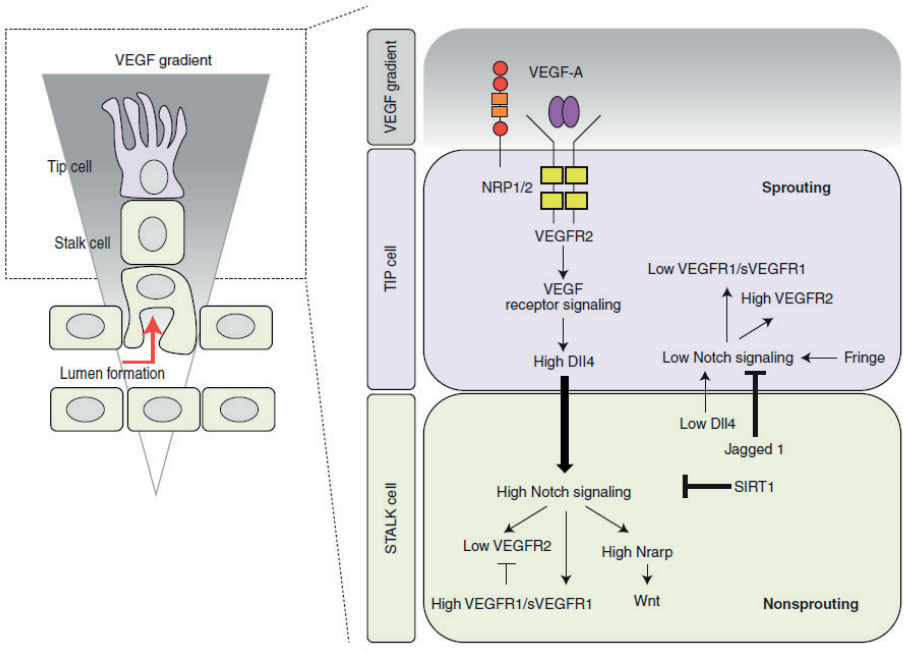

Figure 6: Selection of tip and stalk cells during sprouting angiogenesis. Activation of the VEGF signaling pathway leads to the overexpression of Dll4 ligand by tip cells. Binding of Dll4 with Notch receptors activates Notch signaling pathways in stalk cells resulting in inhibition of VEGR-2 expression and promoting expression of VEGF-R1. Activation of Notch signaling in stalk cells allows inhibition of the tip cell phenotype in these cells. Overexpression of Jagged 1 by stalk cells inhibits Notch signaling in the tip cells [20].

A high concentration of VEGF-A induces tip cell formation. Indeed, VEGF-A binds its receptor VEGFR2 (expressed by quiescent endothelial cells), which leads to the activation of downstream signaling pathways and results in filopodia extension and ECM degradation. VEGF signaling is reinforced

in tip cells by the overexpression of Neuropilin-1 (NRP1) which acts as a receptor for VEGF ligands. The interaction of VEGF-A with VEGFR2 induces high expression of the Notch ligand Dll4 in tip cells. In turn, Dll4 ligand activates Notch signaling in adjacent cells (stalk cells) inhibiting the tip cell phenotype in these cells. Indeed, binding of Dll4 to Notch leads to the cleavage of its NICD (Notch Intracellular Domain), resulting in inhibition of VEGFR-2 expression and promoting VEGFR-1 expression. VEGFR-1 (membrane and soluble) in stalk cells decreases VEGF signaling by sequestering VEGF-A, preventing its interaction with VEGFR2 [3,5,9,16,18,19,25,30].

Moreover, stalk cells overexpress Jagged 1, another Notch ligand, in order to maintain activation of Notch in stalk cells and inactivation of Notch in tip cells. Indeed, Jagged 1 competes with the Dll4 expressed by stalk cells, inhibiting Dll4/Notch signaling in tip cells due to the weak activation of Notch resulting from Jagged1/Notch interactions [19,20,30].

For long, angiogenic sprouting was considered as a static process with a single tip cell leading the growing vessel. However, it has been shown recently (in mice and zebrafish) that tip cell/stalk cell phenotypes are not irreversible and that endothelial cells can exchange at the tip position [31,32].

1.3.3. Lumen formation

During angiogenesis, while the new vessel migrates and elongates towards angiogenic signals, it generates a vascular lumen in order to support blood flow. Three mechanisms have been proposed for lumen formation: cell hollowing, cord hollowing and plasma membrane invagination (**Figure 7**).

The first mechanism, cell hollowing (**Figure 7 top**), is based on the fusion of small intracellular vacuoles into larger vacuoles that from a central lumen

in the endothelial cell. Then, these central lumina are connected to the lumina of adjacent endothelial cells. [33–36].

The second mechanism, cord hollowing (**Figure 7 middle**), consists of flattening endothelial cells by creating an extracellular space between them. This mechanism requires rearrangements of cellular junctions and deadhesive proteins. VE-cadherin promotes interactions between endothelial cells [33,34,36].

Moreover, endothelial cells express N-cadherin which increases the VE-cadherin quantity at EC-EC junctions. PODXL, a glycoprotein of the CD34 sialomucin family that is localized in vesicles is released by exocytosis at cell-cell contacts by a VE-cadherin dependent mechanism.

The presence of PODXL at cell-cell junctions results in the translocation of VE-cadherin at the cell border. Moreover, the negative charge of PODXL leads to a repulsion of the apical endothelial cell surfaces, creating a small space between them. F-actin is recruited to the apical cell surface bringing the necessary force to extend the lumen. The recruitment of F-actin is mediated by Moesin, which is phosphorylated by protein kinase C (PKC). Finally, VEGF-A activates the ROCK pathway, which is necessary for the localization of non-muscle myosin II to the apical cell surface where F-actin is enriched, thus allowing correct vascular lumen formation [34,38,39].

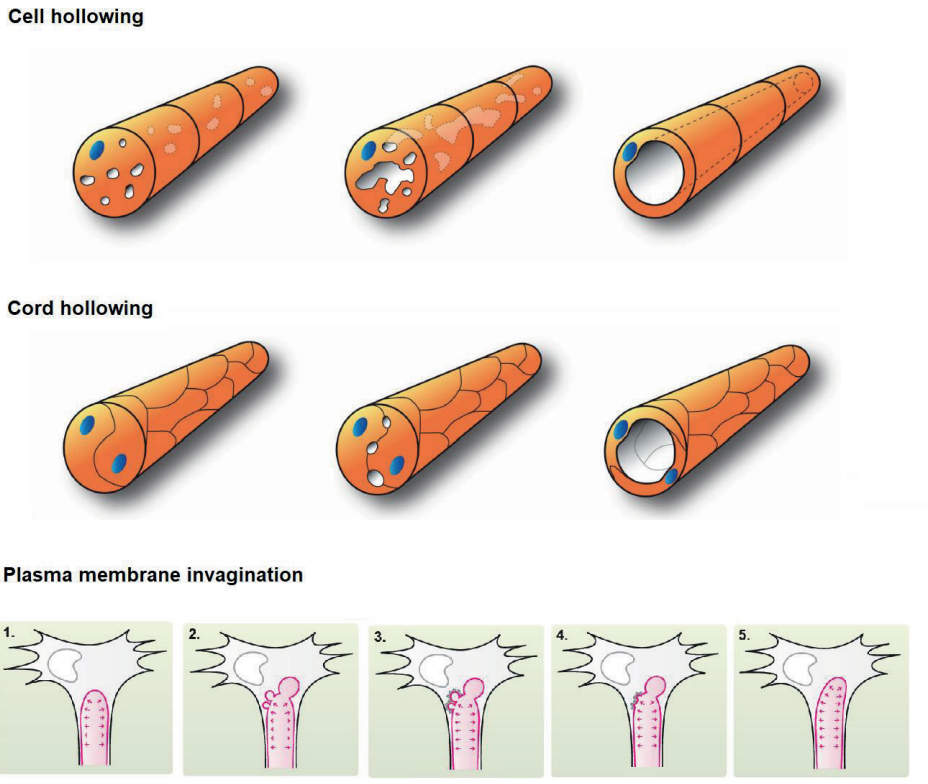

Figure 7: Different models of vascular lumen formation. ***Cell hollowing***: fusion of intracellular vacuoles allowing lumen formation. ***Cord hollowing***: lumen formation resulting from rearrangement of EC-EC junctions creating a small space between endothelial cells. This process requires VE-cadherin, the glycoprotein PODXL, the recruitment of F-actin (by Moesin) and ROCK signaling (activated by VEGF-A). ***Plasma membrane invagination***: lumen expansion by invagination of the plasma membrane of endothelial cells (Adapted from [33,37]).

The third mechanism (**Figure 7 bottom**) was discovered more recently. In this mechanism, lumen formation results from invagination of the apical membrane of tip cells during sprouting angiogenesis. These invaginations are protrusions of the plasma membrane resulting from modification of

cytoskeleton composition. The protrusions, called invert blebbing, display inverted polarity with the apical membrane, which projects into the cell body instead of outside. This process requires haemodynamic forces and actomyosin contraction for lumen expansion. Previous studies suggested that the cell hollowing mechanism was observed during ISV formation in zebrafish. However, a recent study showed that ISV in zebrafish were lumenized via plasma membrane invagination [37].

A fourth mechanism has also been identified, called cavitation. This process requires death by apoptosis of cells from the center of a multicellular structure. The hollow space left allows lumen formation [40]. However, no evidence of this process has been found during zebrafish development [35].

1.3.4. Vessel maturation

The maturation of blood vessels involves the recruitment of mural cells (MC) (pericytes and vascular smooth muscle cells) and the deposition of the extracellular matrix. The recruitment of mural cells is mediated by four different pathways: PDGF-β, Ang1, S1P and TGF-β1 (**Figure 8**) [41].

The PDGF-β/PDGFR-β signaling pathway is crucial for the recruitment of mural cells along the new vessels. During sprouting angiogenesis, tip cells secrete PDGF-β that binds PDGFR-β receptor expressed on mural cells, leading to the proliferation and migration of mural cells [3,5,13,25,41,42].

Once mural cells are recruited along new vessels, they produce Ang1 that binds to Tie2 receptors, inducing the quiescence phenotype. The Ang1/Tie1 interactions stabilize new vessels by promoting MC-EC and ECM-EC interactions. Moreover, binding of Ang1 induces expression of HB-EGF in endothelial cells, which promotes mural cell migration after

binding to epidermal growth factor receptors (EGFRs) expressed by mural cells [3,13,41–43].

EDG1 receptor, expressed by mural cells and endothelial cells, binds sphingosine-1-phosphate (S1P). Activation of S1P/EDG1 signaling in endothelial cells increases the production of ECM proteins, facilitating mural cell recruitment. Moreover, endothelial S1P/EDG1 signaling promotes vessel stability by establishing EC-MC junctions via N-cadherin. Additionally, activation of S1P/EDG1 signaling in mural cells facilitates their migration around the new vessel [13,41,43].

The production of TGF-β1 by endothelial cells promotes activation of the TGF-β1/ALK5 pathway on mural cells, leading to vessel stabilization by stimulating the production of ECM proteins and plasminogen activator inhibitor 1 (PAI1). PAI1 acts by preventing degradation of the extracellular matrix. Moreover the activation of this pathway also leads to the differentiation of mesenchymal cells into mural cells [5,13,25,41–43].

Finally, EC/MC interactions promote the production of inhibitors of metalloproteinases (TIMP2/TIMP3) leading to further stabilization of the ECM [44].

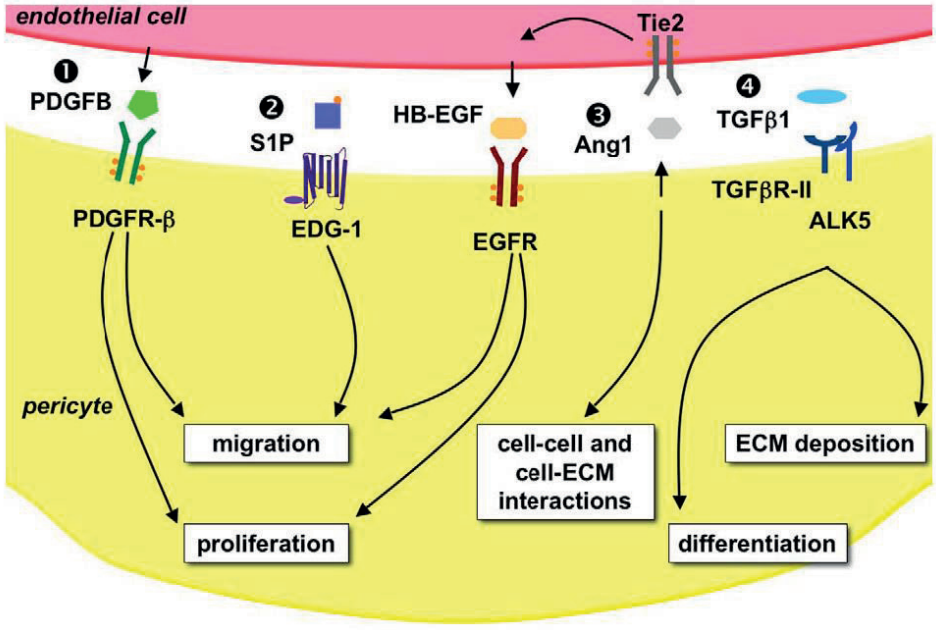

Figure 8: Different signaling pathways between endothelial cells and mural cells implicated in vessel maturation. **(1)** and **(2)** PDGFβ and S1P produced by endothelial cells bind PDGFR-β and EDG-1 respectively, promoting their differentiation and migration. **(3)** Ang1/Tie2 interactions mediate vessel stability by increasing MC-EC and EC-ECM adhesions. Production of HB-EGF resulting from Ang1/Tie2 activation leads to migration and proliferation of mural cells **(4)** TGFβ1/ALK5 pathway stimulates ECM deposition and mesenchymal cell differentiation [41].

2. Vascular permeability

The endothelium constitutes a semi-permeable physical barrier that allows the exchange of proteins, cells and fluids between the blood and the interstitial space. The crucial role of the endothelial barrier is to maintain vascular homeostasis. It also regulates different processes such as angiogenesis and response to inflammation. For example, during sprouting angiogenesis, EC-EC junctions are remodeled allowing migration of endothelial cells and initiation of sprouting. Obviously, alterations of the endothelium barrier have critical consequences for the organism [45,46].

The transport through the endothelial barrier of macromolecules, fluids and cells is effected either by transcellular (through endothelial cells) or paracellular (between endothelial cells) pathways (**Figure 9**).

The transcellular pathways transport macromolecules such as albumin across the endothelium by vesicular trafficking. These pathways include caveolae, vesiculo-vacuolar organelles (VVO) and fenestrations. Caveolae are invaginations of the plasma membrane that form vesicles that can move through the cell. VVO are fused caveolae vesicles that form a channel allowing transport through a single cell. Finally, fenestrations are pinched regions of single cells that form pores allowing rapid exchanges. The paracellular pathway is mediated by the opening and closing of endothelial cell junctions [46–51].

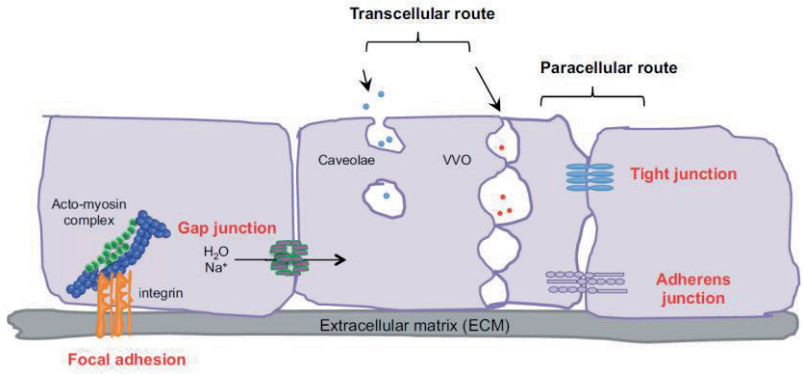

Figure 9: Transcellular and paracellular pathways in endothelial cells. Transport of cells and macromolecules through endothelial cells can occur either by transcellular or paracellular pathways [47].

The endothelium arises from the association of endothelial cells by junctional structures into a monolayer. Although for a long time cell-cell junctions were considered only as the attachment sites of endothelial cells, it is now recognized that endothelial junctions have not only an architectural role but also can control vascular permeability, transmit intracellular signals and limit cell growth [45].

2.1. Molecular organization of endothelial junctions

Two major types of junctions are found in endothelial cells and are named tight junctions (TJs) and adherens junctions (AJs). Other adhesion molecules such as PECAM-1 and nectins are also found in the junctional complex. Moreover, in addition to cell-cell adhesion, GAP junctions form channels between endothelial cells that transport water and ions (**Figure 10**) [45,52–54].

Tight junctions result from the association of different adhesive proteins including claudins, occludins, and ZO proteins. Claudins and occludins are

transmembrane proteins that mediate homophilic interactions with adjacent endothelial cells and ZO-proteins are responsible for connecting claudins and occludins to the actin cytoskeleton. Junctional adhesion molecules (JAMs) and endothelial selective adhesion molecule (ESAMs) associate with TJs and regulate leukocyte transendothelial migration [45,52,55].

Endothelial cells also express platelet endothelial cell adhesion molecule (PECAM), a member of the immunoglobulin family that regulates endothelial junctional integrity via homophilic interactions [56].

Nectin is a member of the immunoglobulin family and associates with both AJs and TJs by mediating homophilic interactions. Nectin binds its intracellular partner afadin, which in turn connects the junction to the actin cytoskeleton. The nectin/afadin complex has been shown to be required for adherens junction formation [53,55].

Adherens junctions constitute about 80% of the total junctions in endothelial cells. Vascular endothelial cadherin (VE-cadherin) is the major component of adherens junctions and its expression is restricted to endothelial cells. VE-cadherin is a transmembrane glycoprotein composed of five extracellular domains that are binding sites for calcium and a cytoplasmic tail that interacts with intracellular partners allowing connection to the actin cytoskeleton. VE-cadherin holds endothelial cells together by interacting with dimers of VE-cadherin expressed on adjacent endothelial cells and providing strong contacts between endothelial cells. Dimerization of VE-cadherin requires the binding of calcium. VE-cadherin interacts via its cytoplasmic tail with the AJ proteins p120 catenin, β-catenin and plakoglobin. The intracellular partners β-catenin and plakoglobin constitute a bridge between VE-cadherin/p120 catenin and the actin cytoskeleton by linking to actin-binding proteins such as α-actinin, vinculin or eplin [45,52,57,58].

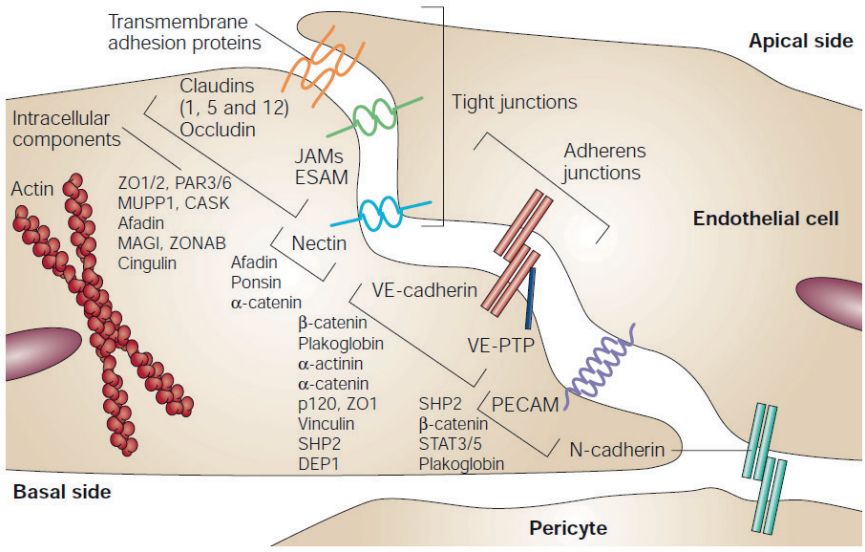

Figure 10: Molecular organization of endothelial junctions. The different endothelial junctions consist of transmembrane adhesion proteins associated with their intracellular partners. Claudins, occludins, junctional adhesion molecules (JAMs) and endothelial cell selective adhesion molecules (ESAMs) compose the tight junctions (TJs). ZO1/2 are intracellular components of TJs that make connections with the actin cytoskeleton. The main adhesive protein of adherens junctions (AJs) is vascular endothelial cadherin (VE-cadherin). VE-cadherin is associated with intracellular partners such as p120, β-catenin and plakogkobin, which constitute a bridge to the actin cytoskeleton by linking to actin-binding proteins such as α-actinin, vinculin or eplin. Nectin, a member of the immunoglobulin family, associates with both TJs and AJs. Nectin links to its intracellular partner afadin, allowing connection to the actin cytoskeleton. Another member of the immunoglobulin family, platelet endothelial cell adhesion molecule (PECAM), is expressed by endothelial cells. PECAM is not associated with TJs or AJs and is implicated in the regulation of endothelial junctional integrity. VE-Cadherin is not the only cadherin expressed by endothelial cells. Neuronal cadherin (N-cadherin) is not found at AJs and mediates heterotypic interactions between endothelial cells and pericytes (Adapted from [45]).

The importance of AJs as compared to TJs has been assessed using mice with null mutations in different endothelial junction components. VE-cadherin$^{-/-}$ and β-catenin$^{-/-}$ genotypes are embryonic lethal in mice. VE-cadherin$^{-/-}$ mice showed large hemorrhages resulting from alterations in vessel formation. B-catenin$^{-/-}$ mice displayed irregular lumina and hemorrhages. Analysis of endothelial junctions in these mice revealed weaker adherens junctions. Null mutations of claudin-5, occludin and PECAM in mice do not lead to embryonic lethality. In these cases no vascular defects have been reported. These results illustrate that AJs are crucial for the maintenance of the endothelial barrier integrity [45].

Besides VE-cadherin, endothelial cells also express another cadherin: neuronal cadherin (N-cadherin), which mediates heterotypic interactions between endothelial cells and pericytes and will be described in a following section.

In this thesis we initially focus our attention on adherens junctions, and more precisely on VE-cadherin. Later focus is on VE-cadherin and the mechanisms that regulate this protein.

2.2. VE-cadherin in vascular permeability

Different mechanisms regulate vascular permeability by opening endothelial cell contacts. These mechanisms include the dissociation of the cadherin-catenin complex due to tyrosine phosphorylation, the disconnection of cadherin-catenin complex from the actin cytoskeleton and finally endocytosis of VE-cadherin (**Figure 11**).

a. Dissociation of the VE-cadherin/p120 catenin complex by tyrosine phosphorylation

The cytoplasmic tail of VE-cadherin can be phosphorylated on different tyrosine and serine residues. Among these residues, Y645, Y658, Y685, Y731 and Y733 seem to be implicated in endothelium barrier integrity. Point mutation studies revealed that phosphorylation of Y658 and Y731 lead to destabilization of endothelial cell junctions. Moreover, phosphorylation of Y645, Y731 and Y733 are required for efficient leukocyte transmigration. It has been reported that Y685 phosphorylation is mediated by VEGF stimulation [59–63]. The binding of VE-cadherin to p120 prevents its internalization. However, activation of Src kinase (activation on Y416 and deactivation on Y527) in turn leads to phosphorylation of VE-cadherin on its Y658 residue. This phosphorylation induces the disruption of the VE-cadherin-p120 interaction and leads to VE-cadherin internalization [64,65].

Phosphatases also control vascular permeability. Vascular endothelial protein tyrosine phosphatase (VE-PTP) is a transmembrane protein that is associated with VE-cadherin. Blocking the dissociation of VE-cadherin/VE-PTP in mice inhibits increases in vascular permeability. Other phosphatases such as PP2A, SHP2 and PTP1 have been reported to stabilize EC junctions. These phosphatases maintain VE-cadherin in a non-phosphorylated state, which in turn increases the stability of cell-cell junctions and decreases endothelial permeability [45,63,65].

b. Disconnection of the VE-cadherin/p120 catenin complex from the actin cytoskeleton

The opening of endothelial contacts has been shown to be a consequence of disconnection of VE-cadherin from the actin cytoskeleton. Once activated after VEGF stimulation, FAK can interact with VE-cadherin and

phosphorylate β-catenin on Y412. This phosphorylation disrupts the interaction between VE-cadherin and β-catenin and leads to the opening of EC junctions. Moreover, phosphorylation of VE-cadherin on Y731 after VEGF stimulation also results in the dissociation of β-catenin. It has been shown that this residue can be phosphorylated by Src kinase [65].

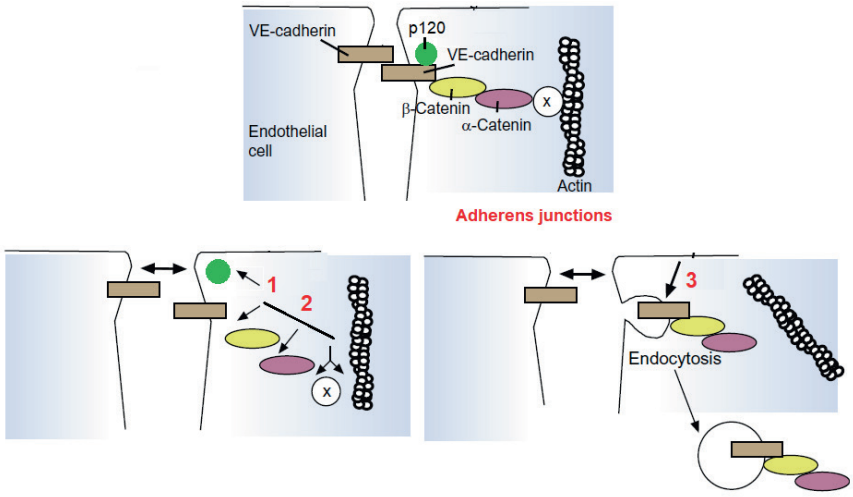

Figure 11: Mechanisms regulating the opening of endothelial cell contacts. (**1**) Dissociation of VE-cadherin/p120 catenin complex. (**2**) Disconnection of VE-cadherin/p120 catenin complex from actin cytoskeleton. (**3**) Endocytosis of VE-cadherin. These 3 mechanisms lead to the opening of endothelial cell junctions (Adapted from [65]).

c. Endocytosis of VE-cadherin

Finally, VE-cadherin can be internalized and degraded by endocytosis. Indeed, phosphorylation of VE-cadherin on S665 mediates the recruitment of β-arrestin-2, which in turn induces the internalization of VE-cadherin into clathrin-coated vesicles. After VEGF stimulation, Src is activated and phosphorylates VAV2, which activates Rac small GTPase. Rac-GTP

activates its downstream target, p21-activated kinase (PAK), which phosphorylates VE-cadherin on S665. The p120 binding site on VE-cadherin is localized near S665. Thus, p120 catenin might regulate endocytosis of VE-cadherin by preventing phosphorylation of S665 [62,63,65,66].

2.3. Regulation of vascular permeability by small GTPases

Different small GTPases have been implicated in the regulation of endothelial permeability. The small GTPases Rap1, Rac1 and Cdc42 are necessary for stabilization and maintenance of endothelial junctions while RhoA activation leads to increased permeability. However, Rac1 has also been identified as playing a role in destabilization of the endothelial barrier under certain conditions (**Figure 12**).

a. Under resting conditions

As previously mentioned, Rac1, Rap1 and Cdc42 are crucial for maintenance and stabilization of endothelial junctions. An increased level of cyclic AMP (cAMP) activates Epac, which in turns activates Rap1. Once activated, Rap1 acts in different ways to stabilize and maintain endothelial junctions. First of all, Rap1 leads to the activation of the small GTPases Rac1 and Cdc42 via activation of Vav2 and Tiam1. These two small GTPases promote cell-cell junction stabilization [55,66,67].

Moreover, activated Rap1 and Rac1 inhibit the activity of RhoA by activating ArhGAP29 and p190RhoGAP respectively, two inhibitors of RhoA. Activation of ArhGAP29 is mediated by Rasip1, a Rap1-effector. Krit1, a Rap1 effector, is recruited to VE-cadherin and mediates a decrease in RhoA activity in endothelial cells. Rap1/Krit interaction allows the indirect binding of Rap1 to adherens junctions. Rap1 can also be activated by PDZ-

GEF but the mechanism responsible for PDZ-GEF activation is still unclear. Rap1 increases stability by recruiting junctional proteins such as Afadin/AF6 to the junctions [55,66–69].

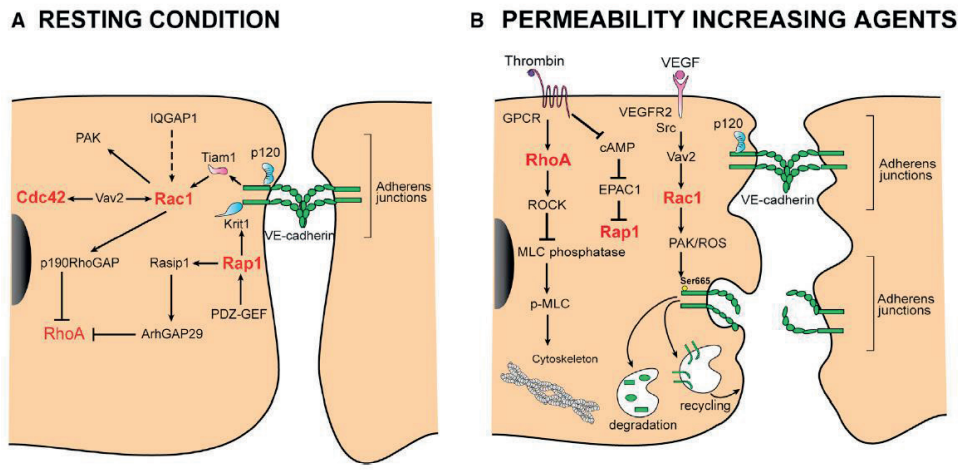

Figure 12: Regulation of vascular permeability by small GTPases. (**A**) Stabilization of the endothelial barrier is mediated by the small GTPases Rap1, Rac1 and Cdc42. Rap1 acts by activating Rac1 and Cdc42 through Tiam1 and Vav2. Rap1 and Rac1 stabilize endothelial junctions by inhibiting RhoA, resulting in a decrease of actomyosin contractility. (**B**) Different agents such as VEGF or thrombin increase vascular permeability by modulating the activity of small GTPases. Thrombin stimulation leads to activation and inactivation of RhoA and Rap1 respectively. VEGF increases permeability by activating Rac1, which leads to the internalization of VE-cadherin (Adapted from [66]).

b. Permeability increasing agents

Destabilization of the endothelial barrier is induced in response to different agents such as VEGF, thrombin, TNFα or EGTA. This destabilization results from the modulation of the activity of different small GTPases (RhoA, Rap1 and Rac1).

Following thrombin stimulation RhoA is activated, leading to the inhibition of MLC phosphatase and increasing MLC II phosphorylation and actomyosin contractility, thus destabilizing the endothelial barrier. Moreover, thrombin stimulation impairs cAMP signaling resulting in inactivation of Rap1 and Rac1; these in turn are able to inactivate RhoA small GTPase.

RhoA can also be activated after VEGF stimulation: this results in an increase of MLC II phosphorylation and actomyosin contractility. However, VEGF stimulation also activates Rac1 via Vav2. Activated Rac1 activates its downstream effector PAK1, which phosphorylates VE-cadherin on S665 resulting in internalization of VE-cadherin and an increase in endothelial permeability [55,66,67].

2.4. Neuronal cadherin (N-cadherin)

As mentioned previously, VE-cadherin is not the only cadherin expressed by endothelial cells. Unlike VE-cadherin, N-cadherin is not endothelial-specific and is also expressed by other cell types in the vasculature, such as pericytes and vascular smooth muscle cells. The importance of N-cadherin in vascular development was assessed by generating N-cadherin null mice (N-cadherin$^{-/-}$). Like VE-cadherin$^{-/-}$, the N-cadherin$^{-/-}$ genotype is embryonic lethal in mice (embryos die at mid-gestation). Specific inactivation of N-cadherin in endothelial cells showed that N-cadherin acts upstream of VE-cadherin. Indeed, reduced expression of VE-cadherin was found in N-cadherin$^{-/-}$ mice. However, another study lead to different results in HUVECs, in which inactivation of N-cadherin did not affect the expression of VE-cadherin [70–72].

The expression of VE-cadherin and N-cadherin seem to be comparable in endothelial cells. However, while VE-cadherin is localized in adherens junctions, N-cadherin is dispersed along the cell membrane [73].

N-cadherin and VE-cadherin have a similar structure and interact with the same intracellular partners. However, these two cadherins have different functions within the endothelium. While VE-cadherin mediates EC-EC junctions, N-cadherin seems to mediate heterotypic interactions between endothelial cells and pericytes. N-cadherin is crucial for the maturation and stabilization of blood vessels [74,75].

Compared to VE-cadherin, the mechanisms by which N-cadherin is regulated are much less studied. S1P (sphingosine-1-phosphate) has been identified as crucial for maturation of blood vessels. Indeed, impaired S1P signaling results in a mislocalization of N-cadherin within EC-pericyte junctions [76].

The recruitment of pericytes during vascular development occurs after mid-gestation. However, N-cadherin$^{-/-}$ mice die at mid-gestation, suggesting that N-cadherin might have another role in addition to the maturation of EC-pericyte junctions. It has been shown that as well as VE-cadherin, N-cadherin is able to inhibit cell growth and apoptosis. Only N-cadherin was found to induce cell motility [65,77].

3. Actin cytoskeleton: crucial for migration and adhesion

During sprouting angiogenesis, tip cells need to migrate towards the pro-angiogenic signal in order to form the new vessel. Migration is an important process that can be divided into different steps. First, cells sense stimuli and display protrusions at the leading edge resulting from actin polymerization. The attachment of these protrusions to the extracellular matrix forms focal adhesions (FAs) which are connected to stress fibers (F-actin). Then, the contraction of stress fibers generates tension to pull the cell body forward. Finally, cell migration requires the disassembly of FAs and stress fibers at the cell rear in order to move. A strict regulation of actin cytoskeleton dynamics is necessary for proper migration and adhesion of endothelial cells during angiogenesis [78–80].

Actin is the most abundant cytoskeleton protein in cells and can be found in two different states: the globular monomeric state of 43 kDa (G-actin) and the filamentous actin state (F-actin) resulting from assembly (polymerization) of G-actin monomers. The G-actin monomer contains three different domains: a barbed end (+ end), a central ATP/ADP binding domain and a pointed end (- end) [81].

The assembly of G-actin monomers leads to the formation of a polarized actin filament. Actin polymerization is a process that can be divided into three phases (**Figure 13**). The first one, nucleation, consists of the assembly of three monomers into a trimer via an ATP-dependent mechanism. The second phase, elongation, consists of preferential incorporation of G-actin monomers at the barbed end of the nascent filament, allowing actin filament growth. Finally the third phase, called

steady-state, occurs when the addition of G-actin-ATP to the barbed end equals the dissociation of G-actin-ADP from the pointed end [81,82].

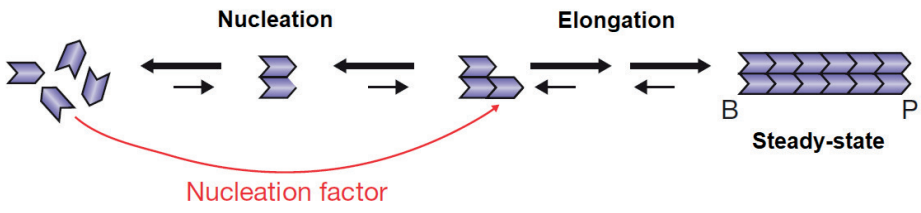

Figure 13: Actin filament polymerization. Nucleation allows association of G-actin monomers into a G-actin trimer by nucleation factors. Once nucleated, the actin filament is elongated by addition of G-actin monomers to the barbed end (B) until reaching a steady-state where association and dissociation of actin monomers to the barbed and pointed ends respectively are equal (Adapted from [82]).

Because spontaneous association of G-actin monomers is instable and slow, initiation of actin polymerization requires nucleation factors. Three classes of actin nucleation factors have been identified: the Arp2/3 complex, spir proteins and formins (**Figure 14**).

The Arp2/3 complex (Actin-related protein 2/3) is composed of 7 proteins and binds the barbed end of G-actin trimers. This interaction stabilizes the G-actin trimers, allowing initiation of actin polymerization. However, the Arp2/3 complex requires previous activation by WASP/WAVE family proteins. Besides its role in the formation of new actin filaments from G-actin trimers, the Arp2/3 complex can bind a pre-existing actin filament and generate a branched actin filament structure. While the new actin filament elongates, the Arp2/3 complex remains attached to the pointed end (- end) of the filament [82–85].

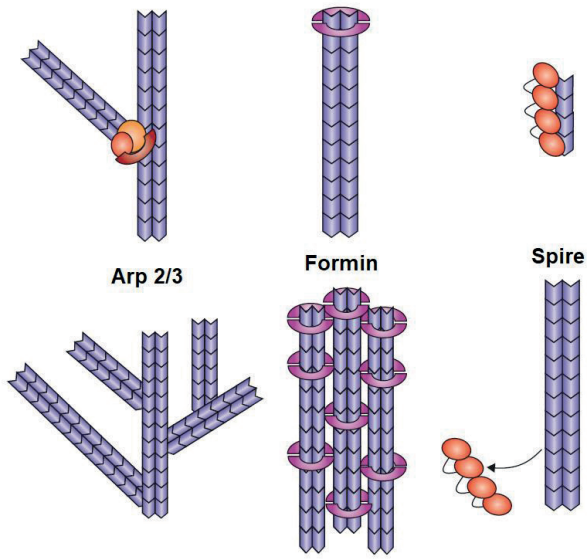

Figure 14: Different classes of actin nucleation factors. The Arp2/3 complex allows formation of actin filaments by stabilizing G-actin trimers and by binding the barbed end of pre-existing filaments, creating a branched network of actin filaments. Formins are dimeric structures that remain attached to the barbed end as it elongates. Spire proteins nucleate actin filaments by stabilization of a G-actin tetramer (Adapted from [82]).

Formins display two conserved regions, called formin homology domain 1 and 2 (FH1 and FH2). All formins act as dimers resulting from dimerization of their FH2 domain. The interaction with actin is mediated by binding to the barbed end through the FH2 domain. After nucleation, unlike the Arp2/3 complex, formins remain associated with the barbed end of actin filament during elongation and do not generate branched actin filament structures. Some formins are able to bundle actin filaments. The presence of formins at the barbed end of an actin filament inhibits association with capping proteins, preventing actin depolymerization. The FH1-domain associates with profilin increasing elongation of actin filaments [81,82,86].

Spire proteins are characterized by the presence of four Wasp homology 2 motifs (WH2) responsible for actin nucleation. Each WH2 motif is able to bind a G-actin monomer, allowing elongation of an actin filament from a G-actin tetramer. Similar to formins, actin filaments resulting from spire-nucleation are not branched [82,87].

Actin nucleation factors are not the only proteins implicated in actin polymerization. Capping proteins can associate either with the barbed end (Gelsolin) or the pointed end (CapZ and CapG). Cap proteins regulate filament length by blocking addition of new G-actin monomers. They also allow specifically directed elongation of actin filaments. Indeed, only uncapped actin filaments can elongate. Moreover, Gelsolin is able to induce a cut in the actin filament and remains attached to the barbed end (+ end) preventing its repolymerization [81,84].

ADF/cofilin (actin depolymerization factor) is responsible for depolymerization and severing of actin filaments. Indeed, ADF/cofilin increases depolymerization at the pointed ends of actin filaments by removing G-actin-ADP. ADF/cofilin generates new barbed ends by severing pre-existing actin filaments. Reversible phosphorylation on a serine residue of ADF/cofilin regulates its activity. The protein is activated after dephosphorylation [81,84,88,89].

ADP/ATP exchange of G-actin is mediated by profilin. The G-actin-ADP removed from the pointed end by ADF/cofilin is converted into G-actin-ATP-cofilin that can be reintroduced at the barbed end [81,88,89].

3.1. Actin structures

As mentioned previously, in order to migrate towards the attractant cells become polarized and generate protrusions at the leading edge that adhere to the substrate (ECM). This is followed by deadhesion and contraction at the cell rear to pull the cell body forward. This process requires the formation of three major actin cytoskeleton structures: filopodia, lamellipodia and stress fibers (**Figure 15**) [90–92].

Filopodia and lamellipodia are protrusive structures that sense and drive migration while stress fibers are contractile structures that contract the whole cell.

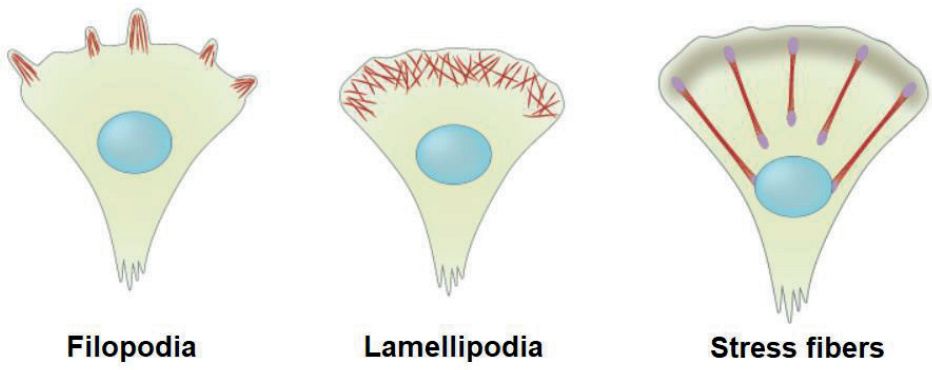

Figure 15: The three actin-based structures involved in endothelial cell migration. Filopodia (**left**) and lamellipodia (**middle**) are protrusive structures found at the leading edge. Stress fibers (**right**) constitute the contractile structure of the endothelial cell (Adapted from [93]).

3.1.1. Lamellipodia

Lamellipodia form a “Y branched” actin filament network at the leading edge during cell migration. After nucleation, the barbed ends of elongating filaments are directed to the leading edge and push the cell membrane

forward. The main mode of actin filament assembly in lamellipodia is via the Arp2/3 complex. The Arp2/3 complex is activated by the WAVE complex, which is itself activated by the small GTPase Rac1. Until recently, it was considered to be well established that Arp2/3 complex activation was mediated by the WAVE complex in a Rac1-dependent manner. However, it has been shown that the Arp2/3 complex can also be activated by N-WASP, which is downstream of the small GTPase Cdc42 [92,94,95].

3.1.2. Filopodia

Filopodia are finger-like structures rising from the lamellipodia at the leading edge. They are constituted of parallel actin filaments organized in bundles that sense the cell environment. The elongation of filopodia is mediated by formins and the Ena/Vasp complex. Indeed, these proteins remain attached to the barbed end during filament growth and are found at the top of the filopodia. The mechanism by which filopodia elongation occurs is well described. However, the mechanism initiating the formation of filopodia is still debated. It is not clear if filopodia are nucleated only by formins or if the Arp2/3 complex also plays a role. However, the nucleation process requires the activation of the small GTPase Cdc42 [92,96,97].

3.1.3. Stress fibers

Stress fibers are actomyosin bundles (abundant in endothelial cells) composed of 10 to 30 actin filaments. These actin filaments exhibit anti-parallel arrangements and are cross-linked together by α-actinin and myosin II. The actomyosin bundles are indispensable for producing the necessary forces for cell movement and are often linked to focal adhesions connecting the extracellular matrix to the actin cytoskeleton [81,92,95].

Different types of stress fibers can be found in the cell depending on their subcellular localization. Dorsal stress fibers are attached to focal adhesions only at one end. These stress fibers do not contain myosin II and are therefore non-contractile structures. Ventral stress fibers are the most abundant stress fibers observed in the cell. They are characterized by actomyosin bundles attached at each end to a focal adhesion. These fibers constitute the major contractile machinery of the cell and are located at the posterior side of the cell. Unlike dorsal and ventral stress fibers, transverse arcs are not directly attached to focal adhesions and are found just behind the lamella. Transverse arcs are curved actomyosin bundles and their association with dorsal stress fibers confers contractile forces. The last type of stress fiber was discovered recently and is called the perinuclear actin cap. It is found above the nucleus and regulates nuclear shape during interphase [98,99].

The assembly of stress fibers requires the activation of the small GTPase RhoA. Once activated, RhoA can activate its downstream targets ROCK and the formin mDia1. The activation of mDia1 provides the nucleating activity required for stress fiber formation. ROCK activation leads to the phosphorylation of MLCII by inhibiting MCLII phosphatase, resulting in an increase of actomyosin contractility [98,99].

It is noteworthy to mention that mechanisms of cell migration are different in 2D systems vs 3D *in vivo*. It is still not established that stress fibers and lamellipodia exist *in vivo*. They might be artefacts of 2D migration systems, which are the systems that have been the most largely used to study cell migration [100,101].

3.2. Integrins: Adhesion receptors

In order to migrate, cells have to make contact with components of the ECM such as fibronectin and collagen. These contacts are mediated by adhesion receptors called integrins.

Integrins are heterodimeric transmembrane structures composed of a large extracellular domain, a transmembrane domain and a short cytoplasmic tail. 24 different integrins have been identified depending on the association of the 18 α and 8 β subunits. Integrin receptors mediate both cell-cell and cell-ECM adhesions and are considered the master regulators of cell adhesion to the extracellular matrix. The non-covalent association of the N-terminal (extracellular) domain of the α and β subunits forms the ligand binding site (**Figure 16**) [102,103].

Two different types of interaction have been observed in integrin signaling: inside-out and outside-in signaling. During inside-out signaling, an intracellular activator binds the β subunit, which induces changes in integrin conformation leading to increased affinity for extracellular ligands. Inside-out signaling controls adhesion to the extracellular matrix (**Figure 16 right**) [102,104,105].

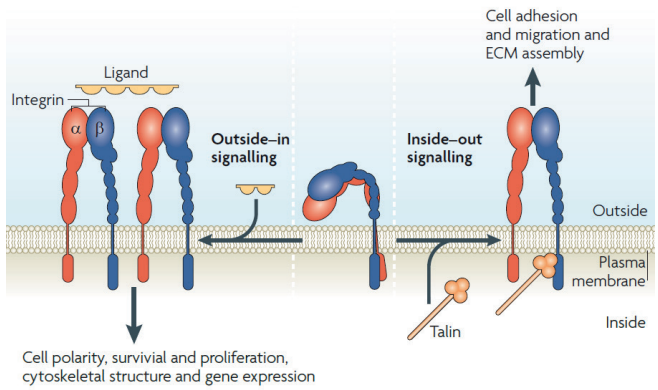

Figure 16: Inside-out and outside-in integrin signaling. *Inside-out signaling (**right**).* Binding of talin (intracellular activator) to the β subunit induces conformational modification of integrin, leading to its activation and increasing its affinity for extracellular ligands. *Outside-in signaling (**left**).* Integrin clustering results from the binding of extracellular ligands, allowing intracellular signal transduction (Adapted from [105]).

In outside-in signaling, the binding of an extracellular ligand changes integrin conformation, leading to the clustering of integrins and allowing intracellular signal transduction (**Figure 16 left**)

Talin plays a key role in integrin activation by binding to the β subunit of integrins. Attachment of cells to the ECM induces integrin clustering on the cell surface. The cytoplasmic domain of the clustered integrins allows recruitment of adaptor proteins that form focal adhesions [106–108].

3.3. Adhesion assembly, maturation and disassembly

Once integrins are activated, more than 50 proteins are recruited transiently to the site of the nascent adhesions. Different types of proteins can be found, including integrin-binding proteins such as Talin; adaptor proteins such as vinculin, paxillin and α-actinin; and kinases such as the FAK/Src complex. Indeed, integrins do not possess intrinsic activity and the FAK/Src complex leads to signal transduction by phosphorylation of downstream targets. All of these proteins allow connection of the cell to the ECM by creating strong linkages to the actin cytoskeleton. This interaction (EC-ECM) provides tension that allows the cell to move during migration [109–112].

Adhesions are highly dynamic structures. The master regulator of adhesion turnover is the FAK/Src complex (*Schematic overview of FAK/Src signaling*

pathways in Figure A in Annex 1). FAK is recruited to the site of adhesion once integrins are activated. FAK is activated by autophosphorylation and binds the Src kinase which in turn phosphorylates FAK, leading to a fully activated FAK/Src complex. This complex phosphorylates a series of downstream targets such as paxillin, Erk and p130-Cas [113,114].

As mentioned previously, actin polymerization is regulated by the Rho small GTPase family. The different Rho GTPases are also implicated in the regulation of adhesion dynamics. Once activated, FAK phosphorylates p130-Cas, which recruits Crk. Crk then activates the small GTPase Rac1. Once phosphorylated by FAK, paxillin is able to activate Cdc42 by activating the Cdc42 activator PKL. Rac1 and Cdc42 activity are required during the first phases of cell spreading. During early spreading, FAK phosphorylates p190RhoGAP, which inhibits RhoA and keeps RhoA activity low, relieving cytoskeletal tension. However, RhoA is activated during late spreading with the formation of stress fibers and the maturation of focal adhesions [115–118].

Although the molecular events that lead to focal adhesion disassembly are not well understood, key regulators have been identified [109,119,120]

Microtubules play a critical role in adhesion disassembly. Extension of microtubules to the site of the adhesion triggers the disassembly [120].

FAK is involved in both assembly and disassembly processes. However, FAK deficiency has a more significant impact on disassembly than on assembly. Indeed, in the absence of FAK an accumulation of mature focal adhesions is observed. The autophosphorylation of FAK (Tyr397) is a crucial event that leads to the subsequent phosphorylation of its kinase domain, allowing full kinase activity. Moreover, the phosphorylation of FAK

on Tyr397 allows the recruitment of dynamin, which is implicated in the internalization of integrins during adhesion disassembly. M-caplain is a protease that plays a role in adhesion disassembly by cleaving proteins such as FAK, paxillin and Talin. It seems that cleaving some components of focal adhesions can facilitate the internalization of integrins [120].

Moreover, Webb showed via analysis of adhesion dynamics that in addition to FAK, Src, paxillin, Erk, p130-Cas and MLCK were implicated in the disassembly process [121].

Different types of structures have been described according to their content, localization, size and lifetime: nascent adhesions, focal complexes (FXs), focal adhesions (FAs) and fibrillar adhesions (FBs) (**Figure 17**). Transitions between these 3 types of adhesion depend on actomyosin contraction and actin polymerization.

Nascent adhesions are formed at the cell periphery via a Rac-dependent mechanism and do not require myosin II. These structures can rapidly disassemble ($t_{1/2}$ ~ 60 seconds) or mature into focal complexes via Rac- and myosin II-dependent mechanisms. FXs are small dot-like structures found at the lamellipodia-lamella boundary that are not connected to stress fibers. FXs can turnover rapidly ($t_{1/2}$ ~ seconds to minutes) or mature into larger adhesions called focal adhesions. FX to FA maturation requires myosin II but also the small GTPase RhoA. FAs are connected to stress fibers, bringing mechanical tension for cell migration. Finally mature FAs are stable ($t_{1/2}$ minutes to hours) and can mature into fibrillar adhesions that are located in the cell body and are the most stable adhesions found in the cell ($t_{1/2}$ hours). From FAs, maturation of FBs requires contractile forces contributed by myosin II [118,122–124].

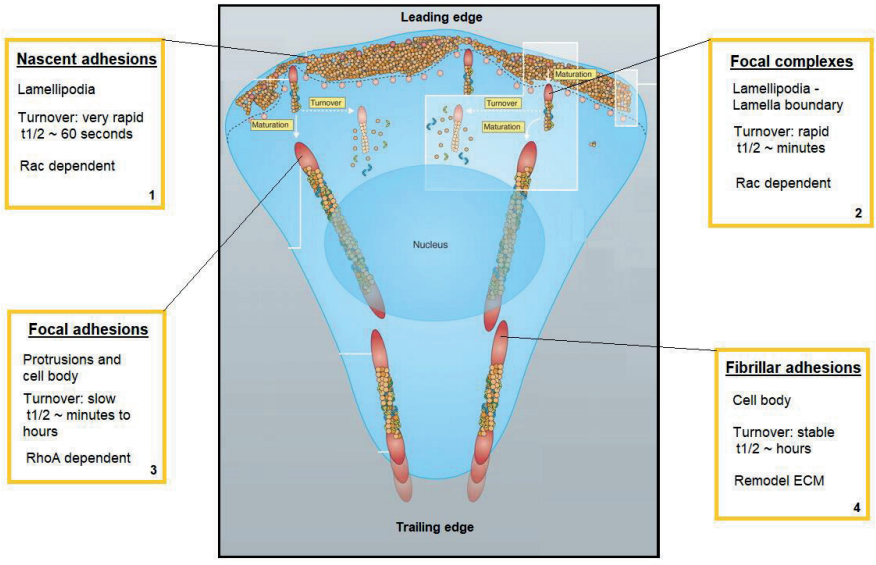

Figure 17: **Representation of different adhesion complexes**. Nascent adhesions (**1**) are formed in the leading edge and rapidly mature into focal complexes via a Rac-dependent mechanism. Focal complexes (**2**) are dot-like structures found at the lamellipodia-lamella boundary and can elongate centripetally and mature into larger focal adhesions (**3**) connected to stress fibers. Finally, focal adhesions mature into fibrillary adhesions (**4**) that are the most stable adhesions found in the cells (Adapted from [122]).

4. The Ras Superfamily of Small GTPases

4.1. Introduction

Small GTPases are low molecular weight proteins (20-30 kDa) that act as binary molecular switches by alternating between an inactive GDP-bound form and an active GTP-bound form, allowing signal transduction. These proteins regulate multiple processes including proliferation, cytoskeleton dynamics, adhesion, migration, membrane trafficking, apoptosis, survival and polarity. The Ras superfamily of small GTPases comprises over 150 human members divided into 5 families based on their functional and sequence similarities. These 5 families are Ras, Rho, Ran, Rab and Arf (**Figure 18**). Briefly, Ras family members play critical roles in cell proliferation, differentiation, survival and apoptosis. Rho family members are considered to be regulators of cytoskeleton dynamics while the Ran protein regulates nucleocytoplasmic transport. Finally, Rab and Arf family members are involved in the regulation of vesicular trafficking [125–127].

	Human genes	Described isoforms	Function
Ras	36	39	Cell proliferation, differentiation, survival, apoptosis, cell-cell adhesion, cell-matrix adhesion
Rho	20	22	Cytoskeletal dynamics, cell shape, adhesion, polarity
Rab	61	63	Membrane and protein traffic
Arf	27	30	Vesicular trafficking, endocytosis and exocytosis
Ran	1	1	Nucleocytoplasmic transport

Figure 18: The Ras superfamily of small GTPases and their known functions (Adapted from [125]).

4.2. Structure and regulation of small GTPases

All members of the Ras superfamily share a conserved domain composed of six β-strands surrounded by 5 α-helices making a 20 kDa "G-domain". Five conserved motifs forming five polypeptide loops are located around the nucleotide-binding site and called G1 - G5 (the G-boxes). Moreover, structural features conserved in all small GTPases are the switch I and switch II regions, where major conformational changes take place upon GTP binding and hydrolysis. The switch I region is called the "effector region" and changes its conformation upon exchange of GTP and GDP. The switch II region plays an important role in nucleotide exchange by GEFs and in stimulating GTP hydrolysis by GAPs (**Figure 19**) [128,129].

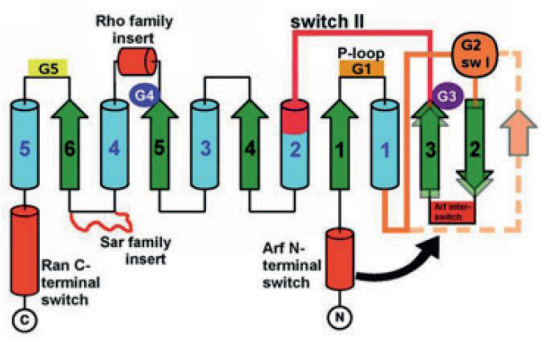

Figure 19: **Structure of the G-domain of Ras superfamily small GTPases** (Adapted from [128]).

Small GTPases display high-affinity binding for GTP and GDP and have low intrinsic GTP hydrolysis and GDP/GTP exchange activities. The activity of small GTPases (GDP/GTP cycle) is regulated by the opposing action of guanine nucleotide exchange factors (GEFs) and GTPase-activating proteins (GAPs). GEFs act by increasing GDP dissociation in

favor of GTP, leading to the activation of the small GTPase while GAPs increase GTP hydrolysis, leading to the inactivation of the protein. Once activated, small GTPases bind a variety of effectors, activating them and allowing signal transduction (**Figure 20**). Besides GEFs and GAPs, some small GTPases (Rho and Rab families) are also regulated by a third class of proteins called guanine nucleotide dissociation inhibitors (GDIs). These proteins act by masking the C-terminal hydrophobic tail of the small GTPases (maintaining the proteins in an "off" state) in the cytosol preventing membrane localization and interaction with effectors [125,130,131].

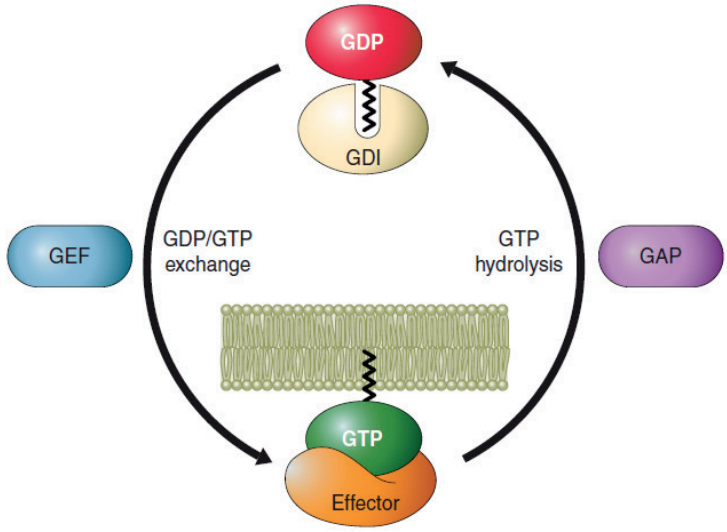

Figure 20: The GDP/GTP cycle. Regulation of the GDP/GTP cycle by GEFs, GAPs and GDIs. Small GTPases are activated by exchange of GDP to GTP by GEFs and inactivated by GTP hydrolysis stimulated by GAPs. GDIs maintain the small GTPase in an inactive state. Specific GEFs and GAPs regulate the different families of small GTPases (Adapted from [131]).

Another common characteristic of most small GTPases is post-translational modification of the C-terminal region by lipids, leading to localization to the membrane where they can be active. Indeed, most of the Ras and Rho members display a tetrapeptide sequence (CAAX) that can be recognized by farnesyltransferase and geranyl-geranyltransferase I, which add farnesyl or geranylgeranyl groups respectively and lead to membrane localization of the proteins [125,132].

It is noteworthy that even if they are still associated with membranes, some small GTPases are not modified by lipids (e.g. RhoBTB, Miro). Moreover, some of them are not modified by lipids and are not bound to membranes (e.g. Rerg and Ran) [125].

Because Rasa3 targets are the small GTPases Rap1 and Ras, the following introduction will focus on these proteins, members of the Ras family.

4.3. Ras small GTPases

There are 3 Ras genes that code for 4 different Ras proteins: H-Ras (Harvey-Ras), N-Ras (Neuroblastoma-Ras) and the two splice variants K-Ras4A (Kirsten-Ras) and K-Ras4B (Kirsten-Ras). These proteins share 80% amino acid sequence identity including a conserved effector domain in the N-terminal, and differ almost exclusively in their C-terminal tails (known as the Hypervariable Region) [133].

As previously mentioned, Ras proteins must be localized at the cellular membrane in order to be active and carry out their biological functions. To achieve this purpose, inactive cytosolic Ras precursors undergo a series of post-translational modifications allowing membrane localization. The first modification of Ras isoforms consists of a farnesylation of cysteine 186 in

the CAAX box, targeting Ras isoforms to the surface of the endoplasmic reticulum. H-Ras, N-Ras and K-Ras4A farnesylation is followed by palmitoylation of the cysteine residue adjacent to cysteine 186 of the CAAX box. H-Ras is palmitoylated on both Cys181 and Cys184 while N-Ras and K-Ras4A are monopalmitoylated. Unlike farnesylation, palmitoylation is a reversible reaction allowing the cell to modify Ras proteins' subcellular localization. H-Ras and N-Ras, once palmitoylated, can be found at the plasma membrane and in the Golgi. On the other hand, K-Ras4B lacks a site for palmitoylation and the mechanism by which it reaches the plasma membrane has not been clearly identified. However, the lysine-rich region found in the hypervariable region of K-Ras4B is involved in membrane anchoring of the protein via interaction with the phospholipids of the plasma membrane [132,134].

In order to assess the function and the redundancy of the Ras isoforms, mouse models have been generated. H-Ras and N-Ras knockout mice are viable, fertile and do not display any developmental defects [135]. However, H-Ras and N-Ras double-knockout mice are still viable and fertile but the number of adults is lower than expected, indicating a potential overlap between H-Ras and N-Ras function [135]. On the other hand, K-Ras knockout is embryonic lethal in mice. These mice died at midgestation (E12.5) and presented heart abnormality, fetal liver defects and anemia. Specific K-Ras4A isoform knockout mice grow normally and were identical to wild-type control mice indicating that K-Ras4A is not essential [136].

Activation of Ras

As mentioned previously, the guanine nucleotide exchange factors (GEFs) increase GDP dissociation in favor of GTP, allowing Ras activation. In recent years many GEFs have been identified that activate the small GTPase Ras. We focus here on the 3 major classes of Ras-GEFs: Sos, Ras-GRFs and Ras-GRPs [137,138].

There are two isoforms of Sos: Sos1 and Sos2. These GEFs activate H-Ras, N-Ras and K-Ras but also act as GEFs for the small GTPase Rac. Sos isoforms consist of a CDC25 domain (also called the Ras-GEF domain) associated with a Ras exchange motif (REM). Sos1 and Sos2 contain (in addition to the CDC25 domain and REM) a Dbl homology domain (DH) and a pleckstrin homology domain in the C-terminal. Activation of Ras by Sos is well characterized. Sos is associated in the cytosol with Grb2 adaptor protein via its SH3 domain in resting conditions. Upon receptor tyrosine kinase activation, the Grb2-Sos complex is recruited to the membrane via attachment of the SH2-Grb2 domain to the cytoplasmic domain of the activated receptor, increasing the proximity of Sos to the Ras small GTPase so activation can occur [139,140]. Another mechanism to activate Ras with the Grb2-Sos complex results from G-protein-coupled receptor activation, leading to the activation of PYK2 tyrosine kinase, which binds Src tyrosine kinase. Once phosphorylated by Src, PYK2 associates with the Grb2-Sos complex and activates the Ras small GTPase [141].

Like Sos, proteins in the second major class of Ras-GEFs, Ras-GRFs (including Ras-GRF1 and Ras-GRF2) possess a REM-CDC25 domain associated with a DH-PH domain. Ras-GRFs contain an additional PH domain in the N-terminal followed by a calmodulin-binding motif (IQ) [138].

These GEFs act on both Ras and Rac small GTPases. Unlike with Sos, Ras activation via Ras-GRFs is mediated by the activation of N-methyl-D-aspartate glutamate ligand-gated ion channel receptors (NMDARs) or G-protein-coupled receptors leading to the accumulation of calcium^{2+} in the cytosol. This Ca^{2+} promotes Ca^{2+} activation by calmodulin (CAM) association with the IQ domain of Ras-GRFs, leading to Ras activation.

Finally, Ras-GRPs (Ras-GRP1, 2, 3 and 4), besides the REM-CDC25 domain in the N-terminal region, contain two tandem Ca^{2+} binding EF hands and a DAG/phorbol ester region called the C1 domain in the C-terminal. In this case, activation of the PLC-linked G-protein coupled receptors leads to the hydrolysis of PIP2 into DAG and IP3. DAG production allows activation of Ras by binding Ras-GRPs (1, 3 and 4) to the membrane through the C1 domain. Regarding Ras-GRP2 (two splice variants were described), it is known that its C1 domain does not bind DAG. It is still not well understood how exactly Ras-GRP2 is associated with the cellular membrane. Moreover it has been shown that both Ras-GRP2 and Ras-GRP3 activate both Ras and Rap1 small GTPases [142].

Once activated, Ras activates a series of downstream signaling pathways (**Figure 21**). The most characterized pathways are the ERK mitogen-activated protein kinase (MAPK) and PI3K-AKT pathways which will be described in the following section.

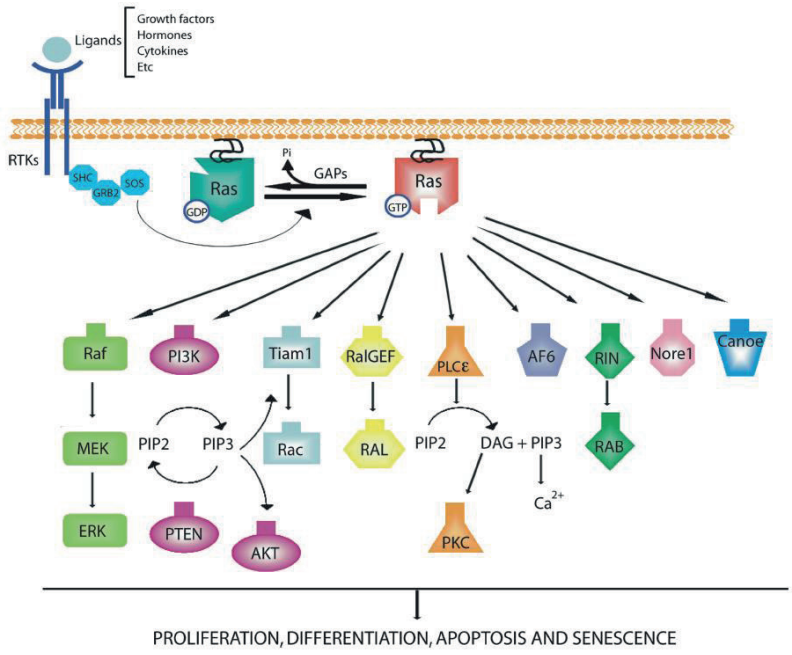

Figure 21: Overview of Ras signaling pathways after Ras activation. Once activated, Ras leads to the activation of multiple signaling pathways. These pathways are involved in proliferation, differentiation, apoptosis and senescence. Of all the signaling pathways, the Ras/Raf/MEK/ERK and the PI3K/Akt pathways are the best characterized. Moreover, activated Ras activates a series of GEFs that regulate other small GTPases such as Rac, Ral and Rab (Adapted from [133]).

Activated Ras promotes recruitment of Raf (a serine/threonine kinase) to the plasma membrane, leading to Raf's activation via a series of phosphorylations by other serine/threonine kinases (PAK, SRC). Once activated, Raf itself phosphorylates and activates the complex MEK1/2 (serine/threonine/tyrosine kinases) which phosphorylates and activates ERK1/2 (serine/threonine kinases). The phosphorylation of ERK leads to its activation and nuclear translocation [143]. Once in the nucleus, ERK phosphorylates a series of transcription factors (Elk1, c-Jun, c-Fos) that

induce expression of genes implicated in proliferation, differentiation, apoptosis and senescence processes.

Phosphatidylinositol-3-kinase (PI3K) is a heterodimeric protein with a regulatory subunit of 85 kDa (p85) and a catalytic subunit of 110 kDa (p110). Once activated, Ras binds and activates the catalytic subunit p110. PI3K acts by converting phosphatidylinositol 4,5-bisphosphate (PIP2) into phosphatidylinositol 3,4,5-trisphosphate (PIP3). Active PI3K leads to the accumulation of PIP3 at the plasma membrane, allowing Akt recruitment via binding to PIP3 by its pleckstrin homology domain. Akt is then phosphorylated and activated by the phosphoinositide-dependent kinases PDK1 and PDK2. After activation, Akt translocates to the nucleus where it affects the activity of a series of transcriptional regulators such as CREB, E2F and NF-κB [133,144]. It is noteworthy that some Ras effectors function as GEFs for other small GTPases. Indeed, Tiam1 and RalGEF are GEFs for Rac and Ral small GTPases respectively. Moreover, Ras effector Rin1 has been described as a GEF for the Rab5 small GTPase [138].

Ras-GAPs increase the hydrolysis activity of small GTPases leading to their inactivation. Unlike Ras-GEFs, these proteins and how they regulate small GTPases are less characterized. However, the majority of GAPs contain an arginine (called an arginine finger) that stabilizes a glutamine residue (61) within the G-protein, facilitating nucleophilic attack during GTP hydrolysis [145]. These proteins are more characterized in the case of cancer, when they have lost their GAP activity or are insensitive to mutant active Ras. For example, P120 RasGAP is insensitive to mutant Ras, and the loss of function of Neurofibromin increases Ras activity [138]. The Ras-GAPs also include the four members of the RasGAP1 subfamily, which includes the GAP Rasa3 (see *Rasa3* section).

4.4. Rap1 small GTPases

Rap1 possesses two distinct isoforms: Rap1a and Rap1b, which are the products of two different genes located on chromosomes 1 and 12 respectively. These proteins share 95% sequence identity. Indeed, Rap1a and Rap1b differ only by 9 amino acid residues at the C-terminal of the proteins [146]. At first, Rap1 was identified as an antagonist to Ras due to the homology of the effector binding region. As such, Rap1 could compete with Ras-signaling by sequestering Ras-effectors such as Raf, resulting in inactivation of Ras signaling pathways. This hypothesis has recently been called into question by studies showing common signaling pathways between the two small GTPases [146–148].

Like Ras, Rap1 requires a post-translational modification of its CAAX region (hypervariable region (HVR)) in order to be localized at intracellular and plasma membranes where it can be active. This modification consists of addition of a geranylgeranyl group on the cysteine of the CAAX region by geranyl-geranyltransferase I [125].

The role of Rap1 isoforms has been assessed by generating mouse models. First, deletion of either Rap1a or Rap1b leads to a partial embryonic lethality. Indeed, $Rap1a^{-/-}$ or $Rap1b^{-/-}$ mice display bleeding and edema around embryonic day E12.5. $Rap1a^{-/-}$ or $Rap1b^{-/-}$ adult homozygous mice can be obtained but with low efficiency, hence the term “partial embryonic lethality”. On the other hand, full $Rap1a^{-/-}$ $Rap1b^{-/-}$ knockout is embryonic lethal in mice due to major malformations between E8.5-E10 [149]. Because bleeding could explain embryonic lethality due to vascular defects, mice with specific deletion of Rap1a or Rap1b in endothelial cells were generated. In both cases, no embryonic lethally was observed. However, deletion of Rap1a and Rap1b together specifically in

the endothelial lineage leads to embryonic lethality due to hemorrhages between E10.5 and E12.5, suggesting a possible redundancy of Rap1 isoform function [150]. Both Rap1a and Rap1b isoforms were shown to have a critical role in angiogenic processes such as migration and sprouting [151].

Compared to Rap1a, the Rap1b isoform is highly expressed in endothelial cells (around 90% of total Rap1) [152]. Moreover, Rap1a is localized at endothelial cell junctions as a pool while Rap1b localization is more cytoplasmic, in the perinuclear region [146].

Activation of Rap1

Currently, six major classes of Rap1 GEFs have been identified: C3G, Epac proteins, Ras-GRPs, PDZ-GEF and the atypical GEFs DOCK4 and Phospholipase C epsilon (**Figure 22**) [153]. Rap-GEFs can be activated following stimulation of various receptors such as receptor tyrosine kinases, cytokine receptors, G-protein-coupled receptors and cell-adhesion molecules. Like Ras-GEFs, all the Rap-GEFs display a CDC25 catalytic domain preceded by a Ras exchange motif (REM) [154].

The Epac family comprises 3 members (Epac1, Epac2 and Repac (related to Epac)). These proteins contain the classic REM/CDC25 domains characteristic of GEFs, a Ras association domain (RA), and a Dishevelled/Egl-10/pleckstrin (DEP) domain (necessary for membrane localization) followed by a cyclic nucleotide binding domain (CNB). Epac2 displays a second CNB in the N-terminal. The third member of the family, Repac, contains only the catalytic region (REM-RA-CDC25). Epac1 and 2 require cAMP binding in order to activate Rap1 and Rap2 [155].

The PDZ-GEF family (PDZ-GEF1 and 2) is characterized by the presence of a PDZ domain, the REM and CDC25 domains, a Ras association domain

(RA) and a region related to the cyclic nucleotide binding domain (RCNB) in the N-terminal [156]. As well as the Epac family, PDZ-GEFs activate both Rap1 and Rap2. The mechanism by which these proteins are activated is still not clear. A main difference between the PDZ-GEF protein family members is the RA domain. Indeed, the RA domain of PDZ-GEF1 interacts with active Rap1 while the RA domain of PDZ-GEF2 interacts with active M-Ras [156].

C3G was the first Rap-GEF identified and seems to be active only on Rap1. The protein contains the characteristic REM-CDC45 region and a proline-rich sequence in the N-terminal that allows binding to the SH3 domain of the adaptor protein Crk. After stimulation, the C3G-Crk complex translocates to the plasma membrane and the activation of C3G is mediated by its phosphorylation on tyrosine residue 504 by different kinases (Src, c-Abl, Hcl and Fyn) [157].

The structures of Ras-GRPs were previously described in the *Ras small GTPases* section. As a reminder, among the four members of the Ras-GRP family, only Ras-GRP2 and Ras-GRP3 (also called CalDAG-GEF1 and CalDAG-GEF3 respectively) activate both Rap and Ras small GTPases.

Dock4 is qualified as an atypical GEF by the fact that it lacks the characteristic REM and CDC25 domains. Instead, it contains a Dock domain in the C-terminal that is responsible for Rap1 binding at the plasma membrane. This protein activates the small GTPases Rap1 and Rac [145]. Phospholipase C epsilon (PLCε) acts as both a Rap1-GEF and a Rap1-effector. Indeed, PLCε contains the catalytic domain CDC25 but also a Ras association domain (RA). It continues to activate Rap1 when Rap1 is already active, acting as a positive feedback loop [145].

Over the years, the involvement of Rap1 in cellular adhesion and in cell-cell junction formation has been largely documented [69,145,153,154].

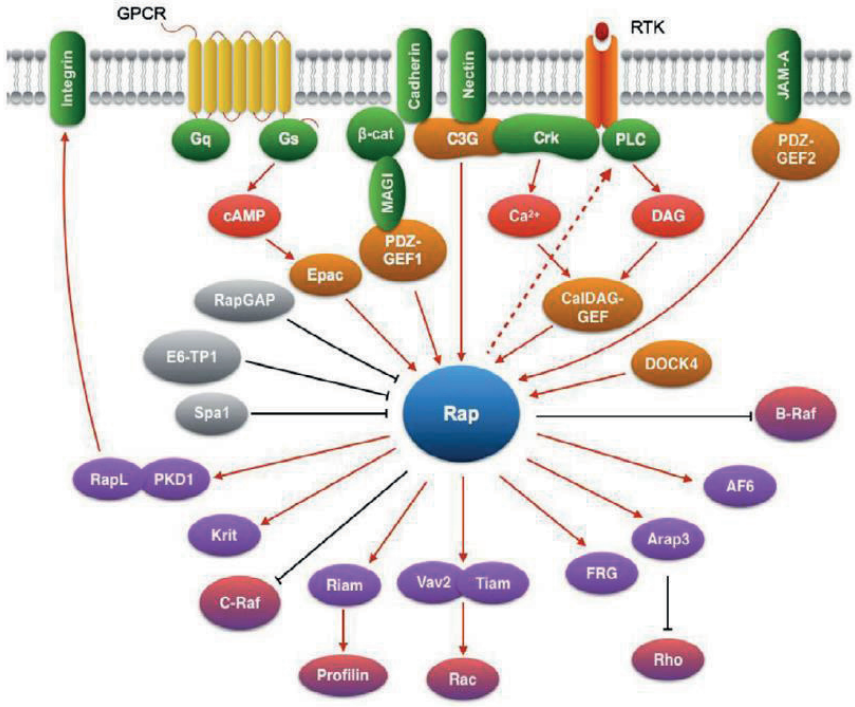

Figure 22: overview of Rap1 signaling patways. Once stimulated by an extra-cellular stimulus, receptors (RTK, GPCR) activate Rap-GEFs (orange) which in turn activate Rap small GTPase (blue). Rap-GAPs (grey) inactivate Rap small GTPase. Rap effectors (purple) are involved in many signaling pathways, such as cell-cell junction formation, cell adhesion and actin cytoskeleton organization (Adapted from [145]).

RapL is a direct effector of Rap1. It has been shown in T cells that active Rap1 interacts with RapL, leading to the binding of RapL to integrin αLβ2 and resulting in its activation. Moreover, RapL is expressed and associated with Rap1 in endothelial cells. Active Rap1 controls cell migration, probably by removing RapL from microtubules [145,158].

Integrin activation by Rap1 was also observed after binding to the serine/threonine kinase PDK1. Indeed, PDK1 promotes β1 integrin activation by regulation of Rap1 activation [159]. On the other hand, Riam stimulates β1 and β2 integrins after binding to active Rap1. Moreover Riam is found in a complex with ADAP and SKAP-55 which are necessary for Rap1 recruitment at the plasma membrane. Then, Riam interacts with profilin, a protein known to regulate actin dynamics [160,161].

The Rap1 effector Krit plays a major role in the regulation of endothelial cell-cell junctions. In endothelial cells, Krit is localized to microtubules. Active Rap1 induces release of Krit from the microtubules to the plasma membrane, and particularly to cell-cell junctions (via an unknown protein) where it can bind junction proteins such as AF-6 (Afadin), β-catenin, VE-cadherin or HEG1 receptor. Moreover, it has been shown that Krit, once released from microtubules, interacts with ICAP-1 and releases it from integrin β1, which induces integrin β1 activation [149,153,162].

As mentioned previously, Rap1 controls processes such as cell adhesion and cell-cell junction formation. Rap1-activated activates some GEFs and GAPs targeting other small GTPases, in particular the Rho family (Cdc42, Rac1 and RhoA), known to play a critical role in actin remodeling. Indeed, active Rap1 activates the Rac-GEFs Tiam and Vav2. By an unknown mechanism, Rap1 mediates CDC42 activation through the activation of the CDC42-GEF FRG. Finally, requiring PI3K activity, active Rap1 activates the Rho-GAP Arap3 resulting in Rho inhibition [161]

The Rho GTPase family is essential to control cytoskeleton organization and adhesion assembly. Briefly, RhoA promotes actin stress fiber and focal adhesion assembly. CDC42 promotes filopodium formation and Rac1 promotes lamellipodium formation [125].

Rap-GAPs are much less characterized in comparison to Rap-GEFs. However a series of GAPs were identified as interacting with Rap: Rap1GAP, SPAR, Spa-1, the GAP1 family (Rasa3, Rasa4 and RasaL (see *Rasa3* section)) and SynGAP.

Unlike Ras proteins, Rap proteins do not contain the glutamine (61) residue which is stabilized by the arginine finger of the Ras-GAPs, but instead display a threonine residue (61). Moreover, instead of an arginine finger, it is an “asparagine thumb” that is used by Rap-GAPs to position the water molecule allowing nucleophilic attack during GTP hydrolysis. This tiny difference makes the regulation between Rap and Ras activity more specific [145].

Rap1GAPs (Rap1GAP1 and Rap1GAP2) contain a GoLoco region (in addition to the GAP domain) allowing the binding of active Gα in response to activation of a G-protein-coupled receptor. This interaction results in the translocation of Rap1GAPs to the plasma membrane where they can inactivate Rap1 [154].

Spa-1 and SPAR proteins (SPAR1, 2 and 3) are Rap-GAPs characterized by the presence of a PDZ domain (protein-protein interaction domain), allowing interaction with other proteins possessing this domain such as transmembrane receptors, in which case they can locally inactivate Rap1 (and Rap2) [145,154].

SynGAP (active on both Rap1 and Ras) was found to be regulated by Ca^{2+}/calmodulin-dependent kinase II [138].

4.5. Ras and Rap1 in cancers

Ras genes (H-Ras, N-Ras and K-Ras) were the first oncogenes identified in human cancers. In approximately 30% of tumors Ras proteins are mutated. Most of the time Ras genes display single missense mutations that result in amino acid substitutions leading to constitutively active Ras-GTPs. Indeed, these mutations damage the intrinsic GTP hydrolysis activity of Ras small GTPases as well as the efficiency of GAP proteins. K-Ras mutations represent 85% of all Ras mutations in human cancers while N-Ras and H-Ras represent respectively 12% and 3%. The most mutated residues are glycine 12 (G12), glycine 13 (G13) and glutamine 61 (Q61). Specific mutations were found preferentially between the Ras isoforms. G12 mutation represents 83% of all K-Ras mutations. Q61 mutation represents 61% in N-Ras. On the other hand, the 3 mutations G12, G13 and Q61 are found equally in H-Ras (around 30% each) [148,163,164].

By contrast, mutations in Rap1 have rarely been examined in human cancers. However, a study conducted on myelodysplastic syndrome (MDS) patients revealed that in 29 patients, only one presented two mutations in Rap1B (G12R and K42R) and zero in Rap1A [165].

Ras/Rap1GAPs catalyze the GTP hydrolysis of Ras/Rap1-GTP leading to their inactivation. The loss of GAPs would be expected to increase Ras/Rap activation. The best characterized case of a GAP no longer deactivating Ras concerns the Ras-GAP neurofibromin. Indeed, germline mutations or deletion of the NF1 gene result in neurofibromatosis type 1 (the development of tumors called neurofibromas). Moreover, studies showed that this gene was mutated or inactivated in a series of cancers such as leukemia, glioblastoma and lung adenocarcinoma. In sporadic cancers it has been shown that NF1 can be inactivated either by genetic

loss or proteasomal degradation. Other Ras-GAPs, DAB2IP and Rasal2, were found inactivated by epigenetic silencing in different tumors (lung, breast and prostate). Unlike Ras proteins (which are usually directly mutated), Ras-GAPs seem to be inactivated by non-genetic mechanisms such as epigenetic silencing, proteasomal degradation and transcriptional repression [166,167].

5. RASA3: RAS p21 protein activator 3

RASA3 (GAPIII, R-Ras GAP or GAP1IP4B) belongs to the GAP1 subfamily, which is composed of 4 members: RASA2 (or GAP1m), RASA4 (or CAPRI), RASAL (or RASAL1) and RASA3. All the members of the GAP1 subfamily function as dual GAPs (GTPase-activating proteins) for Rap1 and Ras small GTPases [168].

5.1. RASA3 expression / structure / cellular localization

The human and mouse genes comprise 24 exons and generate 4191 bp and 4402 bp transcripts respectively. These transcripts encode an 834 amino acid protein with a molecular weight of 96 kDa. Northern blot and western blot analyses revealed that Rasa3 mRNA and protein expression are ubiquitous, with especially high expression in the brain and spleen [169–172].

The RASA3 protein consists of two C_2 domains (C_{2A} and C_{2B}) at the N-terminal end of the protein, a highly conserved central catalytic GAP domain (active on Rap1 and Ras but not on Rac, Rho or Rab family members) and a pleckstrin homology (PH) domain followed by a Bruton tyrosine kinase (Btk) motif at the C-terminal end of the protein, called the PH/Btk domain (**Figure 23**) [168,173].

Usually, C_2 domains allow membrane association and/or activation of the protein via phospholipid binding motifs upon elevation of the intracellular free calcium concentration ([Ca2+]i). P.J Cullen revealed that the C_2 domains of RASA3 (as well as RASA2) do not contain the C_2 conserved motif implicated in calcium-dependent phospholipid binding. An increase in

([Ca2+]i) does not affect the binding of phospholipids to C_2 domains of RASA3 [168,174]. Moreover, deletion of the C_{2A} or C_{2B} domain doesn't alter RASA3 membrane localization [169]. Currently, the biological role of Rasa3 C_2 domains remains unclear.

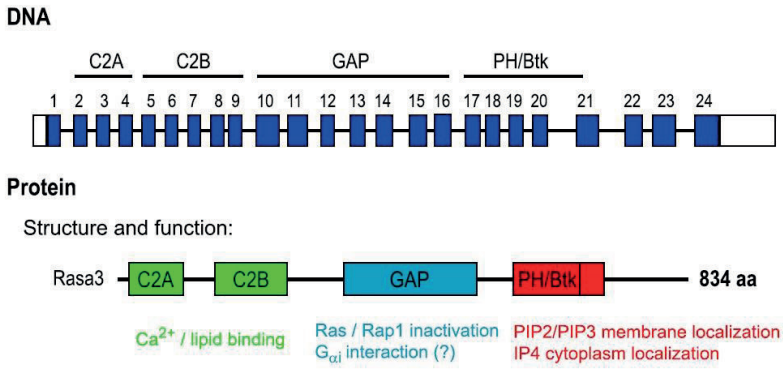

Figure 23: RASA3 gene and protein structure. The top panel represents the DNA structure consisting of 24 exons. The bottom panel represents the different domains of the RASA3 protein with their known functions (Adapted from [175]).

The PH/Btk domain regulates RASA3 localization at the cellular plasma membrane via binding to phosphoinositides. This domain binds, with high affinity, PIP3 (phosphatidylinositol 3,4,5-trisphosphate), IP4 (inositol-1,3,4,5-tetrakisphosphate) and PIP2 (phosphatidylinositol 4,5 bisphosphate) [169,174,176]. At its N-terminal region, the PH/Btk domain contains the core sequence KKR (residues 599 to 601) constituting a positively charged cluster of amino acids. Point mutations of the KKR core sequence that neutralize the positive charge within the PH/Btk domain result in decreased IP4 binding [174]. Moreover, these same point mutations affect the cellular localization of RASA3, leading to its accumulation in the cytosol [169]. These results suggest that RASA3 localization might be

regulated by the competition of IP4 and phospholipid binding. Because the PIP2-binding site within the RASA3 PH/Btk domain overlaps the IP4-binding site, PIP2 is the most probable candidate [177]. The hypothesis is that once IP4 is generated, RASA3 could be displaced from the plasma membrane to the cytosol. However, the accuracy of this hypothesis remains uncertain due to the fact that contradictory results have been observed. Indeed, Maréchal showed translocation of RASA3 from the plasma membrane to the cytosol after treatment with ATP or cell-permeable IP4 ester [178]. On the contrary, no dissociation of RASA3 from the plasma membrane was observed by Cullen following histamine treatment [174].

For many years, it was accepted that the PH/Btk domain of RASA3 was responsible for its plasma membrane localization. However, identification of a missense mutation (G125V) in the RASA3 gene of the *scat* mouse (a spontaneous, autosomal recessive mutant from the BALB/cBy inbred mouse strain) conflicts with preceding studies [172]. This missense mutation (a G-to-V transversion) is located in exon 5 of the RASA3 gene (between the C_{2A} and C_{2B} domains) and affects RASA3 localization, resulting in accumulation of the protein in the cytosol. Blanc revealed that G125 is highly conserved across metazoans and that the G125V mutation would modify function. This result is quite surprising because as mentioned above, deletion of the C_{2A} or C_{2B} domain doesn't affect the membrane localization of RASA3. Notably, the plasma membrane localization of GAP1 family members RASAL and CAPRI is regulated by their C2 domains in a calcium dependent manner [176].

5.2. RASA3 functions *in vitro* and *in vivo*

The first knock-out mouse model for RASA3 was described by Iwashita [171]. These mice express a catalytically inactive truncated RASA3 protein. Exon 11 and 12 (an arginine located in exon 12 is critical for GAP activity) were replaced by a neomycin cassette, leading to the production of a RASA3 protein lacking 88 amino acids. All RASA3$^{-/-}$ mice died during embryonic life between E12.5 and E13.5 from massive subcutaneous and intraparenchymal bleeding. On the contrary, all RASA3$^{+/-}$ mice grew normally and survived until adulthood. Because some E12.5 homozygous embryos presented massive hemorrhages from the brain, blood vessels were examined by electron microscopy. The development of adherens junctions between capillary endothelial cells was reduced in homozygotes compared with heterozygotes or wild-type mice [171].

A positive correlation between the downregulation of RASA3 and neurite outgrowth of PC12 (rat pheochromocytoma) cells has been observed [171]. Indeed, Iwashita found that mRNA and protein levels of RASA3 were reduced following NGF (nerve growth factor) treatment in PC12 cells. Transfection of RASA3 cDNA and a dominant negative H-Ras (N17) suppressed neurite outgrowth of PC12 cells. Taken together, these results revealed that downregulation of RASA3 is necessary for R-Ras activation, which appears crucial for neurite outgrowth of PC12 cells.

A yeast two-hybrid screen of a GH4ZR7 cDNA library allowed the identification of RASA3 as a $G_{\alpha i}$ binding protein. In GH4ZR7 cells, depletion of RASA3 blocked dopamine D2S-induced inhibition of TRH-(thyrotropin-releasing hormone) and induced ERK1/2 activation. These results indicate that RASA3 binds $G_{\alpha i}$ proteins, causing inhibition of G_q-induced Ras/ERK1/2 activation [179].

Walker investigated the relationship of RASA3 and intracellular free Ca^{2+} concentration ($[Ca^{2+}]_i$) in HeLa cells [180]. Indeed, as mentioned above, RASA3 is able to bind IP4 and regulation of $[Ca^{2+}]_i$ has been linked to a potential role of IP4. However, overexpression and depletion of RASA3 both failed to produce any effect on $[Ca^{2+}]_i$ following histamine stimulation [180].

RASA3 has been identified as a PIP3-binding protein in human platelets, acting as a key regulator of integrin $\alpha_{IIb}\beta_3$ outside-in signaling [181]. Recently, RASA3 was shown to act downstream of integrin $\alpha_{IIb}\beta_3$ by inactivating Rap1. In this pathway, PIP3 generated by integrin-mediated PI 3-kinase activity inhibits RASA3 Rap1GAP activity, leading to Rap1 activation and cell spreading [181].

In 1990 Peters described a new autosomal recessive mouse mutation *scat* (severe combined anemia and thrombocytopenia) [182]. Homozygous mice show a cycling phenotype alternating between crisis and remission episodes, with crisis episodes characterized by severe anemia and thrombocytopenia. The first crisis episode starts *in utero*, lasts until postnatal day 9 and is followed by a remission phase, in which the phenotype reverts to normal for the homozygous mice that survive (there is 10-15% mortality after the first crisis). This remission phase is transient and followed by a second crisis leading to the death of 94% of the remaining mice by postnatal day 30. As mentioned previously, Blanc identified a missense mutation (G125V) in the RASA3 gene leading to RAZA3 protein mislocalization in the cytosol and associated with an increase in active Ras. Defective erythropoiesis and megakaryopoiesis were observed in *scat* mice during crisis episodes [172].

Irradiated adult SCID (Severe Combined Immune Deficient) mice reconstituted with E12.5 liver from RASA3$^{-/-}$ embryos were generated in order to study the impact of a catalytically inactive form of RASA3 on the hematopoietic system [183]. This mouse model allows bypassing of the embryonic lethality reported in RASA3$^{-/-}$ mice by Iwashita. Most homozygous mice (20/24) died within 14 months after reconstitution, presented defects during megakaryopoiesis and thrombocytopenia, and were predisposed to develop pre-leukemia. Development, adhesion, motility, actin cytoskeleton and capacity to differentiate into proplatelets were all altered in megakaryocytes from SCID RASA3$^{-/-}$ mice. Molina showed that these megakaryocyte alterations were associated with an increase in active Rap1 and a constitutive activation of inside-out and outside-in integrin signaling [183].

Importantly, there are phenotypic differences between SCID RASA3$^{-/-}$ mice and *scat* mice (RASA3 G125V mutation). Indeed, G125V mutation leads to a mislocalization of RASA3 in the cytosol and mice present a cyclic phenotype [172] which is not observed in RASA3$^{-/-}$ mice (with catalytically-inactive RASA3 protein) [183]. Moreover, Molina was unable to detect any erythropoiesis defects in *scat* mice. At this time, the reasons for these major phenotypic differences between RASA3$^{-/-}$ and RASA3$^{scat/scat}$ mice are not known. However, the relocalization of RASA3 protein to the cytosol observed in RASA3$^{scat/scat}$ mice might offer an explanation. Indeed, the presence of RASA3 in the cytosolic compartment may create a new function for RASA3, leading to the cyclic phenotype observed in *scat* mice.

Another missense mutation (H794L) in the RASA3 gene was identified in a thrombocytopenic mouse strain, hlb381 (RASA3^{hlb}) [184]. Interestingly, peripheral platelet counts were significantly higher in these mice compared

to that observed in other RASA3 knockout/mutated mice [172,183]. Moreover, compared to WT cells, RASA3 expression was strongly reduced in lysates from RASA3$^{hlb/hlb}$ platelets, providing a unique model for studying platelet functions. These platelets exhibited an increase in active Rap1 along with integrin $\alpha_{IIb}\beta_3$ activation. The thrombocytopenia was attributed to an increase in platelet clearance rather than impairment of platelet production. These results identified RASA3 as a negative regulator of platelet activation that operates by antagonizing the Rap1 activation that is mediated by the RAP-GEF CalDAG-GEFI [184].

5.3. Role of RASA3 in disease

RASA3 has been found mutated in several tumors including in colon, bladder and renal cancers [185,186]. Moreover, RASA3 expression is downregulated in rat bladder tumors and in human and dog colorectal cancer cells [187,188]. Tang *et al*. identified RASA3 as a potential colorectal tumor suppressor gene. Indeed, cell growth of HCT116 cells (and other colorectal cancer cells) was induced after reducing RASA3 expression via siRNA [187]. As discussed in the *small GTPases* section, Ras small GTPase is the most mutated protein found in human cancers (around 30%) [189]. These mutations render Ras constitutively active (GTP-bound), leading to Ras pathway activation in the absence of extracellular stimuli. As mentioned previously, GAPs inactivate small GTPases by increasing GTP hydrolysis. However, even in mutant Ras cancers in which the intrinsic activity of GAPs is not altered, the inactivation of GAP members constitutes an alternative mechanism to hyperactivate Ras in tumors. Although none of the members of the GAP1 family have yet been found to be inactivated in cancers, Neurofibromin 1 (GAP) is a characteristic example of a protein that can lose its GAP activity, resulting in hyperactivation of Ras [189,190].

6. Zebrafish: in vivo model for vascular development

6.1. Introduction

The zebrafish (*Danio rerio*) is a small tropical fish used as an *in vivo* model for studying different processes such as embryogenesis and vascular development. The attractiveness of the zebrafish as an *in vivo* model comes from its numerous advantages.

First, zebrafish organs are similar at anatomical, physiological and molecular levels to those of humans. Additionally, their short generation time and small size allow their maintenance at high densities within the laboratory. Females can produce large quantities of eggs. These eggs are fecundated by males and develop externally, allowing analysis during early vascular development. Zebrafish embryos are transparent until 7 days post-fertilization (dpf) and the addition of phenylthiourea prolongs this transparency until up to 14 dpf [191,192].

More and more zebrafish transgenic lines have been created through the years. In order to analyze embryonic processes during zebrafish development, the Tg(fli1:EGFP)^{y1} line was generated (**Figure 24**). In this line green fluorescent protein (GFP) is specifically expressed in endothelial cells, facilitating analysis of zebrafish vasculature during development [193,194].

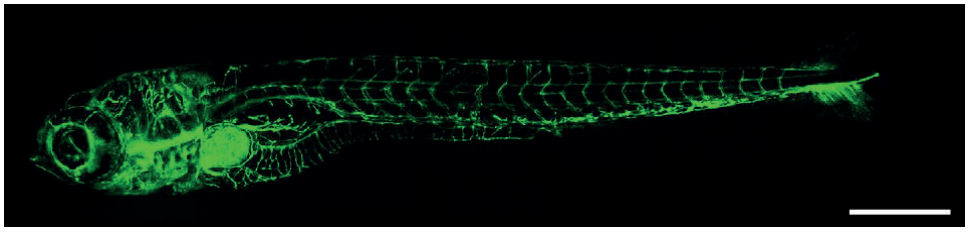

Figure 24: Representation of zebrafish transgenic line Tg(fli1:EGFP)^{y1} at 3 days post-fertilization (dpf). Expression of GFP specifically in endothelial cells allows visualization of zebrafish vessels during vascular development. (Scale bar = 500 µm) (Adapted from [193]).

Using microinjection of morpholinos or generation of knock-out fish, it is easy to perform analyses of protein function. Moreover, zebrafish have the ability to survive a few days with major cardiovascular defects. Indeed, the small size of zebrafish embryos allows oxygen distribution by passive diffusion and can permit relatively normal development of embryos even with severe defects [195,196].

The life of a zebrafish can be divided into different stages. Embryo state (0 – 72h) is followed by larva state (3 – 29 days). The juvenile state starts at 30 days and lasts until 90 days, when fish are considered to be mature adults. Zebrafish live on average 3 to 4 years and can be bred up until they are 2 years old [195].

6.2. Vascular development of the zebrafish

As in mammals, vascular development in zebrafish is divided into two stages. Initially vessels are formed by vasculogenesis, then extension of these vessels occurs by angiogenesis.

Vasculogenesis in zebrafish

The first two vessels formed in zebrafish are the dorsal aorta (DA) and the posterior cardinal vein (PCV). These vessels are formed by vasculogenesis and result from the coalescing of angioblasts. Formation starts at 14-18 hours post-fertilization (hpf) and lasts until 28-30 hpf, at which point the DA and PCV are functional and lumenized.

VEGF and Notch signaling pathways have been identified as crucial for arterial and venous specification. Moreover, before the DA and PCV are formed, zebrafish angioblasts express either EphrinB2 or EphrinB4, which result in the formation of arteries or veins respectively [197,198].

Angiogenesis in zebrafish

During zebrafish development, several vessels are formed by angiogenesis. Some of them are formed via the extension of the DA and PCV. The major vessels studied in zebrafish are the intersegmental vessels (ISVs), the sub-intestinal vessels (SIV) and the caudal vein plexus (CVP). The ISVs are the vessels analyzed during this PhD and the following section will focus on the development of these particular vessels [199–201].

The formation of ISVs consists of two successive waves of angiogenic sprouting from the DA and PCV (**Figure 25**). The first wave starts at around 24 hpf from the DA and forms arterial ISVs. Endothelial cells sprout from the DA and grow dorsally until reaching the dorsal roof where they connect to anterior and posterior neighbors. This fusion leads to the formation of the Dorsal Longitudinal Anastomotic vessel (DLAV). ISVs are formed from each lateral side of the embryos, leading to the formation of two distinct DLAVs. The second wave of angiogenic sprouting starts from the PCV at around 32 hpf. Endothelial cells sprouting from the PCV either connect to an existing arterial ISV, transforming it into venous ISV, or fuse at the midline to form the first lymphatic vessel [197,199].

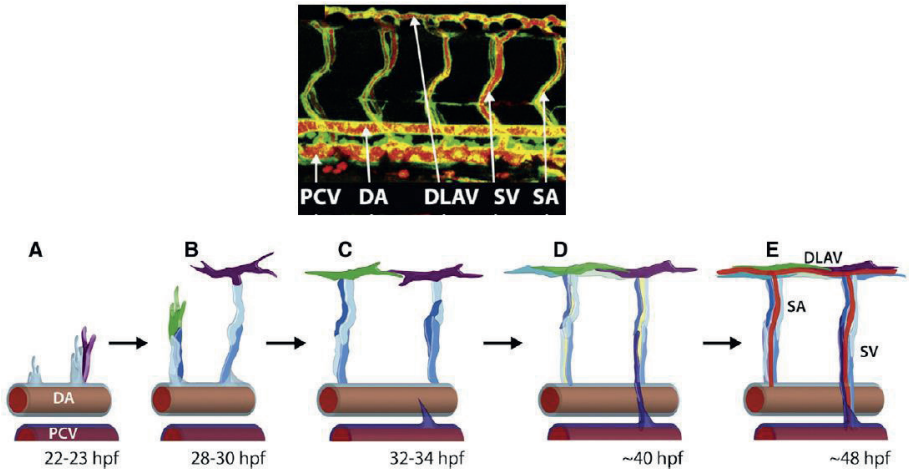

Figure 25: Representation of ISV and DLAV formation. Top image represents a part of the zebrafish trunk vasculature. Endothelial cells sprout from the DA at 22 hpf and migrate towards the dorsal line where they connect with adjacent endothelial cells to form the DLAV. At 32 hpf the second wave of sprouts from the PCV fuses with pre-existing ISVs, turning them into venous ISVs. ISVs and DLAVs are functional and lumenized at 48 hpf. PCV: posterior cardinal vein; DA: dorsal aorta; DLAV: dorsal longitudinal anastomotic vessel; SV: segmental vein; SA: segmental artery (Adapted from [197]).

As opposed to the endothelial cells sprouting from the DA, those sprouting from the PCV do not reach the dorsal line. Finally, vessels are functional and fully lumenized at 48 hpf [197,199]. The different molecular mechanisms of sprouting angiogenesis (VEGF/Notch signaling) and the different processes by which vessels can be lumenized were discussed in the *vascular development* section.

FMNL3, a member of the formin family, was identified as a critical cytoskeletal regulator of endothelial cell elongation. Depletion of FMNL3 in zebrafish led to ISVs defects. Sprouting of the ISV occurred but ECs failed to elongate [202]

Aim of the study

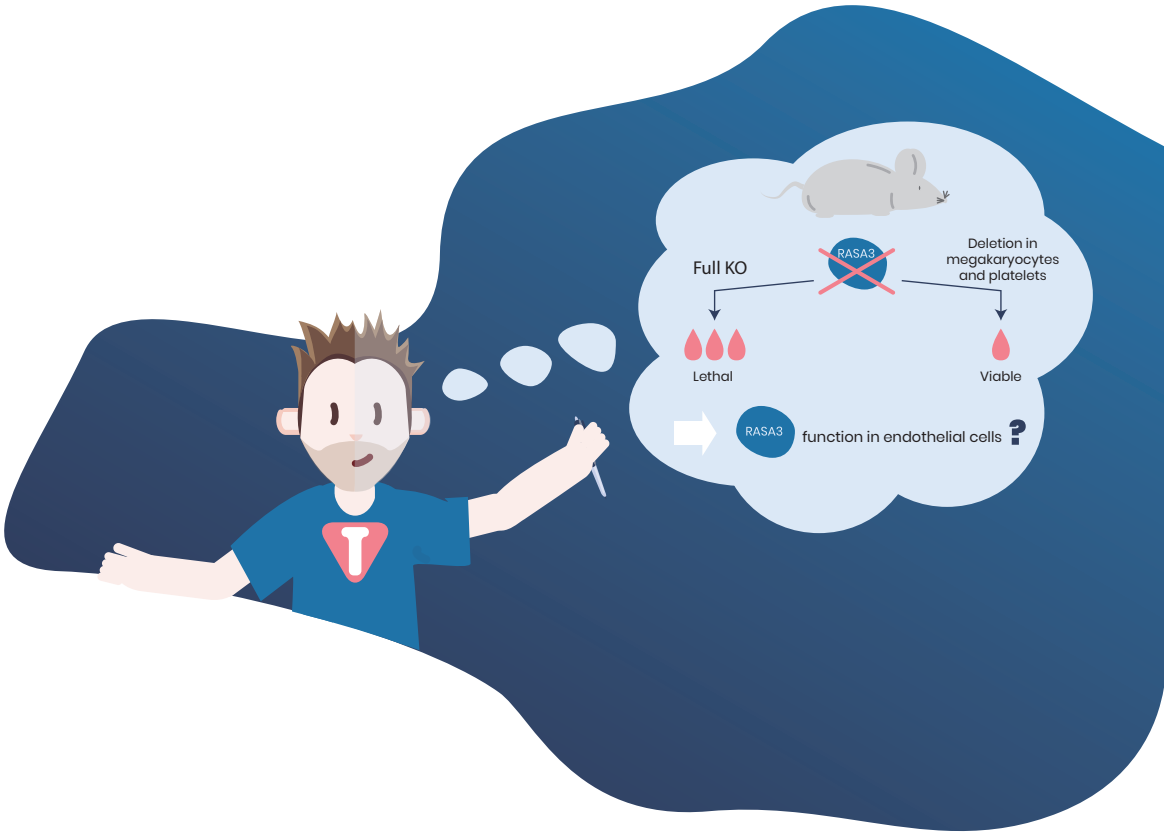

Rasa3 is a member of the GAP1 family and has the ability to control both Ras and Rap1 small GTPases. Mice expressing inactive mutants of Rasa3 die during mid-embryonic life and display many hemorrhages and severe thrombocytopenia [171,183,184]. However, biological function of Rasa3 underlying these defects remains unclear.

The embryonic bleeding and mortality can be potentially explained by low levels of platelets. Mice with specific inactivation of Rasa3 in megakaryocyte lineage display megakaryocyte alterations and severe thrombocytopenia, as expected [183]. However, these mice were obtained at Mendelian ratios and were viable, although with reduced life span.

Another study from Stefanini et al reported that the hemorrhagic phenotype in mice where Rasa3 is inactivated specifically in megakaryocyte lineage are much less severe compared to full Rasa3$^{-/-}$ mice. These authors suggested that embryonic bleeding and lethality resulting from Rasa3 inactivation might be related to its function in a different cell compartment from megakaryocyte lineage. We speculated that this cell compartment might be the endothelial lineage. Indeed, endothelial defects might explain the hemorrhagic phenotype leading to the embryonic lethality observed in full Rasa3$^{-/-}$ mice [184].

The vascular system plays an essential role by delivering oxygens and nutrients to all tissues in the body. Angiogenesis, formation of new blood vessels from pre-existing ones, is a crucial process that allows formation of a complex vascular system.

Here, in collaboration with Patricia Molina Ortiz (laboratory of Stephane Schurmans), we analyzed Rasa3 function in endothelial lineage using *in vivo* (mice and zebrafish) and *in vivo* (HUVECs) approaches. All mice experiments were performed by Patricia Molina Ortiz while experiments in zebrafish and HUVECs were conducted by Tanguy Orban, Maud Martin and Audrey Habets.

Results

1. Rasa3 is expressed in endothelial cells (ECs)

Before investigating the angiogenic functions of Rasa3 in ECs, it was necessary to examine its expression in these cells. Indeed, studying the role of Rasa3 in angiogenic properties had not been done previously. Regarding the expression profile of Rasa3, we see that the protein is expressed ubiquitously throughout the body with a predominance in the brain. In order to validate the choice of our *in vitro* model, human umbilical vein endothelial cells (HUVECs), we examined the mRNA and protein expression levels of Rasa3 in different endothelial cell lines and in HeLa cells. The relative Rasa3 mRNA expression (**Figure 26A**) and the protein expression level of Rasa3 (**Figure 26B**) showed that the protein is well expressed in endothelial cells. For subsequent experiments we decided to continue with the HUVECs as our *in vitro* model.

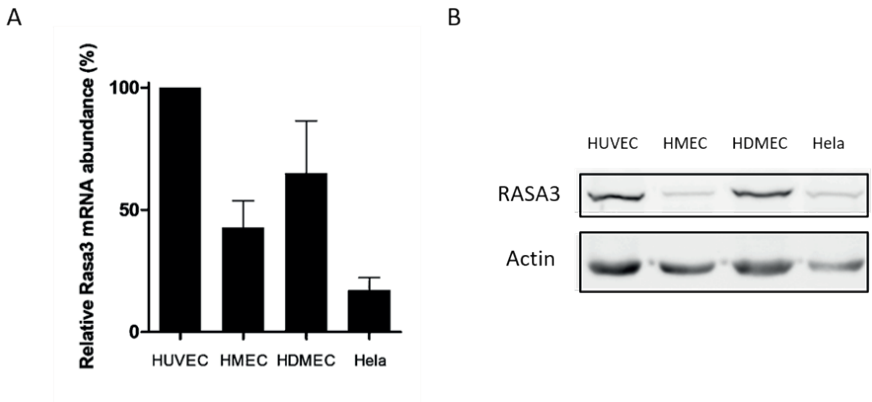

Figure 26: **Expression of Rasa3 in different endothelial cell lines**. Rasa3 expression was examined by RT-qPCR (**A**) and western blot (**B**) analysis in different endothelial cell lines and HeLa cells. HUVEC (Human Umbilical Vein Endothelial Cell); HMEC (Human Microvascular Endothelial Cell); HDMEC (Human Dermal Microvascular Endothelial Cell) and HeLa (Henrietta Lacks, cancer cell line).

To assess the role of Rasa3 in the angiogenic properties of ECs, we designed two small interfering RNA (siRNA) that efficiently reduced its expression in HUVECs. The efficiency of Rasa3 siRNA was checked by RT-qPCR and Western blot. In both cases (**Figure 27A and 27B**) we observed that expression of Rasa3 mRNA and protein is reduced after transfection with siRNA targeting Rasa3.

Importantly, we then checked whether these siRNAs affected the viability or proliferative capacity of the cells. As showed in **Figures 27C and 27D,** the siRNAs targeting Rasa3 didn't drastically affect the viability or proliferation of the cells.

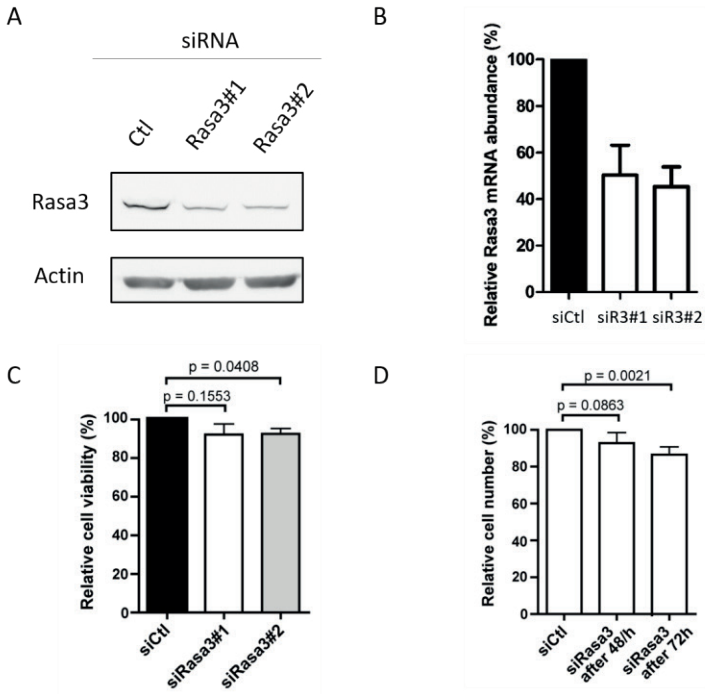

Figure 27: Rasa3 siRNAs reduced Rasa3 expression and didn't affect viability or proliferation properties of ECs. HUVECs were transfected with siRNA targeting Rasa3 or non-related siRNA (siCtl). Seventy-two hours after

transfection, RNA and protein were extracted and analyzed by RT-qPCR (**A**) and western blot (**B**) respectively. GAPDH was used as an internal control for RT-qPCR and Actin was used as a loading control for western blot. (**C**) Seventy-two hours after transfection, control and Rasa3-depleted cells were submitted to a viability assay (MTS) as described in the methods section. (**D**) Twenty-four hours after transfection control and Rasa3-depleted cells were counted and seeded with the same number for each condition. Forty-eight and seventy-two hours post-transfection, HUVECs were harvested and counted (p values are shown, One sample t-test).

2. Loss of Rasa3 affects endothelial angiogenesis and tube formation

Once the siRNA efficiency was validated, we analyzed the impact of Rasa3 inactivation on angiogenic activity via a tubulogenesis assay (matrigel assay). This test is based on the capacity of the cells to form a vascular-like network. Forty-eight hours after transfection, Ctl and Rasa3-depleted cells were seeded on a matrigel matrix, which is enriched in growth factors and allows the formation of tubes by ECs. As showed in **Figures 28A and 28B left**, silencing of Rasa3 expression using two independent siRNAs impaired drastically the formation of vascular-like structure. Quantifications (**Figures 28A and 28B right**) consisted of measuring the cumulative tube length of the network using the siRNA control condition as reference (100%). In order to discriminate the capacity to form from the capacity to maintain a vascular-like network we performed time-lapse microscopy of a matrigel assay. We observed that Rasa3-deficient HUVECs initially formed branched networks but these branches were unstable, leading to rapid collapse of the network.

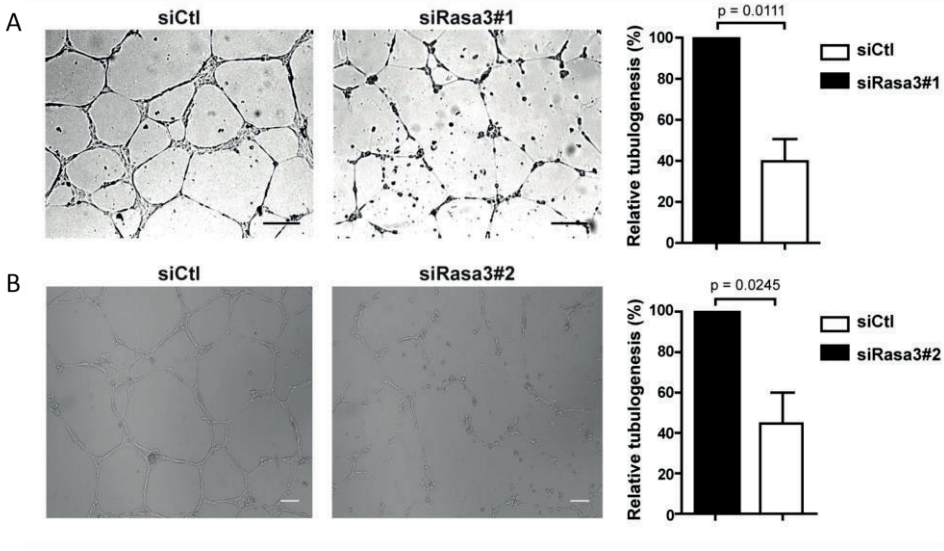

Figure 28: Depletion of Rasa3 impairs tubulogenesis in HUVECs. (**A**) Representative micrographs of a tube-like formation assay in matrigel using HUVECs treated with siControl or with siRasa3#1. Images are representative of 3 independent experiments. Bar = 100 µm. Histograms represent mean ± SD of relative tubulogenesis of capillary-like structures measured in five different fields from 3 independent experiments. The p values are shown (One sample t-test). (**B**) Same as (**A**) using a second siRasa3.

The matrigel assay has the disadvantage that the tubes of the vascular-like network do not display a real lumen. Moreover, it has been shown that the matrigel matrix, due to its enrichment in growth factors, is able to induce formation of vascular-like networks from cell lines not expected to be able to form them, such as fibroblasts. We decided to additionally perform a 3-dimensional spheroid assay to support a role of the Rasa3 protein in tubulogenesis.

Twenty-four hours after transfection, control and Rasa3-depleted HUVECs were harvested in order to form spheroids. The next day, spheroids were

harvested and embedded into a collagen matrix in order to allow the extension of sprouts. We observed (**Figure 29A**) that depletion of Rasa3 using two independent siRNAs impaired the extension of sprouts out of the spheroids. Quantification (**Figure 29B**) revealed that Rasa3 depletion reduced the number of sprouts extending from the spheroids.

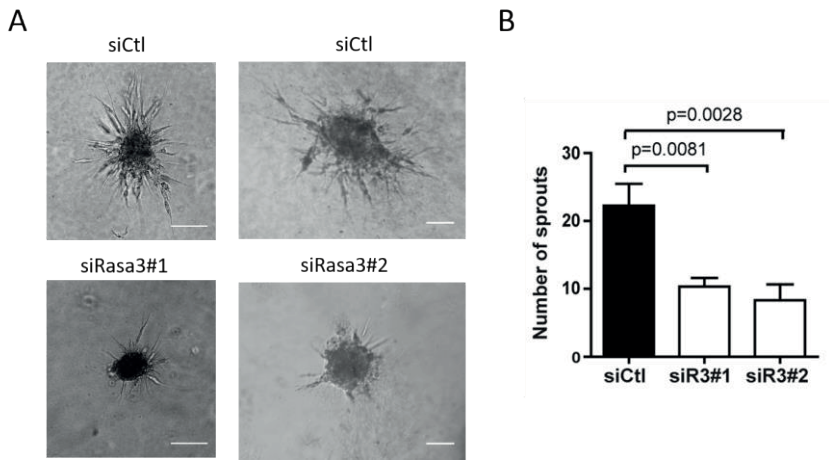

Figure 29: Rasa3 is necessary for endothelial sprouting. (**A**) Representative micrographs of a spheroid sprouting assay with HUVECs treated with siControl or with 2 different siRasa3 (siRasa3#1 and siRasa3#2).This experiment is representative of 3 independent experiments. Bar = 100 µm. (**B**) Histogram represents number of sprouts per spheroid measured on 22 and 15 spheroids, for siRasa3#1 and siRasa3#2 respectively. The p values are shown (Student's t-test).

Patricia Molina Ortiz generated mice expressing a catalytically inactive form of Rasa3 specifically in the endothelial cells ($R3^{f/f}$ iEC-Cre). The effects of EC Rasa3 inactivation on capillary formation were also analyzed in an *ex vivo* model of adult aortic ring in which lumenized endothelial outgrowth emerging from mouse aortic explants can be examined. Inactivation of Rasa3 was achieved by daily tamoxifen IP injection of adult $R3^{f/f}$ iEC-Cre mice for 3 consecutive days, then aortas were isolated, placed

in a 3D collagen I matrix and analyzed at day 5. Compared to control $R3^{f/f}$ mice, the capacity of the aortic endothelium from $R3^{f/f}$ iEC-Cre mice to form neovessels was dramatically impacted, with neovessels severely reduced in number (*Figure 2B in Annex 2*). Altogether, these results validate a critical role of the Rasa3 protein in angiogenic processes.

3. Knockdown of Rasa3 in zebrafish induces tubulogenesis defects in the trunk vasculature

As mentioned previously, Patricia Molina Ortiz generated mice expressing a catalytically inactive form of Rasa3 specifically in the endothelial cells. These mice recapitulate completely the phenotype of Rasa3 full-knockout mice. When she analyzed more precisely the retinal vascular plexus, she observed that these vessels often displayed constricted regions and lacked a continuous lumen (*Figure 2C in Annex 2*). In order to corroborate the results obtained in mice, we decided to analyze the lumenization processes using a second *in vivo* model and taking advantage of the zebrafish model (*Danio rerio*). First, in order to assess the role of Rasa3 in vascular development, we designed a translation-blocking morpholino (ATG-blocking). This morpholino targets the start codon of Rasa3 mRNA, preventing its translation into protein. Using 2.5ng/µl of Rasa3 morpholino (corresponding to 1.31 pg of morpholino), we observed partial reduction of Rasa3 expression, demonstrating the efficiency of the morpholino (**Figure 30A**). In this study we used the transgenic line *Tg(fli1a:eGFP)y1*, which allows visualization of vascular development via expression of GFP protein by endothelial cells. Before conducting any phenotyping analysis, we ensured that our morpholino concentration wasn't toxic and didn't affect the global morphology of the fish. Rasa3 morpholino was injected into one-cell stage zebrafish embryos at 2.5ng/µl. As shown in **Figure 30B**, forty-eight

hours after injection Rasa3 morphant embryos didn't display any general morphological alterations allowing analysis of potential defects in vascular development.

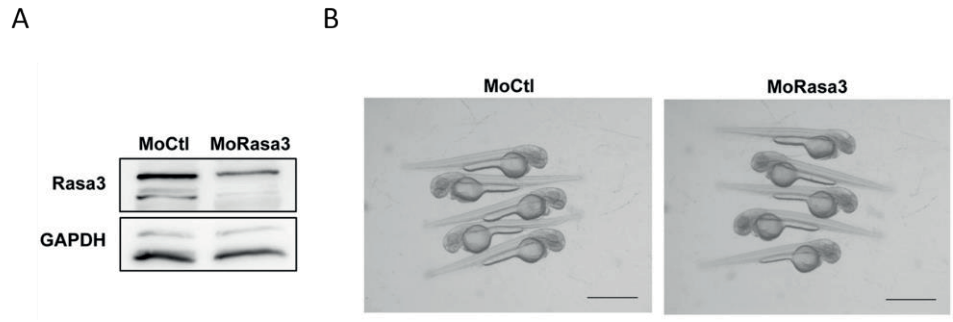

Figure 30: Rasa3 morpholino reduced Rasa3 expression and didn't affect general embryo morphology. (**A**) Detection of Rasa3 level in lysates from Control (Ctl) and Rasa3 morphant embryos. GAPDH was used as a loading control. (**B**) General morphology of Ctl and Rasa3 morphant embryos.

It is well established in the literature that the primitive circulatory loop (consisting of the dorsal aorta (DA) and the posterior cardinal vein (PCV)) of the zebrafish is formed by vasculogenesis. This primitive circulatory loop later extends into a complex vascular network via angiogenesis. To corroborate the lumenization defects observed in mice, we decided to focus our attention on the lumenization of intersomitic vessels (ISVs). These vessels constitute the most documented example of sprouting angiogenesis in zebrafish and are easily observable under the microscope. As mentioned in the introduction section, the formation of these vessels is a two-step process consisting of two sprouting waves, from the DA and the PCV at 22 and 32 hpf respectively, leading to the creation of the dorsal longitudinal anastomotic vessel (DLAV).

We first analyzed the lumenization of ISVs at 48 hpf, a time when these vessels are fully formed and lumenized. Representative confocal images are presented in **Figure 31A**. We observed that knockdown of Rasa3 by injecting a specific morpholino was associated with thinner ISVs and DLAV. Quantification consisted of counting the percentage of lumenized ISVs at 48 hpf for 10 ISVs/embryos in 50 embryos/condition. We showed that the percentage of lumenized ISVs was reduced in Rasa3 morphant embryos compare to control embryos (**Figure 31B left**). We excluded a potential developmental delay by doing the same quantification on 25 embryos/condition at 72hpf (**Figure 31B right**) at which time we observed exactly the same results.

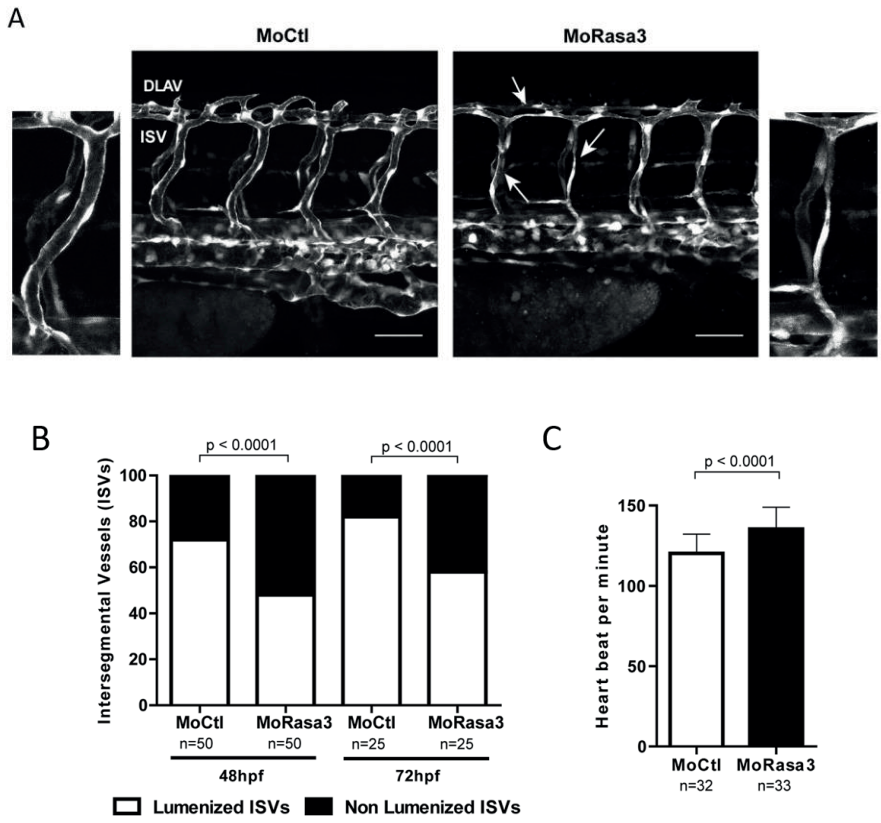

Figure 31: Knockdown of Rasa3 in zebrafish induces tubulogenesis defects in the trunk vasculature. (**A**) Tg(fli1a:eGFP)y1 embryos were injected with control morpholino (MoCtl) or with morpholino targeting Rasa3 (MoRasa3). Confocal pictures of the trunk vasculature were taken at 48 hpf. Ctl embryos present normal ISVs and DLAVs with open lumen (arrow head) whereas Rasa3 morphant embryos show thinner, non-lumenized vessels (arrows). Bars = 50 mm. ISV, intersegmental vessel; DLAV, dorsal longitudinal anastomotic vessels. (**B**) Quantification of lumenized ISVs in Ctl and Rasa3 morphant embryos at 48 (left) and 72 hpf (right). The p values are shown (Fisher's exact test). Results are mean from 10 ISVs/embryo in 50 embryos at 48 hpf and 25 embryos at 75 hpf. (**C**) Heart rates in 32 Ctl and 30 Rasa3 morphant embryos. Histograms are mean ± SD from 35 embryos. The p value is shown (Student's t-test).

These lumenization defects prompted us to analyze the cardiac rhythm of Rasa3 morphants. Possibly, fish presenting lumenization defects could compensate for these defects by increasing their cardiac rhythm. To do so, we counted heartbeats per minute in control and Rasa3 morphant embryos and we observed that Rasa3 knockdown resulted in an increase in cardiac rhythm that could be a compensatory mechanism for these circulatory defects (**Figure 31C**).

4. Depletion of Rasa3 increases adhesion and decreases migration of ECs

Although the exact molecular mechanism of vascular lumen formation and stabilization is still controversial, a common theme is the importance of EC migration/adhesion properties. To understand how Rasa3 might control vascular lumenization, we assessed the ability of Rasa3-silenced HUVECs (siRasa3 HUVECs) to migrate randomly using a scratch-wound assay. We found (**Figure 32**) that downregulation of Rasa3 correlated with a

significant decrease in HUVEC migratory capacity using 2 independent siRNAs targeting Rasa3. Using phase contrast microscopy we showed that control and Rasa-depleted cells didn't display any directionality defects (*Figure B in Annex 1*), meaning that the migration delay previously observed might be due to stronger adhesion of the cells to the substrate.

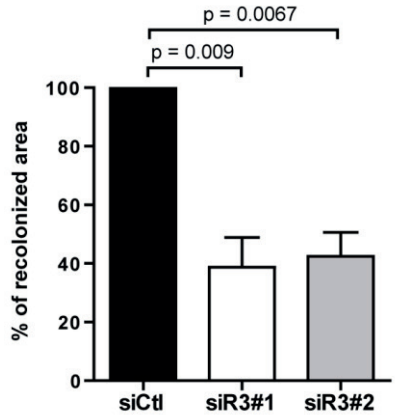

Figure 32: Depletion of Rasa3 decreases migration of ECs. In a scratch-wound migration assay, the recolonized area was analyzed at 8 hours in HUVECs transfected with siControl or one of two different siRasa3. The means ± SD of 3 independent experiments are presented, relative to the siControl condition. The p values are shown (One sample t-test).

Cell migration is a process that relies heavily on assembly and disassembly of EC-ECM (extracellular matrix) focal contacts. We thus assessed the ability of Rasa3-depleted cells to attach to major extracellular matrix components. We found that knockdown of Rasa3 was associated with a significant increase in cell adhesion onto fibronectin On the contrary, adhesion onto vitronectin, laminin and collagen were unaffected (**Figures 33A and 33B**).

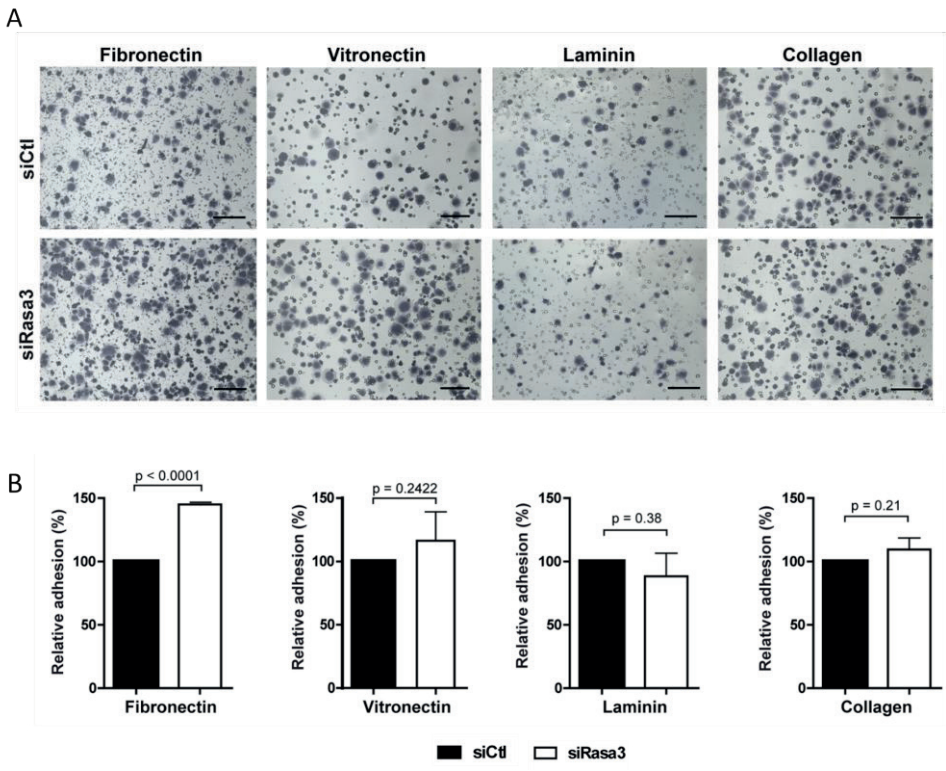

Figure 33: Depletion of Rasa3 increases adhesion of ECs. (**A**) Effects of Rasa3-silencing on HUVEC adhesion onto fibronectin, collagen, vitronectin or laminin. Bars = 100 µm. Representative micrographs of an adhesion assay with HUVECs treated with siControl or siRasa3. Images are representative from 3 to 5 independent experiments. (**B**) Histograms are mean ± SD of 3 independent experiments. The p values are shown (One sample t-test).

Integrins are heterodimeric proteins composed of an α and β subunit and are the major protein implicated in EC/ECM interactions. Using an antibody specific to the clustered form (active form) of the β1 integrin, we found that the enhanced adhesion of siRasa3 HUVECs was associated with a significant increase in β1 integrin clustering. This result was observed by immunofluorescence (**Figure 34A**) and by FACS analysis (**Figure 34B**).

We ensured that the total level of β1 integrin was unchanged in Rasa3-depleted cells compared to control cells (**Figure 34C**). Interestingly, the enhanced clustering of β1 integrin was also observed in sprouts from $R3^{f/f}$ iEC-Cre aortic explants (*Figure 4B in Annex 2*).

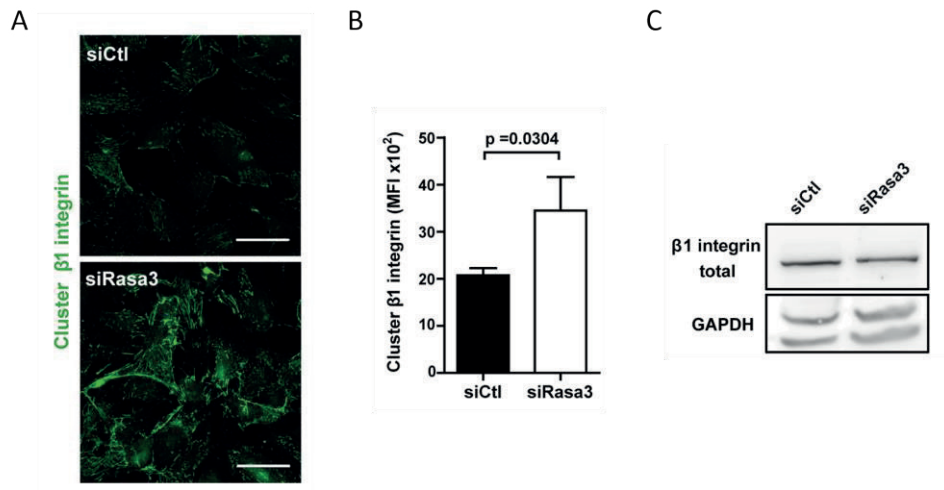

Figure 34: Increased β1 integrin activity in Rasa3-depleted cells. Activation of β1 integrin was analyzed in HUVECs transfected with siControl or siRasa3 by confocal microscopy (**A**) and FACS analysis (**B**) using an antibody specific for clustered β1 integrin. Representative images are shown. Bars = 50 µm. (**B**) Histogram represents mean ± SD of clustered β1 integrin mean fluorescence intensity (MFI) from 3 independent experiments. The p value is shown (Student's t-test). (**C**) Immunodetection of total integrin β1 levels by Western blotting on total extracts from HUVECs transfected with control or Rasa3 siRNA. GAPDH was used as a loading control.

5. Rasa3 is required for normal adhesion turnover

We then wanted to understand how Rasa3-depleted cells adhered more to the substrate. Cell-ECM adhesions found at membrane protrusions are usually divided into two types, depending on their maturation stage. The first adhesions to appear are nascent adhesions (NA) and focal complexes (Fx), which are highly unstable small dot-like structures that form at the lamellipodium and lamellipodium-lamellum interface. While most of the Fx are unstable, a few elongate centripetally and mature into larger (area > 1μm^2) focal adhesions (FAs) connected to actin filaments (F-Actin). We analyzed focal adhesions with immunofluorescence, using paxillin as a specific marker of adhesions.

Knockdown of Rasa3 resulted in profound alterations in the pattern of EC-ECM adhesions. As demonstrated in **Figure 35A**, Rasa3-depleted cells spread onto fibronectin displayed a higher proportion of large FAs, which were localized more centripetally, whereas the number of small adhesions at the cell periphery was notably reduced. Different quantification methods were used in order to confirm these alterations. First, we analyzed the average size of all adhesions and observed that this number was higher in the siRasa3 HUVECs (**Figure 35B**).

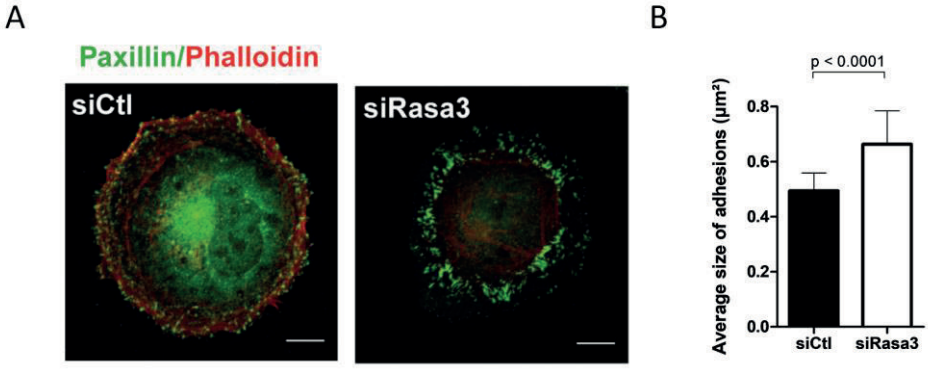

Figure 35: Rasa3 inactivation results in an accumulation of mature focal adhesions (FAs) in Fibronectin-plated HUVECs. (**A**) Adhesions were analyzed by confocal microscopy in Fibronectin-plated HUVECs transfected with siControl or siRasa3 using an anti-Paxillin antibody (green). F-actin was visualized using Phalloidin (red). Representative images are shown. Bars = 10µm. (**B**) Histogram represent the average sizes of all adhesions in 35 siControl- and 33 siRasa3-treated cells. The p values are shown (Student's t-test).

We then created size categories for adhesions: small (0.2-0.5 μm^2), medium (0.5-1 μm^2) and large (>1 μm^2). We showed that depletion of Rasa3 resulted in an increase in large adhesions and a decrease in small adhesions compared to control cells (**Figure 35C**). Finally, in order to determine whether large FAs were closer to the center, a ratio was established (*Figure C in Annex 1 for method*). This ratio consisted of the measure of the distance of all adhesions > 1 μm^2 from the center of the cell to the adhesion divided by the distance of all adhesions > 1 μm^2 from the cell center to the cell periphery (**Figure 35D**). This ratio is smaller in Rasa3-depleted cells meaning that adhesions are closer to the center and then more mature.

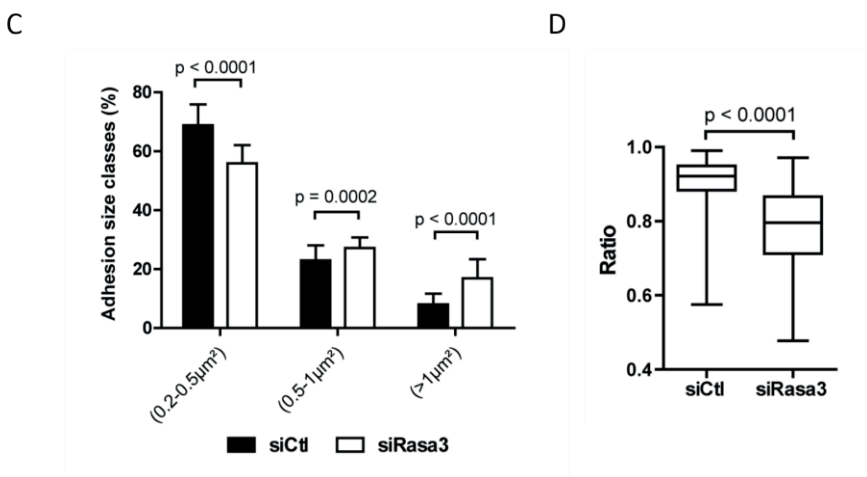

Figure 35: Rasa3 inactivation results in an accumulation of mature focal adhesions (FAs) in Fibronectin-plated HUVECs (*rest*). (**C**) Histograms represent size distributions of paxillin-positive adhesions in 35 siControl- and 33 siRasa3-treateds cells. Adhesions were classified into three size categories: (0.2-0.5 μm^2), (0.5-1 μm^2) and (>1 μm^2). The p values are shown (Student's t-test). (**D**) Quantification of the ratio of the distance between the cell center and the mature focal adhesion (>1 μm^2) versus the distance between the cell center and the cell periphery (n = 244 and n = 343 for siCtl and siRasa3, respectively). The p value is shown (Student's t-test).

We performed the same experiment during VEGF-driven migration of ECs (which also involves activation of the integrin signaling pathway). Interestingly, depletion of Rasa3 again promoted accumulation of larger and more mature adhesions (**Figure 36A**). Here again we analyzed the average size of all the adhesions (**Figure 36B**) and created size categories in order to analyze proportions (**Figure 36C**).

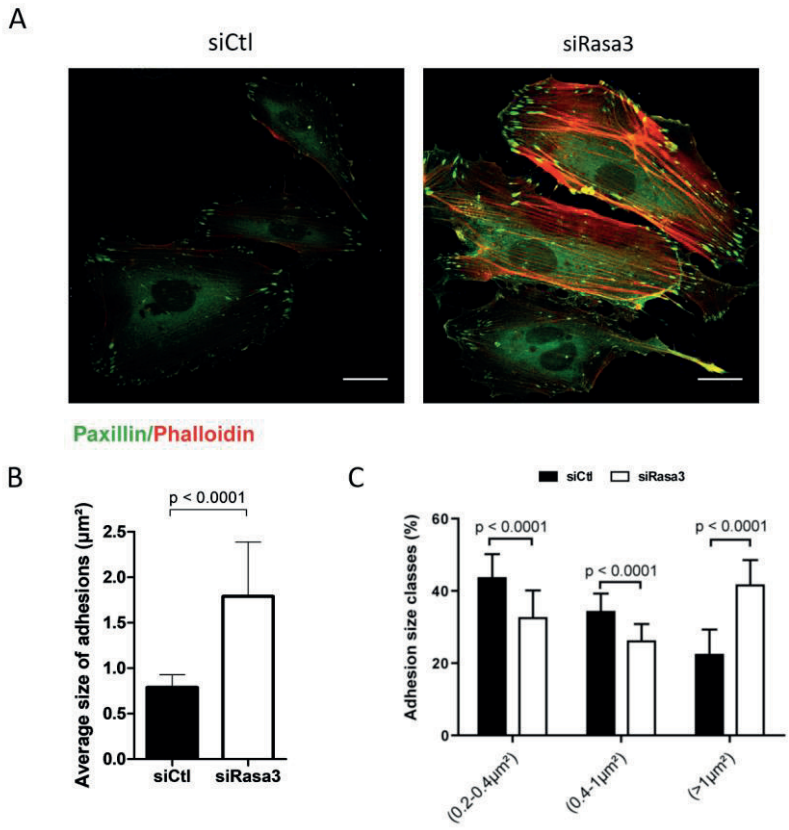

Figure 36: Rasa3 inactivation results in an accumulation of mature focal adhesions (FAs) in VEGF-treated HUVECs. (**A**) Adhesions were analyzed by confocal microscopy in VEGF-treated HUVECs transfected with siControl or siRasa3 using an anti-Paxillin antibody (green). Representative images are shown. Bars = 25µm. (**B**) Histogram represent the average size of all the adhesions in 21 siControl and 23 siRasa3-treated cells. The p values are shown (Student's t-test). (**C**) Histograms represent size distribution of paxillin-positive adhesions in 21 siControl- and 23 siRasa3-treated cells. Adhesions were classified into three size categories: (0.2-0.4 μm^2), (0.4-1 μm^2) and (>1 μm^2). The p values are shown (Student's t-test).

Deletion of Rasa3 results in an accumulation of larger FAs, indicating a potential defect in adhesion turnover. To analyze precisely the dynamics of adhesion assembly and disassembly during EC migration, we performed total internal reflection fluorescence microscopy on migrating GFP-paxillin positive HUVECs and acquired GFP-paxillin signals at 120 second intervals over 10 hours. We focused our analysis on FAs maturing just below the lamella, which appeared both larger and longer lived in siRasa3 cells (**Figure 37A**). We measured changes in Paxillin-GFP over time to evaluate assembly and disassembly, and we determined parameters of FA dynamics as described in *Methods section*. The red and green lines in **Figure 37B** are respectively a logistic fit of the assembly and an exponential fit of the adhesion experiment shown. Adhesion lifetimes were defined by fluorescence intensity above the half-maximum of the fit (**Figure 37B**). Assembly and disassembly rates of FA were significantly decreased in siRasa3 HUVECs. As a result, FA lifetime was increased about twofold in the absence of Rasa3 (**Figure 37C**).

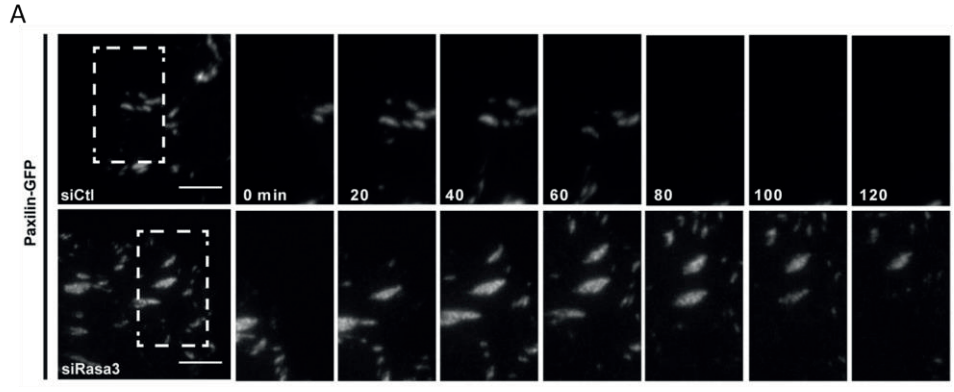

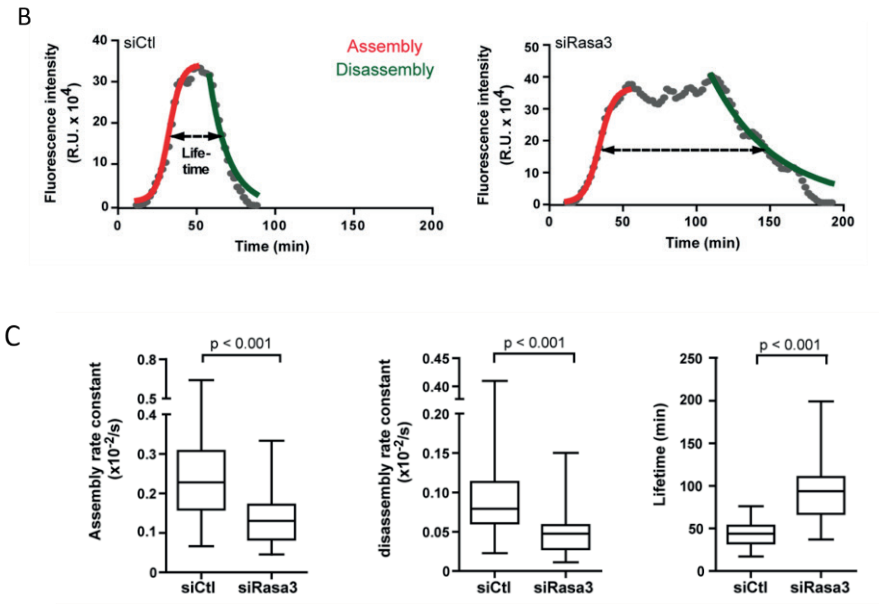

Figure 37: Rasa3 is required for normal adhesion turnover. (**A**) Time-lapse sequences of paxillin-GFP dynamics in migrating HUVECs transfected with control or Rasa3 siRNA. (**B**) Graphs represent turnover dynamics in one representative adhesion experiment in control and Rasa3-depleted cells. Maximum intensity projections over the 200 minutes time-lapse sequences are shown as three-frame running averages. The red and green lines are respectively a logistic fit of the assembly and an exponential fit of the disassembly phase. Adhesion lifetimes are indicated by dashed arrows and defined by fluorescence intensity above the half-maximum of the fit. In the adhesion experiment shown, assembly (0.0041/s in control versus 0.0033/s in Rasa3-depleted cells) and disassembly (0.0010/s in control versus 0.0004/s in Rasa3-depleted cells) rate constants were decreased in Rasa3-depleted cells, as compared with control cells. A lag between the assembly and the disassembly was only observed in Rasa3-depleted cells. FA lifetime was increased in Rasa3-depleted cells (105 minutes) compared to control cells (32 minutes) (**C**) Analysis of adhesion assembly rates, disassembly rates and lifetimes in 35 and 34 adhesions from control and Rasa3-depleted migrating HUVECs, respectively. The p values are shown (Wilcoxon – Mann Whitney test).

Altogether, our data demonstrate that Rasa3 is important to regulate EC-ECM adhesion dynamics and stability. The accumulation of mature FAs in Rasa3-depleted cells results from a decrease of assembly and disassembly rates leading to a stronger adhesion of the cells to the substrate, affecting the angiogenic properties of the cells.

6. Depletion of Rasa3 impairs activation of the FAK-Src complex.

We then decided to look at signaling pathways that could explain the different defects that we observed. We focused our attention on the activation of the FAK-Src complex, whose activation is triggered by cell adhesion to a substrate. By initiating local tyrosine phosphorylation events, the FAK-Src signaling module is a master regulator of adhesion dynamics. This prompted us to investigate FAK/Src signaling in siRasa3 HUVECs. In agreement with decreased turnover of adhesion dynamics, we observed that reduction of Rasa3 expression was associated with diminished activation of FAK and Src following HUVEC adhesion onto fibronectin (**Figure 38A**). Supporting these observations, knockdown of Rasa3 was correlated with reduced phosphorylation of the downstream FAK/SRC targets paxillin and ERK (**Figure 38B**).

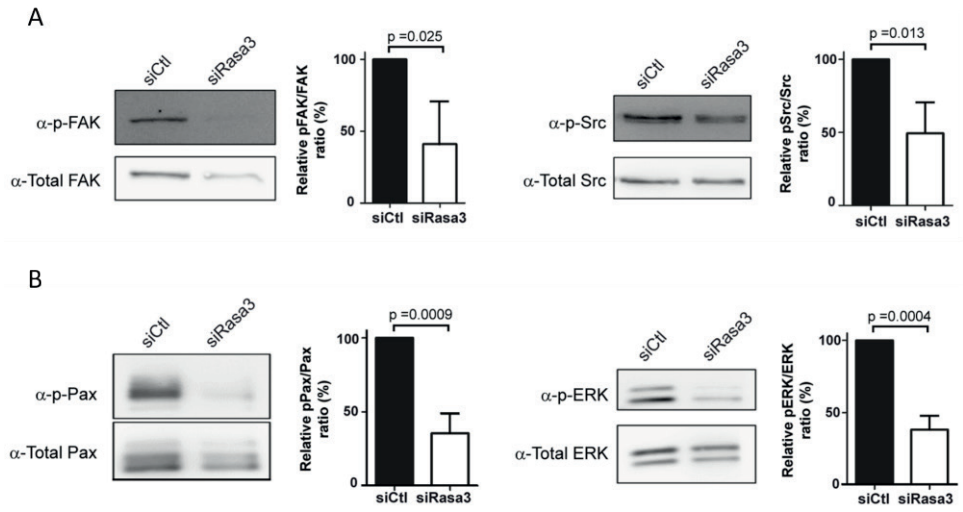

Figure 38: Rasa3 depletion impairs activation of FAK-Src complex in Fibronectin-plated HUVECs. (**A**) Detection of FAK and Src phosphorylation levels in lysates from fibronectin-plated siControl- and siRasa3-transfected cells by western blotting. Total FAK and Src levels respectively were used as controls. Quantifications are shown as the ratio of phospho-specific signal to total protein signal, relative to control HUVECs. (**B**) Detection of ERK and Paxillin phosphorylation levels in lysates from fibronectin-plated siControl- and siRasa3-transfected cells by western blotting. Total ERK and Paxillin levels respectively were used as controls. Quantifications are shown as the ratio of phosphor-specific signal to total protein signal, relative to control HUVECs. (**A**) and (**B**) Results are expressed as means ± SD from 3 independent experiments. The p value are shown (One sample t test).

We previously showed that Rasa3 depletion lead to an accumulation of mature FAs following adhesion onto fibronectin but also following VEGF stimulation (**Figure 36A**). We also investigated FAK/Src signaling in siRasa3 HUVECs following VEGF stimulation. Here again, we observed a complete downregulation of FAK/Src complex activation (**Figure 39A**) as well as the FAK/Src targets phosphorylated paxillin and ERK (**Figure 39B**).

Importantly, impaired FAK activation was also observed in ECs of aortic ring sprouts from tamoxifen-treated $R3^{f/f}$ iEC-Cre mice (*Figure D in Annex 1*).

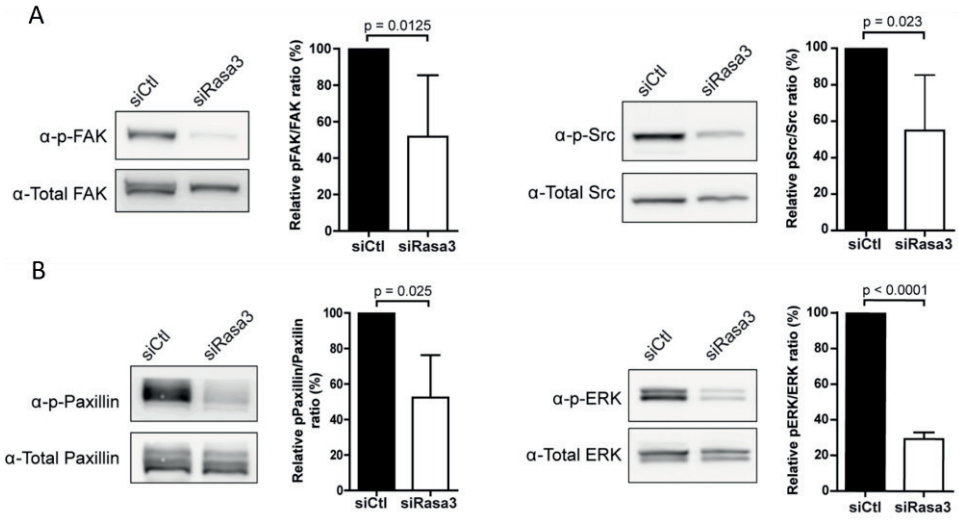

Figure 39: Rasa3 depletion impairs activation of the FAK-Src complex in VEGF-treated HUVECs. (**A**) Detection of FAK and Src phosphorylation levels in lysates from VEGF-treated siControl- and siRasa3-transfected cells by western blotting. Total FAK and Src levels respectively were used as controls. Quantifications are shown as the ratio of phospho-specific signal to total protein signal, relative to control HUVECs. (**B**) Detection of ERK and Paxillin phosphorylation levels in lysates from fibronectin-plated siControl- and siRasa3-transfected cells by western blotting. Total ERK and Paxillin levels respectively were used as controls. Quantifications are shown as the ratio of phosphor-specific signal to total protein signal, relative to control HUVECs. (**A**) and (**B**) Results are expressed as means ± SD from at least 3 independent experiments. The p values are shown (Student's t-test).

7. Rasa3 regulates EC cytoskeleton plasticity

In addition to dynamic contacts with the underlying ECM, lumen morphogenesis also requires profound plasticity of the EC cytoskeleton, in order to support cell shape changes associated with expansion of the luminal compartment [203]. Tubulin acetylation is an indicator of stabilized microtubules. We observed in siRasa3 HUVECs plated onto fibronectin compared to control cells a significant decrease in tubulin acetylation, indicating that Rasa3 depletion correlates with destabilized microtubules (**Figure 40A**). In addition, we observed an increase in the level of actin stress fibers (**Figure 40B**), which are known to suppress acetylation. Because a decrease in tubulin acetylation and an increase in polymerized actin stress fibers may indicate increased actomyosin contractility, we examined nonmuscle myosin IIA activity. We found that cells lacking Rasa3 displayed a higher level of phosphorylated MLCII (**Figure 40C**). Moreover, decreased tubulin acetylation and increased stress fibers were observed in sprouts from R3f/f iEC-Cre mouse aortic explants (*Figure 5D in Annex 2*), supporting the idea that Rasa3 is important for EC cytoskeleton architecture.

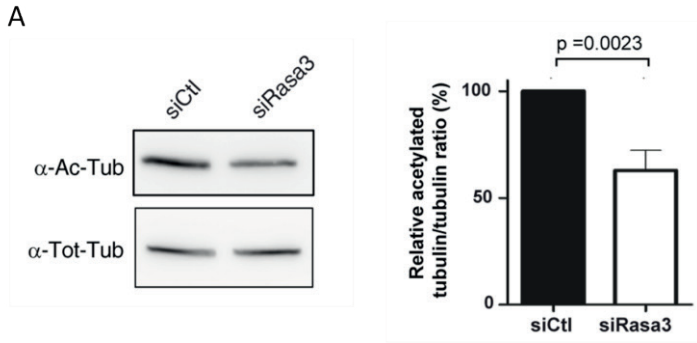

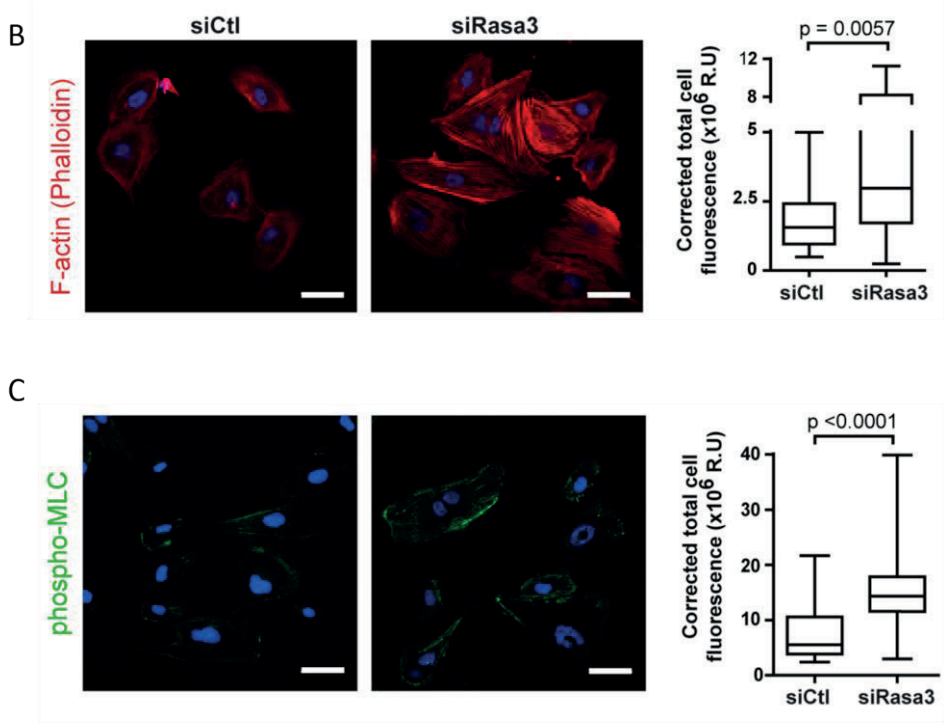

Figure 40: Rasa3 controls EC cytoskeleton plasticity. (**A**) Detection of tubulin acetylation levels in lysates from fibronectin-plated siControl- and siRasa3-transfected cells by western blotting. Total tubulin (Tot-tub) levels were used as control. Tubulin acetylation was quantified (lower) as the ratio of acetylated tubulin signal to the total tubulin signal, relative to control HUVECs. Results are expressed as mean ± SD from 3 independent experiments. The p value is shown (One sample t-test) (**B**) and (**C**) Representative confocal microscopy images of control (siCtl) and Rasa3-depleted (siRasa3) HUVECs plated on fibronectin and stained for F-actin (phalloïdin; red) (**B**) and phospho-MLC (Green) (**C**). Nuclei are stained with Hoechst (blue). Bars are 50µm. Quantifications of F-actin and phospho-MLC signals were performed on 26 cells from 3 independent experiments and are expressed as corrected mean fluorescence intensities (MFI). Results are expressed as mean ± SD from 3 independent experiments. The p value are shown (Student's t-test).

8. Rasa3 depletion resulted in Rap1 hyperactivation

Rasa3 is a dual GAP acting on both Rap1 and Ras small GTPases. Recent findings showed that Rasa3 controls Rap1 but not Ras activation in megakaryocytes [183] [184]. On the contrary, Blanc identified a missense mutation (G125V) in the RASA3 gene of *scat* mice that leads to a mislocalization in the cytosol of RASA3 protein and is associated with an increase in active Ras. We assessed the levels of these active small GTPases in ECs lacking Rasa3. Decreasing Rasa3 expression in HUVECs significantly increased active Rap1 levels (**Figure 41A**), but had no effect on Ras levels (**Figure 41B**).

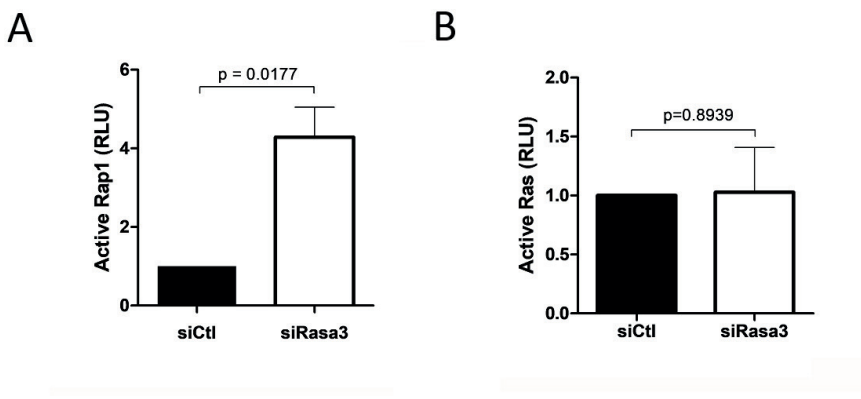

Figure 41: Rap1 is activated upon depletion of Rasa3. (**A**) The densitometric quantification of active Rap1 detected by western blotting on protein extracts from siControl and siRasa3 HUVECs is expressed as mean ± SD from 3 independent experiments. RLU: Relative Luminescence Unit. The p value is shown (One sample t-test). (**B**) The densitometric quantification of active Ras detected by western blotting on protein extracts from siControl and siRasa3 HUVECs is expressed as means ± SD from 3 independent experiments. RLU: Relative Luminescence Unit. The p value is shown (One sample t-test).

These observations were also confirmed *in vivo* in mice expressing a catalytically inactive form of Rasa3 specifically in the endothelial cells. Arteries, veins and plexus of $R3^{f/f}$ iEC-Cre retina displayed dramatically higher levels of active Rap1. Moreover, analysis of aortic sprouts from R3f/f and R3f/f iEC-Cre aortic explants also showed that deletion of Rasa3 was correlated with significantly higher levels of active GTP-bound Rap1 (*Figure 6B in Annex 2*).

9. Rasa3 depletion stabilizes endothelial VE-cadherin-based cell-cell junctions.

Rap1 is involved in the activation of β1-integrins in ECs and plays a key role in integrin-dependent angiogenic functions of ECs such as sprouting, migration and adhesion [149], all of which are affected by Rasa3 depletion in ECs. In addition, Rap1 is known to promote stability of endothelial VE-cadherin-based cell-cell junctions [69]. ECs display two types of VE-cadherin containing junctions [204]. Junctions of the first type localize linearly along cell-cell borders and are considered stable adherens junctions (AJs). Junctions of the second type appear as short linear structures that are almost orthogonal to the cell-cell borders and are remodeling junctions called focal AJs (FAJs). The impact of Rasa3 depletion on proportions of VE-cadherin-containing junctions was evaluated using a specific VE-cadherin antibody by immunofluorescence (**Figure 42A**). Quantification of the total length of FAJs in single cells relative to the total junction length revealed that siRasa3 HUVECs had a reduced proportion of FAJs, indicating that cell-cell junctions are more stable when Rasa3 is knocked down, consistent with increased Rap1 activity (**Figure 42B**).

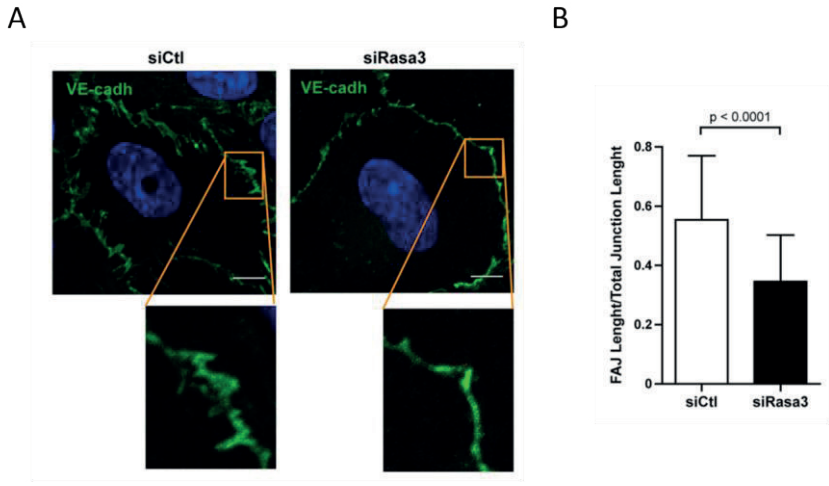

Figure 42: Inactivation of Rasa3 increases stability of VE-Cadherin-based cell-cell junctions. (**A**). Effect of Rasa3-silencing on endothelial cell junctions. Adherent junctions were analyzed by confocal microscopy in HUVECs transfected with siControl or siRasa3 using an anti-VE-cadherin antibody (green). Representative images are shown. Bars = 10 µm. (**B**) Histograms are mean ratio of FAJ length to total junction length per cell. Results are from 30 cells. The p value is shown (Student's t-test).

In line with this, we evaluated the stability of cell-cell junctions after treatment with EGTA, a destabilizing agent that acts by chelating calcium. To do so, siControl and siRasa HUVECs were seeded on coverslips followed the next day by 5 minutes of EGTA treatment. Immunofluorescence was performed using anti-VE-cadherin antibody. We observed that junctions of Rasa3-knockdown HUVECs were more resistant to the cell-cell junction-destabilizing agent EGTA than those of control cells (**Figure 43**). Whereas VE-cadherin was completely internalized in control cells after 5 minutes of EGTA treatment, it was still partially localized at the cell membrane in siRasa3 HUVECs, indicating more resilient cell-cell junctions.

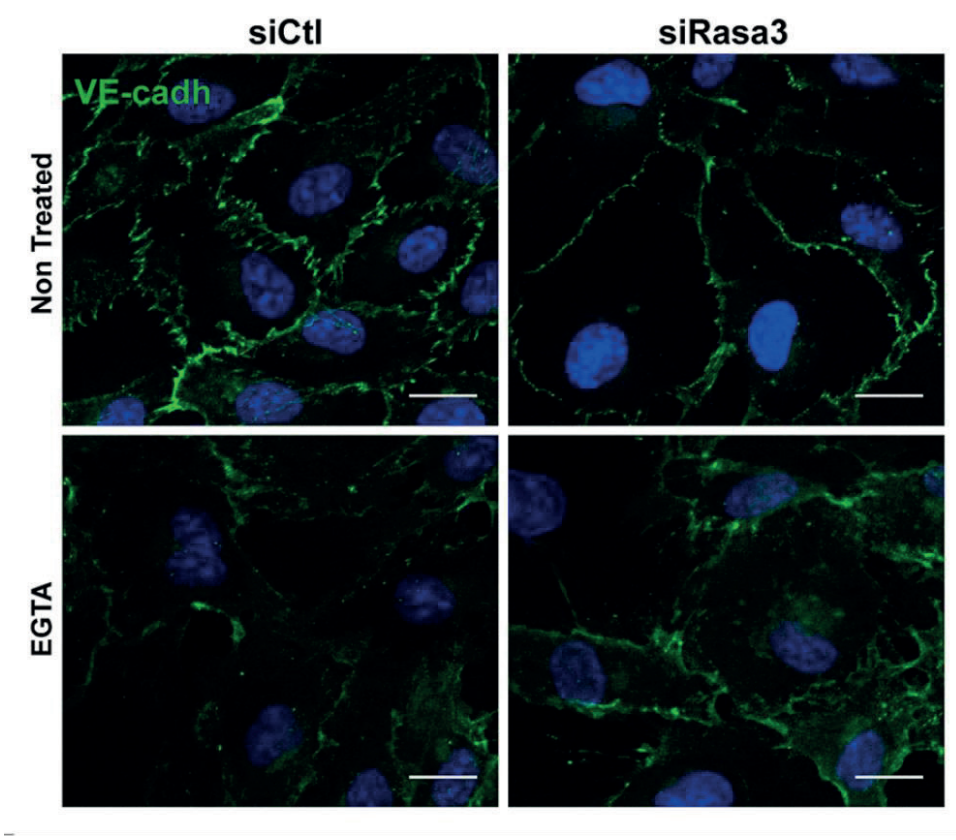

Figure 43: Inactivation of Rasa3 increases stability of VE-Cadherin-based cell-cell junctions after EGTA treatment. VE-cadherin internalization was analyzed by confocal microscopy using an anti-VE-cadherin antibody (green) in control and Rasa3-depleted cells after an EGTA treatment (4 mM). Bars = 50µm

To reinforce the idea that cell-cell junctions are more stable in Rasa3-deficient HUVECs, we performed an EGTA-induced vascular permeability assay by assessing solute flux across an EC monolayer. Briefly, an insert was placed in a 24-well plate defining a top and a bottom chamber. The test is based on the capacity of FITC-Dextran (a fluorescent molecule) to pass from the top to the bottom chamber through a confluent monolayer of HUVECs, depleted or not for Rasa3. We observed that after EGTA

treatment, vascular permeability is reduced when Rasa3 is knocked down, validating a higher stability for these junctions (**Figure 44**). No significant differences were observed in absence of EGTA treatment between the 2 conditions.

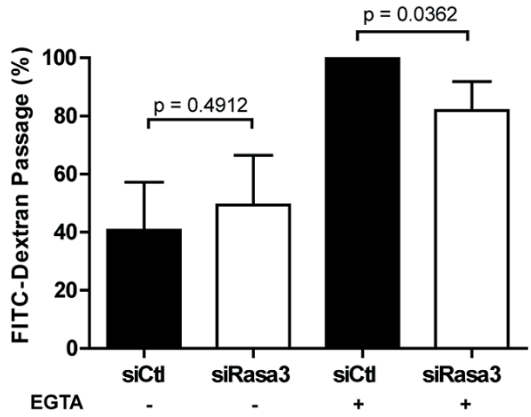

Figure 44: Rasa3 inactivation is associated with a decrease of permeability. Effect of Rasa3-silencing on endothelial permeability after an EGTA treatment (4 mM). Results are mean quantification of FITC-dextran ± SD from 4 independent experiments and relative to EGTA-treated control cells. The p values are shown (non-treated cells: Student's t-test; EGTA-treated cells: One sample test).

VE-cadherin interaction with p120 prevents internalization and degradation of VE-cadherin. VE-cadherin can be phosphorylated on different residues and phosphorylation on the residue tyrosine 658 disrupts the interaction with p120, leading to its internalization. Moreover it has been shown that the phosphorylation of this residue (Y658) is mediated by Src. Through phosphorylation of VE-Cadherin, Src has emerged as a prominent mediator of VE-cadherin-mediated AJ destabilization and vascular permeability [62].

We previously showed (**Figure 38A**) that reduction of Rasa3 expression was associated with diminished activation of FAK and Src following HUVEC adhesion onto fibronectin or VEGF treatment. Consistent with our previous observations of their more stable cell-cell junctions, siRasa3 HUVECs showed reduced phosphorylation of VE-cadherin Y658 and Src activation (**Figure 45A and 45B**).

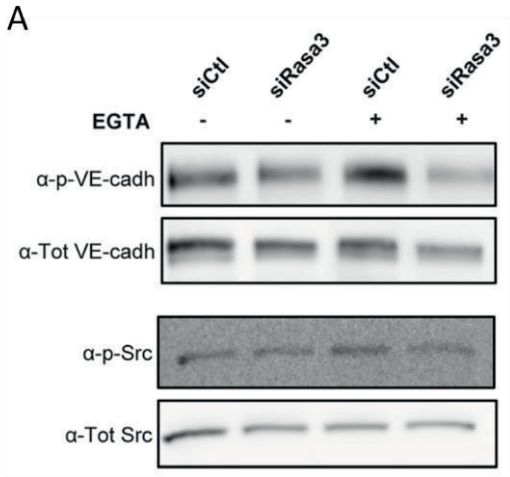

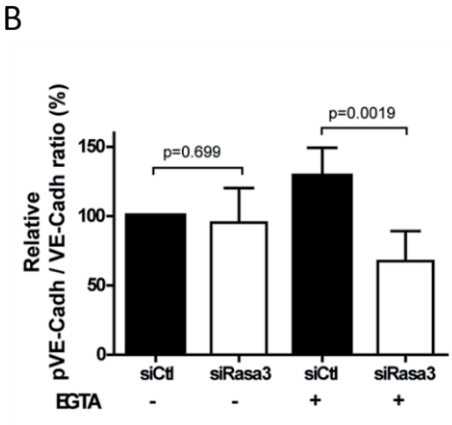

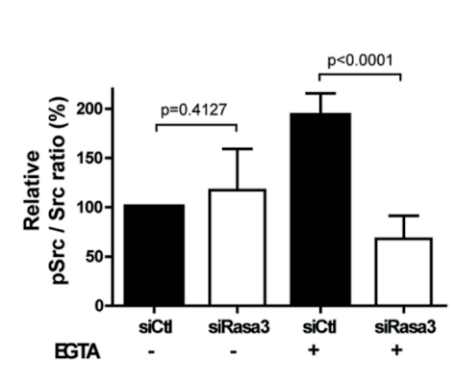

Figure 45: Rasa3 inactivation reduces VE-cadherin internalization. (**A**) Detection of VE-cadherin and Src phosphorylation levels in total lysates from non-treated and EGTA-treated siControl- and siRasa3-transfected cells by western blotting with phospho-specific antibodies. Total VE-cadherin and Src levels respectively were used as controls. (**B**) Histograms consist in the ratio of phosphorylated protein signal to the total protein signal, relative to control HUVECs. Results are expressed as means ± SD from 4 independent experiments. The p values are shown (non-treated cells: One sample t-test; EGTA-treated cells: Student's t-test).

Altogether, these results revealed that Rasa3 depletion increases cell-cell junctions' stability due to an accumulation of VE-cadherin at the cell membrane, resulting from a decrease of phosphorylation by Src that prevents its internalization.

10. Inactivation of Rap1 rescues the Rasa3-depleted phenotypes

We previously showed that decreasing Rasa3 expression in HUVECs significantly increased active Rap1 levels but had no effect on R-Ras levels. In order to test whether suppression of Rap1 by Rasa3 played a role during EC lumen formation, we inhibited Rap1 activity in siRasa3 HUVECs.

Rap1 membrane localization where it is active results from a posttranslational modification mediated by the geranylgeranyltransferase enzyme. This enzyme is inhibited by the Rap1 inhibitor GGTI298, which does not affect the activity of R-Ras (The other target of Rasa3). Using the Rap1 inhibitor GGTI298, the tubulogenesis defects of siRasa3 HUVECs were completely reverted (**Figure 46A**).

Even if GGTI298 is considered a specific inhibitor of Rap1 by the scientific community, as mentioned above, this inhibitor inhibits the geranylgeranyltransferase enzyme. To further validate our results, we prevented Rap1 hyperactivation with siRNAs. Rap1 possesses 2 isoforms, Rap1a and Rap1b, both independently targetable using specific siRNAs.

The efficiency of siRNAs was checked by RT-qPCR. We observed that expression of Rap1a and Rap1b mRNA were reduced after transfection with siRNAs targeting Rap1a and Rap1b respectively (**Figure 46B**).

We then performed the tubulogenesis assay after preventing Rap1 hyperactivation using suboptimal concentrations of either Rap1a or Rap1b siRNAs. Neither siRap1a nor siRap1b alone had an effect on *in vitro* tubulogenesis of control HUVECs. However, siRap1b, but not siRap1a, almost completely rescued the tubulogenesis defects in Rasa3 deficient HUVECs (**Figure 46C**).

Representative images from Figure 46A and 46C are shown in Figure E and F respectively in Annex 1.

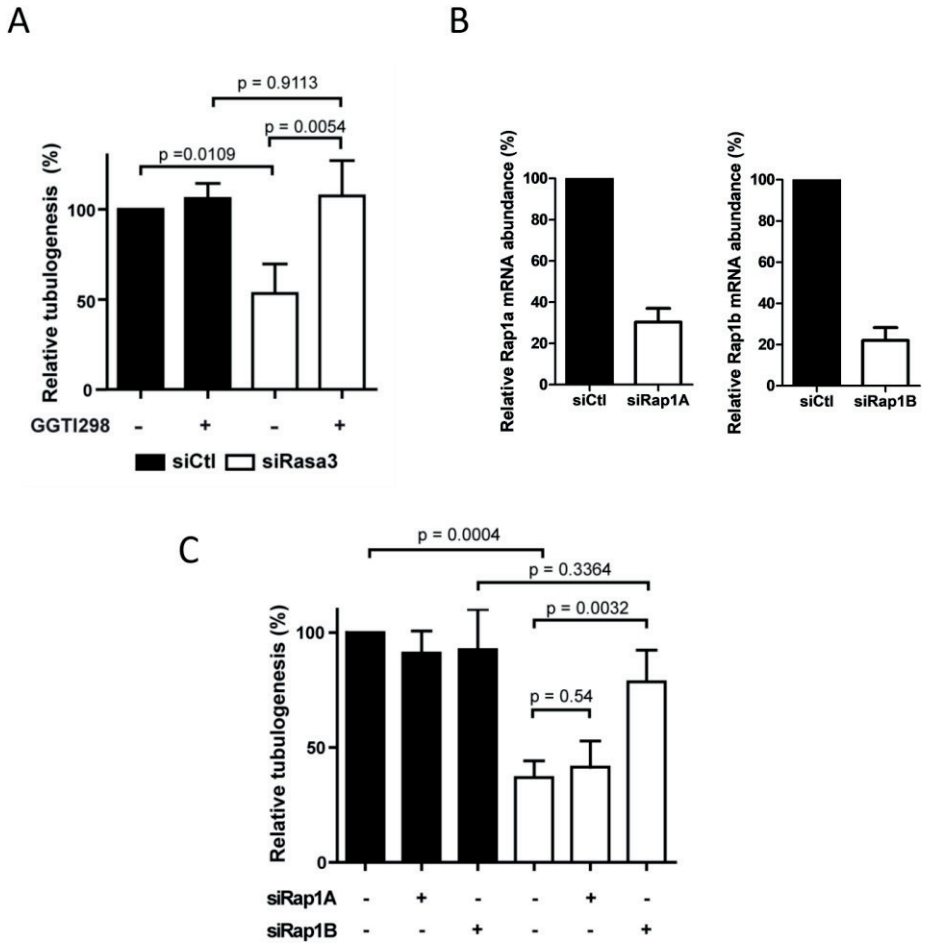

Figure 46: Inactivation of Rap1 rescues the Rasa3-depleted phenotypes. (**A**) Quantification of capillary-like network formation in siControl vs siRasa3 HUVECs treated or not with GGTI298 (10 µM). Results are expressed as mean ± SD cumulative length of capillary-like structures measured in 5 different fields per experiment from 3 independent experiments, relative to non-treated siControl HUVECs. The p value are shown (Student's t-test). (**B**) HUVECs were transfected with siRNA targeting Rap1A, Rap1B or non-related siRNA (siCtl). Seventy-two hours after transfection, RNA and protein were extracted and analyzed by RT-qPCR. GAPDH was used as an internal control. (**C**) Quantification of capillary-like

network formation in siControl vs siRasa3 HUVECs co-transfected with siRap1A, siRap1B or a second control siRNA. Results are expressed as mean ± SD cumulative length of capillary-like structures measured in 5 different fields per experiment from 3 independent experiments, relative to double siControl HUVECs. The p values are shown (Student's t-test).

We were also able to partially rescue the migration delay observed with Rasa3-depleted cells by using the Rap1 inhibitor GGTI298 (**Figure 46D**). Rescue experiments were also performed *in vivo* in zebrafish. We showed that inactivation of Rasa3 by a specific morpholino targeting Rasa3 in zebrafish altered ISV lumenization (**Figure 31A**). In line with this, Control and Rasa3 morphant embryos were treated with Rap1 inhibitor GGTI298 from 40hpf until 48hpf and the same quantifications as in **Figure 31B** were made. The lumen defects were partially rescued in the presence of the Rap1 inhibitor (**Figure 46E**).

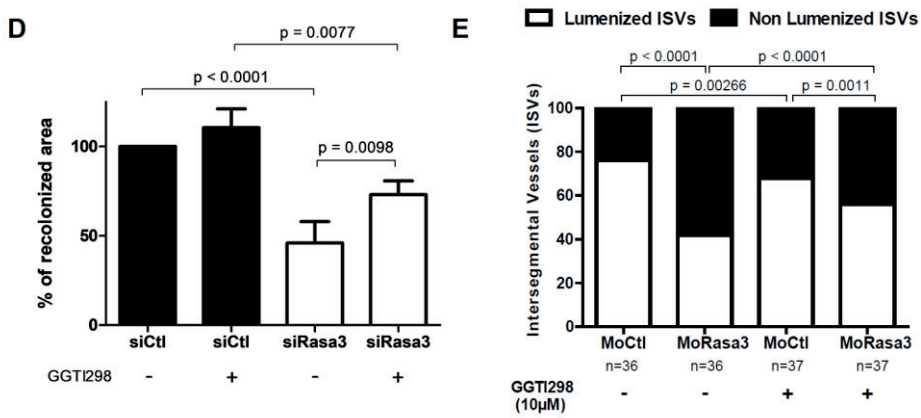

Figure 46: Inactivation of Rap1 rescues the Rasa3-depleted phenotypes (rest**).** (**D**) In a scratch-wound migration assay, the recolonized area was analyzed at 8 hours in HUVECs transfected with siControl or siRasa3 and treated or not with GGTI298 (10 µM). The mean ± SD of 3 independent experiments are presented, relative to the siControl condition. The p values are shown (One sample t-test). (**E**)

Rescue experiment using GGTI298 (10 μM). Quantification of lumenized ISVs in Ctl and Rasa3 morphant embryos at 48hpf. Results are mean from 10 ISVs/embryo in 35 embryos. The p values are shown (Fisher's exact test).

Moreover, Rap1 inhibition by treatment with GGTI298 increased by almost three-fold the number of sprouts from $R3^{f/f}$ iEC-Cre aortic explants, while it dramatically reduced the sprouting ability of control $R3^{f/f}$ aortic rings (*Figure 7B in Annex 2*).

The majority of the results presented above were published in January 2018 in the journal PLoS Genetics.

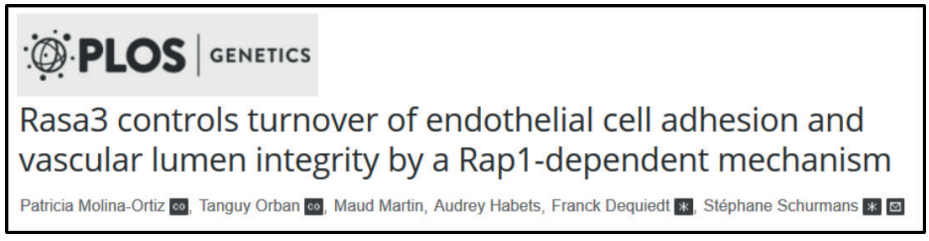
PLOS GENETICS

Rasa3 controls turnover of endothelial cell adhesion and vascular lumen integrity by a Rap1-dependent mechanism

Patricia Molina-Ortiz, Tanguy Orban, Maud Martin, Audrey Habets, Franck Dequiedt, Stéphane Schurmans

11. Endothelial depletion of Rasa3 increases EC-Pericyte interactions

While characterizing blood vessels in $R3^{f/f}$ iEC-Cre mouse retinas, Patricia Molina Ortiz noticed that surrounding pericytes often display an altered morphology. Because pericytes are known to participate in vessel stability, she investigated this phenotype further. Alterations of pericyte morphology were evidenced in $R3^{f/f}$ iEC-Cre mouse retinas by rounder nuclei, suggesting a decrease in pericyte spreading over the abluminal surface of the vessels (*Figure G left in Annex 1*). Supporting this, the relative contact area between pericytes and arterial endothelial cells was significantly reduced, whereas the number of pericytes per endothelial cell surface was increased in R3f/f iEC-Cre mouse vessels (*Figure G right in Annex 1*).

Based on these observations, we suspected that adhesion between pericytes and Rasa3-null ECs might be perturbed. To test this, we adapted an *in vitro* assay in which normal pericytes were left adhering for 30 minutes onto a confluent layer of siRasa3-treated HUVECs. After 30 minutes, a higher number of pericytes had attached to the monolayer of Rasa3-depleted ECs, suggesting excessive adhesion between ECs and pericytes (**Figure 47A**).

In order to recapitulate the pericyte spreading defects observed *in vivo* in mice, we adapted the previous assay by letting pericytes adhere for 8 hours on top of a Rasa3-deficient confluent monolayer before performing immunofluorescence. Pericytes left adhering on Rasa3-depleted ECs showed reduced spreading, as indicated by a lower number of branches (**Figure 47B**). Altogether, these observations indicate that Rasa3-deficient

HUVECs exhibit increased heterotypic adhesion properties, which prevent normal spreading and coverage by pericytes.

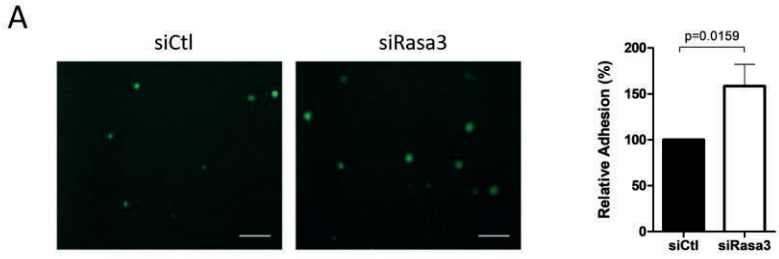

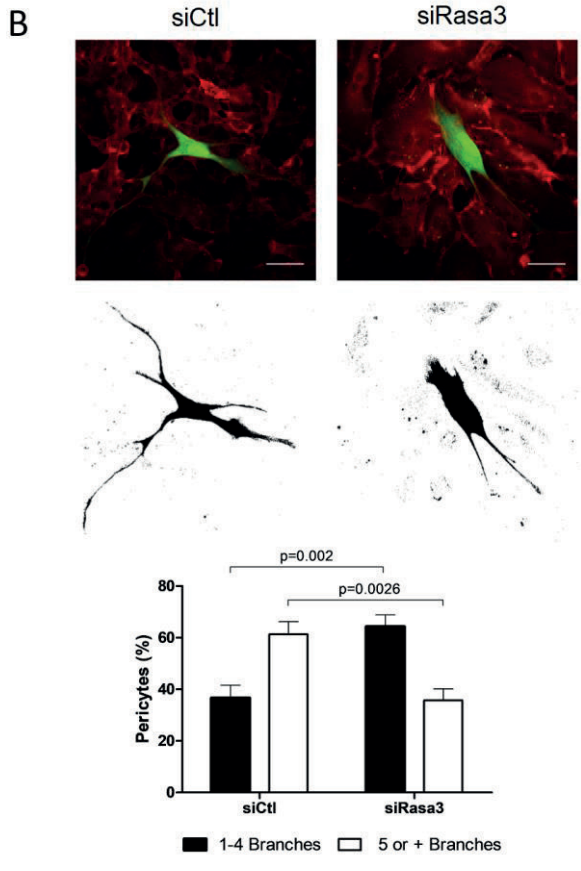

Figure 47: Rasa3 is involved in EC-pericyte interactions. (**A**) Effects of silencing Rasa3 in HUVECs on pericyte adhesion. Representative immunofluorescence images of pericytes labeled with Celltracker (Thermofisher C2925, green) and left to adhere for 30 minutes on a confluent monolayer of siRasa3-treated HUVECs. After washing, attached pericytes were quantified. Bars = 100 µm. Histogram represents mean ± SD of the number of pericytes per image from 7 independent images per experiment from 4 independent experiments. The p value is shown (One sample t-test). (**B**) Representative immunofluorescence images (upper) of pericytes labeled with Celltracker and spread 8 hours on a confluent monolayer of siRasa3-treated HUVECs, labeled with anti-CD31 antibody (red). Binary cell masks (lower) were analyzed with ImageJ. Quantification of pericyte spreading is shown as mean ± SD (histogram) of pericytes (n=300) with 1-4 or >5 branches from 3 independent experiments. The p value are shown (Student's t-test).

HUVECs express VE-cadherin and N-cadherin, two members of the superfamily of cadherins. VE-cadherin is endothelial specific, but N-cadherin is expressed in different cell types and is the cadherin predominantly expressed in vascular smooth muscle cells (VSMC) and pericytes. Currently, a model suggests that VE-cadherin mediates homotypic adhesion between endothelial cells, while N-Cadherin mediates contact between endothelial cells and mural cells (pericytes) [77,205]. We decided to analyze expression of these two cadherins in Rasa3-depleted cells along with β-catenin.

By western blot analysis, using confluent control and Rasa3-depleted cells, we observed that N-cadherin expression was significantly higher following Rasa3 depletion compared to control cells (**Figure 48A**). On the contrary, no significant differences were observed regarding the expression of VE-cadherin or β-catenin (**Figure 48A**). This experiment was repeated using

non-confluent ECs (“sparse cells”) or confluent cells treated with VEGF. In both cases we obtained the same results, indicating that these observations were not dependent on cell confluency.

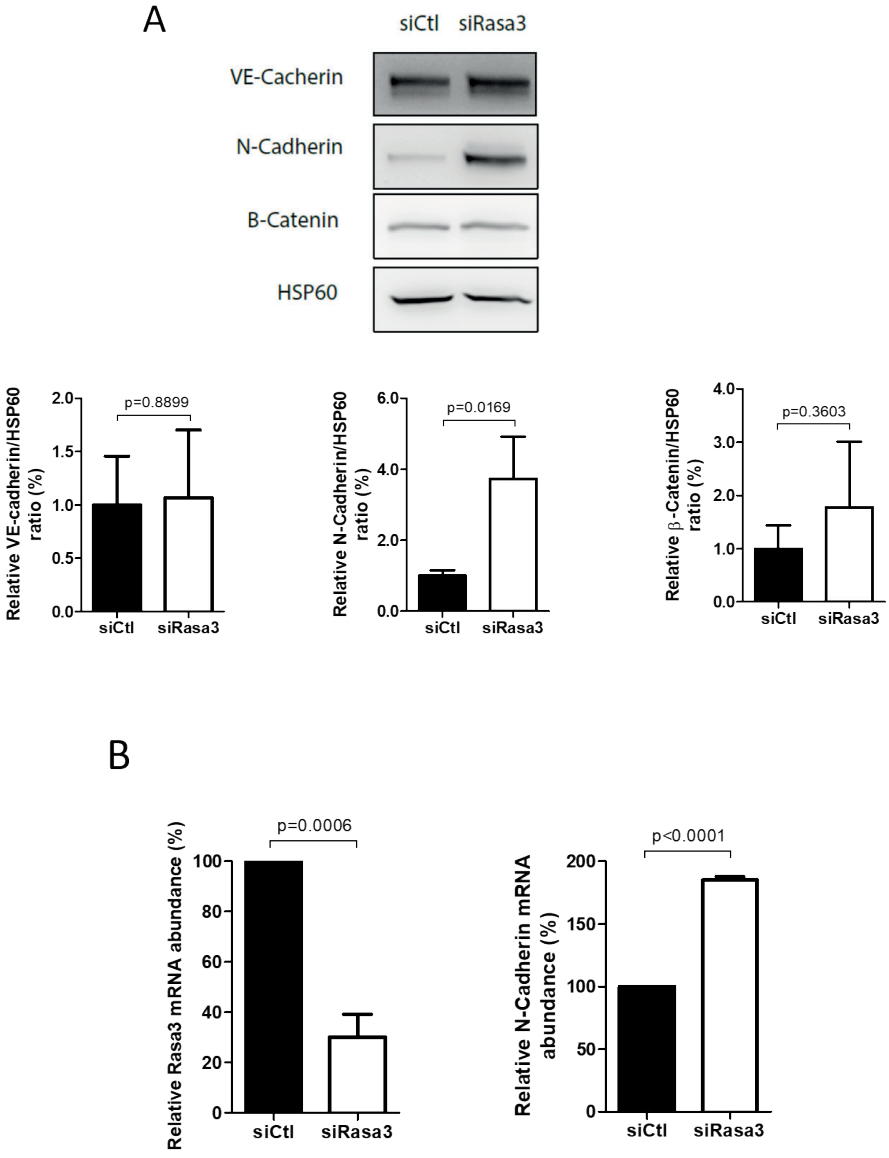

Figure 48: N-cadherin expression is increased upon Rasa3 depletion. (**A**) Detection of N-cadherin, VE-cadherin and β-catenin levels in lysates from confluent siControl- and siRasa3-transfected cells by western blotting. Quantifications are shown as the ratio of specific signal to control protein signal (HSP60), relative to control HUVECs. (**B**) N-cadherin and Rasa3 expression were examined by RT-qPCR using confluent control and siRasa3-transfected HUVECs. GAPDH was used as an internal control.

Higher N-cadherin expression was also observed by RT-qPCR after Rasa3 depletion (**Figure 48B**). Moreover, sprouts from $R3^{f/f}$ iEC-Cre mouse aortic explants also displayed increased N-cadherin (*Figure H in Annex 1*).

Because N-cadherin is a target of β-catenin [77], we hypothesized that increased expression of N-cadherin could be the result of an increase in β-catenin activation. We first analyzed β-catenin localization using cytoplasmic/nuclear fractionation. As represented in **figure 49A**, β-catenin localization was not altered after Rasa3 depletion. Indeed, the same proportion of cytoplasmic and nuclear β-catenin were found in control and Rasa3-depleted cells.

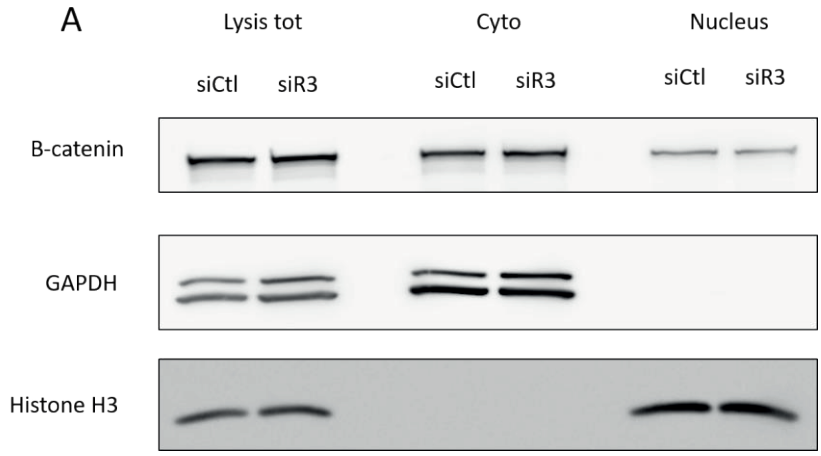

B

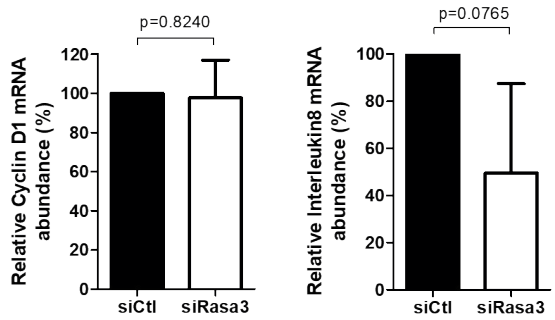

Figure 49: Inactivation of Rasa3 doesn't affect β-catenin localization or expression of β-catenin target genes. (**A**) A cytoplasmic/nuclear lysis was performed on confluent HUVECs transfected with siControl or siRasa3 and β-catenin localization was analyzed by western Blot. GAPDH was used as a specific control of the cytoplasmic fraction while Histone H3 was used as a specific control of the nuclear fraction. (**B**) Expression analysis by RT-qPCR of β-catenin target genes using confluent control or Rasa3-depleted HUVECs.

Moreover, we checked expression of β-catenin target genes by RT-qPCR and no significant differences were observed in Rasa3-depleted cells compared to control cells (**Figure 49B**). These results suggested that the higher N-cadherin expression observed did not result from stronger β-catenin activation.

Discussion & perspectives

Rasa3 controls turnover of endothelial cell adhesion and vascular lumen integrity by a Rap1-dependent mechanism

Different groups have shown that mice expressing inactive mutants of Rasa3 die during mid-embryonic life [171,183,184]. These mice displayed hemorrhages and severe thrombocytopenia resulting from developmental defects during megakaryopoiesis. Because low levels of platelets could potentially explain embryonic bleeding and mortality, Patricia Molina Ortiz generated mice specifically inactivated for Rasa3 in the megakaryocyte lineage. These mice displayed megakaryocyte alterations and severe thrombocytopenia but surprisingly, mice were obtained at Mendelian ratios and were viable even if a reduced lifespan was observed [183].

An independent study conducted by Stefanini and peers reported similar observations. They observed that the hemorrhagic phenotype was much less severe in mice where Rasa3 is specifically inactivated in the megakaryocytes lineage compared to full Rasa3$^{-/-}$ mice. These results suggest that the embryonic bleeding and lethality associated with Rasa3 inactivation might be related to its function in a cell compartment different from megakaryocyte lineage [184].

Patricia Molina Ortis generated mice with specific deletion of Rasa3 in endothelial cells. These mice recapitulate exactly the phenotype observed in full Rasa3$^{-/-}$ mice indicating that Rasa3 is required during mice embryonic development.

In our study we showed by using a combination of *in vitro* cell biology approaches and loss of function studies in mouse and zebrafish, we identified a key role for Rasa3 in the maintenance of vascular integrity in

vertebrates. The use of zebrafish for analyzing Rasa3 function has been performed already by Blanc et al [172]. They noticed severe thrombocytopenia as it was observed previously in mice. However, the role of Rasa3 in vascular development was not investigated in zebrafish in the study from Blanc et al.

We first showed that Rasa3 protein was expressed in ECs. Rasa3 mRNA and protein expression are rather ubiquitous even if some studies pointed out a highly expression in brain and spleen [169–172].

We analyzed further the importance of Rasa3 in angiogenic processes using *in vitro* (HUVECs) and *in vivo* (zebrafish) models. In both models we observed that a deletion of Rasa3 impaired angiogenic processes validating results observed by Patricia Molina Ortiz in mice expressing a catalytically inactive form of Rasa3. Indeed, in absence of Rasa3, *in vitro* endothelial cells are unable to maintain a vascular-like network (matrigel assay) or forming structures called sprout out of spheroids.

In zebrafish, we focused our attention on ISVs formation and quantified the percentage of lumenized ISVs compared to non-lumenized ISVs in control and Rasa3 morphant embryos using Tg(fli1eGFP)^{y1}. Performing a microangiography, which consists in injecting fluorescent dye (such as dextran) into the sinus venosus, would allow the detection of zebrafish vasculature in order to confirm our lumenization defects. Moreover, analysis of heart rate should be analyzed in unsedated embryos since tricaine has an effect on cardiac rhythm.

Morpholinos are known to have off-target effects on zebrafish embryos development. We should repeat our experiments using a second morpholino. Moreover, rescue experiment should be performed by co-

injecting Rasa3 morpholino with human Rasa3 mRNA which is not affected by the morpholino. In order to exclude potential off-target effects due to the morpholino, Rasa3 knockout fish should be generated using the CRISPR technique [206–208].

It would be interesting to extend our analysis of zebrafish vasculature in Rasa3 morphant embryos. Development of sub-intestinal vessel (SIV) and caudal vein plexus (CVP) are well described in the literature and are easy to analyze using Tg(fli1eGFP)^{y1} [193,194].

The caudal vein plexus (**Figure 50**) is generated by sprouting angiogenesis from the PCV (active angiogenesis). It starts around 26 hpf, angiogenic sprouts from the PCV migrate towards the avascular environment (ventral region of the zebrafish embryo). The primordial vein plexus is formed at 30 hpf and angiogenic rate slows down in this region. The primordial vein plexus continues to mature, remodel and is lumenized by 36 hpf. The CVP is fully formed and functional at 48 hpf. Regarding molecular regulators of CVP formation, unlike ISVs that formation is regulated by VEGF-a, CVP formation is regulated by the bone morphogenetic protein (BMP). BMP activates the small GTPase Cdc42 through Arhgef96 that stimulates Formin-like 3 which in turn promotes filopodia extensions allowing CVP formation [209–211].

The sub-intestinal vessels (**Figure 50**) are responsible for vascularization of digestive system. The formation of these vessels by angiogenesis is still poorly understood. It starts at 32 hpf by ventral sprouting of angioblasts from the PCV. Around 41 hpf, avascular loops are formed resulting from the fusion of adjacent sprouts. SIV plexus is completely formed and functional at 72 hpf. VEGF and BMP signaling have been identified as molecular pathways implicated in SIV formation [201,212].

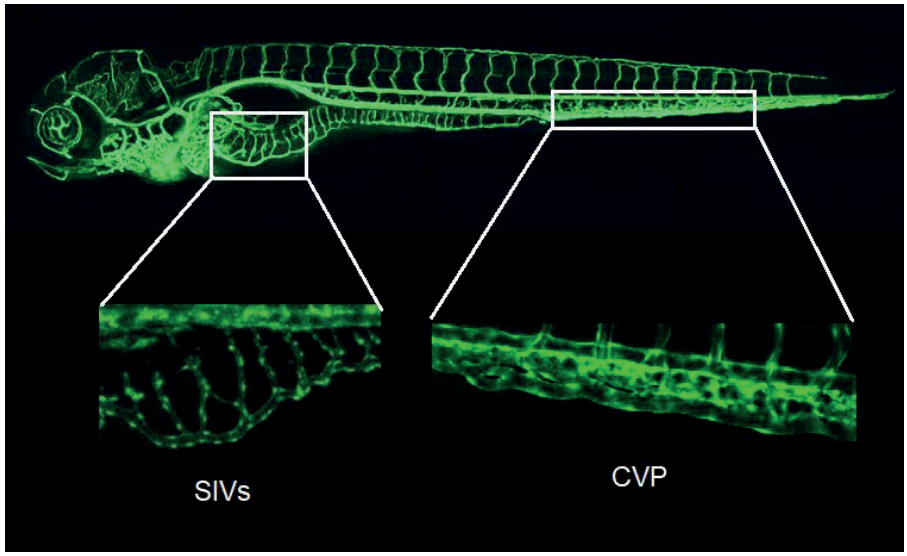

Figure 50: Representation of the caudal vein plexus (CVP) and the sub-intestinal vessels in zebrafish Tg(fli1:EGFP)y1 transgenic line at 72 hpf.

Preliminary results (*Figure I in Annex 1*) revealed that CVP formation was affected in Rasa3 morphant embryos. The process by which lumenization occurs in this structure is still unclear. However, lumenization requires proper migration and adhesion of endothelial cells. CVP alterations observed following Rasa3 depletion using a morpholino are consistent with decreased migration and increased adhesion observed *in vitro* in HUVECs.

The observation of vascular lumen defects in both mice and zebrafish showed that Rasa3 is essential to maintain normal blood vessel tubulogenesis and vascular integrity *in vivo*. Numerous studies have documented that vascular lumen instability or occlusions often lead to hemorrhages and mid-or late gestation embryonic lethality [34,213–215].

Cellular migration and adhesion are key processes required during angiogenesis. Indeed, sprouting angiogenesis requires cytoskeleton remodeling of endothelial cells in order to migrate. Expression of Rasa3 in endothelium is not surprising since it has already been showed that Rasa3 regulates these two processes, migration and adhesion, in megakaryocytes [183]. Reduced migration and increased adhesion were observed in endothelial cells following Rasa3-depletion resulting from accumulation of mature focal adhesions. These results could be indicative of general effect of Rasa3 on migration and adhesion processes.

Using siRNA targeting Rasa3 we showed that Rasa3 implication in angiogenic processes was crucial and that its deletion impacted migration and adhesion properties of endothelial cells. As utilization of siRNAs has been shown to have off-target effect on cells [216], we confirmed our results using a second siRNA targeting Rasa3 and obtained similar results. Only matrigel, spheroid, scratch wound and adhesion assays were performed with the second siRNA. In order to exclude any off-target effects on cells, all experiments should be repeated with the second siRNA.

Rasa3 has the ability to control both Ras and Rap1 smallGTPases in vitro [176]. In vivo, the specificity of Rasa3 towards Ras and Rap1 remains unclear. Scat mice, bearing the G125V mutation in Rasa3 presented increased Ras activity in erythrocytes, which could explain the delayed erythropoiesis phenotype [172]. In megakaryocytes and platelets of mice, Rasa3 deletion leads to upregulation of Rap1 activity without affecting Ras activity [183,184].

Here we showed that absence of Rasa3 in ECs correlates with increased Rap1 *in vivo* (mice) and in cultured endothelial cells (HUVECs). By contrast, no effect was observed on active Ras levels when Rasa3 was knockdown in HUVECs.

Importantly, even if Rap1 activity was not tested in zebrafish, inhibition of Rap1 using the GGTI298 inhibitor partially rescued lumen defects *in vivo* indicating a probable hyperactivation of Rap1 in zebrafish when Rasa3 is knockdown. A rescue of tubulogenesis defects was also observed *in vitro* using GGTI298 inhibitor or specific siRNAs targeting Rap1.

Rap1 exists as two isoforms, Rap1a and Rap1b, within endothelial cells. Rap1b is the most abundant isoform (90% of total Rap1) and is more present in the cytoplasm [152] while Rap1a is localized at EC-EC junctions [146]. Moreover, Rap1b is required for proper endothelial cell-cell junction formation. Inactivation of Rap1b in HUVECs reduces 90% of total Rap1 and residual Rap1 (likely Rap1a) failed to localize to endothelial junctions. Besides its localization, the role of Rap1a isoform is still unclear [217]. In zebrafish, Rap1b is indispensable for vascular integrity. Indeed, inactivation of Rap1b using a morpholino resulted in brain hemorrhages [217].

As previously stated, we have been able to rescue tubulogenesis defects *in vitro* by targeting Rap1b isoform using specific siRNA. No rescue was observed using siRNA targeting Rap1a. These results were not surprising considering the high expression of Rap1b compared to Rap1a in endothelial cells and its role in ECs junction formation. Co-injection of Rasa3 morpholino with Rap1b morpholino should be performed in the future in order to rescue lumen defects *in vivo* via another way than using Rap1 inhibitor GGTI298.

These observations identify Rap1, specifically the Rap1b isoform, and not Ras as the main target of Rasa3 in ECs. This is consistent with the idea that Rap1 and Ras largely act in different signaling pathways and are selectively regulated by specific GAPs and GEFs *in vivo* [161].

Rap1 signaling has been associated with multiple aspects of vascular development and endothelial cell biology [149]. As for other cell types, Rap1 is predominantly involved in the control of integrin- and cadherin-mediated adhesion dynamics in endothelial cells [218,219]. In mice, EC specific inactivation of Rap1 leads to hemorrhages and vascular rupture. More interestingly, these mice exhibit microvessel dilatation [220]. In cultured endothelial cells, depletion of Rap1 diminishes adhesion to the ECM, promotes VE-cadherin-based cell-cell junction remodeling and increases endothelial permeability [221,222]. These effects have been partlially linked to the role of Rap1 in the regulation of integrin β1 affinity and clustering [149]. All these described Rap1 functions are entirely consistent with the phenotype of Rasa3-depleted HUVECs, which exhibit Rap1 hyperactivation and concomitantly increase in β1 integrin clustering and decrease in focal adhesion dynamics, permeability and cell-cell junction remodeling.

Remarkably, decreasing the expression of Rap1 annihilates EC tubulogenesis *in vitro*, similarly to depleting Rasa3. This supports the idea that tube formation relies on a tight balance of EC adhesion dynamics and places Rasa3-Rap1 signaling as a critical hub in this process.

We showed that Rasa3 regulates EC cytoskeleton plasticity. Cytoskeleton remodeling is a crucial step in order to support cell shape change during expansion of luminal compartment. We observed that depletion of Rasa3 resulted in an increase in actin stress fiber levels and in non-muscle myosin IIA (MLCII) activity. It is known that an increase of RhoA small GTPase activity is associated with an increase of actin stress fibers and MLCII activity [99]. Once activated, RhoA activates its downstream effector ROCK which in turn inhibits MLC phosphatase leading to an increase of MLCII

phosphorylation. Our *in vitro* data indicate that the small GTPase RhoA might be activated following Rasa3 depletion. Hyperactivation of RhoA was observed *in vivo* by Patricia Molina Ortiz in mice expressing a catalytically inactive form of Rasa3 (*Figure J in Annex 1*). We have already shown that Rasa3 depletion was associated with a hyperactivation of Rap1 small GTPase *in vitro* and *in vivo*. However both Rap1 and RhoA hyperactivation would be surprising since Rap1 has been identified as a negative regulator of RhoA activity. Indeed, different studies showed that Rap1 inhibits RhoA by activating RhoGAPs such as ARAP3 [219,223]. Nevertheless, increased RhoA activity in absence of Rasa3 could be explained by the low activity of the FAK/Src module observed. The Src kinase is responsible for the phosphorylation of different RhoGAPs such as p190RhoGAP, RhoGAP3, RhoGAP5, RhoGAP42 or RhoGAP32 [224]. Therefore reduced GAP activity of these proteins in Rasa3-depleted cells could explain the hyperactivation of RhoA. We tested the phosphorylation of P190RhoGAP and no differences were observed between control and Rasa3-depleted cells (*data not shown*). Analysis of phosphorylation levels of these proteins in control and Rasa3-depleted cells should be performed in the future.

A recurrent theme in the field of endothelial tubulogenesis is the coordinated control of adhesion processes and cytoskeleton dynamics of ECs [225]. In the model of cord hollowing, the initial VE-cadherin-based AJs between ECs relocalize laterally to allow initial opening of the lumen [34]. It is likely that accumulation of VE-cadherin-based EC-EC junctions towards the cord periphery is achieved through VE-cadherin internalization at the apical cell surface and recycling at the lateral positions, requiring coordinated VE-cadherin phosphorylation events [226].

In this regard, our observation that Rasa3-depleted HUVECs exhibit stable VE-cadherin-based AJs and decreased phosphorylation of VE-cadherin Y658 is consistent with a lower FAK/Src signaling, as both kinases have been extensively documented to promote EC junction turnover [114,120,227]. Moreover, our results are consistent with those observed by Gore et al in HUVECs. They showed that Rap1b is required for suitable endothelial cell-cell junction formation. Rap1b siRNA-treated HUVECs monolayers displayed less stable VE-cadherin-based AJs [217].

In this study we have only focused our attention on VE-cadherin Y658 phosphorylation. Cytosolic part of VE-cadherin displays different tyrosine residues that have been identified as phosphorylation sites for different kinases. Further analysis of VE-cadherin should be investigated in order to highlight crucial phosphorylation sites implicated in Rasa3-Rap1 signaling. Y685 and Y731 are two residues that are directly phosphorylated by the Src kinase. Phosphorylation of S665 requires the activation of Src even if it doesn't mediate direct phosphorylation of the residue [60]. In view of our results, decreased FAK/Src activity in Rasa3-depleted cells, we should expect a decrease of phosphorylation on these different sites in absence of Rasa3.

VE-cadherin Y658 phosphorylation disrupts its interaction with p120 and leads to VE-cadherin internalization. Co-immunoprecipation of VE-cadherin-p120 should further confirm higher stability of VE-cadherin-based AJs in Rasa3-depleted HUVECs. The phosphorylation of VE-cadherin on Y731 disrupts its interaction with β-catenin [60]. Co-immunoprecipitation of VE-cadherin-β-catenin should also be performed. We expect stronger interactions between VE-cadherin/p120 and VE-cadherin/β-catenin in Rasa3-depleted cells reflecting higher stability of AJs.

In this research we only investigated VE-cadherin-based AJs. However, EC-EC junctions comprise also tight junctions (TJs). It should be interesting to analyze the stability of TJs in Rasa3-depleted cells. Analysis of TJs stability can be done by performing immunofluorescences (+- EGTA) and staining TJs specific markers such as ZO-1, occludin or claudin [228].

VE-cadherin also influences actin cytoskeleton remodeling, which is required for the EC shape changes necessary to accommodate the growth of the luminal compartment. VE-cadherin signaling thus plays a critical role in vascular tubulogenesis as illustrated by the lumenization defects observed in VE-cadherin deficient mice and zebrafish [229,230].

Lumen expansion also requires ECs to establish dynamic contacts with the underlying ECM. Loss of β1 integrin during development of the mouse vascular network prevents lumen formation in medium and small sized arteries [213]. In contrast, excessive stability of EC-ECM adhesions impairs ISVs lumenization in zebrafish [231]. When Rasa3 is deleted in HUVECs, turnover of β1 integrin-dependent EC adhesion is impaired and EC-ECM based adhesion contacts accumulate. Together with our observations here, it is thus becoming evident that a tight regulation of adhesion complexes between ECs and the ECM is required to allow vascular lumen formation and maintenance.

Recent observations support the existence of crosstalk between integrin-based cell-matrix and cadherin-based cell-cell contacts. Both of which may operate separately on lumen formation or stabilization [213,232,233]. Strikingly, a number of these studies have converged on Rap1, thus placing this small GTPase at the crossroads of multiple outside-in and inside-out adhesion signaling pathways [231].

Finally, we shed light on the critical function of Rasa3, a poorly characterized protein in vascular development. The first and main cause of embryonic lethality associated with Rasa3 inactivation appears to be excessive activation of Rap1, which leads to dysregulation of EC-adhesion properties and signaling.

As a result, Rasa3 depleted ECs are unable to integrate and coordinate integrin and VE-cadherin signaling, preventing formation of a functional lumen. Our results thus uncovered an important but previously unknown coordinator of multiple adhesion processes during vascular tubulogenesis (**Figure 51**).

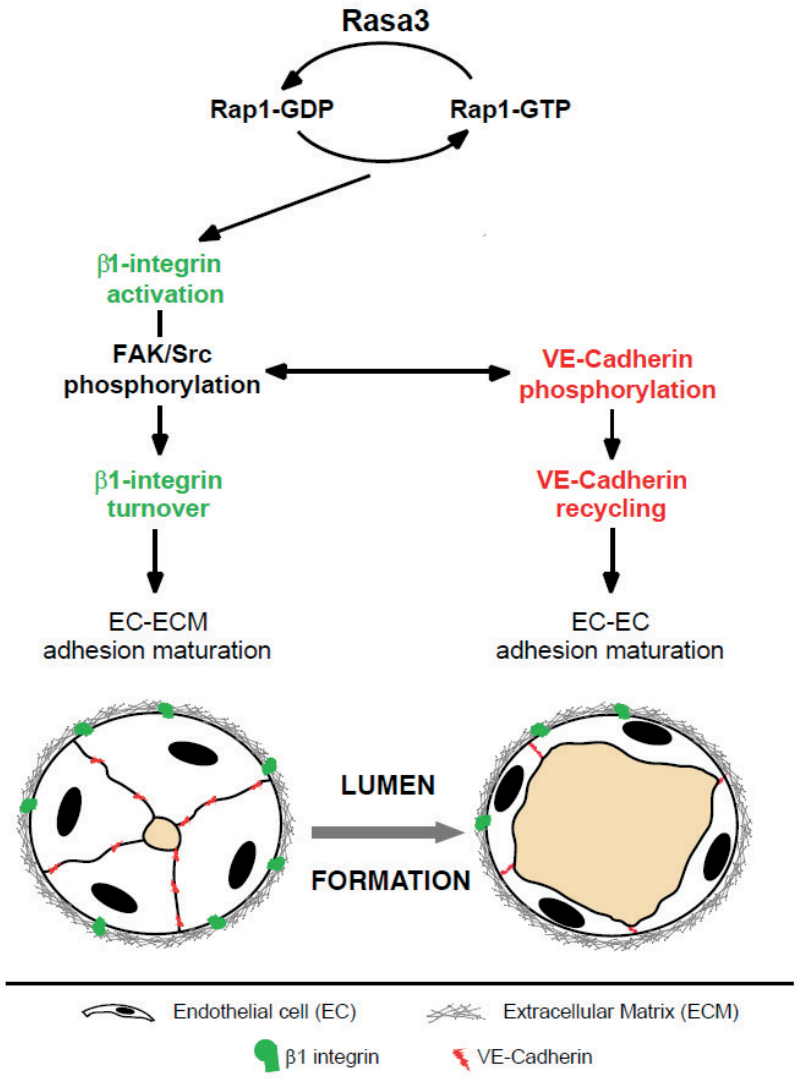

Figure 51: Model for Rasa3 control on endothelial lumen formation. Rap1 inactivation by Rasa3 GAP activity regulates activation of β1 integrin- and VE-cadherin-based adhesions. Following integrin activation, Rasa3 inactivates Rap1 to allow turnover of integrin- and VE-cadherin-based adhesions, via the FAK/Src signaling module. Failure to turnover and recycle EC-ECM and junctional adhesion complexes between EC results in vascular tubulogenesis defects.

Rasa3 controls endothelial cell and pericyte interactions

The maturation of blood vessels is required for good functioning of vascular system. This implies the recruitment of pericytes and deposition of new basal membrane [13]. Patricia Molina Ortiz observed alterations of pericytes in $R3^{f/f}$iEC-Cre mice. These observations were supported *in vitro* in siRasa3-treated HUVECs where pericytes adhered more and spread less around a confluent monolayer of HUVECs.

Endothelial cells express VE-cadherin and N-cadherin. While VE-cadherin is endothelial specific, N-cadherin is also expressed in pericytes. The current model suggests that N-cadherin mediates contact between endothelial cells and pericytes. Here we observed an upregulation of N-cadherin expression in Rasa3-depleted HUVECs. Similar observations were obtained *in vivo* in mice. These results are consistent with our phenotype. Excessive N-cadherin lead to increase of EC-pericyte interactions and prevent spreading of pericytes.

N-cadherin is a target of β-catenin transcription factor [77]. However, we have not been able to observe upregulation of target genes of β-catenin in absence of Rasa3. Moreover β-catenin nuclear localization was not affected following Rasa3 depletion. These results suggested that increase of N-cadherin expression does not result from stronger β-catenin activation. A β-catenin activity assay would exclude any implication of β-catenin in this process and should be performed in the future.

Rap1 has been found hyperactivated following Rasa3 depletion. Implication of Rap1 in regulation of EC-EC and ECM-EC adhesions is well described in the litterature. However, to our knowledge, there is no

evidence that Rap1 signaling was involved in pericyte-EC interactions. The only link between Rap1 and N-cadherin was observed in neurons where Rap1 upregulate membrane localization of N-cadherin [234]. Knowing this, it could be possible that an equivalent mechanism regulates the membrane localization of N-cadherin in endothelial cells. Thus, an increase of Rap1 activity would lead to an increase of N-cadherin expression which is consistent with the phenotype observed in Rasa3-depleted cells.

Rap1 implication in EC-pericyte interactions must be validated in the future by doing rescue experiments using Rap1 inhibitor GGTI298 or specific siRNAs targeting Rap1a or Rap1b.

Recruitment of pericytes around vessels in zebrafish starts at 3dpf [44]. It would be interesting to analyze pericytes recruitment in Rasa3 morphant embryos in order to validate mice observations. In addition, the implementation of rescue experiments in zebrafish is easier compared to mice. Indeed, inhibitors can simply add to zebrafish medium and do not require injection.

S1P1 mediates vessel stabilization by placing the N-cadherin at plasma membrane [76]. We have already excluded the implication of S1P/S1P1 signaling in Rasa3-depleted cells. No differences in term of activation of S1P1 signaling were detected in following Rasa3 depletion (*data not shown*).

Together with EC-ECM and EC-EC adhesion defects, abnormalities in pericyte coverage might contribute to vascular instability and occlusions observed in Rasa3 KO mice. However, the mechanism by which Rasa3 controls endothelial cell-pericyte interactions remains unclear.

GAP1 family members display distinct non redundant functions

Different studies on GAP1 family members identified distinct functions for these proteins. The GAP1 family comprises Rasa2, Rasa3, Rasa4 and RasaL. Besides Rasa2, every member of the GAP1 family has the ability to control both Ras and Rap1 small GTPases *in vitro* [176].

Like Rasa3, Rasa2 is ubiquitously distributed. Rasa4 is predominantly expressed in the spleen and the lymphe nodes while RasaL is largely found in thyroid and adrenal glands [235].

Rasa2 is the least studied member of GAP1 family and the only one acting on Ras and not on Rap1. Nowadays, no knockout mice for Rasa2 have been described. Rasa2 was found mutated in 5% of melanomas (analysis performed on 501 melanomas) and 27% of these mutations result in a loss of function. Downregulation of Rasa2 resulted in excessive activation of Ras that was associated with reduced patient survival. Authors concluded that loss of Rasa2 acts as a melanoma driver [236].

Rasa4-deficient mice are viable and appear to be normal. However, Rasa4-deficient mice are more susceptible to bacterial infection resulting from impaired phagocytosis in macrophages [237]. Depletion of Rasa4 in human mammary epithelial cells promotes cell transformation implicating Rasa4 as a tumor suppressor [238]. Additionally, Rasa4 is silenced in juvenile myelomonocytic leukemia due to hypermethylation of CpG islands [239].

RasaL-deficient mice are viable and grow normally. However, these mice are susceptible to liver fibrosis. Reduced RasaL expression was found in different cancers such as colon, gastric, liver, bladder, thyroid cancers

which indicated that RasaL may act as a tumor suppressor [240,241]. RasaL is also reduced through CpG methylation in many human cancers [242].

These studies revealed that the different members of GAP1 family have distinct non redundant physiological function and Rasa3 seems to be the only member implicated in regulation of vascular development.

Therapeutic implications

Different studies showed that Rasa3 expression was downregulated in different cancer cells. These results suggested that Rasa3 could act as a tumor suppressor gene [185–187]. Here, using a combination of *in vitro* and *in vivo* approaches, we showed that specific inactivation of Rasa3 protein in endothelial cells decreases angiogenic processes. Then, besides its role in cancer cells, the inactivation of Rasa3 could have an anti-angiogenic role in endothelial cells.

The next step of this study would be to analyze the role of Rasa3 protein in tumoral angiogenesis. Patricia Molina Ortiz obtained preliminary results in mice showing that specific inactivation of Rasa3 in endothelial cells reduces the development of tumors (tumors size smaller in absence of Rasa3). She observed that vasculature was reduced inside the tumors from mice expressing an inactive form of Rasa3 in endothelial cells. (*Figure K in Annex 1*).

The role of Rasa3 in tumoral angiogenesis should be confirmed using the zebrafish model following Rasa3 depletion with a morpholino. Indeed, Nicoli et al developed a method to study tumor angiogenesis in zebrafish called the zebrafish/tumor xenograft angiogenesis assay [243]. This method is based on the injection of mammalian tumor cells into the perivitelline space of zebrafish embryos at 48 hpf. Tumor grafts induce a neovascular

response coming from the developing sub-intestinal vessels (SIV) [243,244]. Moreover, in the case of new Rasa3 inhibitor being created, the zebrafish/tumor xenograft model may represent a suitable model for testing it as a novel angiogenesis inhibitor.

Conclusion


RASA3
RAP1
GTP
RAP1
GTP
ß1-int
FAK/Src
P
VE-Cad
P
ß1-int
VE-Cad
P
EC-ECM adhesion
EC-EC adhesion
Lumen Formation

In this study, using a combination of *in vivo* (mice and zebrafish) and *in vitro* (HUVECs) approaches, we identify for the first time a key role of Rasa3 in the maintenance of vascular integrity in vertebrate. Inactivation of Rasa3 is associated with a hyperactivation of Rap1 smallGTPase *in vitro* and *in vivo*.

We showed that Rasa3 depletion in endothelial cells affects EC-EC, EC-ECM and EC-pericyte adhesions. These adhesions defects prevent formation of a patent lumen and result in occluded blood vessels in mice and zebrafish.

Here we identify a critical function of Rasa3 in the endothelial lineage and highlight the causes of embryonic lethality observed in full Rasa3$^{-/-}$ mice.

Methods

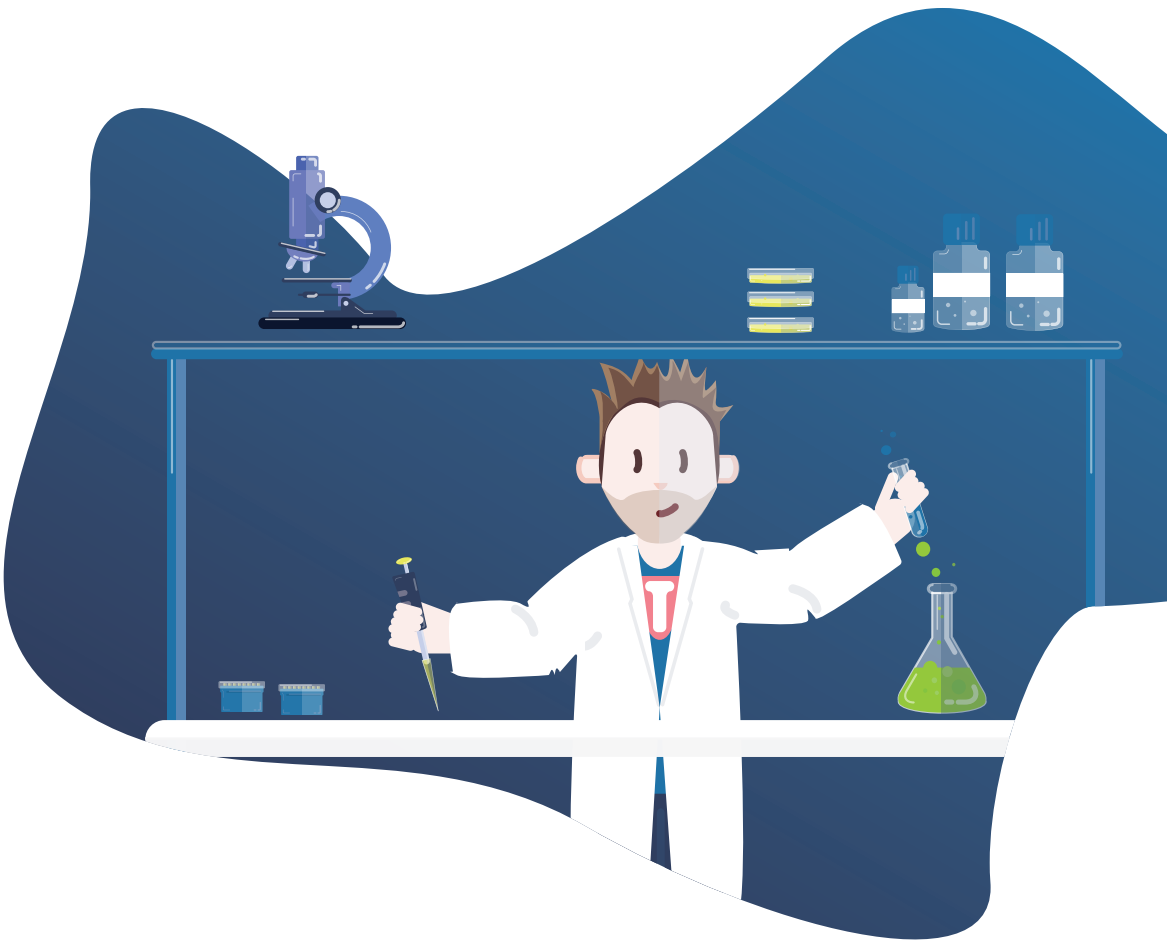

1. Cell culture and siRNA transfection

Human Umbilical Vein Endothelial Cells (HUVECs) were obtained from Lonza and grown at 37°C, in 5% CO_2, in endothelial basal medium (EBM) supplemented with epidermal growth factor (10ng/ml), gentamicin (50µg/ml), amphotericin B (50ng/ml), bovine brain extract (12µg/ml), hydrocortisone (1µg/ml), 10% Fetal Bovine Serum (FBS, Gibco), and 1% antibiotics (penicillin and streptomycin) (Lonza). SiRNA transfections in HUVECs were performed using the GeneTrans 2 reagents (MoBiTec) according to the manufacturer's protocol. Briefly (for a 6well condition), 1µl of siRNA (100µM) is mixed with 24µl of Diluent B (Tube 1). In parallel, 3.5µl of GeneTrans (transfection reagent) is mixed with 21.5µl of DEMEM medium without serum (Tube 2). After 5 minutes the content of tube 1 is introduced in tube 2 and incubate 5 minutes at room temperature. Finally the mix is dropped on the cells and the medium is changed after 4 hours of incubation at 37°C.

Human Brain Vascular Pericytes (HBVPs) were obtained from Sciencell Research Laboratories and grown on poly-L-lysine (2 µg/cm2) (Sciencell Research Laboratories) coated flasks at 37°C, in 5% CO2, in pericyte medium (Sciencell Research Laboratories) supplemented with 10% Fetal Bovine Serum (FBS, Gibco), 1% pericyte growth supplement and 1% penicillin /streptomycin solution.

Control siRNA and siRNA targeting Rasa3, Rap1A and Rap1B were purchased from Eurogentec and presented in **Table 1**.

siRNA	Sequence 5' → 3'
siControl	(SR-CL000-005)
siRasa3#1	GCGCTTTGGGATGAAGAAT
siRasa3#2	CCTGAAGTTTGGAGATGAA
siRap1A	GCAAGACAGTGGTGTAACT
siRap1B	GTCTGCTTTGACTGTACAA

Table 1: siRNA sequences

2. Antibodies and Reagents

Primary antibodies used in this study are listed in **Table 2**.

Antibody	Company	Reference
Rasa3	Santa Cruz	sc-166442
Paxillin	BD BioSciences	610051
Phospho-paxillin	Cell Signaling	2541S
Rap1	Cell Signaling	8825S
FAK	Abcam	ab72140
phosphoFAK	Thermo-fisher	44-624G
ERK	Cell Signaling	9102s
PhosphoERK	Cell Signaling	9101s
SRC	Cell Signaling	2123
PhosphoSRC	Cell Signaling	2101S
VE-cadherin	Santa Cruz	sc-9989
Phospho- VEcadherin	Invitrogen	44-1144G
B1 integrin	EMD Millipore	MAB-1965
Activated B1 integrin	BD Pharmigen	550531
GAPDH	SantaCruz	sc-166545
pMLC2	Cell Signaling	3674
Alpha-tubulin	Sigma	T6199
Acetyl alpha-tubulin	EMD Millipore	MABT868
Ras	Cell Signaling	8832S

Phalloidin (F-Actin) conjugated to Alexa Fluor® 568 dye	Thermo-fisher	A12380
CD31	Dako	M0823
N-cadherin	BD transduction Lab	610920
B-catenin	Santa Cruz	sc-7199
HSP60	Enzo	ADI-SPA-806-F
Histone H3	Santa Cruz	sc-8654
Actin	Santa Cruz	sc-1616

Table 2: List of primary antibodies.

DAPI, FITC-Dextran (FD405) and Rap1 inhibitor GGTI298 (G5169) were obtained from Sigma. VEGF (#100-20) was from Peprotech. Laminin (23017-015) and collagen (A1048301) were from Invitrogen, vitronectin (cc080) was from Millipore and fibronectin (33010018) was from Gibco.

3. qRT-PCR

RNA was extracted with NucleoSpin RNA Kit (Macherey-Nagel) according to manufacturer's protocol and reverse-transcribed with random primers (Thermo Fisher Scientific). qRT-PCR was performed on lightCycler 480 (Roche) using SYBR Green as probe. mRNA quantification was done with the 2-deltadeltaCt method using GAPDH as housekeeping gene for normalization. Primers used during this study are presented in **Table 3**.

Target gene	Forward primer	Reverse primer
Rasa3	TTCCGAGGAAACTCACTGGC	TCAGTGATGGCGTGGAAGAC
GAPDH	TTGCCATCAATGACCCCTTCA	CGCCCCACTTGATTTTGGA
Rap1A	GGATACTGCAGGGACAGAGC	CCCTGCTCTTTGCCAACTAC
Rap1B	GGGAAGGAACAAGGTCAAAA	ATGACTTTTTGCGAGCCTTC
N-cadherin	ATTGGACCATCACTCGGCTTA	CAGGTTCCACTTGAGCTTGTTC
Cyclin D1	ATGTTCGTGGCCTCTAAGATGA	CAGGTTCCACTTGAGCTTGTTC

IL8	ATGACTTCCAAGCTGGCCGTGG CT	TCTCAGCCCTCTTCAAAAACTT CTC

Table 3: Primers sequences.

4. Tube formation assay (Matrigel Assay)

Forty-eight hours after transfection, HUVECs were subjected to the matrigel assay. This angiogenic test is based on the capacity of the cells to form a vascular-like network. 220µl of Matrigel Basement Membrane Matrix (BD Bioscience) were coated in 12 wells 3 hours before harvesting the cells and then 50 x 103 cells were cultivated on it for 16h. Quantification was done by measuring the cumulative tube length in three random microscopic fields using imageJ software.

5. Sprouting assay (Spheroid Assay)

Twenty-four hours after transfection, HUVECS were harvested, counted, mixed in methylcellulose matrix (20%) (Sigma) and EBM medium (80%) and introduced into round bottom 96wells plate (100µl per well) in order to form spheroids of more or less 500 cells. The next day, spheroids were carefully harvested, resuspended in 1ml of methylcellulose and mixed with 1ml of 10X M199 (Sigma), 80% collagen (Gibco), 2% Hepes (1M) and NaOH 0.1M to get a pH around 6.9 and 7.4 (keep the mix on ice before mixing with spheroids). 1 ml of the mixture is added in 24 wells, incubated for 30 min at 37°C and 100µl of EBM medium is added into each well before incubating the plate overnight in the 37°C incubator. Quantification of angiogenic activity was done by counting the number of sprouts of at least 5 spheroids/condition using ImageJ Software.

6. Wound healing (Scratch Wound Assay)

Seventy-two hours after transfection, a confluent monolayer of HUVECs was scraped in order to create a cell free zone. Pictures were taken directly after the scrappage and 8 hours after it. Quantification of cell migration was done by measuring the percentage of recolonized area 8 hours after injury using ImageJ Software.

7. Permeability Assay

One day after transfection, 6 x 104 HUVECs were plated onto insert (FisherBioblock W2127C) precoated with fibronectin (50µg/ml) defining a top and a bottom chamber. Seventy-two hours after transfection, the medium was changed in both chambers and cells were treated with medium containing EGTA (4mM) and FITC-Dextran (1mg/ml) for 30min. Samples from the bottom chamber were analyzed by measuring the fluorescence at 492nm. Insert without cells and insert without addition of FITC-dextran were used respectively as positive and negative control.

8. Adhesion Assay

One day before doing the adhesion assay, 6x 5µl of each substrate were placed carefully in the center of a 96 wells and incubated overnight at 4°C. PBS-CaCl2 (1mM) is used as negative control. The next day, 100µl of blocking solution (For 100ml of blocking solution: 50ml Tris 1M pH6.8, 2.22ml NaCl 5M, 0.25ml CaCl2 2M, 1g BSA, up to 100ml with deionized water) were added into each well and incubated for 30min. Seventy-two hours after transfection, HUVECs were harvested (in RPMI medium + 0.1% BSA + ITS (Invitrogen 41400045) 1/100), counted with trypan blue and 20 000 per well were incubated in fibronectin- (50µg/ml), collagen 1-

(50µg/ml), vitronectin- (10µg/ml), or laminin-precoated (50µg/ml) 96 wells plate for 30min. The cells were washed until nothing left adhere on the PBS-CaCl2 condition, and then stained with crystal violet (20% methanol + 0.5% crystal violet) for 5 min at room temperature. The plate was washed several times with water and dry at room temperature. In order to release the crystal violet of the cells, 100µl of release solution (50% ethanol, 50% NaAc 0.1M) were added into each well and incubated 15 min at room temperature. Relative adhesion is measured by reading absorbance at 560 nm after release of incorporated dye.

9. Zebrafish

The Tg(fli1a:eGFP)y1 line, where endothelial cells express the GFP, was used in this study and maintained conforming to EU regulations on laboratory animals. Knockdown experiments were performed by injecting embryos at the one-cell stage with 2.5 ng of Control (Ctl) or Rasa3 morpholino. Ctl (5'-CCTCTTACCTCAGTTACAATTTATA-3') and Rasa3 (5'-AAGCCCTTCTTCTTCGACCGCCATG-3') morpholinos were purchased from Genetools. The injected embryos were placed in E3 medium and incubated at 28°C. Around 24 hpf (hours post fertilization), E3 medium was replaced with E3 medium + PTU (1-phenyl-2-thiourea) in order to prevent pigmentation of embryos. Phenotype analysis consisted of percentage of ISVs (Intersegmental Vessels) lumenized from 10 ISVs per embryo. Confocal and white light pictures were taken on living embryos using respectively a Zeiss confocal microscope and a stereomicroscope at 48 hpf. For the rescue experiment, the Rap1 inhibitor (GGTI298 10µM) was added to the E3 medium at 40 hpf until 48 hpf when the quantification were made. Heart rates of embryos were measured on

sleeping embryos using a binocular microscope. The embryos were anesthetized in E3 medium + tricaine at a final concentration of 0.16mg/ml

10. SDS-PAGE and Western blotting

HUVECs cells were harvested and total extracts were obtained by lysing cells in Laemmli buffer containing 50mM of Dithiothreitol (DDT) by scrapping the plate. Lysates were sonicated for 5 seconds and boiled for 10 minutes. For zebrafish proteins extraction, 30 embryos were collected and euthanized with tricaine. Embryos were washed with Ringer solution (116mM NaCl, 2.9mM KCl, 5mM HEPES, adjusted to pH 7.2) in order to remove the yolk and incubated 30min at -80°C (after removing the Ringer solution). Embryos were then triturated with a syringe in Lysis buffer (10mM TRIS pH 7.4, 2% Triton X100 + proteases inhibitors) and incubate for 30 minutes at 4°C on wheel. After centrifugation, the supernatant was collected and stored at -80°C. SDS-PAGE and Western blot analysis were performed according to standard procedures and developed with ECL detection kit (GE Healthcare Bio-Sciences). Quantification of bands intensity was determined with ImageJ Software.

11. Rap1/Ras smallGTPases activity assay

Seventy-two hours after transfection, HUVECS were seeded 30 minutes on fibronectin (50µg/ml) and Rap1 and Ras activity were measured using Active Rap1 (#8818) and Active Ras detection (#8821) kit from Cell Signaling following the manufacturer's guidelines. Briefly, cell lysate was incubated for 1 hour on rotation at 4°C with GST-RalGDS-RBD (Rap1) or GST-Raf1-RBD (Ras) and glutathione agarose beads. Bound active Rap1 or Ras were eluted from the beads and analyzed by western blotting using respectively Rap1 or Ras antibody.

12. FACS analysis

Seventy-two hours after transfection, cells were washed three times in blocking solution (PBS 1% FBS) and incubated for one hour with the anti-activated β1 integrin primary antibody. Cells were then washed with blocking solution and incubated with a FITC-conjugated secondary antibody. After washing, the expression of the clustered β1 integrin was quantified by flow cytometry using FACScan Cytometer (Becton Dickinson).

13. Confocal imaging analysis

In adhesion experiments, HUVECs were seeded for 30 minutes onto fibronectin-coated coverslips, 72 hours after siRNA transfection. In VEGF treated experiments, HUVECs were seeded 48 hours after siRNA transfection and, the next day, were treated during 5 minutes with VEGF (50ng/ml) and processed for imaging. For EGTA-treated experiments, HUVECs were seeded 24 hours after siRNA transfection in order to have a confluent monolayer of cells. Two days after, cells are treated for 5 minutes in with EGTA (4mM) and processed for imaging. For confocal analysis, cells were fixed in 4% paraformaldehyde or 100% methanol, permeabilized in 0.1% Triton X-100, blocked in BSA and incubated overnight with the appropriate primary antibodies. Samples were then incubated with the corresponding Alexa-conjugated secondary antibodies (Invitrogen) and, after washing, mounted with Mowiol. All images were acquired with a Nikon A1 confocal microscope. The average size and the adhesion size distribution of focal adhesions were measured using the “analyze particles” plugin of ImageJ Software. Quantification of the ratio of the length between the center and the mature focal adhesion versus the

ratio length between the center and the cell periphery was done manually after isolation of mature focal adhesion (>1µm2) using the “analyze particles” plugin of ImageJ Software. Quantifications of F-actin (phalloidin) and phospho-MLC2 signals were performed using ImageJ Software with this method (https://sciencetechblog.com/2011/05/24/measuring-cell-fluorescence-using-imagej/). Quantification of the total length of FAJs (focal adherens junctions) in single cells relative to the total junction length were performed manually using ImageJ Software.

14. Focal Adhesion Dynamics

HUVECs were co-transfected with siRNA and paxillin-GFP. Focal adhesion dynamics were analyzed using time-laps TIRF (total internal reflection fluorescence) microscopy. Live-cell TIRF imaging was performed on a Nikon Eclipse Ti-E inverted microscope equipped with perfect focus system, CFI apo TIRF 100x oil objective (Nikon), a QuantEM 512SC EMCCD camera (photometrics, Roper Scientific), a TI-TIRF-E motorized TIRF illuminator (Nikon) and a stage top incubator maintaining 37°C and 5% CO2 (Tokai hit). Images were captured every 120 seconds over 10 hours. Quantifications were performed as described by Stehbens and Wittman [245].

15. Adhesion/Spreading Pericytes Assay

On the same day than HUVECs transfection, HBPVs are stained with celltracker green (C2925 invitrogen). Briefly, cells were cultivated in serum-free Pericyte medium supplemented with celltracker green (10µM) for 40 minutes and then replaced with Pericyte medium 10% serum. Forty-eight hours after transfection, HUVECs were harvested and seeded in order to have a confluent monolayer on the next day. Seventy-two hours after

staining HBPVs were harvested, counted and 5000 were added on the confluent monolayer of HUVECS for 20 minutes. After 2 washes, HBPVs left on the monolayer of HUVECS were counted from 7 different field under microscope. For rescue experiment, GGTI298 (10µM) was added to the medium 2 hours before doing the experiment. The protocol of the Spreading Pericytes Assay was the same than the Adhesion Pericytes Assay except that the HPBVs were left spread 8 hours before performing an immunofluorescence staining endothelial cells with CD31 primary antibody. For quantification, the number of branches of 300 pericytes per condition were done using Nikon A1R microscope.

16. Nuclear/cytoplasmic fractionation

Seventy-two hours after transfection, confluent HUVECs are harvested in PBC. The procedure must be done on ice. Cell pellet is triturated 5 times with ice-cold 0.1% NP40-PBS. Keep an aliquot as the whole cell sample. Spin the remainder for 10 seconds and transfer the supernatant to new tube. The supernatant is the cytoplasmic fraction. Resuspend the pellet with ice-cold 0.1% NP40-PBS, spin the tube for 10 seconds and discard supernatant. Repeat this step twice. The nuclear pellet is resuspended and sonicated in Laemmli sample buffer.

17. Statistical analysis

Graph values are presented as mean +/- standard deviation from at least three independent experiments. Statistical analysis were performed with Graphpad Prism. The test used for each experiment is described in the corresponding legend. For each test, a difference of P-value<0.05 was considered significant (*: $p<0.05$; **: $p<0.01$; ***: $p<0.001$).

Bibliography

1. Risau, W. Mechanisms of angiogenesis. *Nature* **386,** 671–674 (1997).

2. Risau, W. & Flamme, I. Vasculogenesis. *Annu. Rev. Cell Dev. Biol.* **11,** 73–91 (1995).

3. Udan, R. S., Culver, J. C. & Dickinson, M. E. Understanding vascular development. *Wiley Interdiscip. Rev. Dev. Biol.* **2,** 327–46 (2013).

4. Ribatti, D., Nico, B. & Crivellato, E. The development of the vascular system: a historical overview. *Methods Mol. Biol.* **1214,** 1–14 (2015).

5. Herbert, S. P. & Stainier, D. Y. R. Molecular control of endothelial cell behavior during blood vessel morphogenesis. *Nat. Rev. Mol. Cell. Biol.* **12,** 551–564 (2012).

6. Carmeliet, P. Angiogenesis in life, disease and medicine. *Nature* **438,** 932–936 (2005).

7. Schmidt, A., Brixius, K. & Bloch, W. Endothelial precursor cell migration during vasculogenesis. *Circ. Res.* **101,** 125–136 (2007).

8. Drake, C. J. Embryonic and adult vasculogenesis. *Birth Defects Res. Part C - Embryo Today Rev.* **69,** 73–82 (2003).

9. Patel-Hett, S. & D'Amore, P. A. Signal transduction in vasculogenesis and developmental angiogenesis. *Int. J. Dev. Biol.* **55,** 353–63 (2011).

10. Eichmann, A. *et al.* Vascular development: From precursor cells to branched arterial and venous networks. *Int. J. Dev. Biol.* **49,** 259–267 (2005).

11. Jin, S.-W. & Patterson, C. The opening act: vasculogenesis and the origins of circulation. *Arterioscler. Thromb. Vasc. Biol.* **29,** 623–9 (2009).

12. Goldie, L. C., Nix, M. K. & Hirschi, K. K. Embryonic vasculogenesis and hematopoietic specification. *Organogenesis* **4,** 257–263 (2008).

13. Jain, R. K. Molecular regulation of vessel maturation. *Nat. Med.* **9,** 685–693 (2003).

14. Herzog, Y., Guttmann-Raviv, N. & Neufeld, G. Segregation of arterial and venous markers in subpopulations of blood islands before vessel formation. *Dev. Dyn.* **232,** 1047–1055 (2005).

15. Chong, D. C., Koo, Y., Xu, K., Fu, S. & Cleaver, O. Stepwise arteriovenous fate acquisition during mammalian vasculogenesis. *Dev. Dyn.* **240,** 2153–2165 (2011).

16. Rice, J. J., Gerwins, P. & Kilarski, W. W. Mechanisms of angiogenesis: Perspectives from antiangiogenic tumor therapies. *Curr. Angiogenes.* **1,** 139–147 (2012).

17. Leite De Oliveira, R., Hamm, A. & Mazzone, M. Growing tumor vessels: More than one way to skin a cat - Implications for angiogenesis targeted cancer therapies. *Mol. Aspects Med.* **32,** 71–87 (2011).

18. Adams, R. H. & Alitalo, K. Molecular regulation of angiogenesis and lymphangiogenesis. *Nat. Rev. Mol. Cell Biol.* **8,** 464–478 (2007).

19. Carmeliet, P., De Smet, F., Loges, S. & Mazzone, M. Branching morphogenesis and antiangiogenesis candidates: Tip cells lead the way. *Nat. Rev. Clin. Oncol.* **6,** 315–326 (2009).

20. Blanco, R. & Gerhardt, H. VEGF and Notch in tip and stalk cell selection. *Cold Spring Harb. Perspect. Med.* **3,** 1–19 (2013).

21. Mentzer, S. J. & Konerding, M. A. Intussusceptive angiogenesis: Expansion and remodeling of microvascular networks. *Angiogenesis* **17,** 499–509 (2014).

22. Kurz, H., Burri, P. H. & Djonov, V. G. Angiogenesis and vascular remodeling by intussusception: From form to function. *News Physiol. Sci.* **18,** 65–70 (2003).

23. Kilarski, W. W., Samolov, B., Petersson, L., Kvanta, A. & Gerwins, P. Biomechanical regulation of blood vessel growth during tissue vascularization. *Nat. Med.* **15,** 657–664 (2009).

24. Greenwood, V. & Kilarski, W. W. Looping angiogenesis Angiogenèse d ' un troisième type contrôlée par les forces contractiles. (2010).

25. Otrock, Z. K., Mahfouz, R. A. R., Makarem, J. A. & Shamseddine, A. I. Understanding the biology of angiogenesis: Review of the most important molecular mechanisms. *Blood Cells, Mol. Dis.* **39,** 212–220 (2007).

26. Maisonpierre, P. C. *et al.* Angiopoetin-2 a Natural Antagonist for Tie2 that disrupts in vivo Angiogenesis. **277,** (1997).

27. Fukuhara S.; Sako K., Zhang J., Minami M., M. N. Angiopoietin-1 / Tie2 receptor signaling in vascular quiescence and angiogenesis. *Histol Histopathol* **25,** 387–396 (2010).

28. Yana, I. *et al.* Crosstalk between neovessels and mural cells directs the site-specific expression of MT1-MMP to endothelial tip cells. *J. Cell Sci.* **120,** 1607–1614 (2007).

29. Neve, A., Cantatore, F. P., Maruotti, N., Corrado, A. & Ribatti, D. Extracellular matrix modulates angiogenesis in physiological and pathological conditions. *Biomed Res. Int.* **2014,** (2014).

30. Benedito, R. & Hellström, M. Notch as a hub for signaling in angiogenesis. *Exp. Cell Res.* **319,** 1281–1288 (2013).

31. Jakobsson, L. *et al.* Endothelial cells dynamically compete for the tip cell position during angiogenic sprouting. *Nat. Cell Biol.* **12,** 943–953 (2010).

32. Bentley, K. *et al.* The role of differential VE-cadherin dynamics in cell rearrangement during angiogenesis. *Nat. Cell Biol.* **16,** 309–321 (2014).

33. Xu, K. & Cleaver, O. Tubulogenesis during blood vessel formation. *Semin. Cell Dev. Biol.* **22,** 993–1004 (2011).

34. Zeeb, M., Strilic, B. & Lammert, E. Resolving cell-cell junctions: Lumen formation in blood vessels. *Curr. Opin. Cell Biol.* **22,** 626–632 (2010).

35. Kamei, M. *et al.* Endothelial tubes assemble from intracellular vacuoles in vivo. *Nature* **442,** 453–456 (2006).

36. Nelson, K. S. & Beitel, G. J. More Than a Pipe Dream: Uncovering Mechanisms of Vascular Lumen Formation. *Dev. Cell* **17,** 435–437 (2009).

37. Gebala, V., Collins, R., Geudens, I., Phng, L. K. & Gerhardt, H. Blood flow drives lumen formation by inverse membrane blebbing during angiogenesis in vivo. *Nat. Cell Biol.* **18,** 443–450 (2016).

38. Strilić, B. *et al.* The Molecular Basis of Vascular Lumen Formation in the Developing Mouse Aorta. *Dev. Cell* **17,** 505–515 (2009).

39. Sacharidou, A., Stratman, A. N. & Davis, G. E. Molecular mechanisms controlling vascular lumen formation in three-dimensional extracellular matrices. *Cells Tissues Organs* **195,** 122–143 (2011).

40. Sigurbjörnsdóttir, S., Mathew, R. & Leptin, M. Molecular mechanisms of de novo lumen formation. *Nat. Rev. Mol. Cell Biol.* **15,** 665–676 (2014).

41. Chantrain, C. F. *et al.* Mechanisms of pericyte recruitment in tumour angiogenesis: A new role for metalloproteinases. *Eur. J. Cancer* **42,** 310–318 (2006).

42. Bergers, G and Steven, S. The role of pericytes in blood-vessel formation and maintenance. *Neuro. Oncol.* **7,** 452–464 (2005).

43. Armulik, A., Abramsson, A. & Betsholtz, C. Endothelial/pericyte interactions. *Circ. Res.* **97,** 512–523 (2005).

44. Stratman, A. N. & Davis, G. E. Endothelial cell-pericyte interactions stimulate basement membrane matrix assembly: influence on vascular tube remodeling, maturation, and stabilization. *Microsc. Microanal.* **18,** 68–80 (2012).

45. Dejana, E. Endothelial cell-cell junctions: Happy together. *Nat. Rev. Mol. Cell Biol.* **5,** 261–270 (2004).

46. Weis, S. M. Vascular permeability in cardiovascular disease and cancer. *Curr. Opin. Hematol.* **15,** 243–249 (2008).

47. Azzi, S., Hebda, J. K. & Gavard, J. Vascular Permeability and Drug Delivery in Cancers. *Front. Oncol.* **3,** 1–14 (2013).

48. Mehta, D. & Malik, A. B. Signaling mechanisms regulating endothelial permeability. *Physiol. Rev.* **86,** 279–367 (2006).

49. Komarova, Y. & Malik, A. B. *Regulation of Endothelial Permeability via Paracellular and Transcellular Transport Pathways*. *Annual Review of Physiology* **72,** (2010).

50. Simionescu, M., Popov, D. & Sima, A. Endothelial transcytosis in health and disease. *Cell Tissue Res.* **335,** 27–40 (2009).

51. Claesson-Welsh, L. Vascular permeability - The essentials. *Ups. J. Med. Sci.* **120,** 135–143 (2015).

52. Wallez, Y. & Huber, P. Endothelial adherens and tight junctions in vascular homeostasis, inflammation and angiogenesis. *Biochim. Biophys. Acta - Biomembr.* **1778,** 794–809 (2008).

53. Bazzoni, G. Dejana, E. Endothelial Cell-to-Cell Junctions: Molecular Organization and Role in Vascular Homeostasis. *Physiol. Rev.* **84,** 869–901 (2004).

54. Hartsock, A. & Nelson, W. J. Adherens and Tight Junctions: Structure, Function and Connection to the Actin Cytoskeleton. *Biochim Biophys Acta* **1778,** 660–669 (2008).

55. Cerutti, C. & Ridley, A. J. Endothelial cell-cell adhesion and signaling. *Exp. Cell Res.* **358,** 31–38 (2017).

56. Privratsky, J. R. & Newman, P. J. PECAM-1: regulator of endothelial junctional integrity. *Cell Tissue Res.* **355,** 607–19 (2014).

57. Niessen, C. M. & Gottardi, C. J. Molecular components of the adherens junction. *Biochim. Biophys. Acta - Biomembr.* **1778,** 562–571 (2008).

58. Bravi, L., Dejana, E. & Lampugnani, M. G. VE-cadherin at a glance. *Cell Tissue Res.* **355,** 515–522 (2014).

59. Dejana, E. & Orsenigo, F. Endothelial adherens junctions at a glance. *J. Cell Sci.* **126,** 2545–2549 (2013).

60. Dejana, E., Orsenigo, F. & Lampugnani, M. G. The role of adherens junctions and VE-cadherin in the control of vascular permeability. *J. Cell Sci.* **121,** 2115–2122 (2008).

61. Sidibé, A. & Imhof, B. A. VE-cadherin phosphorylation decides: Vascular permeability or diapedesis. *Nat. Immunol.* **15,** 215–217 (2014).

62. Gavard, J. Endothelial permeability and VE-cadherin. *Cell Adh. Migr.* **7,** 465–471 (2013).

63. Harris, E. S. & Nelson, W. J. VE-cadherin: at the front, center, and sides of endothelial cell organization and function. *Curr. Opin. Cell Biol.* **22,** 651–8 (2010).

64. Perez-Moreno, M. & Fuchs, E. Guilt by association: What p120-catenin has to hide. *J. Cell Biol.* **199,** 211–214 (2012).

65. Dejana, E. & Vestweber, D. *The role of VE-cadherin in vascular morphogenesis and permeability control*. *Progress in Molecular Biology and Translational Science* **116,** (Elsevier Inc., 2013).

66. Giannotta, M., Trani, M. & Dejana, E. VE-cadherin and endothelial adherens junctions: Active guardians of vascular integrity. *Dev. Cell* **26,** 441–454 (2013).

67. Spindler, V., Schlegel, N. & Waschke, J. Role of GTPases in control of microvascular permeability. *Cardiovasc. Res.* **87,** 243–253 (2010).

68. Wilson, C. W. & Ye, W. Regulation of vascular endothelial junction stability and remodeling through Rap1-Rasip1 signaling. *Cell Adhes. Migr.* **8,** 76–83 (2014).

69. Kooistra, M. R. H., Dube, N. & Bos, J. L. Rap1: a key regulator in cell-cell junction formation. *J. Cell Sci.* **120,** 17–22 (2006).

70. Ferreri, D. M., Minnear, F. L., Yin, T., Kowalczyk, A. P. & Vincent, P. A. N-cadherin levels in endothelial cells are regulated by monolayer maturity and p120 availability. *Cell Commun. Adhes.* **15,** 333–49 (2008).

71. Luo, Y. & Radice, G. L. N-cadherin acts upstream of VE-cadherin in controlling vascular morphogenesis. *J. Cell Biol.* **169,** 29–34 (2005).

72. Radice, G. *et al.* Developmental Deffect in Mouse Embryos Lacking N-Cadherin. *Dev. Biol.* **181,** 64–78 (1997).

73. Navarro, P., Ruco, L. & Dejana, E. Differential localization of VE- and N-cadherins in human endothelial cells: VE-cadherin competes with N-cadherin for junctional localization. *J. Cell Biol.* **140,** 1475–1484 (1998).

74. Cavallaro, U., Liebner, S. & Dejana, E. Endothelial cadherins and tumor angiogenesis. *Exp. Cell Res.* **312,** 659–667 (2006).

75. Tillet, E. *et al.* N-cadherin deficiency impairs pericyte recruitment, and not endothelial differentiation or sprouting, in embryonic stem cell-derived angiogenesis. *Exp. Cell Res.* **310,** 392–400 (2005).

76. Paik, J. H. *et al.* Sphingosine 1-phosphate receptor regulation of N-cadherin mediates vascular stabilization. *Genes Dev.* **18,** 2392–2403 (2004).

77. Giampietro, C. *et al.* Overlapping and divergent signalling pathways of N- and VE-cadherin in endothelial cells. *Blood* **119,** 2159–2170 (2012).

78. Bayless, K. J. & Johnson, G. A. Role of the cytoskeleton in formation and maintenance of angiogenic sprouts. *J. Vasc. Res.* **48,** 369–385 (2011).

79. Lamalice, L., Le Boeuf, F. & Huot, J. Endothelial cell migration during angiogenesis. *Circ. Res.* **100,** 782–794 (2007).

80. Ladoux, B. & Nicolas, A. Physically based principles of cell adhesion mechanosensitivity in tissues. *Reports Prog. Phys.* **75,** (2012).

81. Blanchoin, L., Boujemaa-Paterski, R., Sykes, C. & Plastino, J. Actin dynamics, architecture, and mechanics in cell motility. *Physiol. Rev.* **94,** 235–63 (2014).

82. Chhabra, E. S. & Higgs, H. N. The many faces of actin: Matching assembly factors with cellular structures. *Nat. Cell Biol.* **9,** 1110–1121 (2007).

83. Goley, E. D. & Welch, M. D. The ARP2/3 complex: An actin nucleator comes of age. *Nat. Rev. Mol. Cell Biol.* **7,** 713–726 (2006).

84. Disanza, A. *et al.* Actin polymerization machinery: The finish line of signaling networks, the starting point of cellular movement. *Cell. Mol. Life Sci.* **62,** 955–970 (2005).

85. Lambrechts, A., Van Troys, M. & Ampe, C. The actin cytoskeleton in normal and pathological cell motility. *Int. J. Biochem. Cell Biol.* **36,** 1890–1909 (2004).

86. Paul, A. S. & Pollard, T. D. Review of the mechanism of processive actin filament elongation by formins. *Cell Motil. Cytoskeleton* **66,** 606–617 (2009).

87. Ducka, A. M. *et al.* Structures of actin-bound Wiskott-Aldrich syndrome protein homology 2 (WH2) domains of Spire and the implication for filament nucleation. *Proc. Natl. Acad. Sci.* **107,** 11757–11762 (2010).

88. Lee, S. H. & Dominguez, R. Regulation of actin cytoskeleton dynamics in cells. *Mol. Cells* **29,** 311–325 (2010).

89. Winder, S. J. Actin-binding proteins. *J. Cell Sci.* **118,** 651–654 (2005).

90. Etienne-Manneville, S. Actin and microtubules in cell motility: Which one is in control? *Traffic* **5,** 470–477 (2004).

91. Rottner, K., Faix, J., Bogdan, S., Linder, S. & Kerkhoff, E. Actin assembly mechanisms at a glance. *J. Cell Sci.* **130,** 3427–3435 (2017).

92. Letort, G., Ennomani, H., Gressin, L., Théry, M. & Blanchoin, L. Dynamic reorganization of the actin cytoskeleton. *F1000Research* **4,** 1–11 (2015).

93. https://www.mechanobio.info/cytoskeleton-dynamics/what-is-the-cytoskeleton/what-are-actin-filaments/how-are-actin-filaments-distributed-in-cells-and-tissues/#how-are-actin-filaments-distributed-in-cells-and-tissues.

94. Small, J. V., Stradal, T., Vignal, E. & Rottner, K. The lamellipodium: Where motility begins. *Trends Cell Biol.* **12,** 112–120 (2002).

95. Stricker, J., Falzone, T. & Gardel, M. L. Mechanics of the F-actin cytoskeleton. *J. Biomech.* **43,** 9–14 (2010).

96. Faix, J. & Rottner, K. The making of filopodia. *Curr. Opin. Cell Biol.* **18,** 18–25 (2006).

97. Breitsprecher, D. *et al.* Molecular mechanism of Ena/VASP-mediated actin-filament elongation. *EMBO J.* **30,** 456–467 (2011).

98. Tojkander, S., Gateva, G. & Lappalainen, P. Actin stress fibers - assembly, dynamics and biological roles. *J. Cell Sci.* **125,** 1855–1864 (2012).

99. Pellegrin, S. & Mellor, H. Actin stress fibres. *J. Cell Sci.* **120,** 3491–3499 (2007).

100. Hakkinen, K. M., Harunaga, J. S., Doyle, A. D. & Yamada, K. M. Direct Comparisons of the

Morphology, Migration, Cell Adhesions, and Actin Cytoskeleton of Fibroblasts in Four Different Three-Dimensional Extracellular Matrices. *Tissue Eng. Part A* **17,** 713–724 (2011).

101. Lee, S. & Kumar, S. Actomyosin stress fiber mechanosensing in 2D and 3D. *F1000Research* **5,** 2261 (2016).

102. Campbell, I. D. & Humphries, M. J. Integrin Structure, Activation, and Interactions. *Cold Spring Harb. Perspect. Biol.* **3,** a004994–a004994 (2011).

103. Newham, P. & Humphries, M. J. Integrin adhesion receptors: Structure, function and implications for biomedicine. *Mol. Med. Today* **2,** 304–313 (1996).

104. Calderwood, D. A. Integrin activation. *J. Cell Sci.* **117,** 657–666 (2004).

105. Shattil, S. J., Kim, C. & Ginsberg, M. H. The final steps of integrin activation: The end game. *Nat. Rev. Mol. Cell Biol.* **11,** 288–300 (2010).

106. Calderwood, D. A. & Ginsberg, M. H. Talin forges the links between integrins and actin. *Nat. Cell Biol.* **5,** 694–697 (2003).

107. Klapholz, B. & Brown, N. H. Talin – the master of integrin adhesions. *J. Cell Sci.* jcs.190991 (2017). doi:10.1242/jcs.190991

108. Ginsberg, M. H. Integrin activation. *BMB Rep.* **47,** 655–659 (2014).

109. Wu, C. Focal Adhesion. *Cell Adh. Migr.* **1,** 13–18 (2007).

110. Giancotti, F. G. & Ruoslahti, E. Integrin signaling. *Science (80-.).* **285,** 1028–1032 (1999).

111. Berrier, A. L. & Yamada, K. M. Cell–matrix adhesion. *J. Cell. Physiol.* **213,** 565–573 (2007).

112. Harburger, D. S. & Calderwood, D. A. Integrin signalling at a glance. *J. Cell Sci.* **122,** 1472–1472 (2009).

113. Wozniak, M. A., Modzelewska, K., Kwong, L. & Keely, P. J. Focal adhesion regulation of cell behavior. *Biochim. Biophys. Acta - Mol. Cell Res.* **1692,** 103–119 (2004).

114. Mitra, S. K. & Schlaepfer, D. D. Integrin-regulated FAK-Src signaling in normal and cancer cells. *Curr. Opin. Cell Biol.* **18,** 516–523 (2006).

115. Huveneers, S. & Danen, E. H. J. Adhesion signaling - crosstalk between integrins, Src and Rho. *J. Cell Sci.* **122,** 1059–1069 (2009).

116. Tomar, A. & Schlaepfer, D. D. Focal adhesion kinase: switching between GAPs and GEFs in the regulation of cell motility. *Curr. Opin. Cell Biol.* **21,** 676–83 (2009).

117. Schaller, M. D. Cellular functions of FAK kinases: insight into molecular mechanisms and novel functions. *J. Cell Sci.* **123,** 1007–1013 (2010).

118. Parsons, J. T., Horwitz, A. R. & Schwartz, M. A. Cell adhesion: integrating cytoskeletal dynamics and cellular tension. *Nat. Rev. Mol. Cell Biol.* **11,** 633–43 (2010).

119. Webb, D. J., Parsons, J. T. & Horwitz, A. F. Adhesion assembly, disassembly and turnover in migrating cells - Over and over and over again. *Nat. Cell Biol.* **4,** (2002).

120. Nagano, M., Hoshino, D., Koshikawa, N., Akizawa, T. & Seiki, M. Turnover of focal adhesions and cancer cell migration. *Int. J. Cell Biol.* **2012,** (2012).

121. Webb, D. J. *et al.* FAK-Src signalling through paxillin, ERK and MLCK regulates adhesion disassembly. *Nat. Cell Biol.* **6,** 154–161 (2004).

122. Vicente-Manzanares, M. & Horwitz, A. R. Adhesion dynamics at a glance. *J. Cell Sci.* **124,** 3923–3927 (2011).

123. Geiger, B. & Yamada, K. M. Molecular Architecture and Function of Matrix Adhesions. 1–22 (2011). doi:10.1101/cshperspect.a005033

124. Byron, A., Morgan, M. R. & Humphries, M. J. Adhesion signalling complexes. *Curr. Biol.* **20,** R1063–R1067 (2010).

125. Wennerberg, K., Rossman, K. L. & Der, C. J. The Ras superfamily at a glance. *J. Cell Sci.* **118,** 843–6 (2005).

126. Colicelli, J. Human RAS Superfamily Proteins and Related GTPases. *Sci. Signal.* **2004,** re13-re13 (2004).

127. Goitre, L., Trapani, E., Trabalzini, L. & Retta, S. F. The Ras superfamily of small GTPases: the unlocked secrets. *Methods Mol. Biol.* **1120,** 1–18 (2014).

128. Vetter, I. R. The Structure of the G Domain of the Ras Superfamily. 25–51 (2014). doi:10.1007/978-3-7091-1806-1

129. Vetter, I. R. & Wittinghofer, A. The Guanine in Switch Three Dimensions. *Science (80-.).* **294,** 1299–1304 (2001).

130. Bos, J., Rehmann, H. & Wittinghofer, A. GEFs and GAPs : Critical Elements in the Control of Small G Proteins. *Cell* 865–877 (2007). doi:10.1016/j.cell.200

131. Cherfils, J. & Zeghouf, M. Regulation of Small GTPases by GEFs, GAPs, and GDIs. *Physiol. Rev.* **93,** 269–309 (2013).

132. Ahearn, I., Zhou, M. & Philips, M. R. Posttranslational Modifications of RAS Proteins. *Cold Spring Harb. Perspect. Med.* a031484 (2018). doi:10.1101/cshperspect.a031484

133. Castellano, E. & Downward, J. Role of RAS in the Regulation of PI 3-Kinase. in *Current topics in microbiology and immunology* **346,** 143–169 (2010).

134. Castellano, E. & Santos, E. Functional specificity of Ras isoforms: So similar but so different. *Genes and Cancer* **2,** 216–231 (2011).

135. Esteban, L. M. *et al.* Targeted Genomic Disruption of H- ras and N- ras , Individually or in Combination , Reveals the Dispensability of Both Loci for Mouse Growth and Development Targeted Genomic Disruption of H- ras and N- ras , Individually or in Combination , Reveals the Di. **21,** 1444–1452 (2001).

136. Johnson, L. *et al.* K-ras is an essential gene in the mouse with partial functional overlap with N-ras. *Genes Dev.* **11,** 2468–2481 (1997).

137. Quilliam, L. A., Rebhun, J. F. & Castro, A. F. A growing family of guanine nucleotide exchange factors is responsible for activation of ras-family GTPases. **71,** 391–444 (2002).

138. Mitin, N., Rossman, K. L. & Der, C. J. Signaling interplay in ras superfamily function. *Curr. Biol.* **15,** 563–574 (2005).

139. Schlessinger, J. How receptor tyrosine kinases activate Ras. 273–275 (1993).

140. Egan, S. E. & Weinberg, R. A. The pathway to signal achievement. *Nature* **365,** 781–783 (1993).

141. Pierce, K. L., Luttrell, L. M. & Lefkowitz, R. J. New mechanisms in heptahelical receptor signaling to mitogen activated protein kinase cascades. *Oncogene* **20,** 1532–1539 (2001).

142. Stone, J. C. Regulation and function of the rasGRP family of ras activators in blood cells. *Genes and Cancer* **2,** 320–334 (2011).

143. Wortzel, I. & Seger, R. The ERK cascade: Distinct functions within various subcellular organelles. *Genes and Cancer* **2,** 195–209 (2011).

144. McCubrey, J. A. *et al.* Mutations and Deregulation of Ras/Raf/MEK/ERK and PI3K/PTEN/Akt/mTOR Cascades. *Oncotarget* **3,** 954–987 (2012).

145. Guo, X. X. *et al.* Rap-Interacting Proteins are Key Players in the Rap Symphony Orchestra. *Cell. Physiol. Biochem.* **39,** 137–156 (2016).

146. Wittchen, E. S., Aghajanian, A. & Burridge, K. Isoform-specific differences between Rap1A and Rap1B GTPases in the formation of endothelial cell junctions. *Small GTPases* **2,** 65–76 (2011).

147. Hariharan, I. K. Ras and Rap: Are former enemies now friends? *Dev. Cell* **8,** 303–304 (2005).

148. Shah, S., Brock, E. J., Ji, K. & Mattingly, R. R. Ras and Rap1: A tale of two GTPases. *Semin. Cancer Biol.* 0–1 (2018). doi:10.1016/j.semcancer.2018.03.005

149. Chrzanowska-Wodnicka, M. Distinct functions for Rap1 signaling in vascular morphogenesis and dysfunction. *Exp. Cell Res.* **319,** 2350–9 (2013).

150. Chrzanowska-Wodnicka, M., White, G. C., Quilliam, L. A. & Whitehead, K. J. Small GTPase Rap1 is essential for mouse development and formation of functional vasculature. *PLoS One* **10,** 1–16 (2015).

151. Carmona, G. *et al.* Role of the small GTPase Rap1 for integrin activity regulation in endothelial cells and angiogenesis. *Angiogenesis* **113,** 488–497 (2009).

152. Chrzanowska-Wodnicka, M., Kraus, A. E., Gale, D., White, G. C. & Vansluys, J. Defective angiogenesis, endothelial migration, proliferation, and MAPK signaling in Rap1b-deficient mice. *Blood* **111,** 2647–2656 (2008).

153. Pannekoek, W. J., Kooistra, M. R. H., Zwartkruis, F. J. T. & Bos, J. L. Cell-cell junction formation: The role of Rap1 and Rap1 guanine nucleotide exchange factors. *Biochim. Biophys. Acta - Biomembr.* **1788,** 790–796 (2009).

154. Bos, J. L., De Rooij, J. & Reedquist, K. A. Rap1 signalling: Adhering to new models. *Nat. Rev. Mol. Cell Biol.* **2,** 369–377 (2001).

155. Cheng, X., Ji, Z., Tsalkova, T. & Mei, F. Epac and PKA: A tale of two intracellular cAMP receptors. *Acta Biochim. Biophys. Sin. (Shanghai).* **40,** 651–662 (2008).

156. Kuiperij, H. B. *et al.* Characterisation of PDZ-GEFs, a family of guanine nucleotide exchange factors specific for Rap1 and Rap2. *Biochim. Biophys. Acta - Mol. Cell Res.* **1593,** 141–149 (2003).

157. Radha, V., Mitra, A., Dayma, K. & Sasikumar, K. Signalling to actin: role of C3G, a multitasking guanine-nucleotide-exchange factor. *Biosci. Rep.* **31,** 231–244 (2011).

158. Fujita, H. *et al.* Local activation of Rap1 contributes to directional vascular endothelial cell migration accompanied by extension of microtubules on which RAPL, a Rap1-associating molecule, localizes. *J. Biol. Chem.* **280,** 5022–5031 (2005).

159. Medeiros, R. B. *et al.* Protein kinase D1 and the β1 integrin cytoplasmic domain control β1 integrin function via regulation of Rap1 activation. *Immunity* **23,** 213–226 (2005).

160. Lafuente, E. M. *et al.* RIAM, an Ena/VASP and Profilin ligand, interacts with Rap1-GTP and

mediates Rap1-induced adhesion. *Dev. Cell* **7,** 585–95 (2004).

161. Raaijmakers, J. H. & Bos, J. L. Specificity in Ras and Rap Signaling. *J. Biol. Chem.* **284,** 10995 (2009).

162. Glading, A., Han, J., Stockton, R. A. & Ginsberg, M. H. KRIT-1/CCM1 is a Rap1 effector that regulates endothelial cell-cell junctions. *J. Cell Biol.* **179,** 247–254 (2007).

163. Simanshu, D. K., Nissley, D. V. & McCormick, F. RAS Proteins and Their Regulators in Human Disease. *Cell* **170,** 17–33 (2017).

164. Kodaz, Hilmi Osman Kostek, Muhammet Bekir Hacioglu, Bulent Erdogan, C. E. K. & Ilhan Hacibekiroglu, Esma Turkmen, Sernaz Uzunoglu, I. C. Frequency of RAS Mutations (KRAS, NRAS, HRAS) in Human Solid Cancer. *Eurasian J. Med. Oncol.* **1,** 1–7 (2017).

165. Gyan, E. *et al.* Mutation in RAP1 is a rare event in myelodysplastic syndromes. *Leukemia* **19,** 1678–1680 (2005).

166. Maertens, O. & Cichowski, K. An expanding role for RAS GTPase activating proteins (RAS GAPs) in cancer. *Adv. Biol. Regul.* **55,** 1–14 (2014).

167. Vigil, D., Cherfils, J., Rossman, K. L. & Der, C. J. Ras superfamily GEFs and GAPs: validated and tractable targets for cancer therapy? *Nat. Rev. Cancer* **10,** 842–57 (2010).

168. Cullen, P. J. *et al.* Identification of a specific Ins(l,3,4,5)P4-binding protein as a member of the GAP1 family. *Nature* **376,** 527–530 (1995).

169. Lockyer, P. J. *et al.* Distinct subcellular localisations of the putative inositol 1,3,4,5tetrakisphosphate receptors GAP1(IP4BP) and GAP(1m) result from the GAP1(IP4BP) PH domain directing plasma membrane targeting. *Curr. Biol.* **7,** 1007–1010 (1997).

170. McNulty, T. J., Letcher, A. J., Dawson, A. P. & Irvine, R. F. Tissue distribution of GAP1IP4BP and GAP1m: Two inositol 1,3,4,5-tetrakisphosphate-binding proteins. *Cell. Signal.* **13,** 877–886 (2001).

171. Iwashita, S. *et al.* Versatile roles of R-Ras GAP in neurite formation of PC12 cells and embryonic vascular development. *J. Biol. Chem.* **282,** 3413–3417 (2007).

172. Blanc, L. *et al.* Critical function for the Ras-GTPase activating protein RASA3 in vertebrate erythropoiesis and megakaryopoiesis. *Proc. Natl. Acad. Sci.* **109,** 12099–12104 (2012).

173. Bottomley, J. R., Reynolds, J. S., Lockyer, P. J. & Cullen, P. J. Structural and functional analysis of the putative inositol 1,3,4, 5-tetrakisphosphate receptors GAP1(IP4BP) and GAP1(m). *Biochem. Biophys. Res. Commun.* **250,** 143–9 (1998).

174. Cullen, P. J. Bridging the GAP in inositol 1,3,4,5-tetrakisphosphate signalling. *Biochim. Biophys. Acta - Mol. Cell Biol. Lipids* **1436,** 35–47 (1998).

175. Schurmans, S., Polizzi, S., Scoumanne, A., Sayyed, S. & Molina-Ortiz, P. The Ras/Rap GTPase activating protein RASA3: From gene structure to invivo functions. *Adv. Biol. Regul.* **57,** 153–161 (2015).

176. Yarwood, S., Bouyoucef-Cherchalli, D., Cullen, P. J. & Kupzig, S. The GAP1 family of GTPase-activating proteins: spatial and temporal regulators of small GTPase signalling. *Biochem. Soc. Trans.* **34,** 846–50 (2006).

177. Cozier, G. E. *et al.* GAP1IP4BP contains a novel group I pleckstrin homology domain that directs constitutive plasma membrane association. *J. Biol. Chem.* **275,** 28261–8 (2000).

178. Marechal, Y. *et al.* Inositol 1,3,4,5-tetrakisphosphate controls proapoptotic Bim gene

expression and survival in B cells. *Proc. Natl. Acad. Sci.* **104,** 13978–13983 (2007).

179. Nafisi, H., Banihashemi, B., Daigle, M. & Albert, P. R. GAP1(IP4BP)/RASA3 mediates Gαi-induced inhibition of mitogen-activated protein kinase. *J. Biol. Chem.* **283,** 35908–35917 (2008).

180. Walker, S. A. *et al.* Analyzing the role of the putative inositol 1,3,4,5-tetrakisphosphate receptor GAP1IP4BP in intracellular Ca2+ homeostasis. *J. Biol. Chem.* **277,** 48779–48785 (2002).

181. Battram, A. M. *et al.* The phosphatidylinositol 3,4,5-trisphosphate (PI(3,4,5)P3) binder Rasa3 regulates phosphoinositide 3-kinase (PI3K)-dependent integrin αIIbβ3outside-in signaling. *J. Biol. Chem.* **292,** 1691–1704 (2017).

182. Peters, L. L., McFarland-Starr, E. C., Wood, B. G. & Barker, J. E. Heritable severe combined anemia and thrombocytopenia in the mouse: Description of the disease and successful therapy. *Blood* **76,** 745–754 (1990).

183. Molina-Ortiz, P. *et al.* Rasa3 Controls Megakaryocyte Rap1 Activation, Integrin Signaling and Differentiation into Proplatelet. *PLoS Genet.* **10,** (2014).

184. Stefanini, L. *et al.* RASA3 is a critical inhibitor of RAP1-dependent platelet activation. *J. Clin. Invest.* **125,** 1419–1432 (2015).

185. Choi, Y. J. *et al.* Whole-exome sequencing identified the genetic origin of a mucinous neoplasm in a mature cystic teratoma. *Pathology* **48,** 372–376 (2016).

186. Abaan, O. D. *et al.* The Exomes of the NCI-60 Panel: A Genomic Resource for Cancer Biology and Systems Pharmacology. *Cancer Res.* **73,** 4372–4382 (2013).

187. Tang, J. *et al.* Cancer driver–passenger distinction via sporadic human and dog cancer comparison: a proof-of-principle study with colorectal cancer. *Oncogene* **33,** 814–822 (2014).

188. Yao, R., Yi, Y., Grubbs, C. J., Lubet, R. A. & You, M. Gene expression profiling of chemically induced rat bladder tumors. *Neoplasia* **9,** 207–21 (2007).

189. Karnoub, A. E. & Weinberg, R. A. Ras oncogenes: split personalities. *Nat. Rev. Mol. Cell Biol.* **9,** 517–31 (2008).

190. Grewal, T., Koese, M., Tebar, F. & Enrich, C. Differential Regulation of RasGAPs in Cancer. *Genes Cancer* **2,** 288–97 (2011).

191. Goldsmith, J. R. & Jobin, C. Think small: Zebrafish as a model system of human pathology. *J. Biomed. Biotechnol.* **2012,** (2012).

192. Ny, A., Autiero, M. & Carmeliet, P. Zebrafish and Xenopus tadpoles: Small animal models to study angiogenesis and lymphangiogenesis. *Exp. Cell Res.* **312,** 684–693 (2006).

193. Chávez, M. N., Aedo, G., Fierro, F. A., Allende, M. L. & Egaña, J. T. Zebrafish as an emerging model organism to study angiogenesis in development and regeneration. *Front. Physiol.* **7,** 1–15 (2016).

194. Lawson, N. D. & Weinstein, B. M. In vivo imaging of embryonic vascular development using transgenic zebrafish. *Dev. Biol.* **248,** 307–318 (2002).

195. Parmentier, C. Pourquoi le poisson zèbre.pdf. *Rev. Fr. Histotechnologie* **22,** 49–62 (2009).

196. Grillitsch, S. The influence of environmental PO2 on hemoglobin oxygen saturation in developing zebrafish Danio rerio. *J. Exp. Biol.* **208,** 309–316 (2005).

197. Ellertsdóttir, E. *et al.* Vascular morphogenesis in the zebrafish embryo. *Dev. Biol.* **341,** 56–65 (2010).

198. Hermkens, D. M. A., Duckers, H. J. & Schulte-merker, S. Vascular Development in the Zebrafish. 47–57 (2015). doi:10.1007/978-1-4939-2907-8

199. Isogai, S. Angiogenic network formation in the developing vertebrate trunk. *Development* **130,** 5281–5290 (2003).

200. Schuermann, A., Helker, C. S. M. & Herzog, W. Angiogenesis in zebrafish. *Semin. Cell Dev. Biol.* **31,** 106–114 (2014).

201. Hen, G. *et al.* Venous-derived angioblasts generate organ-specific vessels during zebrafish embryonic development. *Development* **142,** 4266–4278 (2015).

202. Hetheridge, C. *et al.* The formin FMNL3 is a cytoskeletal regulator of angiogenesis. *J. Cell Sci.* **125,** 1420–1428 (2012).

203. Bayless, K. J. & Johnson, G. A. Role of the cytoskeleton in formation and maintenance of angiogenic sprouts. *J. Vasc. Res.* **48,** 369–85 (2011).

204. Millán, J. *et al.* Adherens junctions connect stress fibres between adjacent endothelial cells. *BMC Biol.* **8,** 11 (2010).

205. Liebner, S., Cavallaro, U. & Dejana, E. The multiple languages of endothelial cell-to-cell communication. *Arterioscler. Thromb. Vasc. Biol.* **26,** 1431–1438 (2006).

206. Bedell, V. M., Westcot, S. E. & Ekker, S. C. Lessons from morpholino-based screening in zebrafish. *Brief. Funct. Genomics* **10,** 181–188 (2011).

207. Eve, A. M. J., Place, E. S. & Smith, J. C. Comparison of Zebrafish tmem88a mutant & morpholino knockdown phenotypes. *PLoS One* **12,** 1–17 (2017).

208. Sertori, R., Trengove, M., Basheer, F., Ward, A. C. & Liongue, C. Genome editing in zebrafish: A practical overview. *Brief. Funct. Genomics* **15,** 322–330 (2016).

209. Choi, J. *et al.* Aplexone targets the HMG-CoA reductase pathway and differentially regulates arteriovenous angiogenesis. *Development* **138,** 1173–1181 (2011).

210. karthik, S. *et al.* Synergistic interaction of sprouting and intussusceptive angiogenesis during zebrafish caudal vein plexus development. *Sci. Rep.* **8,** 9840 (2018).

211. Wakayama, Y., Fukuhara, S., Ando, K., Matsuda, M. & Mochizuki, N. Cdc42 mediates Bmp - Induced sprouting angiogenesis through Fmnl3-driven assembly of endothelial filopodia in zebrafish. *Dev. Cell* **32,** 109–122 (2015).

212. Goi, M. & Childs, S. J. Patterning mechanisms of the sub-intestinal venous plexus in zebrafish. *Dev. Biol.* **409,** 114–128 (2016).

213. Zovein, A. C. *et al.* β1 Integrin Establishes Endothelial Cell Polarity and Arteriolar Lumen Formation via a Par3-Dependent Mechanism. *Dev. Cell* **18,** 39–51 (2010).

214. Kleaveland, B. *et al.* Regulation of cardiovascular development and integrity by the heart of glass–cerebral cavernous malformation protein pathway. *Nat. Med.* **15,** 169–176 (2009).

215. Cattelino, A. *et al.* The conditional inactivation of the beta-catenin gene in endothelial cells causes a defective vascular pattern and increased vascular fragility. *J. Cell Biol.* **162,** 1111–22 (2003).

216. Jackson, A. L. & Linsley, P. S. Recognizing and avoiding siRNA off-target effects for target

identification and therapeutic application. *Nat. Rev. Drug Discov.* **9,** 57–67 (2010).

217. Gore, A. V., Lampugnani, M. G., Dye, L., Dejana, E. & Weinstein, B. M. Combinatorial interaction between CCM pathway genes precipitates hemorrhagic stroke. *Dis. Model. Mech.* **1,** 275–281 (2008).

218. Boettner, B. & Van Aelst, L. Control of cell adhesion dynamics by Rap1 signaling. *Curr. Opin. Cell Biol.* **21,** 684–693 (2009).

219. Bos, J. L. Linking Rap to cell adhesion. *Curr. Opin. Cell Biol.* **17,** 123–128 (2005).

220. Chrzanowska-Wodnicka, M., White, G. C., Quilliam, L. A. & Whitehead, K. J. Small GTPase Rap1 Is Essential for Mouse Development and Formation of Functional Vasculature. *PLoS One* **10,** e0145689 (2015).

221. Pannekoek, W.-J. *et al.* Epac1 and PDZ-GEF cooperate in Rap1 mediated endothelial junction control. *Cell. Signal.* **23,** 2056–2064 (2011).

222. Yan, J., Li, F., Ingram, D. A. & Quilliam, L. A. Rap1a is a key regulator of fibroblast growth factor 2-induced angiogenesis and together with Rap1b controls human endothelial cell functions. *Mol. Cell. Biol.* **28,** 5803–10 (2008).

223. Post, A., Pannekoek, W. J., Ponsioen, B., Vliem, M. J. & Bos, J. L. Rap1 Spatially Controls ArhGAP29 To Inhibit Rho Signaling during Endothelial Barrier Regulation. *Mol. Cell. Biol.* **35,** 2495–2502 (2015).

224. Ferrando, I. M. *et al.* Identification of Targets of c-Src Tyrosine Kinase by Chemical Complementation and Phosphoproteomics. *Mol. Cell. Proteomics* **11,** 355–369 (2012).

225. Iruela-Arispe, M. L. & Davis, G. E. Cellular and Molecular Mechanisms of Vascular Lumen Formation. *Dev. Cell* **16,** 222–231 (2009).

226. Vestweber, D., Winderlich, M., Cagna, G. & Nottebaum, A. F. Cell adhesion dynamics at endothelial junctions: VE-cadherin as a major player. *Trends Cell Biol.* **19,** 8–15 (2009).

227. Wehrle-Haller, B. Assembly and disassembly of cell matrix adhesions. *Curr. Opin. Cell Biol.* **24,** 569–581 (2012).

228. Steed, E., Balda, M. S. & Matter, K. Dynamics and functions of tight junctions. *Trends Cell Biol.* **20,** 142–149 (2010).

229. Montero-Balaguer, M. *et al.* Stable Vascular Connections and Remodeling Require Full Expression of VE-Cadherin in Zebrafish Embryos. *PLoS One* **4,** e5772 (2009).

230. Carmeliet, P. *et al.* Targeted Deficiency or Cytosolic Truncation of the VE-cadherin Gene in Mice Impairs VEGF-Mediated Endothelial Survival and Angiogenesis. *Cell* **98,** 147–157 (1999).

231. Martin, M. *et al.* PP2A regulatory subunit Bα controls endothelial contractility and vessel lumen integrity via regulation of HDAC7. *EMBO J.* **32,** 2491–2503 (2013).

232. Weber, G. F., Bjerke, M. A. & DeSimone, D. W. Integrins and cadherins join forces to form adhesive networks. *J. Cell Sci.* **124,** 1183–93 (2011).

233. Yamamoto, H. *et al.* Integrin β1 controls VE-cadherin localization and blood vessel stability. *Nat. Commun.* **6,** 6429 (2015).

234. Jossin, Y. Polarization of migrating cortical neurons by Rap1 and N-cadherin: Revisiting the model for the Reelin signaling pathway. *Small GTPases* **2,** 322–328 (2011).

235. King, P. D., Lubeck, B. A. & Lapinski, P. E. Nonredundant functions for Ras GTPase-activating proteins in tissue homeostasis. *Sci. Signal.* **6,** re1 (2013).

236. Arafeh, R. *et al.* Europe PMC Funders Group Recurrent inactivating RASA2 mutations in melanoma. **47,** 1408–1410 (2016).

237. Zhang, J., Guo, J., Dzhagalov, I. & He, Y.-W. An essential function for the calcium-promoted Ras inactivator in Fcgamma receptor-mediated phagocytosis. *Nat. Immunol.* **6,** 911–9 (2005).

238. Westbrook, T. F. *et al.* A genetic screen for candidate tumor suppressors identifies REST. *Cell* **121,** 837–848 (2005).

239. Poetsch, A. R. *et al. RASA4* undergoes DNA hypermethylation in resistant juvenile myelomonocytic leukemia. *Epigenetics* **9,** 1252–1260 (2014).

240. Calvisi, D. F. *et al.* Inactivation of Ras GTPase-activating proteins promotes unrestrained activity of wild-type Ras in human liver cancer. *J. Hepatol.* **54,** 311–9 (2011).

241. Takata, A., Otsuka, M., Kishikawa, T. & Yamagami, M. RASAL1 is a potent regulator liver fibrosis. **8,** 64840–64852 (2017).

242. Jin, H. *et al.* Epigenetic silencing of a Ca2+-regulated Ras GTPase-activating protein RASAL defines a new mechanism of Ras activation in human cancers. *Proc. Natl. Acad. Sci.* **104,** 12353–12358 (2007).

243. Nicoli, S. & Presta, M. The zebrafish/tumor xenograft angiogenesis assay. *Nat. Protoc.* **2,** 2918–2923 (2007).

244. Hollenbach, M., Stoll, S. J., Jörgens, K., Seufferlein, T. & Kroll, J. Different Regulation of Physiological and Tumor Angiogenesis in Zebrafish by Protein Kinase D1 (PKD1). *PLoS One* **8,** 1–12 (2013).

245. Stehbens, S. J. & Wittmann, T. Analysis of focal adhesion turnover: a quantitative live-cell imaging example. *Methods Cell Biol.* **123,** 335–46 (2014).

246. Bolós, V., Gasent, J. M., López-Tarruella, S. & Grande, E. The dual kinase complex FAK-Src as a promising therapeutic target in cancer. *Onco. Targets. Ther.* **3,** 83–97 (2010).

Annex 1

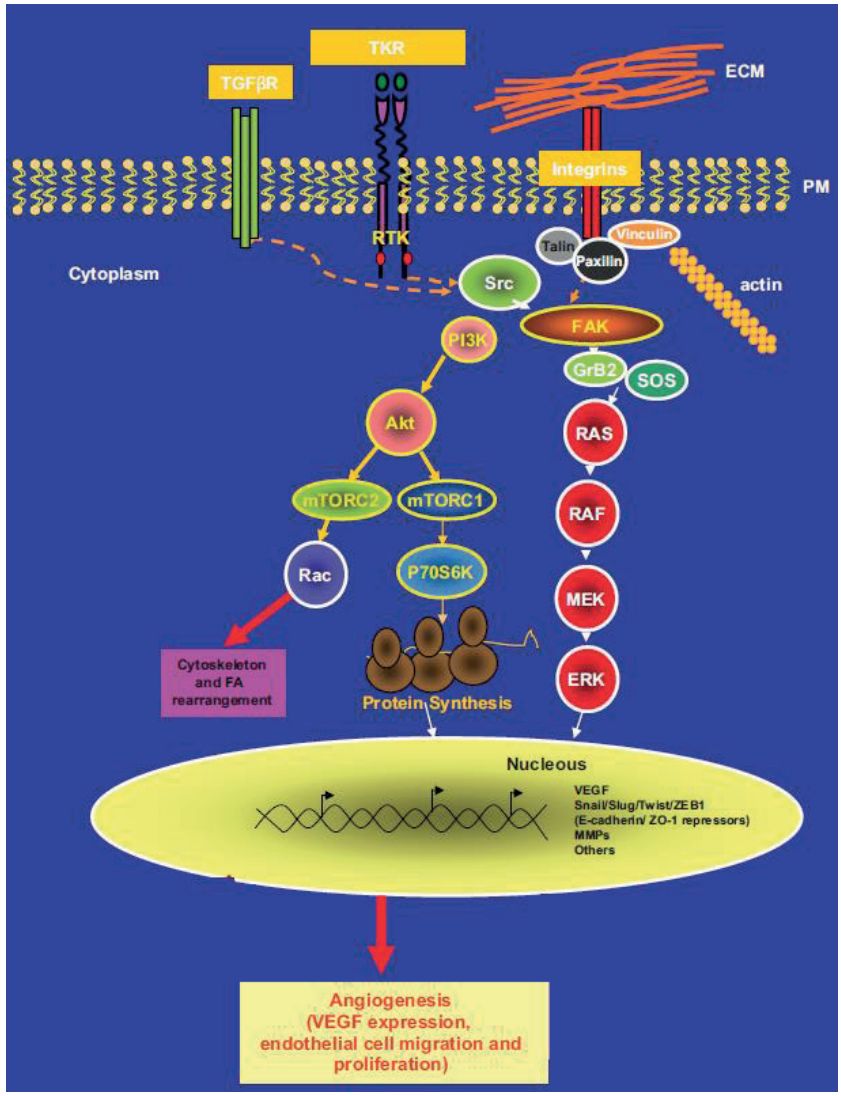

Figure A: FAK/Src signaling pathways. Once activated by integrins or tyrosine kinase receptors, FAK/SRC complex transduces signals through the activation of different intracellular signaling pathways such as PI-3K or MAPK. Activation of FAK leads to the activation of some small GTPases such as Rac leading to FA rearrangement. (Adapted from [246])

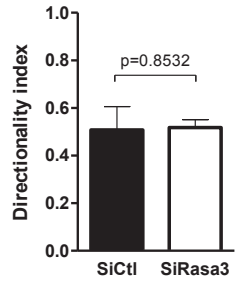

Figure B: Rasa3-depleted cells didn't display any directionality defects. A directionality index of 1 represents completely directional movement in a straight line perpendicular to the wound edge and a directionality index of 0 represents totally random cell movement. Directionality index were calculated using imageJ software.

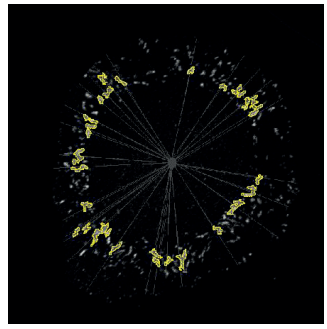

Figure C: How the ratio in Figure 35D is calculated. Using ImageJ software, all adhesions >1 μm^2 are isolated. The center of the cell is marked approximatively. The distance of all adhesions > 1 μm^2 from the center of the cell to the adhesion (a) and the distance of all adhesions > 1 μm^2 from the cell center to the cell periphery are calculated (p). The ratio is a divided by p

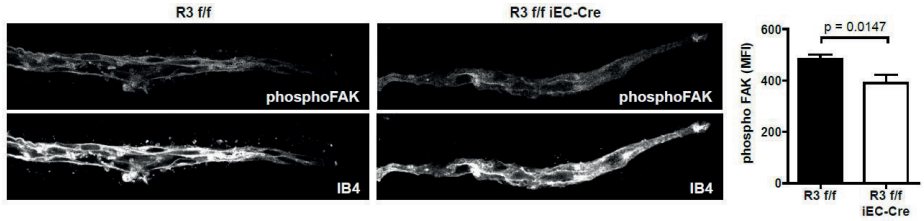

Figure D: Depletion of Rasa3 impairs activation FAK in vivo. Immunofluorescence analysis of aortic ring sprouts from $R3^{f/f}$ and $R3^{f/f}$ iEC-Cre mice stained for the IB4 endothelial marker (lower) and with an anti-phospho-FAK antibody (upper).

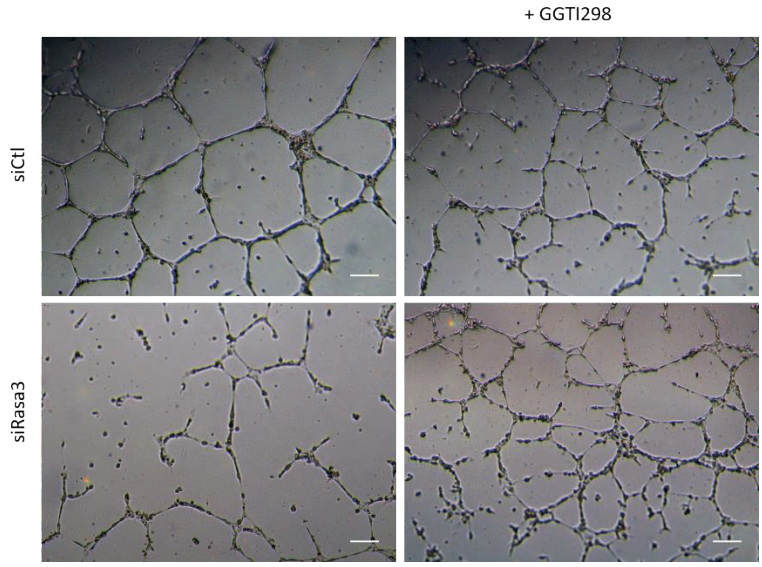

Figure E: Representative images from Figure 46A (Matrigel). Representative images of a tube-like formation assay in matrigel using ctl or siRasa3-HUVECs treated or not with Rap1 inhibitor (GGTI298).

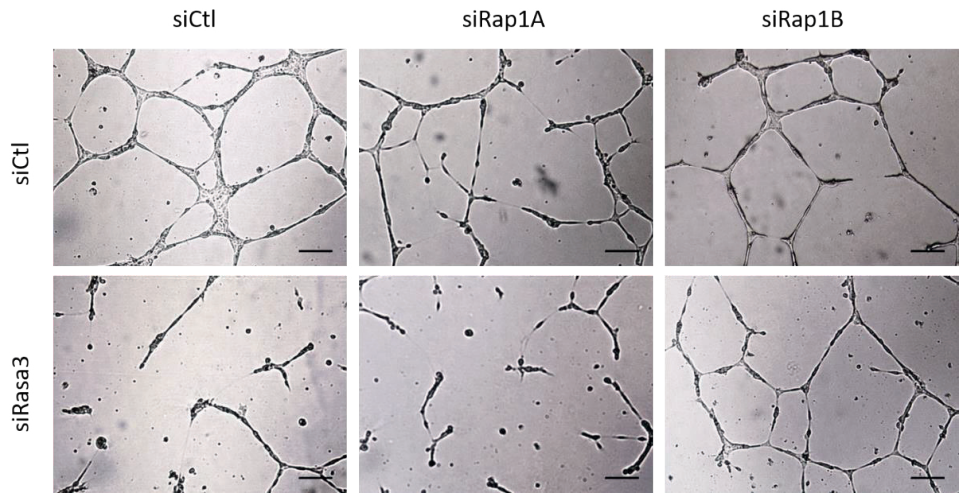

Figure F: Representative images from Figure 46C (Matrigel). Representative images of a tube-like formation assay in matrigel using ctl or siRasa3-HUVECs treated or not with siRap1a or siRap1b.

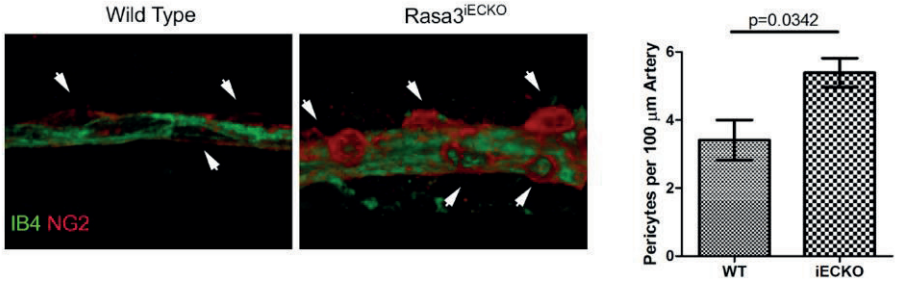

Figure G: Alterations of pericyte morphology in R3f/f iEC-Cre mouse retinas. (**Left**) Immunofluorescence analysis of retinas from $R3^{f/f}$ and $R3^{f/f}$ iEC-Cre mice stained for the IB4 endothelial marker and with an anti-NG2 antibody (pericyte marker). (**Right**) Quantification of pericytes per endothelial cell surface.

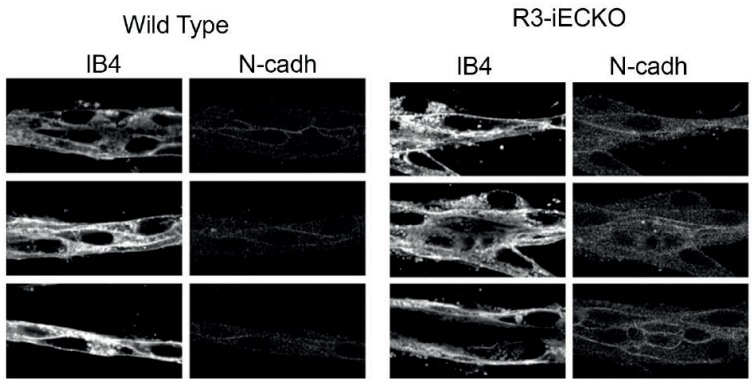

Figure H: N-cadherin expression is increased upon Rasa3 depletion in mice. Immunofluorescence analysis of aortic ring sprouts from $R3^{f/f}$ (wild type) and $R3^{f/f}$ iEC-Cre mice stained for the IB4 endothelial marker and with an anti-N-cadherin antibody.

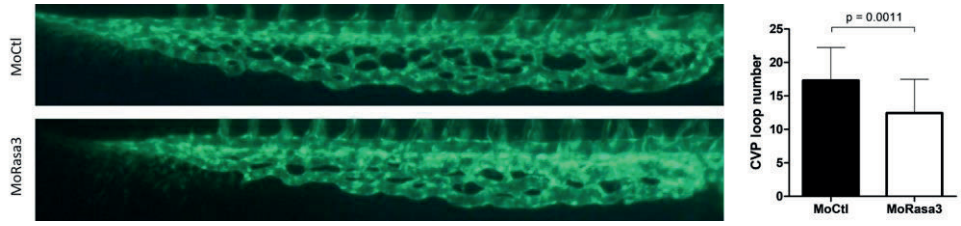

Figure I: Rasa3 depletion reduces loop formation at CVP (caudal vein plexus). (**Left**) Tg(fli1a:eGFP)y1 embryos were injected with control morpholino (MoCtl) or with morpholino targeting Rasa3 (MoRasa3). Pictures of CVP were taken at 48 hpf. (**Right**) Quantification of loop formation at CVP. Histograms are mean ± SD from 25 embryos. The p value is shown (Student's t-test).

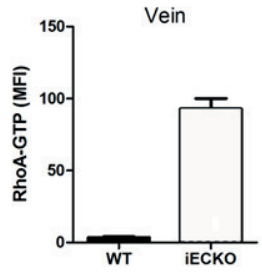

Figure J: RhoA is activated upon depletion of Rasa3 *in vivo*. Quantification of active RhoA-GTP mean fluorescence intensity (MFI) in veins of $R3^{f/f}$ and $R3^{f/f}$ iEC-Cre newborn retinas.

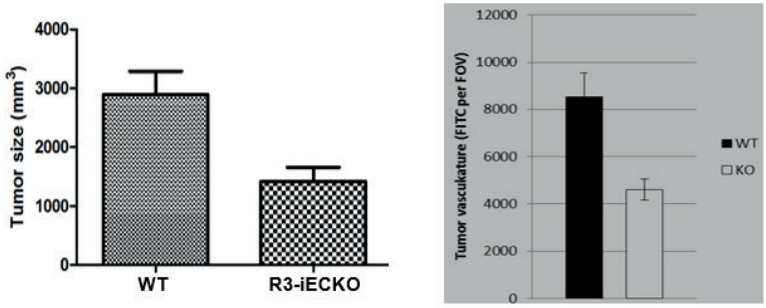

Figure K: Subcutaneous injection of LLC1 cells in $R3^{f/f}$ and $R3^{f/f}$ iEC-Cre mice. (**Left**) Analysis of tumor size in $R3^{f/f}$ and $R3^{f/f}$ iEC-Cre mice 15 days after injection (**Right**) Analysis of tumor vasculature using FITC-Dextran dye.

Annex 2

PLOS GENETICS

RESEARCH ARTICLE

Rasa3 controls turnover of endothelial cell adhesion and vascular lumen integrity by a Rap1-dependent mechanism

Patricia Molina-Ortiz[1☯], Tanguy Orban[2☯], Maud Martin[1,2¤], Audrey Habets[2], Franck Dequiedt[2‡], Stéphane Schurmans[1‡*]

1 Laboratory of Functional Genetics, GIGA-Molecular Biology of Disease, University of Liège, Liège, Belgium, **2** Laboratory of Protein signaling and Interactions Signalisation, GIGA-Molecular Biology of Diseases, University of Liège, Liège, Belgium

☯ These authors contributed equally to this work.
¤ Current address: Cell Biology, Department of Biology, Faculty of Science, Utrecht University, Utrecht, the Netherlands
‡ FD and SS also contributed equally to this work.
* sschurmans@ulg.ac.be

OPEN ACCESS

Citation: Molina-Ortiz P, Orban T, Martin M, Habets A, Dequiedt F, Schurmans S (2018) Rasa3 controls turnover of endothelial cell adhesion and vascular lumen integrity by a Rap1-dependent mechanism. PLoS Genet 14(1): e1007195. https://doi.org/10.1371/journal.pgen.1007195

Editor: Gregory S. Barsh, Stanford University School of Medicine, UNITED STATES

Received: September 13, 2017

Accepted: January 9, 2018

Published: January 30, 2018

Data Availability Statement: All relevant data are within the paper and its Supporting Information files.

Funding: This work was supported by grants from the University of Liège (to SS and FD), the Fonds Léon Frédéricq (to FD), the Belgian National Fund for Scientific Research (FRS-FNRS, grant T.0003.15 to SS), Télévie (to FD), the Interuniversity Attraction Poles Program–Belgian Science Policy (IUAP-BELSPO PVI/28 and PVII/13, to FD). PMO is a Welbio and ARC Post-doctoral

Abstract

Rasa3 is a GTPase activating protein of the GAP1 family which targets R-Ras and Rap1. Although catalytic inactivation or deletion of Rasa3 in mice leads to severe hemorrhages and embryonic lethality, the biological function and cellular location of Rasa3 underlying these defects remains unknown. Here, using a combination of loss of function studies in mouse and zebrafish as well as *in vitro* cell biology approaches, we identify a key role for Rasa3 in endothelial cells and vascular lumen integrity. Specific ablation of Rasa3 in the mouse endothelium, but not in megakaryocytes and platelets, lead to embryonic bleeding and death at mid-gestation, recapitulating the phenotype observed in full *Rasa3* knock-out mice. Reduced plexus/sprouts formation and vascular lumenization defects were observed when Rasa3 was specifically inactivated in mouse endothelial cells at the postnatal or adult stages. Similar results were obtained in zebrafish after decreasing Rasa3 expression. *In vitro*, depletion of Rasa3 in cultured endothelial cells increased β1 integrin activation and cell adhesion to extracellular matrix components, decreased cell migration and blocked tubulogenesis. During migration, these Rasa3-depleted cells exhibited larger and more mature adhesions resulting from a perturbed dynamics of adhesion assembly and disassembly which significantly increased their life time. These defects were due to a hyperactivation of the Rap1 GTPase and blockade of FAK/Src signaling. Finally, Rasa3-depleted cells showed reduced turnover of VE-cadherin-based adhesions resulting in more stable endothelial cell-cell adhesion and decreased endothelial permeability. Altogether, our results indicate that Rasa3 is a critical regulator of Rap1 in endothelial cells which controls adhesions properties and vascular lumen integrity; its specific endothelial cell inactivation results in occluded blood vessels, hemorrhages and early embryonic death in mouse, mimicking thus the *Rasa3*$^{-/-}$ mouse phenotype.

fellowand TO is a FNRS-FRIA PhD student.The fundershad no role in study design, datacollection andanalysis, decisionto publish,or preparationof themanuscript.

Competinginterests: Theauthorshavedeclared thatno competinginterestsexist.

Author summary

Because it delivers oxygen and nutriments to every tissue in the body, the vascular system is essential to vertebrate life. Blood vessels consist of a layer of interconnected endothelial cells delineating a luminal space through which blood flows. Formation of vascular lumens is a critical step in vascular development, as vessels should allow unrestricted blood flow while absorbing the pressure from cardiac activity yet retaining flexibility to adapt to homeostatic needs. Our current knowledge of how lumens are established and maintained is still modest and has come essentially from *in vitro* systems. Here, using a combination of loss of function studies in mouse and zebrafish and *in vitro* cell biology approaches, we show that Rasa3, a GTPase activating protein of the GAP1 family, controls Rap1 activation, endothelial cell adhesion and migration as well as formation of vascular lumens. We also found that inactivation of Rasa3 specifically in mouse endothelial cells lead to embryonic bleeding and death at mid-gestation, recapitulating the phenotype observed in full *Rasa3* knock-out mice.

Introduction

Blood vessels consist of a layer of interconnected endothelial cells (ECs) delineating a luminal space through which blood flows. Our current knowledge of how lumens are established and maintained is still modest and has come essentially from *in vitro* systems. Only recently, studies have investigated vascular lumen formation *in vivo*: adhesion to surrounding extracellular matrix (ECM), remodeling of EC-EC junctions and actin cytoskeleton-driven cell shape changes are common themes in this complex process [1]. Through loss-of-function experiments, these studies also identified several molecular regulators crucial for lumenogenesis, including cell surface and polarity proteins, kinases and phosphatase, actin interactors and regulators, EC-ECM adhesion proteins and small GTPase signaling components [2–11].

The small GTPase superfamily, which includes the Ras, Rho, Ran, Rab and Arf families, is composed of proteins that act as molecular switches in important signaling pathways. These pathways, which relate to cell proliferation and survival, cell-matrix and cell-cell adhesion, and cytoskeleton dynamics are critical for normal development and physiology and, when deregulated, cause severe life-threatening syndromes and pathologies. Small GTPases activity is controlled by the antagonistic actions of activating guanine exchange factors (GEFs) and repressing GTPase-activating proteins (GAPs). Rasa3 (GAP1IP4BP, R-Ras GAP) is a member of the GAP1 subfamily of Ras GAPs and is known to function as a dual GAP for Rap1 and R-Ras small GTPases [12,13]. While R-Ras has been extensively studied due to its involvement in cancer, Rap1 has recently attracted a lot of attention due to its central role in development and morphogenesis of higher organisms, especially in the cardiovasculature [14].

Mouse models have confirmed a critical role for Rasa3 during development and differentiation. Mice homozygous for the *scat* (severe combined anemia and thrombocytopenia) mutation in the *Rasa3* gene exhibit successive episodes of severe bleeding associated with embryonic and postnatal mortality [15]. Massive hemorrhages are also observed in *Rasa3*$^{-/-}$ embryos expressing a catalytically inactive Rasa3 protein and are associated with death at embryonic day (E) 12.5 to E13.5 [16]. We and others reported that loss-of-function of Rasa3 was associated with a severe thrombocytopenia, providing a possible explanation for the embryonic hemorrhages and lethality [15,17,18]. The thrombocytopenic syndrome was attributed to hyperactivation of Rap1-dependent signaling upstream of αIIbβ3 integrin stimulation,

resulting in defects during megakaryopoiesis and/or circulating platelet activation [17,18]. However, compared to full *Rasa3*$^{-/-}$ mice, the hemorrhagic phenotype and embryonic lethality were much less severe in mice in which Rasa3 was deleted specifically in the megakaryocyte lineage, suggesting that they might be caused by defects in a different cell type [18]. Here, we tested the hypothesis that embryonic bleeding and lethality associated with *Rasa3* inactivation relate to its important function in endothelial cells and vascular development. We report that mice with endothelial-specific deletion of Rasa3 exhibited severe hemorrhages and embryonic death, recapitulating the *Rasa3*$^{-/-}$ mouse phenotype. By contrast, Rasa3 inactivation specifically in megakaryocytes caused a severe thrombocytopenia but no embryonic lethality. We also show that lack of Rasa3 in ECs is associated with hyperactivation of Rap1 GTPase signaling, deregulation of EC-ECM and EC-EC adhesions and of endothelial tube morphogenesis. Our study thus identifies Rasa3 as a critical regulator of Rap1 activity, adhesion processes and tubulogenesis in ECs.

Results

Rasa3 inactivation in EC results in severe bleeding and embryonic death

In order to explore the functions of Rasa3 in ECs *in vivo*, we generated a *Rasa3*$^{flox/+}$ (*R3*$^{f/+}$) mutant mouse in which two intronic LoxP sites were introduced upstream of exon 11 and downstream of exon 12 in the *Rasa3* gene (Fig 1A). Exons 11 and 12 of the Rasa3 gene were specifically targeted, as previously described by Iwashita et al. [16]. Deletion of these two exons should lead to the production of a 88 amino acids-truncated catalytically inactive Rasa3 protein, if stable. Doing so, we were sure to inactivate the Rasa3 gene and to reproduce the embryonic lethality of *Rasa3*$^{-/-}$ mice. Crossing *R3*$^{f/+}$ with *PGK-Cre* mice generated *R3*$^{\Delta/+}$ mice with a full body heterozygous deletion of exons 11 and 12, which encodes residues 315–402 of the RASA3 GAP domain. Intercrosses between *R3*$^{\Delta/+}$ mice failed to yield any live *R3*$^{\Delta/\Delta}$ newborns (S1 Table). At E12.5, all *R3*$^{\Delta/\Delta}$ embryos displayed widespread hemorrhages, indicative of abnormalities in the vascular or coagulation systems (Fig 1B). When analyzed by Western blot, *R3*$^{\Delta/\Delta}$ embryos revealed that homozygous deletion of exon 11 and 12 of the *Rasa3* gene resulted in the absence of the Rasa3 protein (Fig 1B). Since in our hands deletion of Rasa3 specifically in megakaryocytes and platelets was not associated with embryonic lethality or hemorrhages (S1 Table and S1 Fig), we investigated whether this phenotype is observed when Rasa3 is inactivated in ECs. We generated *R3*$^{f/+}$ *Cdh5(PAC)*-CreERT2 (*R3*$^{f/+}$ iEC-Cre) mice by crossing *R3*$^{f/f}$ mice with mice expressing the Cre recombinase under the control of a tamoxifen-inducible, EC-specific promoter. *R3*$^{f/f}$ iEC-Cre mice were obtained by intercrossing *R3*$^{f/+}$ iEC-Cre mice. To achieve EC-specific homozygous inactivation of Rasa3, female *R3*$^{f/f}$ mice were bred with male *R3*$^{f/f}$ iEC-Cre mice. Intraperitoneal (ip) injections of tamoxifen in pregnant female *R3*$^{f/f}$ mice at E8.5, E9.5 and E10.5 correlated with embryonic lethality and absence of Rasa3 mutant newborns (S1 Table). Genotyping of E12.5 embryos revealed deletion of Rasa3 exons 11 and 12 in embryos that were positive for the Cre recombinase (Fig 1C). As was previously observed with the *R3*$^{\Delta/\Delta}$ deletion, the lethal phenotype resulting from EC-specific deletion of Rasa3 was 100% penetrant and consistently associated with massive bleeding (S1 Table and Fig 1C). In contrast, sibling *R3*$^{f/f}$ embryos lacking the Cre recombinase transgene did not show any vascular defects.

EC specific inactivation of Rasa3 induces blood vessel lumenization defects *in vivo*

In order to investigate the function of Rasa3 in ECs, we looked at postnatal retinal angiogenesis. Vascularization of the retina starts at postnatal day 0 (P0) and continues until P7-P10. *R3*$^{f/f}$

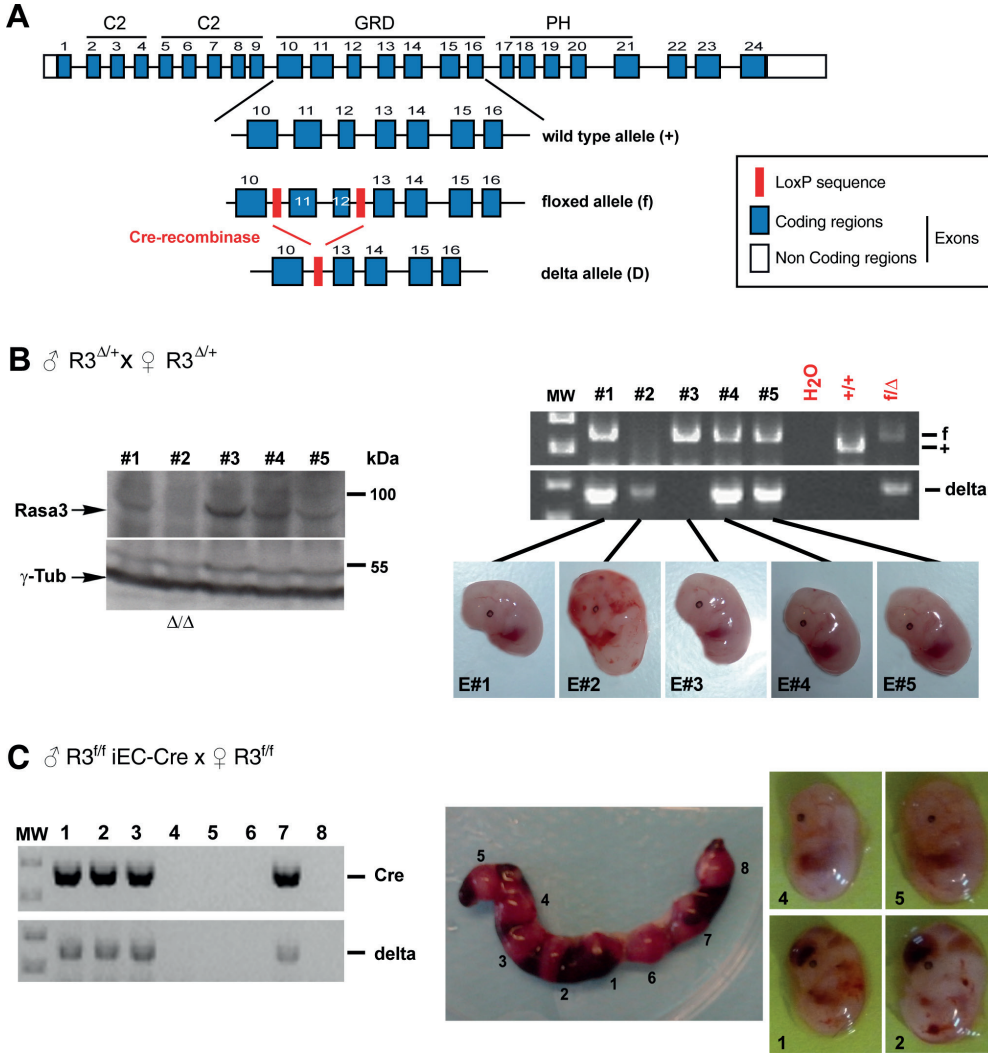

Fig 1. Whole embryo or endothelial-specific inactivation of Rasa3 induces severe bleeding and lethality in E12.5 embryos. A. The mouse *Rasa3* gene structure (boxes denote exons, and exons in blue indicate the coding regions) with the corresponding protein domains, C2 (C2), the GAP-related domain (GRD) and the pleckstrin homology domain (PH), are represented. LoxP site insertions in the floxed (f) allele are indicated (red box). The post-recombination delta (Δ) allele is represented. **B.** (Left) Immunodetection of Rasa3 and γ-Tubulin by Western blotting on extracts isolated from 5 E12.5 embryos from an $R3^{\Delta/+}$ mice intercross. (Right) Genotyping of embryos described at the left by PCR amplification of the genomic region between the LoxP sites (f) or of the delta *Rasa3* allele. E2 embryo is $R3^{\Delta/\Delta}$, E1, E4 and E5 are $R3^{\Delta/+}$ embryos and E3 is the $R3^{f/f}$ embryo (E3). Results are representative of 5 separate experiments. **C.** Uterine horns of a $R3^{f/f}$ female at E12.5 after crossing with a $R3^{f/f}$ iEC-Cre male, and ip injected with tamoxifen (center). Eight embryos were genotyped for the Cre transgene and the $R3^{\Delta}$ allele (left). Only embryos positive for the Cre transgene have the $R3^{\Delta}$ allele (E1, E2, E3 and E7) and present severe bleeding (right). Results are representative of 10 separate experiments.

https://doi.org/10.1371/journal.pgen.1007195.g001

and $R3^{f/f}$ iEC-Cre newborns received tamoxifen at P1, P2 and P3 via intragastric administration and retinal vascularization was analyzed at P5. As expected, tamoxifen led to the deletion of exon 11–12 of the *Rasa3* gene ($R3^{\Delta}$) specifically in $R3^{f/f}$ iEC-Cre pups (Fig 2A). Body weight of control $R3^{f/f}$ and mutant $R3^{f/f}$ iEC-Cre pups were similar, indicating that EC deletion of

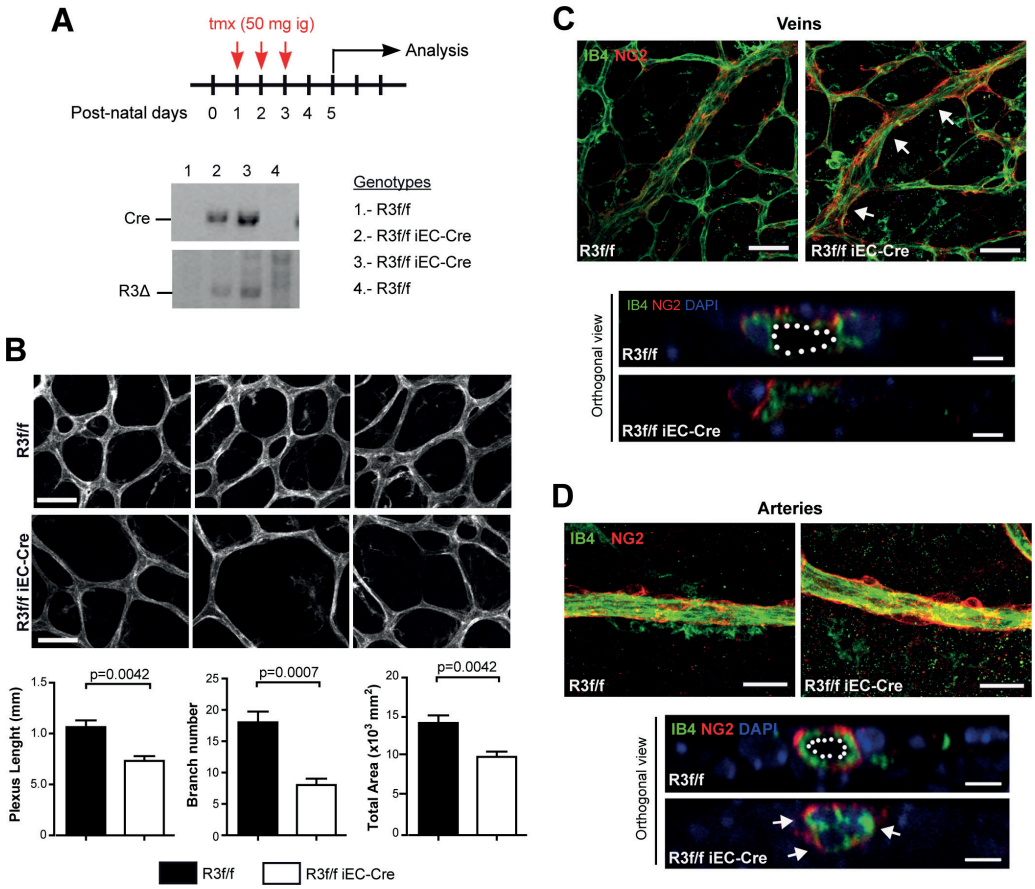

Fig 2. Endothelial deletion of Rasa3 results in defects in retinal vascularization. A. Experimental design of deletion of Rasa3 in $R3^{f/f}$ and $R3^{f/f}$ iEC-Cre pups via tamoxifen (tmx) intragastric (ig) injections at P1, P2 and P3. At P5, the $R3^{\Delta}$ allele was only detected in Cre-positive $R3^{f/f}$ newborns. Lower panels: genotyping of 4 mice by PCR for the Cre transgene (above) and the Rasa3$^{\Delta}$ allele (below) detection. When the Cre transgene is present, the Rasa3$^{\Delta}$ allele appears, indicating the deletion of exons 11 and 12 of the Rasa3 gene. The genotype of the 4 mice is indicated on the right. **B.** Immunofluorescence analysis of $R3^{f/f}$ and $R3^{f/f}$ iEC-Cre retinal plexus stained for the IB4 endothelial cell marker (upper images). Representative images of 4 independent experiments are shown. Bars = 50 μm. (Graphs) Quantification of cumulative length (left), number of branches (center) and area (right) of retinal vascular plexuses from tamoxifen-treated $R3^{f/f}$ and $R3^{f/f}$ iEC-Cre newborns. Data are represented as mean ± SEM. **C.** Immunofluorescence analysis of retinas from $R3^{f/f}$ and $R3^{f/f}$ iEC-Cre newborns using an endothelial (IB4, green) and a pericyte (NG2, red) marker. Representative images of twisted regions (arrows) in $R3^{f/f}$ iEC-Cre veins are shown. (Lower panel) Orthogonal reconstructions of confocal Z-stack in one representative $R3^{f/f}$ iEC-Cre vein showing luminal occlusion. Nuclei were stained with DAPI (blue). **D.** Representative images of arteries in retinas of $R3^{f/f}$ and $R3^{f/f}$ iEC-Cre pups. (Lower panel) Orthogonal reconstructions of confocal Z-stack in one representative $R3^{f/f}$ iEC-Cre artery with luminal occlusion. The lumen is outlined with a white dotted line in the control. Bars are 50 μm. The p values are shown (Unpaired t-test).

https://doi.org/10.1371/journal.pgen.1007195.g002

Rasa3 had no major impact on postnatal growth until P5 (S2A Fig). Vascular expansion in the retina was assessed by measuring the radial progression of the vascular plexus after staining with the EC marker isolectin B4 (IB4). We observed no significant difference in the radial extension of the retinal vasculature network between $R3^{f/f}$ and $R3^{f/f}$ iEC-Cre pups (S2B Fig). However, vascular networks from mutant mice showed reduced complexity, compared to control mice (Fig 2B). This was confirmed by quantifying the cumulative vessel length, the number of branches and the total vascularized area of the retinal plexus, which were all significantly lower in $R3^{f/f}$ iEC-Cre mice as compared with controls (Fig 2B, lower graphs).

After P3, the immature retinal vascular plexus extends and remodels into a hierarchical network, in which arteries and veins can be clearly identified. Interestingly, veins in retinas from $R3^{f/f}$ iEC-Cre mice exhibited reduced diameters (S2C Fig). In addition, these vessels often displayed constricted regions and lacked a continuous lumen (Fig 2C). Arteries of $R3^{f/f}$ iEC-Cre mouse retinas appeared grossly normal (Fig 2D), although their diameters were significantly increased, compared to $R3^{f/f}$ mice (S2D Fig). Careful examination revealed frequent lumen occlusions (Fig 2D, orthogonal view). The lack of arterial lumen correlated with abnormal EC shape, which appeared cuboidal in $R3^{f/f}$ iEC-Cre mice (Fig 2D, arrows). Interestingly, lumenization defects were also observed in a zebrafish model. Knockdown of *Rasa3* by injection of a specific morpholino in the EC specific reporter line *Tg(fli1a:eGFP)y1* didn't affect the global morphology of the fish, but was associated with thinner intersegmental vessels (ISVs) and dorsal longitudinal anastomotic vessels (DLAVs) (S3A–S3C Fig). The lumen was often lacking in these vessels (S3D Fig). We also observed increased heart rate in Rasa3 morphants, which could be a compensatory mechanism for these circulatory defects (S3E Fig).

Loss of Rasa3 affects endothelial angiogenesis and tube formation *in vitro* and *in vivo*

Vascular remodeling and lumenization are dependent on physical forces exerted by blood flow [19]. To examine the effects of Rasa3 disruption outside of any potential perturbation of hemodynamic forces, we assessed the ability of human umbilical vein endothelial cells (HUVECs) deficient for Rasa3 to form capillary-like networks *in vitro*. Silencing of Rasa3 expression using two independent siRNA dramatically impaired formation of a continuous vascular-like network (S4A and S4B Fig), although it did not impact on HUVEC viability or proliferation (S4C and S4D Fig). Time-lapse microscopy showed that whereas Rasa3-deficient HUVECs initially formed branched networks, the branches were hypocellular and unstable leading to rapid collapse of the network (S1 Movie). Similar observations were made in a 3-dimensional spheroid assay, in which downregulation of Rasa3 severely impaired extension of sprouts out of the spheroid (Fig 3A). The effects of EC Rasa3 inactivation on capillary formation were also analyzed in an *ex vivo* model of adult aortic ring in which lumenized endothelial outgrowth emerging from mouse aortic explants can be examined. Inactivation of Rasa3 was achieved by daily tamoxifen ip injection of adult $R3^{f/f}$ iEC-Cre mice for 5 consecutive days and isolated aortas were placed in a 3D collagen I matrix. Compared to control $R3^{f/f}$ mice, the capacity of the aortic endothelium from $R3^{f/f}$ iEC-Cre mice to form neovessels was dramatically impacted, with neovessels severely reduced in number and length (Fig 3B). After 12 days culture, endothelial sprouts from control $R3^{f/f}$ aortas exhibited a large and well-defined lumen. In contrast, the large majority of the few sprouts that grew out of the $R3^{f/f}$ iEC-Cre explants had a significantly reduced or closed lumen (Fig 3C).

Lack of Rasa3 correlates with reduced EC adhesion turnover

Although the exact molecular mechanism of vascular lumen formation and stabilization is still controversial, a common theme is the importance of EC adhesion properties. To understand

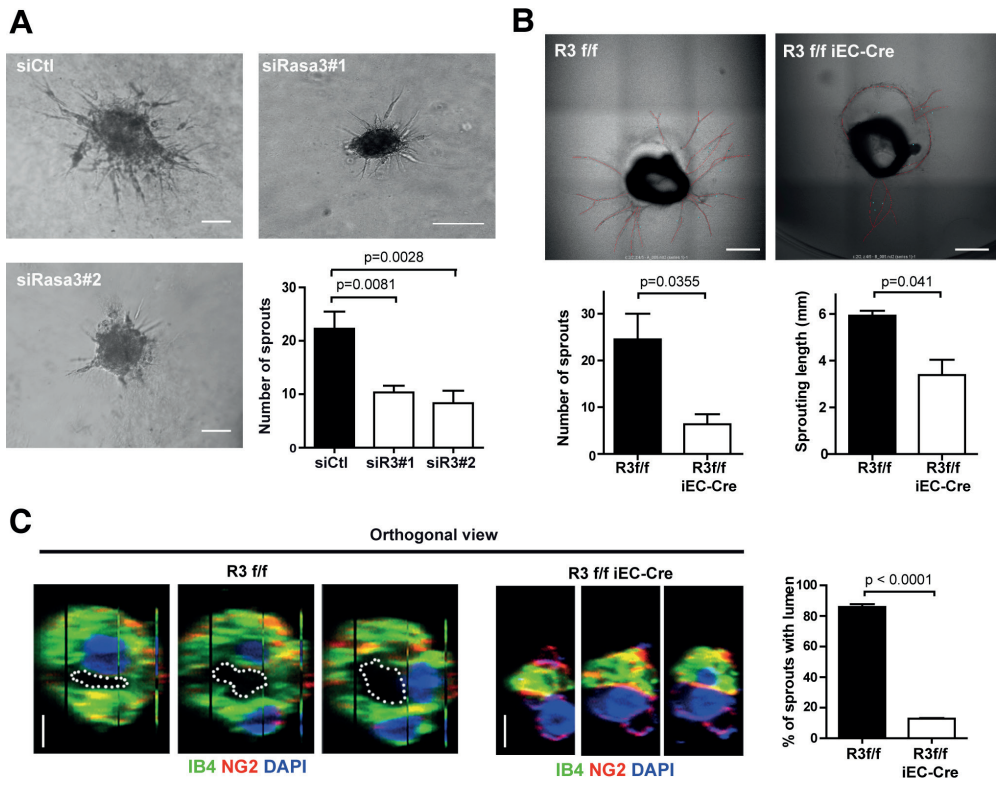

Fig 3. Rasa3 is necessary for endothelial sprouting and lumenization capacities. A. Representative micrographs of a spheroid sprouting assay with HUVECs treated with siControl or with 2 different siRasa3 (siRasa3#1 and siRasa3#2). This experiment is representative of 3 independent experiments. Bar = 100 μm. Histogram represents number of sprouts per spheroid measured on 22 and 15 spheroids, for siRasa3#1 and siRasa3#2 respectively. The p values are shown (Student's t-test). **B.** Representative bright field images of $R3^{f/f}$ and $R3^{f/f}$ iEC-Cre aortic rings after 12 days of 3D collagen I-matrix culture in the presence of VEGF (10 ng/ml). New sprouts are highlighted in red. Images are representative of 5 independent experiments. (Lower graphs) Quantification of sprout number per aortic ring (left) and sprout length (right) in aortic rings isolated from $R3^{f/f}$ and $R3^{f/f}$ iEC-Cre mice **C.** Immunofluorescence analysis of $R3^{f/f}$ and $R3^{f/f}$ iEC-Cre aortic ring sprouts stained for the IB4 (green) endothelial and NG2 (red) pericyte marker. Nuclei were stained with DAPI (blue). Images are representative orthogonal reconstructions of confocal Z-stack showing collapsed lumen in $R3^{f/f}$ iEC-Cre aortic ring sprout. Lumens are outlined with a white dotted line. Bars = 5 μm. (Graph) Percentage of sprouts with a lumen in $R3^{f/f}$ and $R3^{f/f}$ iEC-Cre aortic rings. Data are represented as mean ± SEM of 3 independent experiments. The p values are shown (Unpaired two-tail t-test).

https://doi.org/10.1371/journal.pgen.1007195.g003

how Rasa3 might control vascular lumenization, we assessed the ability of Rasa3-silenced HUVECs (siRasa3 HUVECs) to attach to major extracellular matrix (ECM) components. We found that knockdown of Rasa3 was associated with a significant increase in cell adhesion onto fibronectin (S5A Fig). In contrast, adhesion onto vitronectin, laminin or collagen was unaffected. The enhanced adhesion of siRasa3 HUVECs to fibronectin was associated with a significant increase in β1 integrin clustering (Fig 4A and S5B Fig). Interestingly, the enhanced clustering of β1 integrin was also observed in sprouts from $R3^{f/f}$ iEC-Cre aortic explants (Fig 4B). Because excessive integrin clustering may reflect alterations in focal contact dynamics [20], we decided to further investigate the dynamics of adhesions in siRasa3 HUVECs. First, we examined cell migration, a process that relies heavily on assembly and disassembly of

EC-ECM focal contacts (FCs). Using a scratch-wound assay, we found that downregulation of Rasa3 correlated with a significant decrease in HUVECs migratory capacity, supporting the idea that FC dynamics might be perturbed following Rasa3 silencing (S6A Fig). Cell-ECM adhesions found at membrane protrusions are usually divided into two types, depending on their maturation stage. The first adhesions to appear are nascent adhesions (NA) and focal complexes (Fx), which are small dot-like structures forming at the lamellipodium and lamellipodium-lamellum interface. While most of the Fx are unstable, a few will elongate centripetally and mature into larger (area > $1\mu m^2$) focal adhesions (FAs). Knockdown of Rasa3 resulted in profound alterations in the pattern of EC-ECM adhesions, as detected by labeling the FC component paxillin. Compared to control siRNA-treated HUVECs (siControl HUVECs), siRasa3 cells spreading onto fibronectin had a higher proportion of large FAs, which were localized more centripetally, whereas the number of small adhesions at the cell periphery was notably reduced (S6B and S6C Fig). Interestingly, depletion of Rasa3 also promoted accumulation of larger and more mature adhesions during VEGF-driven migration of ECs (S6D Fig).

To analyze precisely the dynamics of adhesion assembly and disassembly during EC migration, we performed total internal reflection fluorescence (TIRF) microscopy on migrating GFP-paxillin positive HUVECs. We focused our analysis on FAs maturing just below the lamella, which appeared both larger and longer lived in siRasa3 cells (S2 Movie). We measured changes in Paxillin-GFP over time to evaluate functions for assembly and disassembly, and we determined parameters of FA dynamics, as described in Methods (Fig 4C). Assembly and disassembly rates of FA were significantly decreased in siRasa3 HUVECs (Fig 4D). As a result, FA lifetime was increased about twofold in the absence of Rasa3 (Fig 4D). Altogether, our data demonstrate that Rasa3 is important to regulate EC-ECM adhesion dynamics and stability. By initiating local tyrosine phosphorylation events, the FAK-Src signaling module is a master regulator of adhesion dynamics. This prompted us to investigate FAK/Src signaling in siRasa3 HUVECs. In agreement with decreased turnover of adhesion dynamics, we observed that reduction of Rasa3 expression was associated with diminished activation of FAK and Src following HUVECs adhesion onto fibronectin (Fig 5A) or VEGF stimulation (S7A Fig). Supporting these observations, knockdown of Rasa3 correlated with reduced phosphorylation of the downstream FAK/Src targets paxillin (Fig 5A and S7A Fig). Importantly, impaired FAK activation was also observed in EC of aortic ring sprouts from tamoxifen-treated $R3^{f/f}$ iEC-Cre mice (S7B Fig).

Rasa3 regulates EC cytoskeleton plasticity

In addition to dynamic contacts with the underlying ECM, lumen morphogenesis also requires profound plasticity of EC cytoskeleton, in order to support cell shape changes associated with expansion of the luminal compartment [21]. Tubulin acetylation, indicative of stabilized microtubules, was significantly reduced in siRasa3 HUVECs plated on fibronectin, when compared with siControl HUVECs (Fig 5B). In addition, we observed an increase in actin stress fiber level and in nonmuscle myosin IIA activity, which are known to suppress tubulin acetylation (Fig 5C). Observation of stress fibers in 3D cell culture systems such as the ring aortic assay is notoriously less conspicuous than in 2D cell culture. Nevertheless, we also observed decreased tubulin acetylation and increased stress fibers in sprouts from tamoxifen-treated $R3^{f/f}$ iEC-Cre mouse aortic explants, supporting the idea that Rasa3 is important for EC cytoskeleton architecture (Fig 5D).

Defects associated with Rasa3 depletion are mediated by Rap1 hyperactivation

Based on our recent finding that in megakaryocytes Rasa3 controls Rap1 but not R-Ras activation [17], we assessed the levels of these active small GTPases in ECs lacking Rasa3. Decreasing

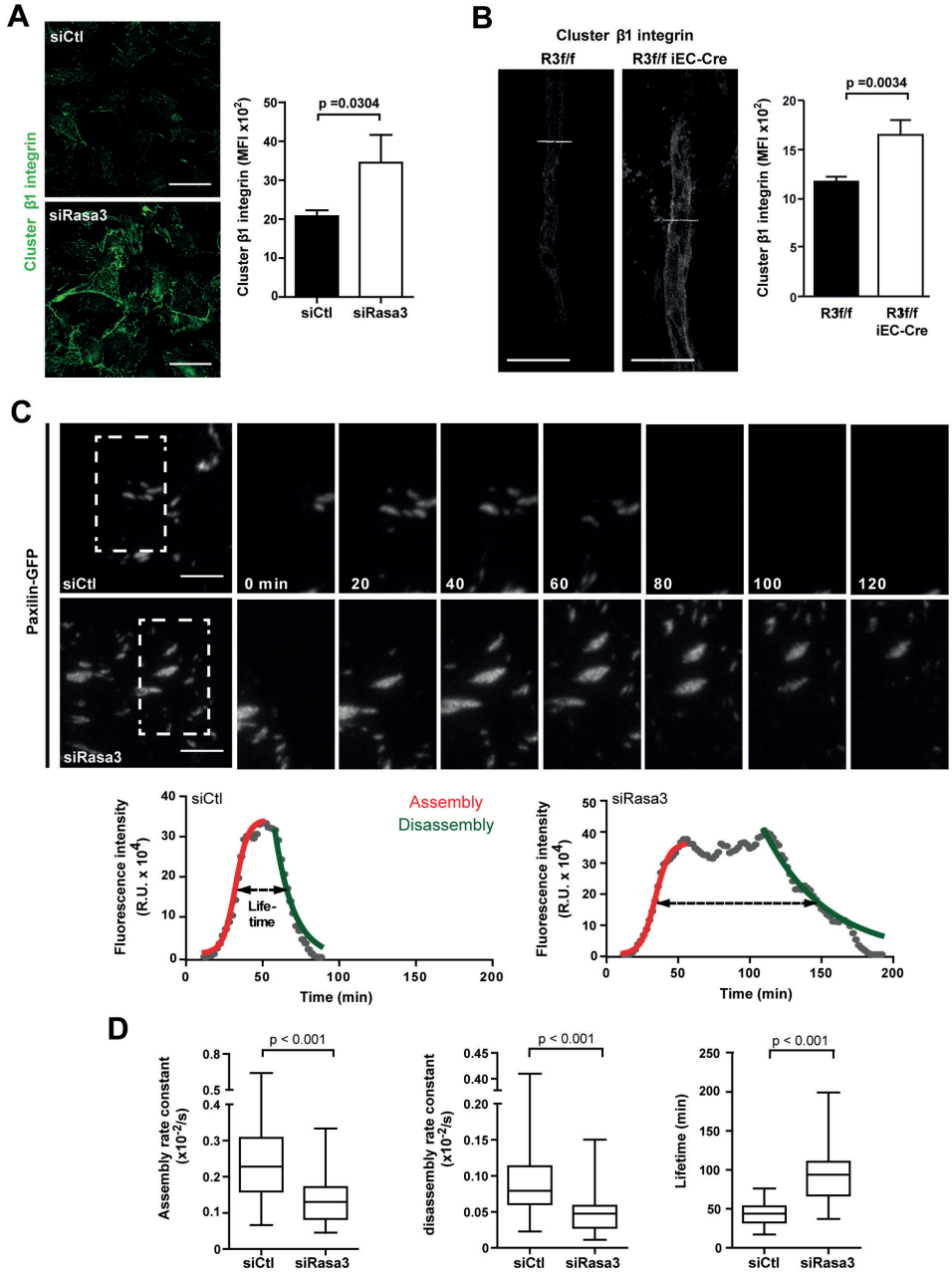
A
siCtl
siRasa3
Cluster β1 integrin
Cluster β1 integrin (MFI x10²)
p =0.0304
siCtl
siRasa3
B
Cluster β1 integrin
R3f/f
R3f/f iEC-Cre
p =0.0034
Cluster β1 integrin (MFI x10²)
R3f/f
R3f/f iEC-Cre
C
Paxilin-GFP
siCtl
siRasa3
0 min
20
40
60
80
100
120
Fluorescence intensity (R.U. x 10⁴)
Assembly
Disassembly
Life-time
Time (min)
D
Assembly rate constant (x10⁻²/s)
p < 0.001
disassembly rate constant (x10⁻²/s)
p < 0.001
Lifetime (min)
p < 0.001
siCtl
siRasa3

Fig 4. Depletion of Rasa3 impairs EC adhesion turnover. A-B. Activation of β1 integrin was analyzed in HUVECs transfected with control or Rasa3 siRNA **(A)** and in $R3^{f/f}$ and $R3^{f/f}$ iEC-Cre aortic ring sprouts **(B)** by confocal microscopy using an antibody specific for clustered β1 integrin. Representative images are shown. Bars = 50 μm. Histograms represent mean ± SD of clustered β1 integrin mean fluorescence intensity (MFI) from 3 independent experiments. The p values are shown (Student's t-test). **C.** Time-lapse sequences of paxillin-GFP dynamics in migrating HUVECs transfected with control or Rasa3 siRNA. The regions indicated are shown at higher magnification. Graphs represent turnover dynamics in one representative adhesion experiment in control and Rasa3-depleted cells. Maximum intensity projections over the 200 min time-lapse sequences are shown as three-frame running averages. The red and green lines are respectively a logistic fit of the assembly and an exponential fit of the disassembly phase. Adhesion lifetimes are indicated by dashed arrows as defined by fluorescence intensity above the half-maximum of the fit. In the adhesion experiment shown, assembly (0,0041/s in control versus 0,0033/s in Rasa3-depleted cells) and disassembly (0,0010/s in control versus 0,0004/s in Rasa3-depleted cells) rate constants were decreased in Rasa3-depleted cells, as compared with control cells. A lag between the assembly and the disassembly was only observed in Rasa3-depleted cells. Lifetime was increased in Rasa3-depleted cells (105 min), as compared with control cells (32 min). **D.** Analysis of adhesion assembly rates, disassembly rates and lifetimes in 35 and 34 adhesions from control and Rasa3-depleted migrating HUVECs, respectively. The p values are shown (Wilcoxon—Mann Whitney test).

https://doi.org/10.1371/journal.pgen.1007195.g004

Rasa3 expression in HUVECs significantly increased active Rap1 levels (Fig 6A), but had no effect on R-Ras levels (S8 Fig), as reported in megakaryocytes. Analysis of aortic sprouts from $R3^{f/f}$ and $R3^{f/f}$ iEC-Cre aortic explants also showed that deletion of Rasa3 correlated with significantly higher levels of active GTP-bound Rap1 (Fig 6B). These observations were also confirmed *in vivo*, as active Rap1 levels were dramatically higher in arteries, veins, and plexus of $R3^{f/f}$ iEC-Cre retina, compared to $R3^{f/f}$ retina (Fig 6C).

Rap1 is involved in the activation of β1-integrins in ECs and plays a key role in integrin-dependent angiogenic functions of ECs such as sprouting, migration and adhesion [14], all of which are affected by Rasa3 depletion in ECs. In addition, Rap1 is known to promote stability of endothelial VE-cadherin-based cell- cell junctions [22]. ECs display two types of VE-cadherin containing junctions [23]. Junctions of the first type localize linearly along cell-cell borders and are considered as stable adherens junctions (AJs). Junctions of the second type appear as short linear structures that are almost orthogonal to the cell-cell borders and are remodeling junctions called focal AJs (FAJs). Quantification of the total length of FAJs in single cells relative to the total junction length revealed that siRASA3 HUVECs had a reduced proportion of FAJs, indicating that cell-cell junctions are more stable when Rasa3 is knockdown, consistent with increased Rap1 activity (S9A Fig). In line with this, we found that junctions of Rasa3 knockdown HUVECs were more resistant to the cell-cell junction-destabilizing agent EGTA than those from control cells. Whereas VE-cadherin was completely internalized in control cells after 5 min of EGTA treatment, it still partially localized at the cell membrane in siRasa3 HUVECs, indicative of more resilient cell-cell junctions (S9B Fig). In addition, EGTA-induced vascular permeability was also reduced in Rasa3-deficient HUVECs, as measured by assessing solute flux across an EC monolayer (S9C Fig). Through phosphorylation of VE-cadherin, Src has emerged as a prominent mediator of VE-cadherin-mediated AJ destabilization and vascular permeability [24]. Consistent with their more stable cell-cell junctions, siRasa3 HUVECs showed reduced phosphorylation of VE-cadherin Y658 and Src activation (S9D Fig).

In order to test whether suppression of Rap1 by Rasa3 played a role during EC lumen formation, we inhibited Rap1 activity in siRasa3 HUVECs. Tubulogenesis defects of siRasa3 HUVECs were completely reverted upon treatment with the Rap1 inhibitor GGTI298 (Fig 7A, left graph). These results were further confirmed when Rap1 hyperactivation was prevented with suboptimal concentrations of either Rap1a or Rap1b siRNAs. Neither siRap1a nor siRap1b alone had an effect on *in vitro* tubulogenesis of control HUVECs. However, siRap1b, but not siRap1a, almost completely rescued the tubulogenesis defects in Rasa3 deficient HUVECs (Fig 7A right graph). Rap1 inhibition by treatment with GGTI298 increased by almost threefold the number of sprouts from $R3^{f/f}$ iEC-Cre aortic explants, while it dramatically reduced the sprouting ability of control $R3^{f/f}$ aortic rings (Fig 7B). More importantly, inhibition of

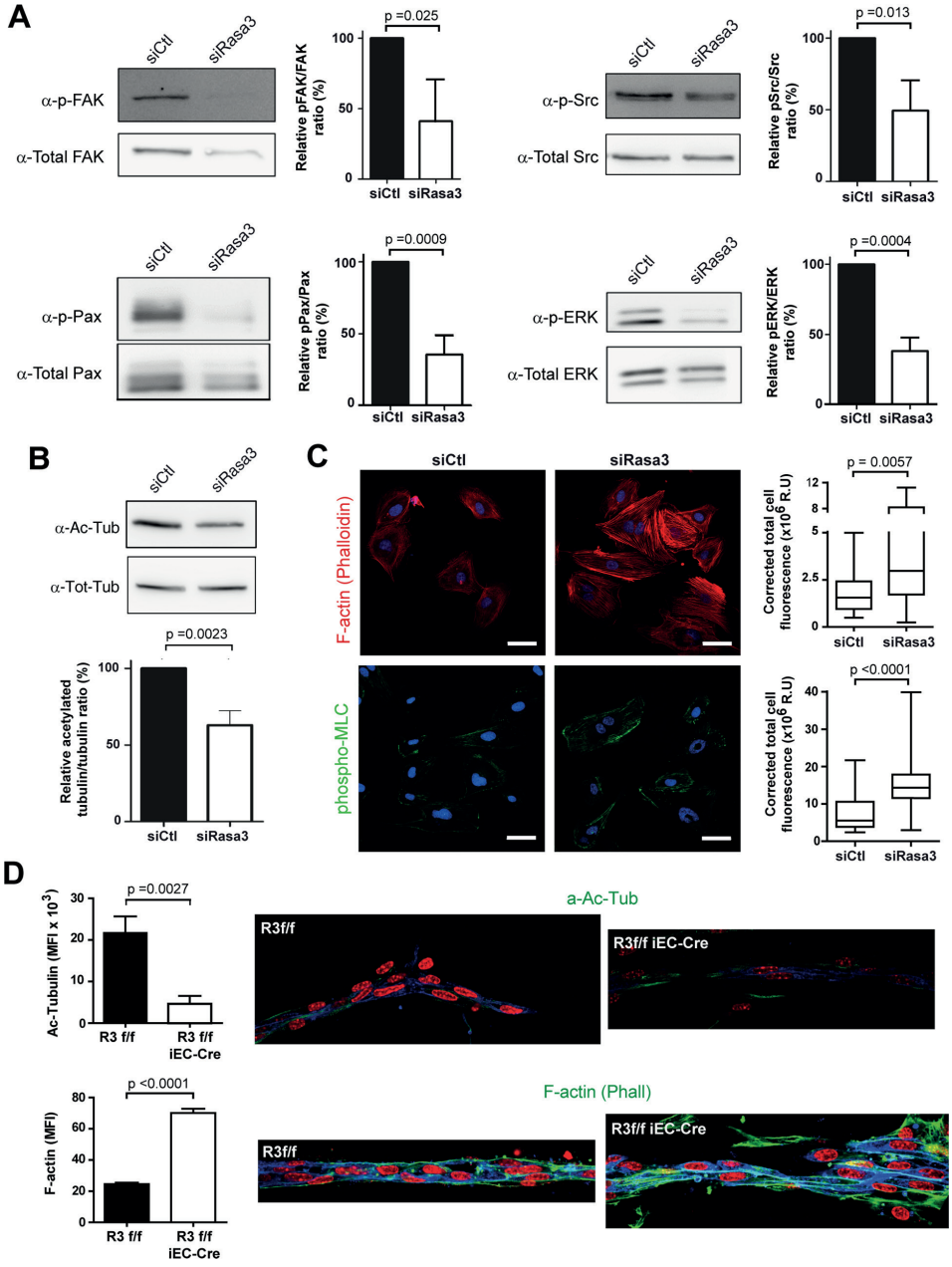
A
siCtl
siRasa3
α-p-FAK
α-Total FAK
Relative pFAK/FAK ratio (%)
p =0.025
α-p-Src
α-Total Src
Relative pSrc/Src ratio (%)
p =0.013
α-p-Pax
α-Total Pax
Relative pPax/Pax ratio (%)
p =0.0009
α-p-ERK
α-Total ERK
Relative pERK/ERK ratio (%)
p =0.0004
B
α-Ac-Tub
α-Tot-Tub
Relative acetylated tubulin/tubulin ratio (%)
p =0.0023
C
F-actin (Phalloidin)
phospho-MLC
Corrected total cell fluorescence (x10^6 R.U)
p = 0.0057
p <0.0001
D
Ac-Tubulin (MFI x 10^3)
p =0.0027
R3 f/f
R3 f/f iEC-Cre
a-Ac-Tub
R3f/f
R3f/f iEC-Cre
F-actin (MFI)
p <0.0001
F-actin (Phall)

Fig 5. Rasa3 controls EC cytoskeleton plasticity. A. Detection of FAK, Src, Paxillin (Pax) and ERK phosphorylation levels in lysates from fibronectin-plated control and siRasa3-transfected cells by Western blotting. Total FAK, Src, Paxillin and ERK levels respectively were used as control. Quantifications are shown as the ratio of phospho-specific signal over total protein signal, relative to control HUVECs. **B.** Detection of tubulin acetylation levels in lysates from fibronectin-plated control and siRasa3-transfected cells by Western blotting. Total tubulin (Tot-tub) levels were used as control. Tubulin acetylation was quantified (lower) as the ratio of acetylated tubulin signal over the total tubulin signal, relative to control HUVECs. Results are expressed as mean ± SD from 3 independent experiments. **C.** Representative confocal microscopy images of control (siCtl) and Rasa3-depleted (siRasa3) HUVECs plated on fibronectin and stained for F-actin (phallodin; red) and phospho-MLC (Green). Nuclei are stained with Hoechst (blue). Bars are 50μm. Quantifications of F-actin and phospoho-MLC signals were performed on 26 cells from 3 independent experiments and are expressed as corrected mean fluorescence intensities (MFI). Results are expressed as mean ± SD from 3 independent expriments. **D.** Immunofluorescence analysis of sprouts from $R3^{f/f}$ and $R3^{f/f}$ iEC-Cre aortic ring stained for the IB4 (blue) and acetylated tubulin (upper) or phalloidin (lower panel) in green. Nuclei are stained with DAPI (red). Representative images of 3 independent experiments are shown. Bars = 50 μm. (Left) Quantification of acetylated tubulin (upper) and Phalloidin (lower) mean fluorescence intensity (MFI). Data are presented as mean ± SEM of 10 sprouts per group in 3 independent experiments. The p values are shown (Student's t-test).

https://doi.org/10.1371/journal.pgen.1007195.g005

Rap1 also increased the number of sprouts from $R3^{f/f}$ iEC-Cre aortic rings that show a visible lumen (Fig 7C). Moreover, in the zebrafish model, the lumen defects were also partially rescued in presence of the GGTI298 Rap1 inhibitor (S3F Fig). Altogether, these observations demonstrate that Rasa3 controls endothelial lumenization by regulating Rap1 dependent signaling.

Discussion

Here, using a combination of *in vitro* cell biology approaches and loss of function studies in mouse and zebrafish, we identify a key role for Rasa3 in the maintenance of vascular integrity in vertebrates. We show that deletion or knockdown of Rasa3 in ECs is associated with hyper-activation of the small GTPase Rap1 and deregulation of EC adhesion properties. When Rasa3

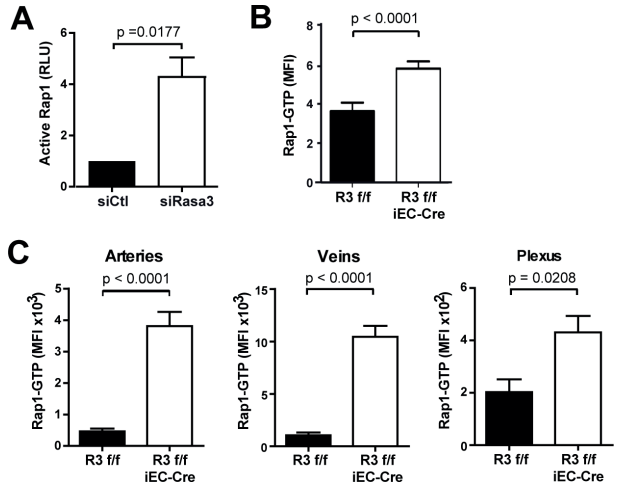

Fig 6. Rap1 is activated upon depletion of Rasa3. A. The densitometric quantification of active Rap1 detected by Western blotting on protein extracts from siControl and siRasa3 HUVECs is expressed as means ± SD from 3 independent experiments. RLU: Relative Luminescence Unit. **B.** Quantification of active Rap1-GTP mean fluorescence intensity (MFI) in aortic ring (n = 10) sprouts from $R3^{f/f}$ and $R3^{f/f}$ iEC-Cre mice (n = 10). Data are epresented as mean ± SEM. **C.** Quantification of active Rap1-GTP mean fluorescence intensity (MFI) in arteries, veins and plexus of $R3^{f/f}$ and $R3^{f/f}$ iEC-Cre newborn retinas (n ≥ 8). Data are represented as mean ± SEM. The p values are shown (Student's t-test).

https://doi.org/10.1371/journal.pgen.1007195.g006

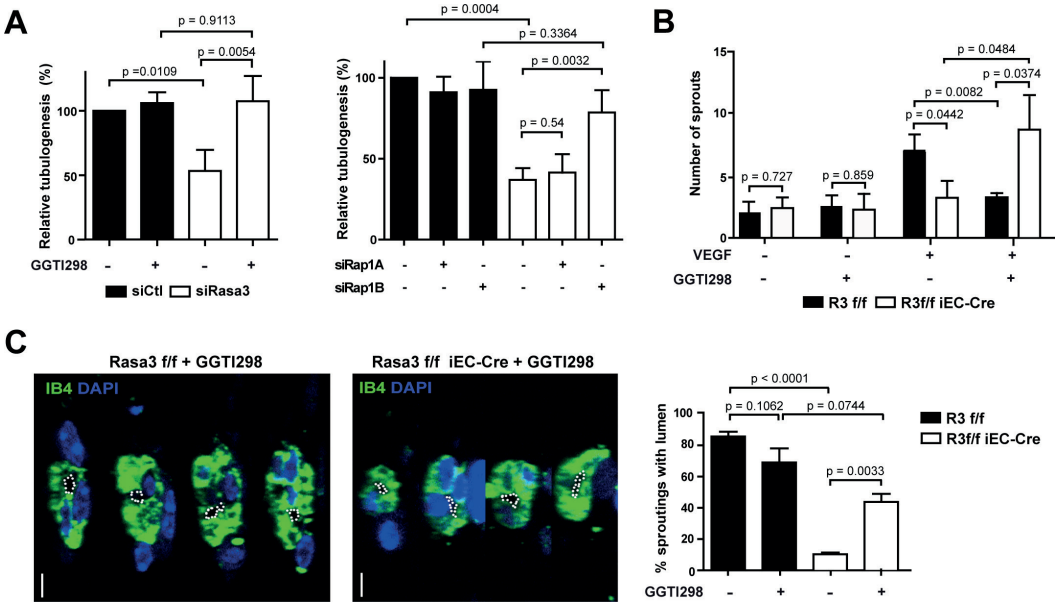

Fig 7. Inactivation of Rap1 rescues the Rasa3-depleted phenotypes. A. Quantification of capillary-like network formation in siControl vs siRasa3 HUVEC treated or not with GGTI298 (left) or co-transfected with siRap1A, siRap1B or a second control siRNA (right). Results are expressed as mean ± SD cumulative length of capillary-like structures measured in 5 different fields per experiment from 3 independent experiments, relative to non-treated siControl HUVECs (left) or to double siControl HUVECs (right), respectively. **B.** Number of sprouts growth out from $R3^{f/f}$ and $R3^{f/f}$ iEC-Cre aortic rings after 8 days of culture in the presence or absence of the Rap1 inhibitor GGTI298. A minimum of 10 aortic rings were analyzed per group in 3 independent experiments. **C.** Representative orthogonal reconstruction images of confocal Z-stacks from $R3^{f/f}$ and $R3^{f/f}$ iEC-Cre aortic ring sprouts, in the presence or absence of the Rap1 inhibitor GGTI298, stained for the IB4 (green) endothelial and nuclei DAPI (blue). Lumens are outlined with a white dotted line. Bars = 5 μm. Graph represent the mean ± SEM of the percentage of lumenized sprouts from $R3^{f/f}$ and $R3^{f/f}$ iEC-Cre aortic rings cultured in the same conditions as in panel B. The p values are shown (Student's t-test).

https://doi.org/10.1371/journal.pgen.1007195.g007

is deleted or knocked down, turnover of β1 integrin-dependent EC adhesion is impaired and EC-ECM basal adhesion contacts accumulate. In addition, EC-EC adhesions are stabilized, leading to decreased endothelial permeability. These adhesion defects prevent formation of a patent lumen and result in occluded blood vessels, hemorrhages and early embryonic death in EC-restricted *Rasa3* KO mice.

We and others have shown that mice expressing inactive mutants of Rasa3 die during mid-embryonic life and display hemorrhages and severe thrombocytopenia resulting from developmental defects during megakaryopoiesis [16–18]. Because low levels of platelets could potentially explain embryonic bleeding and mortality, we generated mice specifically inactivated for *Rasa3* in the megakaryocyte lineage ($R3^{f/f}$ PF4-Cre). As expected, these mice display megakaryocyte alterations and a severe thrombocytopenia. Surprisingly, $R3^{f/f}$ PF4-Cre newborn mice were obtained at Mendelian ratios and were viable, although with reduced life span (S1 Fig and S1 Table). A recent study from Stefanini et al. independently reported similar observations. However, these authors observed that the hemorrhagic phenotype in $R3^{f/f}$ PF4-Cre embryos was much less severe than in $R3^{-/-}$ embryos, suggesting that embryonic bleeding and lethality associated with *Rasa3* inactivation might relate to its function in a cell compartment different from the megakaryocyte lineage. Here, we show that EC-specific deletion of *Rasa3* results in the same lethal phenotype as in full $R3^{-/-}$ embryos, indicating that the specific

requirement for Rasa3 during mouse embryonic development is largely linked to its function in the developing vascular endothelium. EC Rasa3 is thus essential to maintain normal blood vessel tubulogenesis and vascular integrity *in vivo*. Numerous studies have documented that vascular lumen instability or occlusions often lead to hemorrhages and mid- or late gestation embryonic lethality [3,25–27].

Rasa3, like every member of the GAP1 GTPase family besides Rasa2, has the ability to control both R-Ras and Rap1 small GTPases *in vitro* [13]. *In vivo*, the specificity of Rasa3 towards R-Ras or Rap1 remains unclear. *Scat* mice, bearing the G125V mutation in Rasa3 show increased R-Ras activity in erythrocytes, which could explain the delayed erythropoiesis phenotype [15]. In megakaryocytes and platelets, we and others have shown that Rasa3 deletion leads to upregulation of Rap1 activity without affecting R-Ras activity [17,18]. Here, we show that the absence of Rasa3 in ECs correlates with increased Rap1 activity *in vivo* and in cultured endothelial cells. By contrast, no effect was observed on active R-Ras levels when Rasa3 was knockdown in the later cells. Importantly, inhibition of Rap1 using the GGTI298 inhibitor or specific siRNA rescued adhesion and tubulogenesis defects. These observations thus identify Rap1, and not R-Ras, as the main target of Rasa3 in ECs and are consistent with the idea that Rap1 and R-Ras largely act in different signaling pathways and are selectively regulated by specific GAPs and GEFs *in vivo* [28].

Rap1 signaling has been associated with multiple aspects of vascular development and endothelial cell biology [14]. As for other cell types, Rap1 is predominantly involved in the control of integrin and cadherin-mediated adhesion dynamics in endothelial cells [29,30]. In mice, EC specific inactivation of Rap1 leads to hemorrhage and vascular rupture. More interestingly, these mice exhibit microvessel dilation [31]. In cultured endothelial cells, depletion of Rap1 diminishes adhesion to the ECM, promotes VE-cadherin-based cell-cell junction remodeling and increases endothelial permeability [32,33]. These effects have been partly linked to the role of Rap1 in the regulation of integrin β1 affinity and clustering [14]. All these described Rap1 functions are entirely consistent with the phenotype of Rasa3-depleted HUVECs, which exhibit Rap1 hyperactivation and concomitantly increase in β1 integrin clustering and decrease in focal adhesion dynamics, permeability and cell-cell junction remodeling. Remarkably, decreasing expression of Rap1 annihilates EC tubulogenesis *in vitro*, similarly to depleting Rasa3 [33]. This supports the idea that tube formation relies on a tight balance of EC adhesion dynamics and identifies Rasa3-Rap1 signaling as a critical hub in this process.

A recurrent theme in endothelial tubulogenesis is the coordinated control of adhesion processes and cytoskeleton dynamics of ECs [34]. In the model of cord hollowing, the initial VE-cadherin-based AJs between ECs relocalize laterally to allow initial opening of the lumen [26]. It is likely that accumulation of VE-cadherin-based EC-EC junctions towards the cord periphery is achieved through VE-cadherin internalization at the apical cell surface and recycling at the lateral positions, requiring coordinated VE-cadherin phosphorylation events [35]. In this regard, our observation that Rasa3-depleted HUVECs exhibit stable VE-cadherin-based AJs and decreased phosphorylation of VE-cadherin Y658 is consistent with their lower FAK/Src signaling, as both kinases have been extensively documented to increase VE-cadherin phosphorylation and promote EC junction turnover. VE-cadherin also influences actin cytoskeleton remodeling, which is required for the EC shape changes necessary to accommodate the growth of the luminal compartment. VE-cadherin signaling thus plays a critical role in vascular tubulogenesis, as illustrated by the lumenization defects observed in VE-cadherin-deficient mice and zebrafish [36,37].

Lumen expansion also requires ECs to establish dynamic contacts with the underlying ECM. Loss of β1 integrin during development of the mouse vascular network prevents lumen formation in medium and small sized arteries [3]. In contrast, we have previously shown that

excessive stability of EC-ECM adhesions impairs ISV lumenization in zebrafish [4]. Together with our observations here, it is thus becoming evident that a tight regulation of adhesion complexes between ECs and the ECM is required to allow vascular lumen formation and maintenance. Recent observations support the existence of crosstalk between integrin-based cell-matrix and cadherin-based cell-cell contacts, both of which may operate separately on lumen formation or stabilization [3,38,39]. Strikingly, a number of these studies have converged on Rap1, thus placing this small GTPase at the crossroads of multiple outside-in and inside-out adhesion signaling pathways [40].

The developmental consequences of EC Rasa3 ablation in mice, as dissected in this study, shed light on the critical function of this poorly characterized protein in vertebrate development. The first and main cause of embryonic lethality associated with Rasa3 inactivation appears to be excessive activation of Rap1, which leads to dysregulation of EC adhesion properties and signaling. As a result, Rasa3-depleted ECs are unable to integrate and coordinate integrin and VE-cadherin signaling, preventing formation of a functional lumen. Our results thus uncovered an important but previously unknown coordinator of multiple adhesion processes during vascular tubulogenesis (Fig 8). Better understanding of the intricate molecular networks linked to vascular lumen formation should pave the way towards new vascular-targeted therapies.

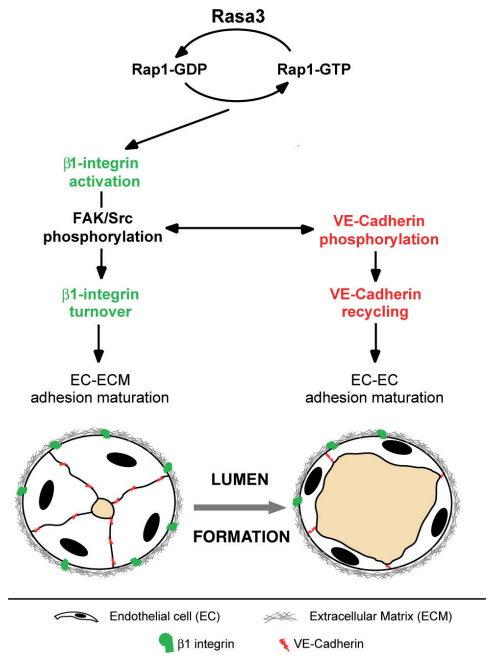

Fig 8. Model for Rasa3 control on endothelial lumen formation. Rap1 inactivation by Rasa3 GAP activity regulates activation of β1 integrin- and VE-cadherin-based adhesions. Following integrin activation, Rasa3 inactivates Rap1 to allow turnover of integrin- and VE-cadherin-based adhesions, via the FAK/Src signalling module. Failure to turnover and recycle EC-ECM and junctional adhesion complexes between EC results in vascular tubulogenesis defects. Thin black arrows indicate signalling pathways. The two-way thin black arrow indicates the interaction between the FAK/Src signalling module and the VE-cadherin signalling pathway.

https://doi.org/10.1371/journal.pgen.1007195.g008

Methods

Ethics statement

Studies on mice were conducted according to internationally-accepted standards. Mice studies were authorized by the Animal Care Use and Review Committee of the University of Liege (approval numbers: 1517, 1628 and 1902).

Mice

Rasa3$^{flox/+}$ (*R3*$^{f/+}$) mice with exons 11 and 12 of the Rasa3 gene flanked by LoxP sites were generated by inGenious Targeting Laboratory, Inc. *R3*$^{f/+}$ mice were crossed with PGK-Cre mice to generate *R3*$^{\Delta/+}$ mice as well as with PF4-Cre mice for megakaryocytes and platelets deletion and with Cdh5(PAC)-CreERT2 (or iEC-Cre) mice for deletion in EC in the presence of tamoxifen [41]. All mice were housed in an animal facility with a 12 h light/12 h dark cycle and had free access to food and water throughout the study period.

Tamoxifen treatments

For studies on embryos, plugged female *R3*$^{f/f}$ mice were ip injected at E8.5 and E10.5 with tamoxifen. For retinal angiogenesis studies in *R3*$^{f/f}$ and *R3*$^{f/f}$ iEC-Cre newborns, intragastric administration of tamoxifen was performed at P1, P2 and P3, according to Pitulescu et al [42]. For aortic ring studies in adult mice, 10 week-old *R3*$^{f/f}$ and *R3*$^{f/f}$ iEC-Cre mice were ip injected with tamoxifen for 5 consecutive days. After tamoxifen treatment, DNA recombination was assessed by PCR detection of the *R3*$^{\Delta}$ allele on tail DNA.

Antibodies and reagents

A list of the primary and secondary antibodies used in this study is presented in S2 Table. TRITC-phalloidin served for F-actin staining (Molecular Probes). DAPI and FITC-Dextran (FD405) were obtained from Sigma. Detection of active GTP-bound Ras and Rap1 in HUVECs was performed with Cell Signaling kits (#8821 and #8818, respectively). The low molecular Rap1 inhibitor GGTI298 was from Sigma. Control (SR-CL000-005) and Rasa3 (5'-GCGCTT TGGGATGAAGAAT-3' and 5'CCTGAAGTTTGGAGATGAA-3') siRNAs were purchased from Eurogentec. Tamoxifen was from Sigma, VEGF was from Peprotech, fibronectin and collagen I were from Gibco, vitronectin was from Millipore and laminin was from Invitrogen.

Whole mount newborn retina assay

For whole mount retina immunofluorescence, we proceeded as Pitulescu et al [42]. Eyes were fixed in 4% paraformaldehyde in PBS at 4˚C overnight and washed in PBS. Retinas were dissected, permeabilized in PBS, 1% BSA, 0.5% Triton X-100 at 4˚C overnight, rinsed in PBS, washed twice in PBlec (PBS, pH 6.8, 1% Triton-X100, 0.1 mM CaCl2, 0.1 mM MgCl2, 0.1 mM MnCl2), and incubated in biotinylated isolectin B4 (Sigma- Aldrich), 20 μg/ml in PBlec at 4˚C overnight. After five washes in PBS, samples were incubated with streptavidin conjugates (Alexa-488, -594, or -647; Molecular Probes) diluted 1:400 in PBS, 0.5% BSA, 0.25% Triton X-100 at room temperature for 3 h. After washing and a brief postfixation in paraformaldehyde, the retinas were either flat-mounted using Prolong (Molecular 2 probes) or processed for multiple labeling. DAPI (1:5000, 20 mg/ml, Sigma) was used for nuclear staining. Flat-mounted retinas were analyzed by confocal laser scanning microscopy using a Nikon A1 microscope. Images were processed using ImageJ. Fields of views at the sprouting vascular front of the retinal vascular network, including regions of capillary-sized vessels directly adjacent to radial

arterioles, were captured using a 40x objective lens. For quantification, at least four fluorescent images/retinas were taken from 8 mice per group.

Aortic ring assay

For aortic ring *ex vivo* culture assay, we proceeded as Baker et al [43]. Freshly dissected aortas isolated from 12 week-old mice were placed in ice-cold OptiMEM, cleaned of fatty tissue under a dissecting microscope, and rinsed in ice-cold OptiMEM three times to remove residual blood before they were sliced into 0.5-mm-thick rings, using a surgical scalpel. The rings were starved overnight at 37˚C in a 5% CO2 humidified incubator before they were embedded in 50 μl of Collagen I matrix. Matrix was overlaid with 100 μl of OptiMEM supplemented with Glutamine, 10% FBS and antibiotics. New sprouts from the rings were induced by adding VEGF (10 ng/ml) to the culture medium for 12 days, with medium change every 2 days. The outgrowth and branching activity of endothelial tubes were counted using a Nikon inverted microscope. A minimum of twelve rings per genotype were used for each assay and each assay was repeated at least 4 times. Aortic rings were immunostained according to Baker et al. 5. Briefly, aortic rings were fixed in 4% paraformaldehyde in PBS and washed in PBS. After, they were permeabilized in PBS, 1% BSA, 0.5% Triton X-100 at 4˚C overnight, rinsed in PBS, washed twice in PBlec (PBS, pH 6.8, 1% Triton-X100, 0.1 mM CaCl2, 0.1 mM MgCl2, 0.1 mM MnCl2), and incubated in biotinylated isolectin B4 (Sigma- Aldrich), 20 μg/ml in PBlec at 4˚C overnight. After five washes in PBS, samples were incubated with streptavidin conjugates (Alexa-488, -594, or -647; Molecular Probes) diluted 1:400 in PBS, 0.5% BSA and 0.25% Triton X-100 at room temperature for 3 h. After washing and a brief post-fixation in paraformaldehyde, the aortic rings were either flat-mounted using Prolong (Molecular probes) or processed for multiple labeling. DAPI (Sigma) served for nuclear staining. Flat mounted aortic rings were analyzed by confocal laser scanning microscopy using a Nikon A1 microscope.

Blood platelets quantification

Eight to twelve week-old male mice were bled under sodium pentobarbital anesthesia from the retro-orbital plexus in EDTA containing tubes. Blood platelets were quantified with a Cell Dyn 3500 analyzer (Abott Diagnostic).

Zebrafish

Knockdown experiments were performed by injecting embryos at the one-cell stage with 2.5 ng of Control (Ctl) or Rasa3 morpholino. Ctl (5'-CCTCTTACCTCAGTTACAATTTATA-3') and Rasa3 (5'-AAGCCCTTCTTCTTCGACCGCCATG-3') morpholinos were purchased from Genetools. The injected embryos were placed in E3 medium and incubated at 28˚C. Confocal pictures were taken on living embryos using a Zeiss confocal microscope at 48 hpf (hours post fertilization). The Tg(fli1a:eGFP)y1 fish were maintained conforming to EU regulations on laboratory animals. For the rescue experiment, the GGTI298 (10 μM) was added to the E3 medium at 40 hpf until 48 hpf when the quantification was made.

HUVEC culture and siRNA transfection

Human Umbilical Vein Endothelial Cells (HUVECs) were obtained from Lonza and grown at 37˚C, in 5% CO_2. SiRNA transfections in HUVECs were performed using the GeneTrans 2 (MoBiTec) reagents according to the manufacturer's protocol.

Tube formation assay

48 hours after transfection, HUVECs were subjected to the Matrigel assay as described Martin et al, 2008 [44]. 50 x 10^3 cells were cultivated for 16 h on 220 μl of Matrigel Basement Membrane Matrix (BD Bioscience). Quantification was done by measuring the cumulative tube length in three random microscopic fields using ImageJ software.

Wound healing

72 h after transfection, a confluent monolayer of HUVECs was scraped in order to create a cell free zone. Quantification of cell migration was done by measuring the percentage of recolonized area 8h after injury using the ImageJ software.

Adhesion assay

72 h after transfection, HUVECs were incubated in fibronectin-, collagen 1-, vitronectin-, or laminin-precoated coverslips for 30 min. The cells were washed and stained with crystal violet. Relative adhesion is measured by reading absorbance at 560 nm after release of incorporated dye.

Focal adhesion dynamics

Focal adhesion dynamics and quantifications were performed as described by Stehbens and Wittman [45]. HUVECs were co-transfected with siRNA and paxillin-GFP. Focal adhesion dynamics were analyzed using time-laps TIRF (total internal reflection fluorescence) microscopy. Live-cell TIRF imaging was performed on a Nikon Eclipse Ti-E inverted microscope equipped with perfect focus system, CFI Apo TIRF 100X oil objective (Nikon), a QuantEM 512SC EMCCD camera (photometrics, Roper Scientific), a TI-TIRF-E motorized TIRF illuminator (Nikon) and a stage top incubator maintaining 37˚C and 5% CO2 (Tokai hit). Images were captured every 120 seconds over 10 h.

Permeability assay

One day after transfection, 6 x 10^4 HUVECs were plated onto insert (FisherBioblock W2127C) precoated with fibronectin. The insert defined a top and a bottom chamber. After transfection (72h), the medium was changed in both chambers, and cells were treated with a medium containing EGTA (4mM) and FITC-Dextran (1mg/ml) for 30 min. Samples from the bottom chamber were analyzed by measuring the fluorescence at 492nm.

Confocal imaging analysis

For lumen quantification, orthogonal reconstructions of the Z-stacks were generated. ImageJ was used for quantification of fluorescence intensity, distances and surfaces. In adhesion experiments, HUVECs were seeded for 30 min onto fibronectin-coated coverslips, 72h after siRNA transfection. In VEGF treated experiments, HUVECs were seeded 48 h after siRNA transfection and, the next day, were treated during 5 min with VEGF (50 ng/ml) and processed for imaging. For EGTA-treated experiments, HUVECs were seeded 24 h after siRNA transfection in order to have a confluent monolayer of cells. Two days after, cells are treated for 5 min with EGTA (4 mM) and processed for imaging. For confocal analysis, cells were fixed in 4% paraformaldehyde or 100% methanol, permeabilized in 0.1% Triton X-100, blocked in BSA and incubated overnight with the appropriate primary antibodies. Samples were then incubated with the corresponding Alexa-conjugated secondary antibodies (Invitrogen) and, after washing, mounted with Mowiol. All images were acquired with a Nikon A1 confocal

microscope. The average size and the adhesion size distribution of focal adhesions were measured using the "analyze particles" plugin of ImageJ software. For *in vivo* and *ex vivo* experiments, Z-sections were acquired for precise structure and fluorescence intensity analyses with ImageJ. All images in the same experiment were acquired and analyzed in the same conditions.

SDS-PAGE and western blotting

Cells were harvested and total extracts were obtained by lysing cells in Laemmli buffer containing 50mM of Dithiothreitol (DDT). SDS-PAGE and Western Blot analysis were performed according to standard procedures and developed with ECL detection kit (GE Healthcare Bio-Sciences). Quantification of bands intensity was determined with ImageJ software.

FACS analysis

72 hours after transfection, cells were washed three times in blocking solution (PBS 1% FBS) and incubated for one hour with the anti-activated β1 integrin primary antibody. Cells were then washed with blocking solution and incubated with a FITC-conjugated secondary antibody. After washing, the expression of the clustered β1 integrin was quantified by flow cytometry using FACScan Cytometer (Becton Dickinson).

Statistics. Statistical analyses were performed with Graphpad Prism 3.0. The test used for each experiment is described in the corresponding legend. For each test, a difference of $P < 0.05$ was considered significant.

Supporting information

S1 Fig. Severe thrombocytopenia but no embryonic lethality in *R3*$^{f/f}$ PF4-Cre mice in which *Rasa3* is specifically inactivated in megakaryocytes and platelets. A. Immunodetection of Rasa3 and γ-Tubulin by Western blotting on washed-platelet extracts isolated from blood of *R3*$^{f/f}$ (1) and *R3*$^{f/f}$ PF4-Cre (2). Image is representative of 5 independent experiments. **B.** Survival curve of *R3*$^{f/f}$ (n = 11) and *R3*$^{f/f}$ PF4Cre (n = 8) mice over a period of 50 weeks. The p value is shown (Log-rank (Mantel-Cox) test). **C.** Blood platelet counts in adult *R3*$^{f/f}$ (n = 8) and *R3*$^{f/f}$ PF4-cre (n = 8) mice. Data are represented as mean ± SEM. The p value is shown (Unpaired t-test). **D.** Quantification of megakaryocytes present in the spleen of *R3*$^{f/f}$ (n = 6) and *R3*$^{f/f}$ PF4-Cre (n = 6) mice. Data are represented as mean ± SEM; the p value is shown (Unpaired t-test).
(TIF)

S2 Fig. Deletion of Rasa3 in *R3*$^{f/f}$ iEC-Cre newborns by daily tamoxifen injections results in vascular defects. A. Quantification of *R3*$^{f/f}$ (n = 18) and *R3*$^{f/f}$ iEC-Cre (n = 8) newborn body weight at P5 after tamoxifen treatment. **B.** Representative image of *R3*$^{f/f}$ (n = 18) and *R3*$^{f/f}$ iEC-Cre (n = 8) newborn retina vasculature, stained with the IB4 (green) endothelial marker. The blue line and the white arrow indicate the total length and the vascular front of the vascular network, respectively. Bars = 2 mm. Quantification of the radial outgrowth of the retinal network is shown. **C-D.** Quantification of the vein (**C**) and arteries (**D**) diameter in P5 newborn retinas of *R3*$^{f/f}$ (n = 8) and *R3*$^{f/f}$ iEC-Cre (n = 8) newborns. Data are represented as mean ± SEM. The p values are shown (Unpaired t-test).
(TIF)

S3 Fig. Knockdown of Rasa3 in Zebrafish induces tubulogenesis defects in the trunk vasculature. A. Detection of Rasa3 level in lysates from Control (Ctl) and Rasa morphant embryos. GAPDH was used as control. **B.** General morphology of Ctl and Rasa3 morphant embryos. **C.**

Tg(fli1a:eGFP)y1 embryos were injected with control morpholino (MoCtl) or with morpholino targeting Rasa3 (MoRasa3). Confocal pictures of the trunk vasculature were taken at 48 hpf. Ctl embryos present normal ISVs and DLAVs with open lumen (arrow head) whereas Rasa3 morphant embryos show thinner, non-lumenized vessels (arrows). Bars = 50 mm. ISV, intersegmental vessel; DLAV, dorsal longitudinal anastomotic vessels. **D.** Quantification of lumenized ISVs in Ctl and Rasa3 morphant embryos at 48 and 72 hpf. The p values are shown (Fisher's exact test). Results are mean from 10 ISVs/embryo in 50 embryos at 48hpf and 25 embryos at 72hpf. **E.** Heart rates in 32 Ctl and 30 Rasa3 morphant embryos. Histograms are mean ± SD from 35 embryos. The p value is shown (Fisher's exact test). **F.** Rescue experiment using GGTI298 (10 μM). Quantification of lumenized ISVs in Ctl and Rasa3 morphant embryos at 48hpf. The p values are shown. Results are mean from 10 ISVs/embryo in 35 embryos.
(TIF)

S4 Fig. Deletion of Rasa3 impairs tubulogenesis in HUVECs. A. Immunodetection of Rasa3 and Actin by Western blotting on total extracts from HUVECs transfected with a control siRNA or two different Rasa3 siRNAs (siRasa3#1 and siRasa3#2). **B.** Representative micrographs of a tube-like formation assay in Matrigel using HUVECs treated with siControl or with two different Rasa-siRNA (siRasa3#1 and siRasa3#2). Images are representative of 3 independent experiments. Bar = 100 μm. Histograms represent mean ± SD of relative tubulogenesis of capillary-like structures measured in five different fields from 3 independent experiments. The p values are shown (One sample t-test). **C.** Histograms represent mean relative cell viability ± SD in siCTL or siRasa3-treated HUVECs from 3 independent experiments. **D.** Histograms represent mean cell number of siRasa3#1 at indicated time points after seeding and relative to the number of cells in siCTL-treated HUVECs. Results are from at least 3 independent experiments. The p values are shown in **B**, **C** and **D** (Student's t-test).
(TIF)

S5 Fig. Depletion of Rasa3 increases adhesion and decreases migration of ECs. A. Effects of Rasa3-silencing on HUVEC adhesion onto Fibronectin, Collagen, Vitronectin or Laminin. Bars = 100 μm. Representative micrograph of an adhesion assay with HUVECs treated with siCTL or siRasa3. Images are representative from 3 to 5 independent experiments. Histograms are mean ± SD of 3 independent experiments. The p values are shown (Student's t-test). **B.** Immunodetection of total integrin β1 levels by Western blotting on total extracts from HUVECs transfected with control or Rasa3 siRNA (related to the experiment described in Fig 5A). Actin was used as a loading control.
(TIF)

S6 Fig. Rasa3 is required for normal adhesion turnover. A. In a scratch-wound migration assay, the recolonized area was analyzed at 5h in HUVECs transfected with siControl or two different siRasa3. The means ± SD of 3 independent experiments are presented, relative to the siControl condition. The p values are shown (One sample t-test). **B.** Adhesions were analyzed in Fibronectin-plated HUVECs transfected with siControl or siRasa3 by confocal microscopy using an anti-Paxillin antibody. Histograms represent size distribution of paxillin positive adhesions in 35 control and 33 siRasa3-treated cells. Adhesions were classified into three size categories: (0.2–0.5 μm^2), (0.5–1 μm^2) and (> 1 μm^2). The p values are shown (Student's t-test). **C.** Adhesions were analyzed in Fibronectin-plated HUVECs transfected with siControl and siRasa3 by confocal microscopy using an anti-Paxillin antibody (green). F-actin is visualized using Phalloidin (red). Representative images are shown. Bars = 10 μm. Quantification of the ratio of the length between the center and the mature focal adhesion (> 1 μm^2) versus the

length between the center and the cell periphery (n = 244 and n = 343 for siCTL and siRasa3, respectively). The p value is shown (Student's t-test). **D.** Adhesions were analyzed in VEGF-stimulated HUVECs transfected with siControl and siRasa3 as described in (**B**) in 21 control and 23 siRasa3-treated cells. The p values are shown (Student's t-test).
(TIF)

S7 Fig. Depletion of Rasa3 impairs activation of the FAK-Src complex. A. Detection of FAK, Src, Paxillin (Pax) and ERK phosphorylation levels in lysates from VEGF-stimulated, control and siRasa3-transfected HUVECs by Western blotting with phospho-specific antibodies. Total FAK, Src, Paxillin and ERK levels were respectively used as control. Phosphorylation levels of FAK, Src, Paxillin and ERK were quantified by densitometry as the ratio of phospho-specific signal over the total protein signal, relative to control HUVECs. Results are expressed as means ± SD from at least 3 independent experiments. The p values are shown (Student's t-test). **B.** Immunofluorescence analysis of aortic ring sprouts from $R3^{f/f}$ and $R3^{f/f}$ iEC-Cre mice stained for the IB4 endothelial marker (lower) and with an anti-phospho-FAK antibody (upper). Representative images of minimum 5 sprouts per genotype in 3 independent experiments are shown. Bars = 50 μm. Quantification of anti-phosphoFAK mean fluorescence intensity (MFI) ± SEM (n = 5). The p value is shown (Unpaired t-test).
(TIF)

S8 Fig. Rasa3 knockdown in HUVECs has no effect on active R-Ras level. The densitometric quantification of active R-Ras detected by Western blotting on protein extracts from siControl and siRasa3 HUVECs is expressed as means ± SD from 3 independent experiments. RLU: Relative Luminescence Unit. The p value is shown (Student's t-test).
(TIF)

S9 Fig. Depletion of Rasa3 stabilizes endothelial VE-Cadherin-based cell-cell junctions. A. Effect of Rasa3-silencing on endothelial cell junctions. Adherent junctions were analyzed in HUVECs transfected with siControl and siRasa3 by confocal microscopy using an anti-VE-cadherin antibody (green). Representative images are shown. Bars = 10 μm. (Right) The signal was quantified. Histograms are mean ratio of FAJ length versus the total junction length per cell. Results are from 30 cells. The p value is shown (Student's t-test). **B.** VE-cadherin internalization was analyzed by confocal microscopy using an anti-VE-cadherin antibody (green) in control and Rasa3-depleted cells after an EGTA treatment (4 mM). Bars = 50μm **C.** Effect of Rasa3-silencing on endothelial permeability after an EGTA treatment (4 mM). Results are mean quantification of FITC-dextran ± SD from 4 independent experiments and relative to EGTA-treated control cells. The p values are shown (non-treated cells: Student's t-test; EGTA-treated cells: One sample test). **D.** Detection of VE-cadherin and Src phosphorylation levels in total lysates from non-treated and EGTA-treated sicontrol and siRasa3-transfected cells by Western blotting with phospho-specific antibodies. Total VE-cadherin and Src levels respectively were used as control. Results are expressed as means ± SD from 4 independent experiments, relative to control HUVECs. The p values are shown (non-treated cells: One sample t-test; EGTA-treated cells: Student's t-test).
(TIF)

S1 Table. Endothelial specific or full deletion of exons 11–12 of the mouse *Rasa3* gene during embryonic life results in embryonic death. Newborns were genotyped 21 days after bird by PCR.
[ff]Plugged $R3^{f/f}$ females were ip injected with 5 mg of tamoxifen at E8.5, E9.5 and E10.5. Statistics (Student's t-test): [ffff]: $P < 0.001$.
(DOCX)

S2 Table. Antibodies used in the manuscript.
(DOCX)

S1 Movie. The ability of control HUVECs and HUVECs deficient for Rasa3 to form capillary-like networks was investigated *in vitro* by time-lapse microscopy. Silencing of Rasa3 expression using siRNA dramatically impaired formation of a continuous vascular-like network. Indeed, whereas Rasa3-deficient HUVECs initially formed branched networks, the branches were hypocellular and unstable leading to rapid collapse of the network.
(MP4)

S2 Movie. Analysis of the dynamics of adhesion assembly and disassembly by TIRF microscopy on migrating GFP-paxillin positive HUVECs depleted or not for Rasa3. The analysis was focused on FAs maturing just below the lamella, which appeared both larger and longer lived in siRasa3 HUVECs than in siControl HUVECs.
(MP4)

Acknowledgments

We would like to thank the Dequiedt and Schurmans laboratories for helpful discussions. We are especially thankful to Jonathan Bruyr and Tina O'Grady from the Dequiedt laboratory for technical help and proofreading of the manuscript, respectively, and Laura Sacré from the Schurmans laboratory for technical help. We thank the GIGA-imaging and flow cytometry, and Animal Housing platforms for their technical support.

Author Contributions

Conceptualization: Patricia Molina-Ortiz, Tanguy Orban, Franck Dequiedt, Stéphane Schurmans.

Formal analysis: Patricia Molina-Ortiz, Tanguy Orban, Maud Martin, Audrey Habets.

Funding acquisition: Franck Dequiedt, Stéphane Schurmans.

Investigation: Patricia Molina-Ortiz, Tanguy Orban, Maud Martin, Audrey Habets.

Methodology: Patricia Molina-Ortiz, Tanguy Orban, Maud Martin, Audrey Habets, Franck Dequiedt, Stéphane Schurmans.

Project administration: Franck Dequiedt, Stéphane Schurmans.

Resources: Franck Dequiedt, Stéphane Schurmans.

Supervision: Franck Dequiedt, Stéphane Schurmans.

Writing – original draft: Franck Dequiedt, Stéphane Schurmans.

Writing – review & editing: Patricia Molina-Ortiz, Tanguy Orban, Maud Martin, Franck Dequiedt, Stéphane Schurmans.

References

1. Neufeld S, Planas-Paz L, Lammert E. Blood and lymphatic vascular tube formation in mouse. Seminars in Cell and Developmental Biology. 2014. pp. 115–123. https://doi.org/10.1016/j.semcdb.2014.02.013 PMID: 24631829
2. Strilić B, Kucera T, Eglinger J, Hughes MR, McNagny KM, Tsukita S, et al. The molecular basis of vascular lumen formation in the developing mouse aorta. Dev Cell. 2009; 17: 505–15. https://doi.org/10.1016/j.devcel.2009.08.011 PMID: 19853564

3. Zovein AC, Luque A, Turlo KA, Hofmann JJ, Yee KM, Becker MS, et al. Beta1 integrin establishes endothelial cell polarity and arteriolar lumen formation via a Par3-dependent mechanism. Dev Cell. Elsevier; 2010; 18: 39–51. https://doi.org/10.1016/j.devcel.2009.12.006 PMID: 20152176
4. Martin M, Geudens I, Bruyr J, Potente M, Bleuart A, Lebrun M, et al. PP2A regulatory subunit Bα controls endothelial contractility and vessel lumen integrity via regulation of HDAC7. EMBO J. 2013; 32: 2491–2503. https://doi.org/10.1038/emboj.2013.187 PMID: 23955003
5. Hayashi M, Majumdar A, Li X, Adler J, Sun Z, Vertuani S, et al. VE-PTP regulates VEGFR2 activity in stalk cells to establish endothelial cell polarity and lumen formation. Nat Commun. 2013; 4: 1672. https://doi.org/10.1038/ncomms2683 PMID: 23575676
6. Wang Y, Kaiser MS, Larson JD, Nasevicius A, Clark KJ, Wadman SA, et al. Moesin1 and Ve-cadherin are required in endothelial cells during in vivo tubulogenesis. Development. 2010; 137: 3119–3128. https://doi.org/10.1242/dev.048785 PMID: 20736288
7. Phng LK, Gebala V, Bentley K, Philippides A, Wacker A, Mathivet T, et al. Formin-mediated actin polymerization at endothelial junctions is required for vessel lumen formation and stabilization. Dev Cell. 2015; 32: 123–132. https://doi.org/10.1016/j.devcel.2014.11.017 PMID: 25584798
8. Hultin S, Zheng Y, Mojallal M, Vertuani S, Gentili C, Balland M, et al. AmotL2 links VE-cadherin to contractile actin fibres necessary for aortic lumen expansion. Nat Commun. 2014; 5: 3743. https://doi.org/10.1038/ncomms4743 PMID: 24806444
9. Barry DM, Xu K, Meadows SM, Zheng Y, Norden PR, Davis GE, et al. Cdc42 is required for cytoskeletal support of endothelial cell adhesion during blood vessel formation in mice. Development. 2015; 142: 3058–3070. https://doi.org/10.1242/dev.125260 PMID: 26253403
10. Xu K, Sacharidou A, Fu S, Chong DCC, Skaug B, Chen ZJJ, et al. Blood vessel tubulogenesis requires Rasip1 regulation of GTPase signaling. Dev Cell. 2011; 20: 526–39. https://doi.org/10.1016/j.devcel.2011.02.010 PMID: 21396893
11. Barry DM, Koo Y, Norden PR, Wylie LA, Xu K, Wichaidit C, et al. Rasip1-Mediated Rho GTPase Signaling Regulates Blood Vessel Tubulogenesis via Nonmuscle Myosin II. Circ Res. 2016; 119: 810–826. https://doi.org/10.1161/CIRCRESAHA.116.309094 PMID: 27486147
12. Schurmans S, Polizzi S, Scoumanne A, Sayyed S, Molina-Ortiz P. The Ras/Rap GTPase activating protein RASA3: From gene structure to invivo functions. Advances in Biological Regulation. 2015. https://doi.org/10.1016/j.jbior.2014.09.006 PMID: 25294679
13. Yarwood S, Bouyoucef-Cherchalli D, Cullen PJ, Kupzig S. The GAP1 family of GTPase-activating proteins: spatial and temporal regulators of small GTPase signalling. Biochem Soc Trans. 2006; 34: 846–50. https://doi.org/10.1042/BST0340846 PMID: 17052212
14. Van Aelst L, Boettner B, Chrzanowska-Wodnicka M. Distinct functions for Rap1 signaling in vascular morphogenesis and dysfunction. Exp Cell Res. Elsevier; 2013; 319: 2350–9. https://doi.org/10.1016/j.yexcr.2013.07.022 PMID: 23911990
15. Blanc L, Ciciotte SL, Gwynn B, Hildick-Smith GJ, Pierce EL, Soltis K a, et al. Critical function for the Ras-GTPase activating protein RASA3 in vertebrate erythropoiesis and megakaryopoiesis. Proc Natl Acad Sci U S A. 2012; 109: 12099–104. https://doi.org/10.1073/pnas.1204948109 PMID: 22773809
16. Iwashita S, Kobayashi M, Kubo Y, Hinohara Y, Sezaki M, Nakamura K, et al. Versatile roles of R-Ras GAP in neurite formation of PC12 cells and embryonic vascular development. J Biol Chem. 2007; 282: 3413–7. https://doi.org/10.1074/jbc.C600293200 PMID: 17179160
17. Molina-Ortiz P, Polizzi S, Ramery E, Gayral S, Delierneux C, Oury C, et al. Rasa3 Controls Megakaryocyte Rap1 Activation, Integrin Signaling and Differentiation into Proplatelet. PLoS Genet. 2014;10. https://doi.org/10.1371/journal.pgen.1004420 PMID: 24967784
18. Stefanini L, Paul DS, Robledo RF, Chan ER, Getz TM, Piatt R, et al. RASA3 is a critical inhibitor of RAP1-dependent platelet activation. J Clin Invest. 2015; 1–34. https://doi.org/10.1172/JCI78652
19. Culver JC, Dickinson ME. The effects of hemodynamic force on embryonic development. Microcirculation. 2010. pp. 164–178. https://doi.org/10.1111/j.1549-8719.2010.00025.x PMID: 20374481
20. Gardel ML, Schneider IC, Aratyn-Schaus Y, Waterman CM. Mechanical Integration of Actin and Adhesion Dynamics in Cell Migration. Annu Rev Cell Dev Biol. 2010; 26: 315–333. https://doi.org/10.1146/annurev.cellbio.011209.122036 PMID: 19575647
21. Bayless KJ, Johnson GA. Role of the cytoskeleton in formation and maintenance of angiogenic sprouts. Journal of Vascular Research. 2011. pp. 369–385. https://doi.org/10.1159/000324751 PMID: 21464572
22. Kooistra MRH, Dube N, Bos JL. Rap1: a key regulator in cell-cell junction formation. J Cell Sci. 2006; 120: 17–22. https://doi.org/10.1242/jcs.03306 PMID: 17182900
23. Millán J, Cain RJ, Reglero-Real N, Bigarella C, Marcos-Ramiro B, Fernández-Martín L, et al. Adherens junctions connect stress fibres between adjacent endothelial cells. BMC Biol. 2010; 8: 11. https://doi.org/10.1186/1741-7007-8-11 PMID: 20122254

24. Gavard J. Endothelial permeability and VE-cadherin: A wacky comradeship. Cell Adhes Migr. 2014; 8: 158–164. https://doi.org/10.4161/cam.29026 PMID: 25422846

25. Cattelino A, Liebner S, Gallini R, Zanetti A, Balconi G, Corsi A, et al. The conditional inactivation of the β-catenin gene in endothelial cells causes a defective vascular pattern and increased vascular fragility. J Cell Biol. 2003; 162: 1111–1122. https://doi.org/10.1083/jcb.200212157 PMID: 12975353

26. Zeeb M, Strilic B, Lammert E. Resolving cell-cell junctions: Lumen formation in blood vessels. Current Opinion in Cell Biology. 2010. pp. 626–632. https://doi.org/10.1016/j.ceb.2010.07.003 PMID: 20678912

27. Kleaveland B, Zheng X, Liu JJ, Blum Y, Tung JJ, Zou Z, et al. Regulation of cardiovascular development and integrity by the heart of glass-cerebral cavernous malformation protein pathway. Nature medicine. 2009. pp. 169–76. https://doi.org/10.1038/nm.1918 PMID: 19151727

28. Raaijmakers JH, Bos JL. Specificity in Ras and Rap signaling. J Biol Chem. 2009; 284: 10995–10999. https://doi.org/10.1074/jbc.R800061200 PMID: 19091745

29. Bos JL. Linking Rap to cell adhesion. Curr Opin Cell Biol. 2005; 17: 123–128. https://doi.org/10.1016/j.ceb.2005.02.009 PMID: 15780587

30. Boettner B, Van Aelst L. Control of cell adhesion dynamics by Rap1 signaling. Curr Opin Cell Biol. 2009; 21: 684–93. https://doi.org/10.1016/j.ceb.2009.06.004 PMID: 19615876

31. Chrzanowska-Wodnicka M, White GC, Quilliam LA, Whitehead KJ. Small GTPase Rap1 is essential for mouse development and formation of functional vasculature. Boggon TJ, editor. PLoS One. Public Library of Science; 2015; 10: e0145689. https://doi.org/10.1371/journal.pone.0145689 PMID: 26714318

32. Pannekoek WJ, van Dijk JJG, Chan OYA, Huveneers S, Linnemann JR, Spanjaard E, et al. Epac1 and PDZ-GEF cooperate in Rap1 mediated endothelial junction control. Cell Signal. 2011; 23: 2056–2064. https://doi.org/10.1016/j.cellsig.2011.07.022 PMID: 21840392

33. Yan J, Li F, Ingram DA, Quilliam LA. Rap1a is a key regulator of fibroblast growth factor 2-induced angiogenesis and together with Rap1b controls human endothelial cell functions. Mol Cell Biol. 2008; 28: 5803–10. https://doi.org/10.1128/MCB.00393-08 PMID: 18625726

34. Iruela-Arispe ML, Davis GE. Cellular and Molecular Mechanisms of Vascular Lumen Formation. Developmental Cell. 2009. pp. 222–231. https://doi.org/10.1016/j.devcel.2009.01.013 PMID: 19217424

35. Vestweber D, Winderlich M, Cagna G, Nottebaum AF. Cell adhesion dynamics at endothelial junctions: VE-cadherin as a major player. Trends Cell Biol. 2009; 19: 8–15. https://doi.org/10.1016/j.tcb.2008.10.001 PMID: 19010680

36. Carmeliet P, Lampugnani MG, Moons L, Breviario F, Compernolle V, Bono F, et al. Targeted deficiency or cytosolic truncation of the VE-cadherin gene in mice impairs VEGF-mediated endothelial survival and angiogenesis. Cell. 1999; 98: 147–157. https://doi.org/10.1016/S0092-8674(00)81010-7 PMID: 10428027

37. Montero-Balaguer M, Swirsding K, Orsenigo F, Cotelli F, Mione M, Dejana E. Stable vascular connections and remodeling require full expression of VE-cadherin in zebrafish embryos. Callaerts P, editor. PLoS One. 2009; 4: e5772. https://doi.org/10.1371/journal.pone.0005772 PMID: 19503615

38. Weber GF, Bjerke MA, DeSimone DW. Integrins and cadherins join forces to form adhesive networks. J Cell Sci. 2011; 124: 1183–1193. https://doi.org/10.1242/jcs.064618 PMID: 21444749

39. Yamamoto H, Ehling M, Kato K, Kanai K, van Lessen M, Frye M, et al. Integrin β1 controls VE-cadherin localization and blood vessel stability. Nat Commun. 2015; 6: 6429. https://doi.org/10.1038/ncomms7429 PMID: 25752958

40. Retta SF, Balzac F, Avolio M. Rap1: A turnabout for the crosstalk between cadherins and integrins. European Journal of Cell Biology. 2006. pp. 283–293. https://doi.org/10.1016/j.ejcb.2005.09.007 PMID: 16546572

41. Monvoisin A, Alva JA, Hofmann JJ, Zovein AC, Lane TF, Iruela-Arispe ML. VE-cadherin-CreERT2 transgenic mouse: A model for inducible recombination in the endothelium. Dev Dyn. 2006; 235: 3413–3422. https://doi.org/10.1002/dvdy.20982 PMID: 17072878

42. Pitulescu ME, Schmidt I, Benedito R, Adams RH. Inducible gene targeting in the neonatal vasculature and analysis of retinal angiogenesis in mice. Nat Protoc. Nature Publishing Group, a division of Macmillan Publishers Limited. All Rights Reserved.; 2010; 5: 1518–34. https://doi.org/10.1038/nprot.2010.113 PMID: 20725067

43. Baker M, Robinson SD, Lechertier T, Barber PR, Tavora B, D'Amico G, et al. Use of the mouse aortic ring assay to study angiogenesis. Nat Protoc. Nature Publishing Group; 2012; 7: 89–104. https://doi.org/10.1038/nprot.2011.435 PMID: 22193302

44. Martin M, Potente M, Janssens V, Vertommen D, Twizere J-C, Rider MH, et al. Protein phosphatase 2A controls the activity of histone deacetylase 7 during T cell apoptosis and angiogenesis. Proc Natl Acad

Sci U S A. National Academy of Sciences; 2008; 105: 4727–32. https://doi.org/10.1073/pnas.0708455105 PMID: 18339811

45. Stehbens SJ, Wittmann T. Analysis of focal adhesion turnover. A quantitative live-cell imaging example. Methods Cell Biol. 2014; 123: 335–346. https://doi.org/10.1016/B978-0-12-420138-5.00018-5 PMID: 24974036

Abstract

Rasa3 is a GTPase activating protein of the GAP1 family which targets Ras and Rap1. Although catalytic inactivation or deletion of Rasa3 in mice leads to severe hemorrhages and embryonic lethality, the biological function and cellular location of Rasa3 underlying these defects remains unknown. Here, using a combination of loss of function studies in mouse (in collaboration with Patricia Molina Ortiz and Stephane Schurmans) and zebrafish as well as in vitro cell biology approaches, we identify a key role for Rasa3 in endothelial cells and vascular lumen integrity.

Specific ablation of Rasa3 in the mouse endothelium, but not in megakaryocytes and platelets, lead to embryonic bleeding and death at mid-gestation, recapitulating the phenotype observed in full Rasa3 knock-out mice. Vascular lumenization defects were observed when Rasa3 was specifically inactivated in mouse endothelial cells at the postnatal or adult stages. Similar results were obtained in zebrafish after decreasing Rasa3 expression using a morpholino. *In vitro*, depletion of Rasa3 in cultured endothelial cells (HUVECs) increased β1 integrin activation and cell adhesion to extracellular matrix components resulting in decreased cell migration and blocked tubulogenesis. During migration, these Rasa3-depleted cells exhibited larger and more mature adhesions resulting from a perturbed dynamics of adhesion assembly and disassembly which significantly increased their life time. These defects were due to a hyperactivation of the Rap1 GTPase and a downregulation of FAK/Src signaling. Moreover, Rasa3-depleted cells showed reduced turnover of VE-cadherin-based adhesions resulting in more stable endothelial cell-cell adhesion and decreased endothelial permeability. Finally, pericytes (cells implicated in heterotypic interactions with endothelial cells) adhere more and spread less around a confluent monolayer of Rasa3-depleted HUVECs.

Altogether, our results indicate that Rasa3 is a critical regulator of Rap1 in endothelial cells which controls adhesions properties and vascular lumen integrity; its specific endothelial cell inactivation results in occluded blood vessels, hemorrhages and early embryonic death in mouse, mimicking thus the full Rasa3-/- mouse phenotype.